이학박사 학위논문

Evolution of the Mesozoic sedimentary basins of the southern Korean Peninsula inferred from geochemistry, sedimentology, and detrital zircon geochronology

한반도 남부의 중생대 퇴적분지들의 발달에 대한 지화학적, 퇴적학적 및 쇄설성 저어콘 연대측정 연구

2020년 2월

서울대학교 대학원

지구환경과학부

이 효 종

ABSTRACT

Evolution of the Mesozoic sedimentary basins of the southern Korean Peninsula inferred from geochemistry, sedimentology, and detrital zircon geochronology

Hyojong Lee
School of Earth and Environmental Sciences
The Graduate School
Seoul National University

Understanding evolution of the Korean Mesozoic sedimentary basins is important to reconstruct the geological history of the Mesozoic Korean Peninsula. This study deals with three topics about sedimentary basins of two different ages in the western Korean Peninsula: (1) the Neungju Basin (Cretaceous), (2) the Chungnam and Gimpo basins with the Seokmun Formation (Triassic to Jurassic). In Chapter 1, facies analysis is carried out to investigate stratigraphic evolution of the Cretaceous Neungju Basin. Four facies associations are recognized: (1) alluvial fan, (2) alluvial plain, (3) sandflat, and (4) playa lake. Vertical and spatial changes in depositional environments were strongly controlled by tectono-volcanic subsidence and source area rejuvenation after active volcanism. The boundary between syneruption and inter-eruption deposits is highly variable according to the relative position in the basin. In proximal environments, erosive boundaries were

formed on syn-eruption deposits after volcanism due to minor influence of tectono-volcanic subsidence. In distal environments, whereas, conformable surface (flooding surface) was formed on syn-eruption deposits due to tectono-volcanic subsidence. In Chapter 2, mudstone geochemistry was examined in the Neungju Basin to investigate compositional contrast due to separation and mixing of different source rocks, in support of previous detrital zircon age data. The Neungju Basin fill of the study area was derived from Precambrian metamorphic rocks, Triassic to Jurassic granites, and Cretaceous volcaniclastic plains on the southern part of the basin. Sediment detritus derived from these source rocks were not fully mixed in the proximal environments (alluvial to sandflat), and thus, the proximal sediments do not reflect the overall compositional characteristics of the surrounding rocks, providing inappropriate information about tectonic settings. On the other hand, sediments deposited in the distal environment (the central playa lake) provide weathering intensities lower than expected, due to the input of unaltered materials from the unstable, southern volcaniclastic plains. In Chapter 3, the tectonic evolution of the western Korean Peninsula during the Early Mesozoic is inferred by mudstone geochemistry and detrital zircon U-Pb age dating. The results suggest (1) the northern distribution of crystalline basement rocks as the hinterland side and southern distribution of metasedimentary cover rocks as the foreland side in the Early Mesozoic orogenic belts, (2) a transition from a collisional to a convergent tectonic setting during their deposition.

Keywords: geochemistry, facies analysis, zircon U-Pb dating, Mesozoic, nonmarine

Student Number: 2010-30111

TABLE OF CONTENTS

LIST OF TABLES

LIST OF FIGURES

INTRODUCTION

Sedimentologists have developed various techniques of provenance analysis to investigate ancient tectonic history. Early researchers focused on modal composition of sandstones to discriminate tectonic setting of ancient basins because types of detrital grains in sediments and sedimentary rocks are strongly influenced by tectonic setting (Dickinson, 1970; Dickinson and Suczek, 1979). Tectonic history such as evolution of magmatic arcs and basement exhumation can be investigated in terms of sandstone petrography (e.g., Kumon and Kiminami, 1994). Mostly during late 1980s to early 2000s, several researchers developed bulk rock geochemistry as a provenance analysis method (e.g., Bhatia, 1983; Roser and Korsch, 1986, 1988; Floyd and Leveridge, 1987; Cullers, 1994; Cullers and Podkovyrov, 2000). Because bulk rock geochemistry can be applied to mudstones as well as sandstones, provenance studies could have been expanded to fine-grained sediment-dominant succession deposited in distal environments such as lakes or deep-seas. Also, subtle changes in source rock composition and/or tectonic setting can be discriminated through bulk rock geochemistry by statistical approaches using a large number of elemental datasets (e.g., Hessler and Lowe, 2006; Joo et al., 2007; Caracciolo et al. 2012). Recently, detrital zircon geochronology has been improved remarkably as a provenance analysis technique. Zircon age data provides exact ages of source rocks, and thus, potential source rocks and sediment pathway can be specified more clearly than provenance analysis using sandstone petrography or bulk rock geochemistry (e.g., Gehrels and Stewart, 1998; Dickinson and Gehrels, 2003; Raines et al., 2013). Each provenance analytic technique has its own advantages and disadvantages, may delivering different fragments of information about a basin. In this study, multi-disciplinary approaches using sedimentology,

geochemistry, and zircon U-Pb geochronology were applied to two different age of nonmarine successions in the Korean Peninsula.

The Neunju Basin fill was deposited in alluvial fan to playa lake environments during Late Cretaceous on the southwestern part of the Korean Peninsula. Jurassic to Triassic granites and Precambrian metamorphic rock broadly distributed in the nearby areas of the basin might be the primary source of sediments. Cretaceous volcaniclastic sediments might also be supplied to the basin. Preferential mixing and separation of sediment detritus originated from different types of source rocks might produce spatial compositional contrast in the basin. Through a combination of facies analysis and zircon age dating for sandstones, the contribution of different types and ages of source rocks was assessed. Mudstones deposited in proximal and distal environments were collected and analyzed geochemically to investigate how sediment mixing/separation influence on tectonic setting and weathering signatures.

The Daedong Supergroup was deposited in nonmarine basins scattered in the southern part of the Korean Peninsula during Triassic to Jurassic under tropical to subtropical climatic conditions (Chun et al., 1988). Based on petrologic and petrographic analyses for conglomerate and sandstone, early researchers suggested that the Daedong Supergroup was derived mainly from mature (meta)sedimentary rocks (e.g., Yu and Lee, 1992; Yu et al., 1992). The overall mature characteristics in the coarse-grained sedimentary rocks of the Deadong Supergroup, however, might be produced by compositional modification through intense chemical weathering under warm and humid climatic conditions and post-depositional diagenesis. In this study, the western Daedong Supergroup (the Nampo Group, the Oseosan Volcanic Complex, the Gimpo Group, and the Seokmun Formation), broadly

distributed in western Korean Peninsula from Gimpo to Boryeong areas, was examined in terms of bulk rock geochemistry and zircon U-Pb geochronology to investigate source rock signatures before compositional modification, and possible regional difference of provenance in the western Daedong Supergroup.

1. STRATIGRAPHIC EVOLUTION OF THE NORTHERN PART OF THE CRETACEOUS NEUNGJU BASIN, SOUTH KOREA

1.1. Introduction

The distribution of depositional environments and vertical stratigraphic evolution of a sedimentary basin are influenced by variable extrinsic factors. In most inland extensional basins, tectonism tends to be a first-order control on the development of a sedimentary succession (Gawthorpe et al., 1994; Gawthorpe and Leeder, 2000). Rapid subsidence may result in the expansion of distal depositional environments, whereas reduced subsidence may result in the progradation of proximal depositional environments (e.g., Jo, 2003). Climate changes may exert an effect of variable magnitude on a basin. Long-term climate changes may influence large-scale stratigraphic architectures (e.g., Allen et al., 2013), whereas short-term climate changes may produce high-frequency fluctuations of lake-levels (e.g., Mtelela et al., 2016).

Volcanism and basin subsidence may occur coevally in many extensional basins (Acocella, 2010), influencing the development of sedimentary successions (e.g., Ashley and Hay, 2002; D'Elia et al., 2018). Instantaneous input of large amounts of volcaniclastic deposits by floods and debris-flow may facilitate aggradational sedimentation during active periods of volcanism, whereas erosion by normal streamflow channels may generate degradational sedimentation during inactive periods of volcanism (Smith, 1987, 1991). The alternation of syn-eruption and inter-eruption sedimentation, however, may not occur if background tectonics played the primary role in the development of the basin (e.g., Sohn et al., 2013).

The East Asian continental margin including the Korean Peninsula was characterized by back-arc to intra-arc settings due to oblique subduction of the Izanagi Plate during the Cretaceous (Lee, 1999). A number of nonmarine basins were formed in the southwestern Korean Peninsula along the NE-SW-trending fault systems under extensional or transtensional tectonic regimes (Ryang, 2013). Factors of basin evolution mentioned above can be seen in the Neungju Basin. The Neungju Basin is the largest among these nonmarine basins. Despite the great paleontological interest in the Neungju Basin due to its preservation of various dinosaur track fossils (e.g., Huh et al., 2003; Huh et al., 2006; Paik et al., 2012; Huh et al., 2013), sedimentological analyses have only been performed on limited parts of the basin (e.g., You et al., 1998; Paik et al., 2007) since early geological surveys (Kim and Park, 1966; Son and Kim, 1966). As a result, the stratigraphic evolution of the basin remains poorly understood. The purposes of this study are (1) to describe and interpret sedimentary facies and depositional environments of the northern part of the Neungju Basin fill, (2) to reconstruct temporal and spatial changes of its paleoenvironments, and (3) to evaluate the influences of tectonics, climate, and volcanism on the development of nonmarine successions.

1.2. Geological settings

The Neungju Basin is one of the nonmarine basins that developed on the southwestern Korean Peninsula during the Cretaceous (Fig. 1-1). The basin is located east of Mudeung Mountain, which was formed by volcanic eruptions during the late-stage development of the Neungju Basin (Ahn et al., 2014). Most of the basin margins remain unclear because

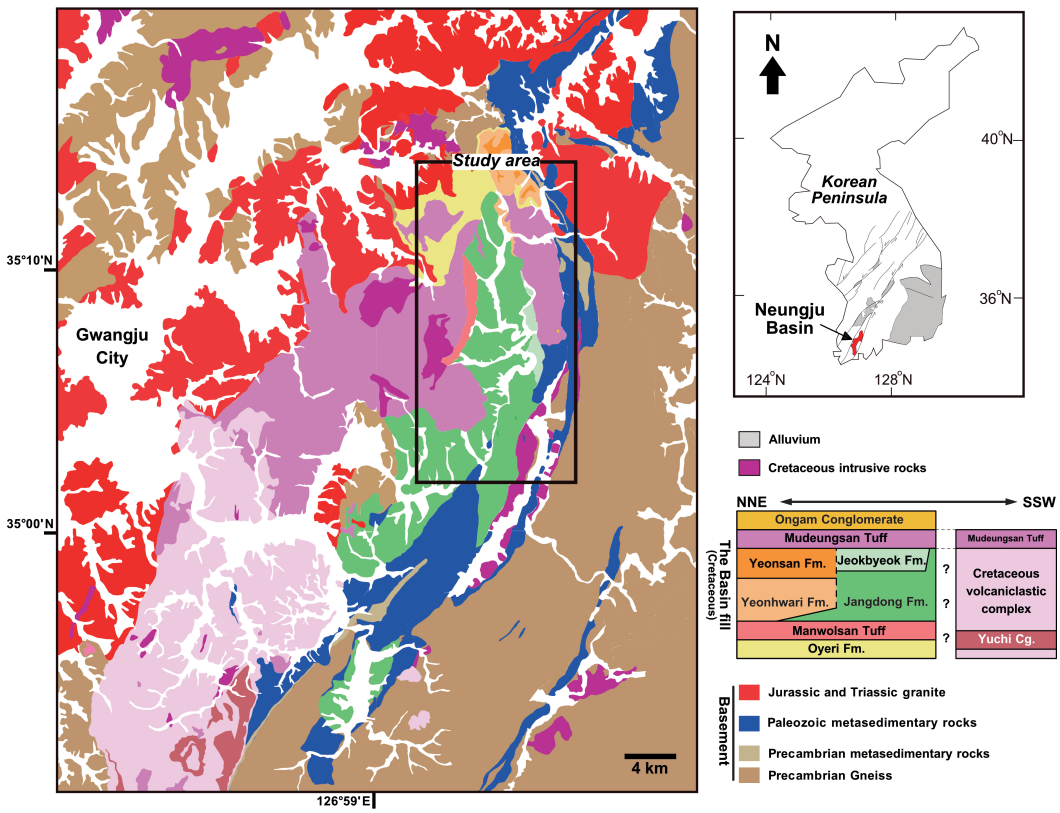

Fig. 1-1. Geological map and stratigraphy of the Neungju Basin (modified after Cheong and Kim, 1966; Kim and Park, 1966; Son and Kim, 1966). The basin fill is bounded by Precambrian gneiss, Paleozoic sedimentary rocks, and Mesozoic granites. The central and northern parts of the basin show mixed deposition of siliciclastic and volcaniclastic deposits, whereas the southern part is mostly filled with volcaniclastic deposits. Most of the basin margin has been covered by volcaniclastic deposits (Mudeungsan Tuff) formed at the late stage of basin development. The study area is indicated by the black square. The depositional ages of the Manwolsan and Mudeungsan Tuffs were reported to be 96 Ma (Kwon, 2018) and 87 to 85 Ma (Ahn et al., 2014), respectively.

volcaniclastic deposits (the Mudeungsan Tuff) associated with the formation of Mudeung Mountain cover most of the basin margins.

The basin fill was deposited in nonmarine environments including alluvial fan, alluvial plain, sandflat, and shallow lacustrine systems, punctuated by intermittent volcanism (Kim and Park, 1966; Son and Kim, 1966; Paik et al., 2007; Roh et al., 2017). Based on lithology, the basin fill is subdivided into the Oyeri Formation, Manwolsan Tuff, Jangdong Formation, Jeokbyeok Formation, Mudeungsan Tuff, and Ongam Conglomerate in ascending order (Fig. 1-1; Kim and Park, 1966; Son and Kim, 1966).

The Oyeri Formation is composed of conglomerate, sandstone, and reddish silty mudstone. The Manwolsan Tuff is gray or greenish lapilli-tuff with minor intercalation of dark gray to black silty mudstones. The Jangdong Formation shows regional variations in lithology. It is mainly composed of dark gray to black silty mudstones and fine sandstones in the northern and central parts of the study area, whereas conglomerates, sandstones, reddish silty mudstones in the southern part of the study area. The Jeokbyeok Formation is composed of dark gray to black silty mudstones and fine sandstones. Early researchers referred the Jangdong and Jeokbyeok formations as the Jangdong and Jeokbyeok tuffs because these successions include a large proportion of volcaniclastic deposits (Kim and Park, 1966; Son and Kim, 1966). In this study, the decameter- to hectometer-thick volcaniclastic deposits in these two successions were dealt separately (the 2nd and 3rd amalgamated tuff beds), and the siliciclastic deposits of the Jangdong and Jeokbyeok tuffs were refereed as the Jangdong and Jeokbyeok formations. The Mudeungsan Tuff is a more than 300 m thick succession of welded dacitic tuffs (Jung et al., 2014). The Ongam Conglomerate is mainly composed of conglomerates and subordinately greenish to reddish

silty mudstones, unconformably overlying the Mudeungsan Tuff. Near the northern basin margin, the Jeokbyeok Formation is not present, and the Yeonhwari and Yeonsan formations composed of conglomerates and sandstones occur between the Jangdong Formation and Mudeungsan Tuff (Fig. 1-1; Son and Kim, 1966). The basin fill is mostly inclined southeast-northeastward (8–29°) in the northern and central parts of the basin (Fig. 1-2). It is inclined west-northwestward near the eastern basin margin, and south-southwestward in the southern part of the study area.

Most of the previous studies focused on dinosaur track-bearing sites in the Jangdong and Jeokbyeok formations, suggestive of their deposition in sandflat to mudflat environments (Huh et al., 2003; Huh et al., 2006; Paik et al., 2007; Roh et al., 2017). The Yeonhwari Formation has been interpreted as an alluvial fan environment (You et al., 1998). Arid to semi-arid climate conditions during the development of the Neungju Basin were suggested based on the occurrence of evaporite casts in mudstones of the Jangdong Formation (Paik et al., 2007).

The depositional age of the basin fill has been constrained as the Late Cretaceous. In a previous study using detrital U-Pb zircon analysis, the Manwolsan Tuff deposited in the early-stage of basin development has yielded the youngest zircon age peak of 96 Ma. Also, the Mudeungsan Tuff deposited in the late-stage of basin development has yielded zircon U-Pb ages between 87 to 85 Ma (Ahn et al., 2014). Thus, the deposition of the Neungju Basin fill was likely initiated in Cenomanian and continued to Santonian.

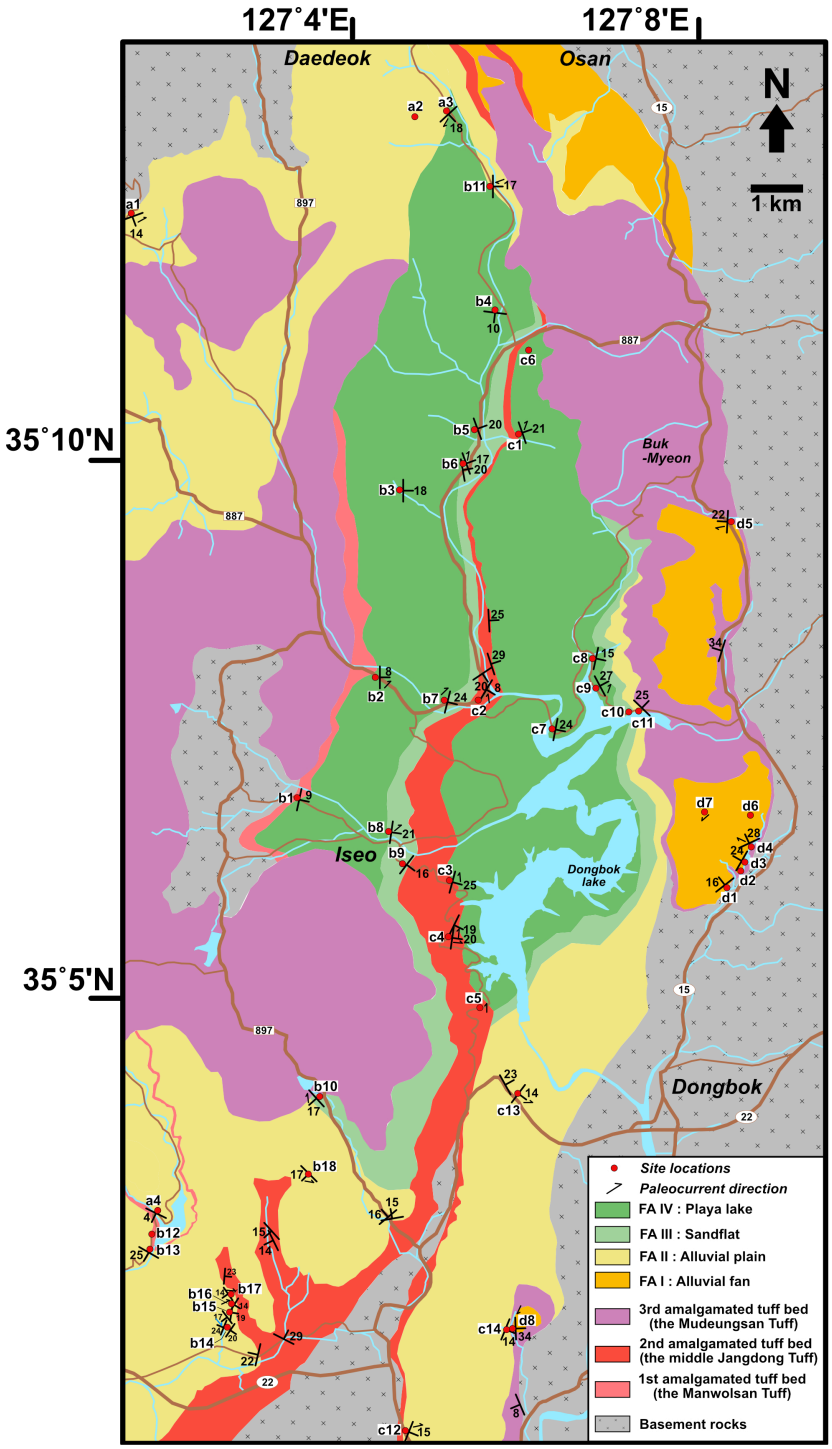

Fig. 1-2. Location map of the measured sections, showing regional distribution of facies associations (modified after Kim and Park, 1966; Son and Kim, 1966). Decameter- to hectometer-thick amalgamated tuff beds occur three times in some stratigraphic horizons, subdividing the basin fill into four conformable Units (I to IV).

1.3. Facies associations

Based on texture, rock colors, and sedimentary structures, ten sedimentary facies are classified in the study area. Their detailed descriptions and interpretations are presented in Table 1-1 and Figure 1-3. Figures 1-4 and 1-5 provide the measured stratigraphic sections in the study area. Site locations and their GPS coordinates are presented in Figure 1-2 and Table 1-2, respectively. These sedimentary facies are grouped into four facies associations representing (1) alluvial fan, (2) alluvial plain, (3) sandflat, and (4) playa lake environments. The occurrences, characteristics, and interpreted depositional environments of the facies associations are described below and are summarized in Table 1-3. The regional distribution of the facies associations is presented in Figure 1-2.

1.3.1. Facies Association I: Alluvial Fan

Facies association I (FA I) occurs along the eastern margin of the basin, corresponding to the upper part of the Yeonhwari Formation, Yeonsan Formation, and the lower part of the Ongam Conglomerate. FA I is composed mainly of disorganized conglomerates (Gd) and horizontally stratified gravelly sandstones (GSh) (Figs. 1-3a and b). The disorganized conglomerate beds are 1 to 4 m thick, forming several meter-thick amalgamated conglomerate bodies (< 23 m). They are mostly massive, clast-supported to matrix-supported conglomerate, but some show crude stratifications. The conglomerate clasts are angular to subangular and are composed of pebble to boulders of schist, quartzite, and granite originated from the northern and eastern margins. In some areas, the disorganized conglomerates overlying the Mudeungsan Tuff (corresponding to the Ongam Conglomerate) contain abundant angular to subangular tuff clasts. The horizontally stratified gravelly sandstones are occasionally amalgamated at the top of the disorganized

Table 1-1. Facies description and interpretation

Facies	Code	Description	Interpretation
Conglomerate facies			
Disorganized conglomerate	Gd (-v)	1–4 m thick; amalgamated up to 23 m thick; clast-supported or matrix-supported; poorly sorted; very coarse to coarse-grained sand matrix or occasionally reddish/greenish silts matrix; angular to subangular pebble to cobble-size extrabasinal clasts, with some boulder-size clasts (e.g., granite, quartzite and schists); (-v) abundant angular to subangular pebble to boulder-size tuff clasts	Debris flow deposits (Nemec & Steel, 1984; Shultz, 1984); hyperconcentrated flow deposits (Pierson & Scott, 1985; Smith, 1986); sheet/longitudinal gravel bars (Steel & Thomson, 1983; Nemec & Steel, 1984; Nemec & Postma, 1993)
Horizontally-stratified gravelly sandstone	GSh	< 1 m thick; occasionally amalgamated at the top of the disorganized conglomerate; crudely stratified or low-angle cross stratified; very coarse to coarse-grained sand matrix; angular to subrounded pebble-size extrabasinal clasts (e.g., granite, quartzite and schists)	Waning flow deposits (Nemec & Steel, 1984); sheetflood deposits (Blair, 1987)
Cross-stratified gravelly sandstone	GSt	Encased in reddish silt to mudstones; 1-3 m thick; sharp, erosional base and flat top; low-angle or trough cross-stratified; alternation of granule- to pebble-size clast-rich layers and very coarse- to coarse-grained sand layers; subangular to subrounded pebble- to cobble-size clast-rich near the bottom (quartzite, schists, reddish mudstone)	Mixed load deposits in gravelly ephemeral braided stream (Reid & Frostick, 1984; Rhee & Chough, 1993); minor channel or scour fills (Miall, 1977; Ryang & Chough, 1997)
Coarse- to fine-grained sandstone facies			
Thick bedded sheet sandstone	Ssh1 (-v)	Decimeter to a few meter thick (0.4-2 m); tabular sheet-like geometry; medium to very coarse-grained; low-angle or trough cross-stratified; low angle lateral-accreted; (-v) tuffaceous	Sandy ephemeral braided stream deposits (Smoot, 1983; Olsen, 1989)
Thin bedded sheet sandstone	Ssh2 (-v)	A few centimeter to decimeter thick; commonly stacked up to a few meter; tabular sheet-like geometry; very fine- to fine-grained; horizontal- or low angle-cross laminated; normal-graded; (-v) tuffaceous	Plane-bed flow deposits under lower or upper flow regime (Bridge & Best, 1988; Best & Bridge, 1992); sheetflood deposits (Smoot, 1983; Olsen, 1989)
Lenticular sandstone	Slc	Decimeter thick; very fine- to medium-grained; lenticular shape; low angle lateral-accreted; trough cross-stratified	Minor crevasse channel deposits (Fielding, 1984, 1986); solitary-channel ephemeral stream deposits (Tunbridge, 1984; Olsen, 1989 and references therein)
Fine grained sandstone to mudstone facies			
Flaser or wavy-bedded fine sandstone to mudstone	MSd	Interlamination of fine sandstone to siltstone and mudstone; dark gray; a few millimeter to centimeter thick; thin flaser or wavy-bedded; occasional presence of mudcracks	Ephemeral stream deposits (Martin, 2000); sheetflood deposits in mudflat environments (Ainsworth et al., 2012; Smoot; 1983; Paik & Kim. 2006)
Reddish siltstone to mudstone	MZr	Siltstone to mudstone; reddish; variable thickness (up to several meters); poorly- or well-sorted; massive or crudely-laminated; occasional inclusion of granule- to sand-size grains	Suspension sedimentation from overflow on floodplain; reddening under oxidizing condition after deposition
Gray siltstone to mudstone	MZg	Siltstone to mudstone; dark gray to greenish gray; a few centimeter to decimeter thick; massive or crudely laminated	Suspension sedimentation from overflow on floodplain or standing water (e.g., pond or lake); graying under waterlogged, reducing condition after deposition
Dark gray siltstone to mudstone	MZd	Siltstone to mudstone; dark gray to black; horizontal or ripple cross-laminations; occasional presence of secondary structures such as mudcracks, gypsum layers, evaporate casts, and dinosaur footprint	Suspension sedimentation in shallow saline water with occasional subaerial exposures (Paik & Kim 2007; Smoot, 2013)

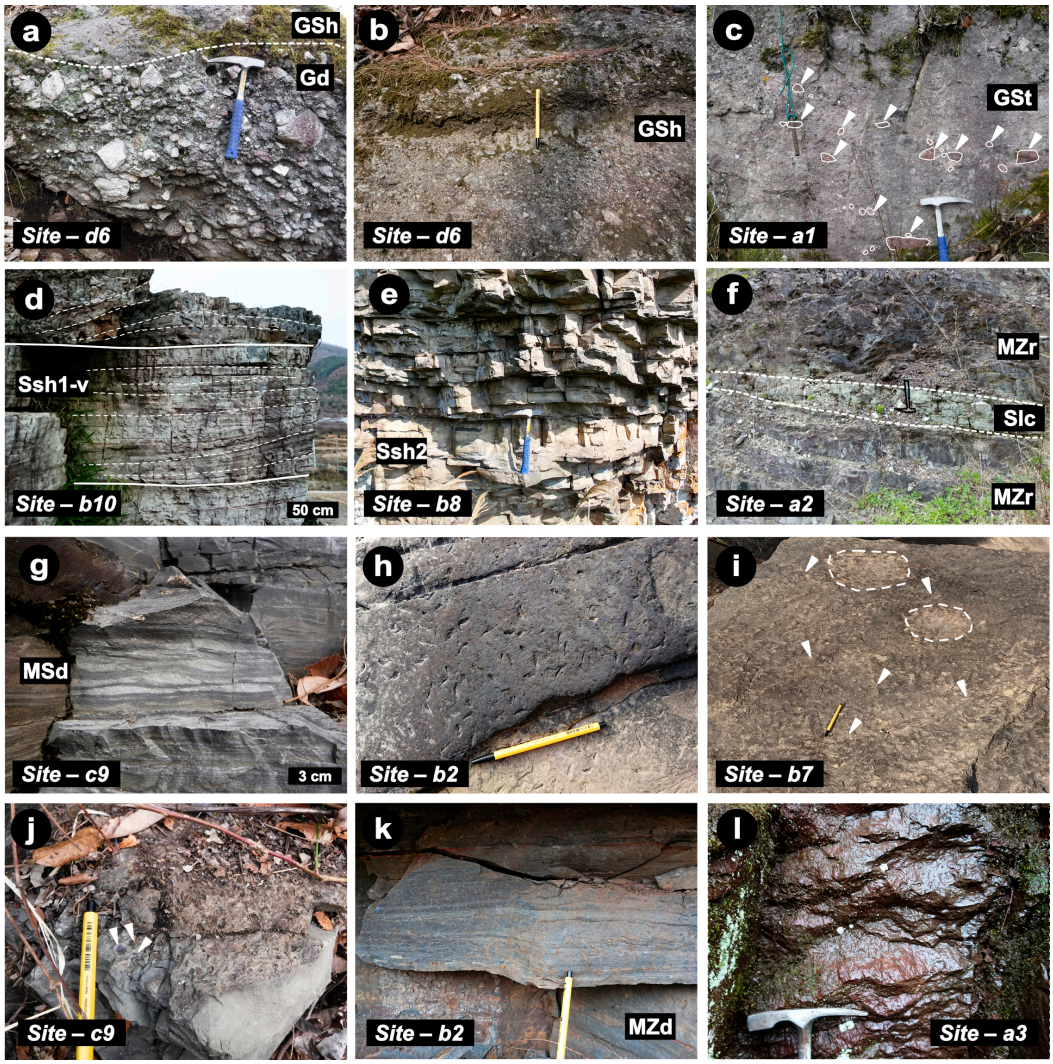

Fig. 1-3. Examples of selected facies and sedimentary structures. (a) Disorganized conglomerate (Gd). Horizontally stratified gravelly sandstone (GSh) are amalgamated with the top of Gd facies. (b) Horizontally stratified gravelly sandstone (GSh). (c) Cross-stratified gravelly sandstone (GSt). White arrows indicate reddish mudstone clasts. (d) Thick-bedded sheet sandstone (Ssh1). Note the sheet-like external geometries with minor lateral accretion. (e) Thin-bedded sheet sandstone (Ssh2). (f) Lenticular sandstone (Slc) encased in reddish siltstone to mudstone (MZr). (g) Flaser or wavy-bedded fine sandstone to mudstone (MSd). (h) Evaporite casts on the surface of MSd facies. (i) One pair of dinosaur footprints on the bedding plane of MSd facies. White arrows indicate mudcracks. (j) Small, dark gray mudstone intraclasts are accumulated in a layer of MSd facies. (k) Dark gray siltstone to mudstone showing horizontal laminations (MZd). (l) Pedogenic slickensides developed in reddish siltstone to mudstone.

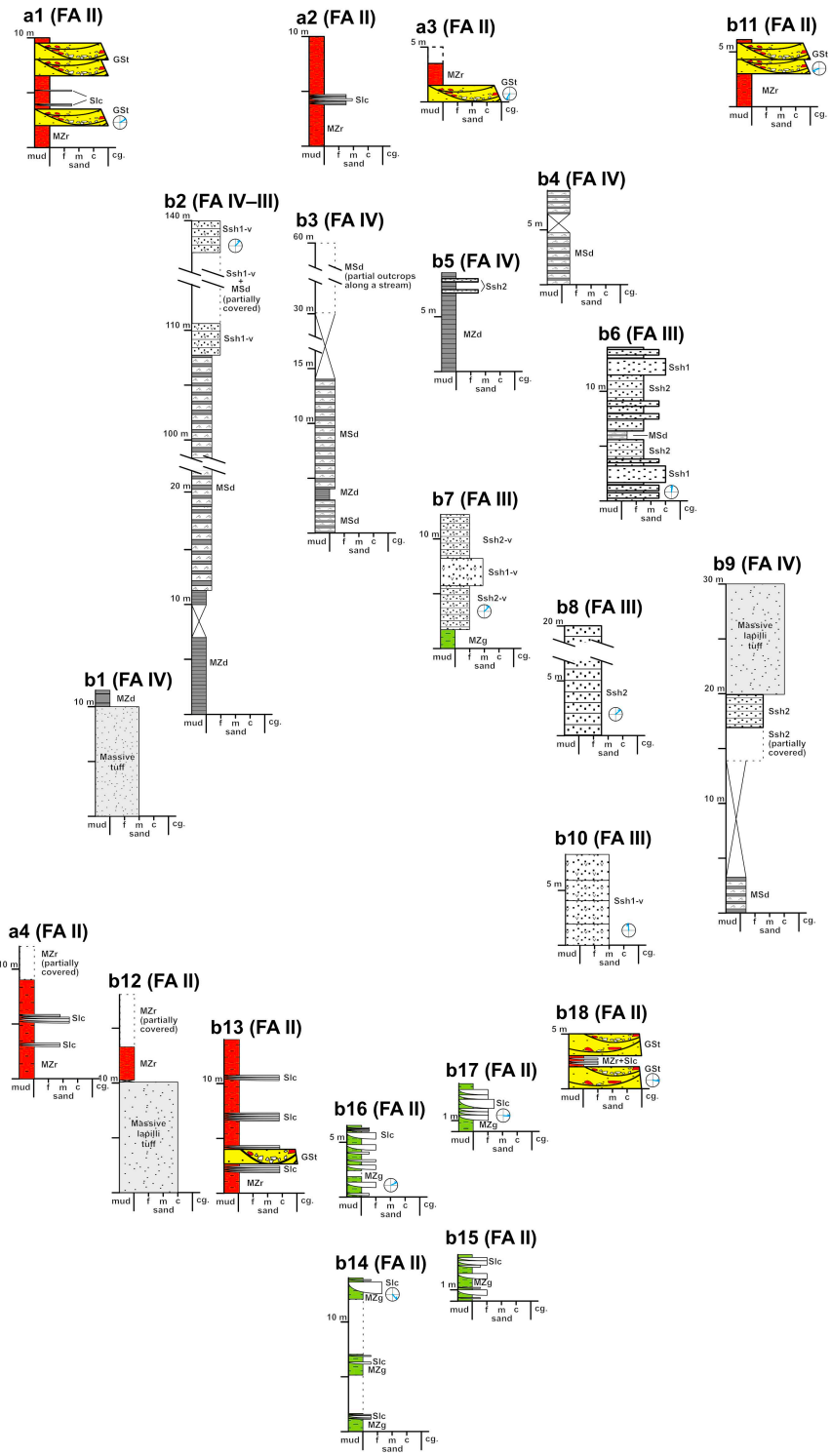

Fig. 1-4. Measured sections from stratigraphic Units I and II. Site locations are shown in Figure 1-2. Blue arrows indicate trough axes, determined by measuring two sides of a trough. Facies codes are presented in Table 1-1.

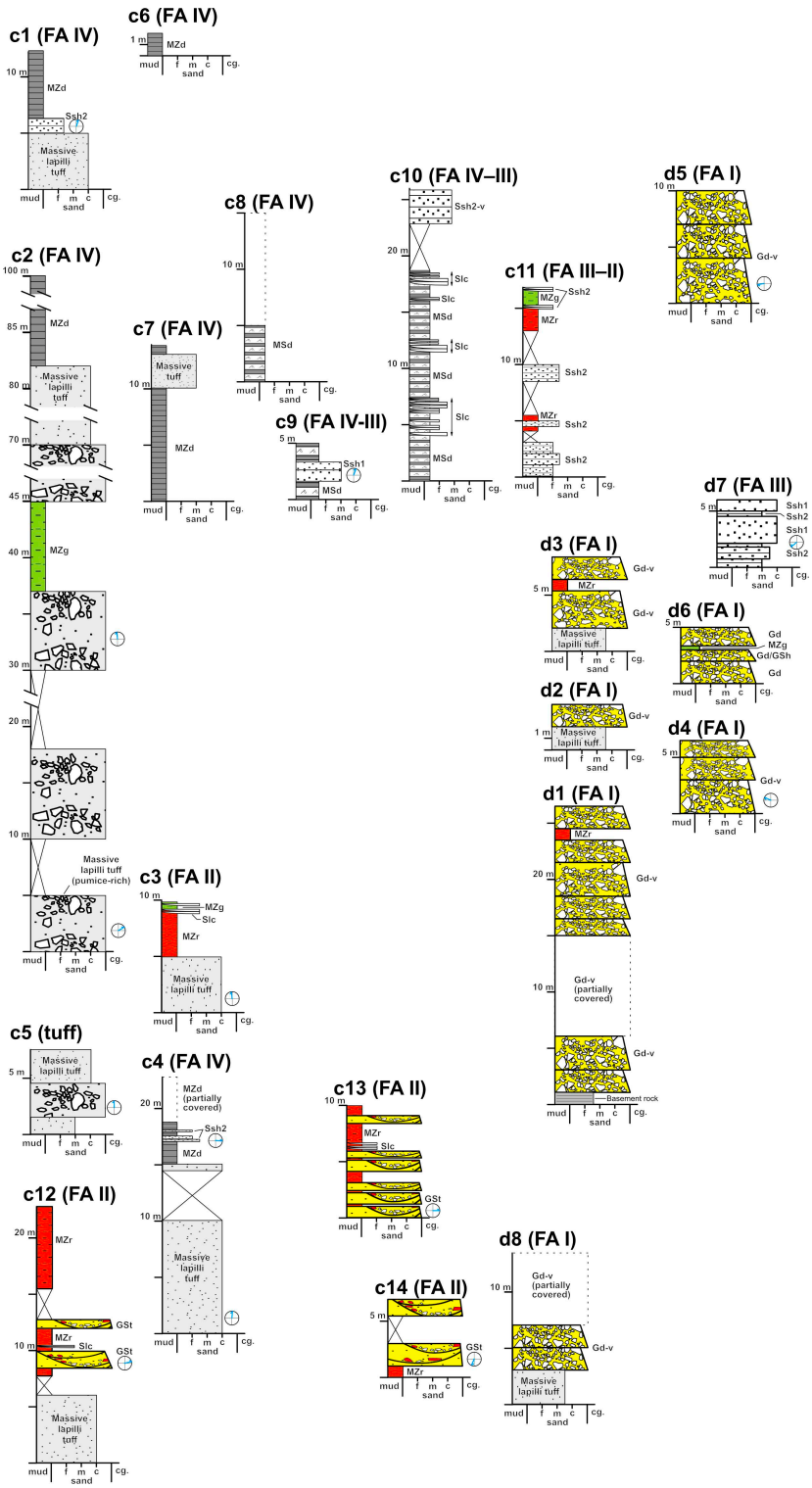

Fig. 1-5. Measured sections from stratigraphic Units III and IV. Site locations are shown in Figure 1-2, and facies codes are presented in Table 1-1.

Table 1-2. GPS coordinates of the measured sections

Site no.	Latitude	Longitude	Site no.	Latitude	Longitude
a1	35°12'29.8"N	127°01'28.7"E	c1	35°10'27.0"N	127°06'05.9"E
a2	35°13'29.0"N	127°04'43.5"E	c2	35°07'57.9"N	127°05'34.8"E
a3	35°13'31.2"N	127°05'12.8"E	c3	35°06'13.4"N	127°05'14.1"E
a4	35°03'07.5"N	127°01'53.6"E	c4	35°05'42.8"N	127°05'14.1"E
b1	35°07'01.7"N	127°03'29.8"E	c5	35°05'03.5"N	127°05'36.8"E
b2	35°08'12.5"N	127°04'21.0"E	c6	35°11'16.9"N	127°06'05.7"E
b3	35°09'57.1"N	127°04'37.8"E	c7	35°07'41.8"N	127°06'25.2"E
b4	35°11'35.3"N	127°05'46.9"E	c8	35°08'21.0"N	127°06'53.1"E
b5	35°10'29.9"N	127°05'33.4"E	c9	35°08'04.7"N	127°06'54.0"E
b6	35°10'10.5"N	127°05'24.2"E	c10	35°07'51.2"N	127°07'20.3"E
b7	35°07'55.9"N	127°05'12.4"E	c11	35°07'51.3"N	127°07'32.1"E
b8	35°06'41.7"N	127°04'33.6"E	c12	35°01'05.0"N	127°04'43.6"E
b9	35°06'24.5"N	127°04'41.5"E	c13	35°04'13.4"N	127°06'02.9"E
b10	35°04'12.7"N	127°03'48.0"E	c14	35°02'00.8"N	127°05'51.8"E
b11	35°12'46.3"N	127°05'45.4"E	d1	35°06'10.2"N	127°08'22.8"E
b12	35°02'54.8"N	127°01'49.8"E	d2	35°06'20.1"N	127°08'35.0"E
b13	35°02'49.3"N	127°01'49.6"E	d3	35°06'24.6"N	127°08'36.1"E
b14	35°02'02.7"N	127°02'41.7"E	d4	35°06'33.0"N	127°08'39.8"E
b15	35°02'12.3"N	127°02'44.9"E	d5	35°09'38.6"N	127°08'23.9"E
b16	35°02'15.6"N	127°02'44.9"E	d6	35°06'52.8"N	127°08'40.1"E
b17	35°02'20.8"N	127°02'44.1"E	d7	35°06'52.5"N	127°08'02.7"E
b18	35°03'29.3"N	127°03'38.1"E	d8	35°02'01.8"N	127°05'57.6"E

Table 1-3. Facies associations and interpretation

Code	Dominant facies	Subordinate facies	Interpretation	Occurrence
FA I	Gd, GSh	MZr, MZg	Alluvial fan	Yeonhwari Fm. (upper part), Yeonsan Fm., Ongam Cg. (lower part)
FA II	GSt, MZr	Slc, MZg	Alluvial plain	Oyeri Fm., Yeonhwari Fm. (lower part), Jangdong Fm.
FA III	Ssh1, Ssh2	Slc, MZg, MZr	Sandflat	Jangdong Fm. (middle and uppermost parts), Jeokbyeok Fm., Ongam Cg. (upper part)
FA IV	MZd, MSd	SSh2	Marginal playa lake	Jangdong Fm.

conglomerates. They are less than 1 m thick and are characterized by crude stratification or low-angle cross-stratification. Reddish or gray siltstone to mudstone facies (MZr, MZg) is occasionally interbedded with these coarse-grained facies (Gd, GSh).

The disorganized conglomerates are poorly sorted and show no distinct stratification, indicating their deposition as debris flows or hyperconcentrated flows (Nemec and Steel, 1984; Shultz, 1984; Pierson and Scott, 1985; Smith, 1986). The gravelly sandstones are commonly amalgamated with the tops of the disorganized conglomerates and are interpreted as waning-flow deposits (Nemec and Steel, 1984) or sheetflood deposits that developed on the surfaces of alluvial fans during flooding (Wasson, 1977; Nemec and Steel, 1984; Blair, 1987). The disorganized conglomerates include boulder-sized angular clasts produced from the northern and eastern margins, indicating their deposition in medial to proximal parts of an alluvial fan, possibly close to the border fault (Spearing, 1974; Nilsen, 1982). The occurrence of abundant tuff clasts in the disorganized conglomerate overlying the Mudeungsan Tuff indicates that volcanic eruption was intense enough to supply a large volume of sediments close to the eastern basin margin, causing significant erosion of volcaniclastic sediments after the volcanism.

1.3.2. Facies Association II: Alluvial Plain

Facies association II (FA II) is broadly distributed near the northern basin margin, corresponding to the Oyeri Formation and the lower part of the Yeonhwari Formation. In the southern part of the study area, most of the Jangdong Formation is also composed of FA II. FA II is dominated by massive or crudely laminated reddish mudstones (MZr). Cross-

stratified gravelly sandstones (GSt), and lenticular sandstones (Slc) are interbedded with the reddish siltstone to mudstones (MZr) (Fig. 1-3c and f). The gravelly sandstones occur as 1- to 3-m-thick beds and are characterized by the alternation of granule- to pebble-size clast-rich layers and very coarse- to coarse-grained sand layers, showing low-angle to trough cross-stratification. The clasts are composed of quartzite, schist, and reddish silt/mudstones and are abundant at the base of the gravelly sandstone beds. The lenticular sandstones are less than 1 m thick and laterally thin and transit into the reddish siltstone to mudstones. In addition to lenticular geometry, they are also characterized by low-angle lateral-accretion and trough cross-stratification.

The reddish siltstone to mudstones can be interpreted as overbank deposits in well-drained floodplain (Friend, 1966; Miall, 1996). The unstratified features in the reddish siltstone to mudstones are likely to have been caused by pedogenesis (Fig. 1-3l). The alternation of gravelly and sandy layers in the gravelly sandstones may be a result of fluctuations in flow velocity during deposition. Similar textures, however, can be produced in gravelly ephemeral streams where gravelly sediments are transported as bed-load and sandy sediments are transported as suspended load (Wasson, 1977; Reid and Frostick, 1984). The concave base and flat top of the lenticular sandstones are suggestive of channel fills. Lateral-accretion also suggests that the channel is sinuous. Based on small grain-size and thickness of the lenticular sandstones relative to the gravelly sandstones, the lenticular sandstones can be interpreted as crevasse channel deposits developed in the floodplain during flooding (Miall, 1985; Miall, 1996). Overall, FA II is interpreted as alluvial plain deposits composed of ephemeral streams and well-drained floodplains (e.g., Rhee and Chough, 1993; Ryang and Chough, 1997).

1.3.3. Facies Association III: Sandflat

Facies association III (FA III) mainly occurs thinly in the central part of the study area (the middle part of the Jangdong Formation), and the areas close to the eastern margin (the uppermost part of the Jangdong Formation to the lower Jeokbyeok Formation). It also occurs in the upper part of the Ongam Conglomerate. FA III is characterized by multiple stacks of thick-bedded (Ssh1), thin-bedded (Ssh2), and lenticular sandstones (Slc). Gray siltstone to mudstones (MZg) is occasionally thinly interbedded with the sandstone (Fig. 1-3d and e). The thick-bedded sandstones are low-angle to trough cross-stratified, coarse- to medium-grained sandstones that occur as 0.4- to 2-m-thick sheets. They are mostly vertically accreted, but in some beds, low-angle lateral accretion is also shown. Thin-bedded sandstones and lenticular sandstones are identical to those of FA II. In some outcrops, a gradual transition from thin-bedded sandstones or lenticular sandstones to thick-bedded sandstones is observed, forming a coarsening- and thickening-upward trend.

The thick-bedded sandstones are somewhat similar to braided stream deposits (Allen, 1983), showing sheet-like external geometries, multiple stacks of sandstones, and dominance of vertical accretion with a minor lateral accretion (Fig. 1-3d). In contrast to typical braided stream deposits, however, they are characterized by nonerosive and flat basal and internal surfaces. In braided stream deposits, the basal and internal surfaces tend to be irregular due to episodic erosion and complex development of variable types of bars. Thus, the thick-bedded sandstones may have been deposited in ephemeral braided stream environments where ephemeral run-off and sheetflood generate poorly defined, nonerosive channels (e.g., Miall, 1985; Olsen, 1989). The thin-bedded sandstones can be interpreted

as sheetflood deposits that developed in alluvial plain areas adjacent to the ephemeral braided stream environments (e.g., Tunbridge, 1984; Miall, 1985; Olsen, 1989). The dominance of sandy sheetflood deposits suggests that FA III is sandflat deposits around shallow playa lake under arid to semi-arid climate conditions (e.g., Smoot, 1983; Paik and Kim, 2006). Although FA III is also similar to the distributary zone deposits of terminal fan environments (cf. Olsen, 1987; Kelly and Olsen, 1993), it is distinguished from terminal fan deposits by the lack of channel bifurcation and interchannel deposits.

1.3.4. Facies Association IV: Playa Lake

Facies association IV (FA IV) broadly occurs in the central and northern parts of the study area, corresponding to most of the Jangdong Formation. FA IV is mainly composed of flaser- or wavy-bedded fine-grained sandstone to mudstone (MSd) and dark gray siltstone to mudstones (MZd) (Figs. 1-3g and k). The dark gray siltstone to mudstones are horizontally or ripple-cross laminated and are characterized by the occurrence of sedimentary features such as mudcracks, evaporite casts, and dinosaur footprints (Figs. 1-3h and i). Laminae including dark gray siltstone to mudstone intraclasts are also rarely observed (Fig. 1-3j).

The alternation of thin sand and mud layers with flaser or wavy bedding is characteristic of marine tidal flat deposits (Reineck, 1967; Reineck and Wunderlich, 1968). Similar sedimentary structures, however, can be developed in ephemeral streams or mudflat environments where sheetfloods repeatedly generate rapid changes in flow velocity (e.g., Smoot, 1983; Martin, 2000; Paik and Kim, 2006). Thus, the flaser- or wavy-bedded fine

sandstone to mudstone may have been deposited in a mudflat environment. The dark gray mudstones may have been deposited in a shallow and stable lake. However, the occurrence of mudcracks, evaporite casts, dinosaur footprints, and intraclast layers indicates that subaerial exposure and minor erosion were common. FA IV is interpreted as a shallow playa lake environment located in the central and northern parts of the study area.

1.4. Amalgamated tuff beds

In the study area, decameter- to hectometer-thick amalgamated tuff beds are recognized in some stratigraphic horizons (Fig. 1-2). They are: (1) 1st amalgamated tuff beds (the Manwolsan Tuff); (2) 2nd amalgamated tuff beds (the middle Jangdong Tuff); and (3) 3rd amalgamated tuff beds (the Mudeungsan Tuff). The respective depositional ages of the 1st and 2nd amalgamated tuff beds have been reported to 96 and 93 M based on zircon U-Pb data (Kwon, 2018). The depositional age of the Mudeungsan Tuff was also reported to be between 87 to 85 Ma (Ahn et al., 2014).

1.4.1. 1st amalgamated tuff beds

Approximately 50-m-thick, the 1st amalgamated tuff beds are exposed on the western side of the study area, overlying alluvial plain deposits (Fig. 1-2). They contain pebble-size subrounded pumice lapilli and angular reddish mudstone clasts in massive coarse ash matrix (Fig. 1-6a). They can be classified as massive lapilli tuff deposited by pyroclastic flows (Cas and Wright, 1987; Branney and Kokelaar, 2002).

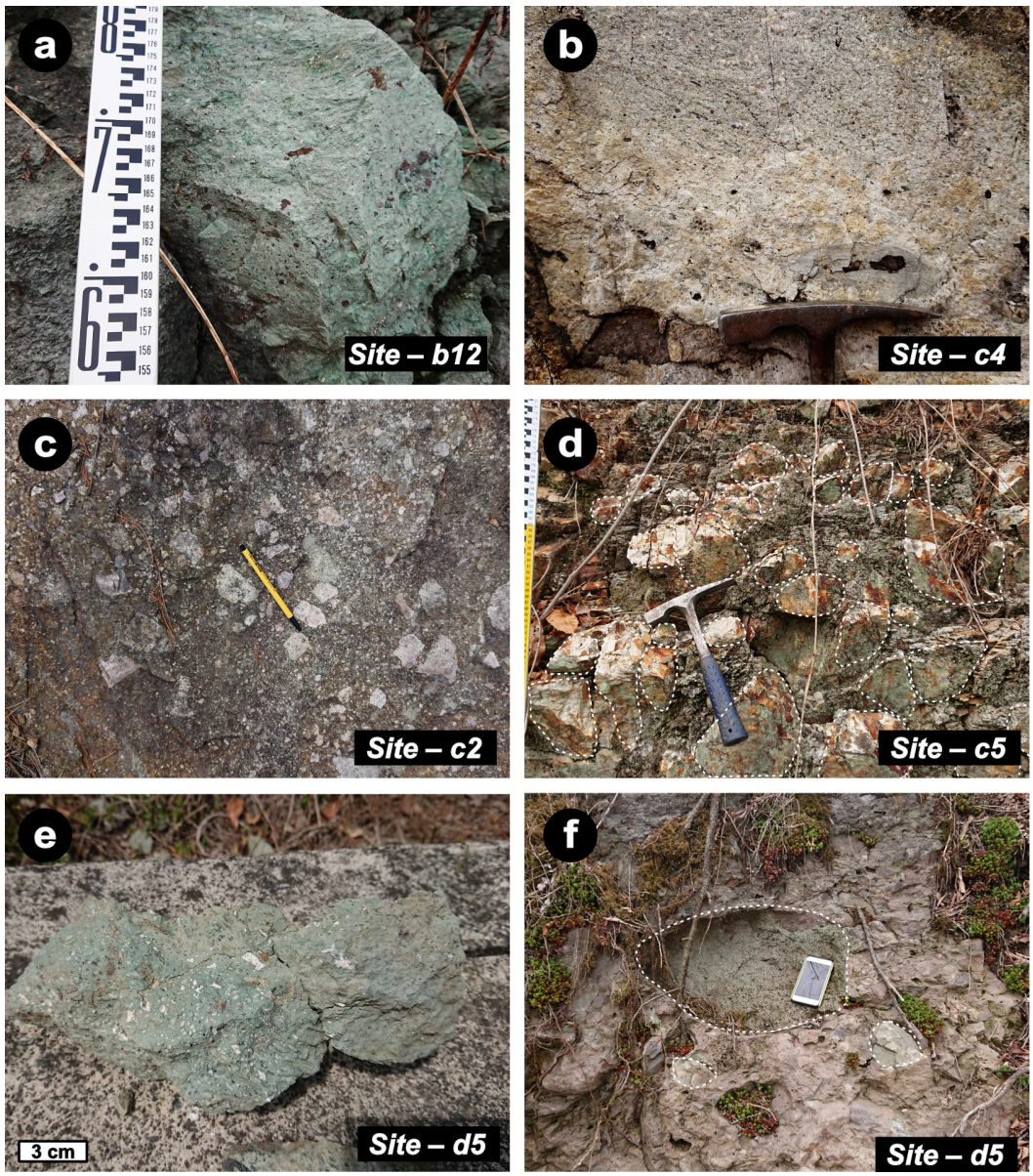

Fig. 1-6. Examples of the thickly amalgamated tuff beds. (a) Massive, greenish lapilli-tuff from the 1st amalgamated tuff beds (the Manwolsan Tuff). (b) Welded lapilli-tuff from the upper part of the 2nd amalgamated tuff beds (the middle Jangdong Tuff). (c) Pebble-size pumice-rich tuff from the middle of the 2nd amalgamated tuff beds. (d) Pebble- to cobble-size pumice-rich tuff from the lower part of the 2nd amalgamated tuff beds. (e) Massive, greenish lapilli-tuff from the 3rd amalgamated tuff beds (the Mudeungsan Tuff). (f) Lapilli-tuff clasts in the disorganized conglomerate of unit IV.

1.4.2. 2nd amalgamated tuff beds

The 2nd amalgamated tuff beds occur in the middle part of the study area (Fig. 1-2). They are amalgamated up to 120 m, showing a difference in pumice abundance (Fig. 1-6b to d). In the lower part of the 2nd amalgamated tuff beds, they contain pebble- to cobble-size subrounded rhyolitic pumice lapilli abundantly, with dark gray to black mudstone clasts (Fig. 1-6d). In the upper part, the 2nd amalgamated tuff beds only include a minor proportion of pebble-size pumices (Fig. 1-6b). The 2nd amalgamated tuff beds characterized by massive textures, although (cross-) stratification and welded textures are occasionally observed (Fig. 1-6b). Paleocurrent data collected from cross-stratification indicate their derivation from the south of the study area (Fig. 1-5). They can be classified as pumice-rich lapilli tuff in the lower part and massive lapilli tuff in the upper part (Branney and Kokelaar, 2002).

1.4.3. 3rd amalgamated tuff beds

The 3rd amalgamated tuff beds are the Mudeungsan Tuff deposited by Mudeunsan volcanic eruption near the northwestern boundary of the Neungju Basin at the late-stage of basin development (Ahn et al., 2014; Fig. 1-1 and 1-2). They are amalgamated more than 300 m in the study area and broadly distributed most part of the Neungju Basin. They are mainly composed of massive coarse to fine ash matrix and contains some granule- to pebble-size rhyolitic pumices and dark gray mudstone clasts (Figs. 1-6e and f). Crude stratification and welded textures are occasionally observed. They can be classified as massive lapilli

tuffs (Branney and Kokelaar, 2002).

1.5. Stratigraphic units

1.5.1. Unit boundaries

Using the amalgamated tuff beds as key beds, the basin fill of the Neungju Basin can be subdivided into four conformable stratigraphic units (I to IV; Fig. 1-7). Unit I is separated from Unit II by the 1st amalgamated tuff beds. In the central part of the study area, dark gray siltstone to mudstones (MZd) of Unit II overlie the 1st amalgamated tuff bed (Fig. 1-8i). On the other hand, reddish siltstone to mudstone (MZd) of Unit II overlie the tuff beds in the southern part. Pebble-size angular tuff clasts in the MZd facies are suggestive of minor erosion (Fig. 1-8h), although an erosional surface has not been clearly observed. The unit boundary is covered partly by the 3rd amalgamated tuff beds (Fig. 1-2) and is difficult to specify in the northern part of the study area.

Unit II and III are separated by the 2nd amalgamated tuff beds. In the central to northern parts of the study area, dark gray siltstone to mudstone (MZd) of Unit III overlie the 2nd amalgamate tuff beds (Fig. 1-8e and g), showing no sign of basal erosion. In the southern part of the study area, on the other hand, reddish siltstone to mudstone (MZd) of Unit III overlie the 2nd amalgamated tuff beds (Fig. 1-8d and f). Irregular top of the 2nd amalgamated tuff beds is suggestive of minor erosion in the southern part of the study area.

Unit III is thickly covered by the 3rd amalgamated tuff beds. The disorganized

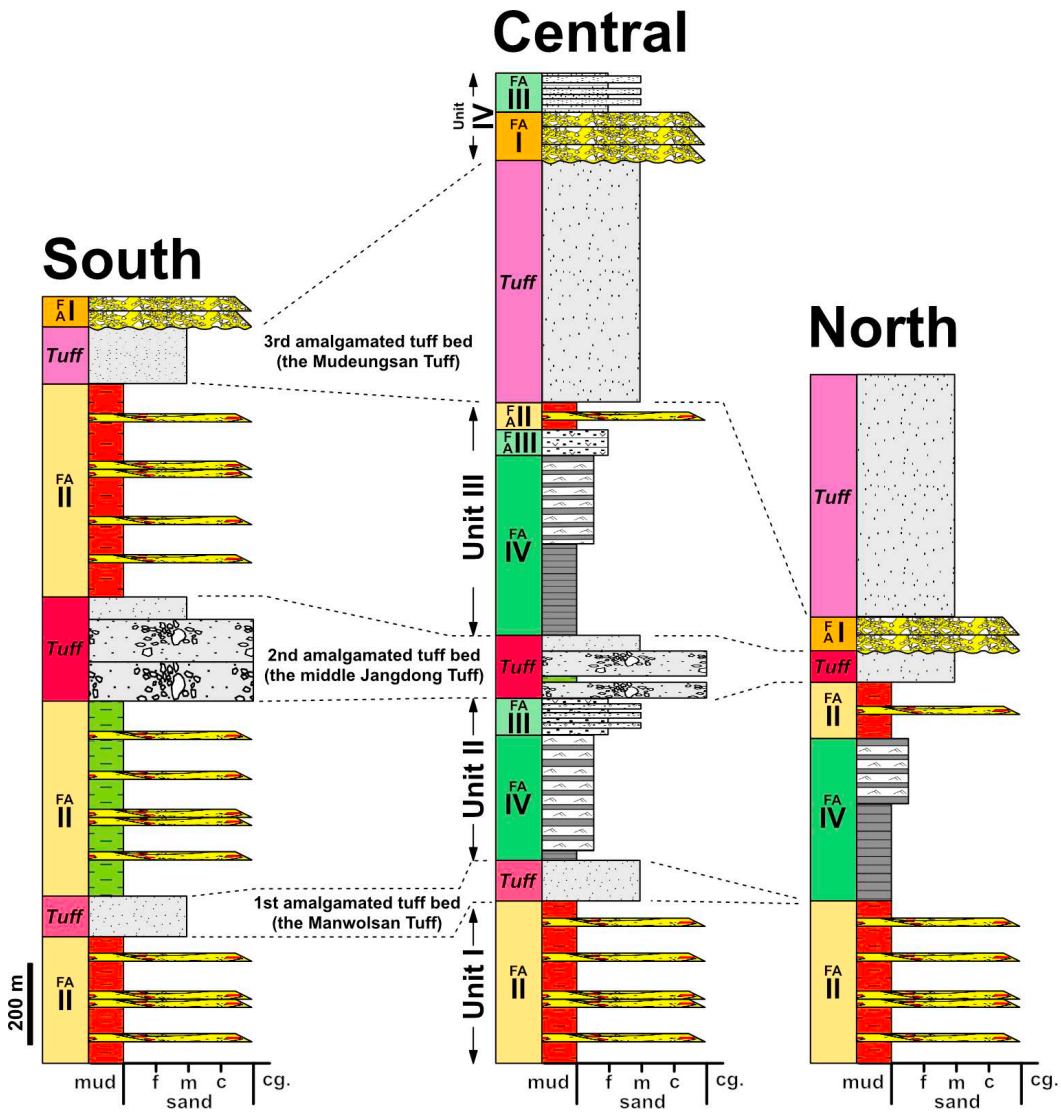

Fig. 1-7. Schematic composite sections of the southern, central, and northern parts of the study area, highlighting the upsection changes in depositional environments.

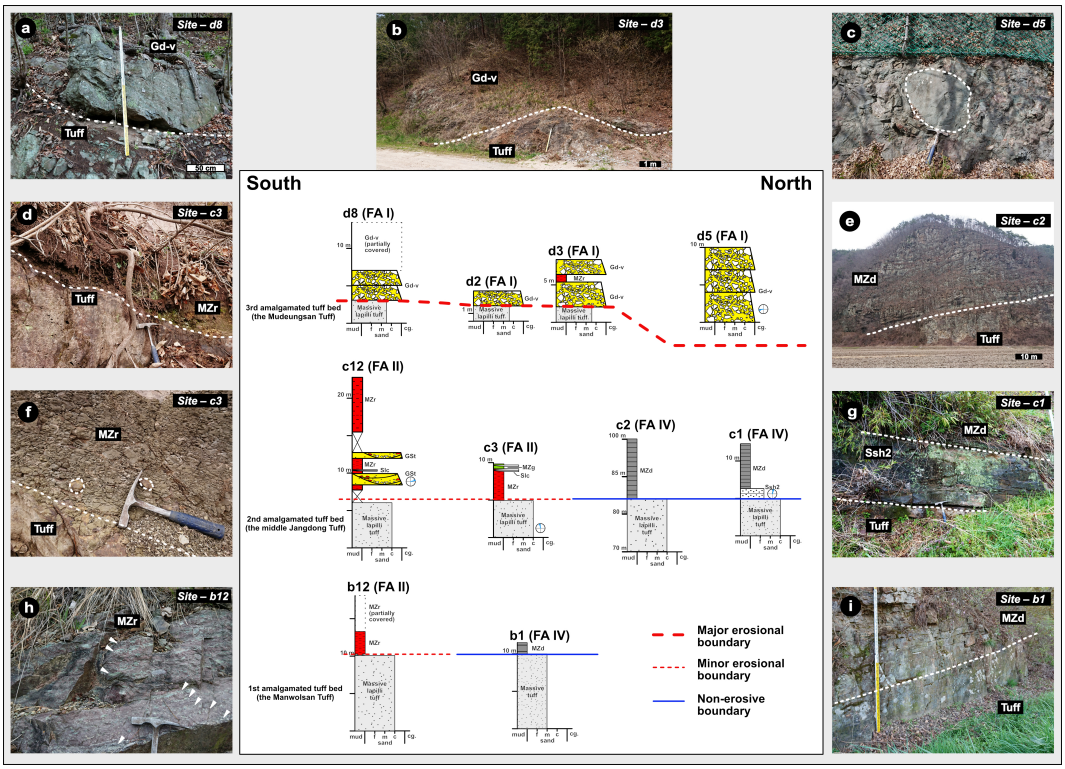

Fig. 1-8. Characteristics of the top of the thickly amalgamated tuff beds and outcrop photographs. (a and b) The disorganized conglomerate erosively overlying the 3rd amalgamated tuff beds (the Mudeungsan Tuff). (c) Boulder-size clasts of the 3rd amalgamated tuff beds in the overlying disorganized conglomerates, indicating significant erosion of the tuff beds below. (d) Minor erosion at the top of the 2nd amalgamated tuff beds (the middle Jangdong Tuff). (e) Marginal playa lake deposits (MZd facies) non-erosively overlying the 2nd amalgamated tuff beds. (f) Carbonate nodules in reddish siltstone to mudstone facies, few cm above the tuff beds. (g) Non-erosive boundary between Ssh2 facies and the underlying tuff beds. (h) Pebble-size angular tuff clasts (white arrows) in reddish siltstone to mudstones. Approximately 1 m above the underlying tuff beds, indicating minor erosion. (i) Non-erosive boundary between MZd facies and the underlying tuff beds.

conglomerates of Unit IV erosively overlie the 3rd amalgamated tuff beds (Fig. 1-8a to c). The common occurrence of cobble-size tuff clasts in the disorganized conglomerates indicates significant erosion of the underlying 3rd amalgamated tuff beds during their deposition.

1.5.2. Stratigraphic Unit I

Stratigraphic Unit I, the lowest unit, is approximately 150 to 250 m thick and is exposed along the western basin margin. This unit is composed of FA II (Fig. 1-7), indicating the development of a broad alluvial plain environment along the western basin margin during the earliest stage of basin evolution (Fig. 1-9). Paleocurrent data indicate eastward flow direction during the deposition of Unit I (Fig. 1-2), suggesting that alluvial fans might exist west of the present basin margin.

1.5.3. Stratigraphic Unit II

Stratigraphic Unit II (approximately 200 m thick) initiates with an abrupt transition from FA II of Unit I to FA IV in the central and northern parts of the study area, indicating a major expansion of the playa lake environment in the areas (Fig. 1-7 and 1-9). The occurrence of FA II in the southern part of the study area indicates that the lake expansion was not expanded to the southern part. The ephemeral braided stream deposits (Ssh1) in Unit II commonly contain abundant tuffaceous materials (Fig. 1-4). North- to northeastward flow directions of the stream deposits (Fig. 1-4) indicate that tuffaceous materials were derived from the volcaniclastic plains developed on the southern part of the

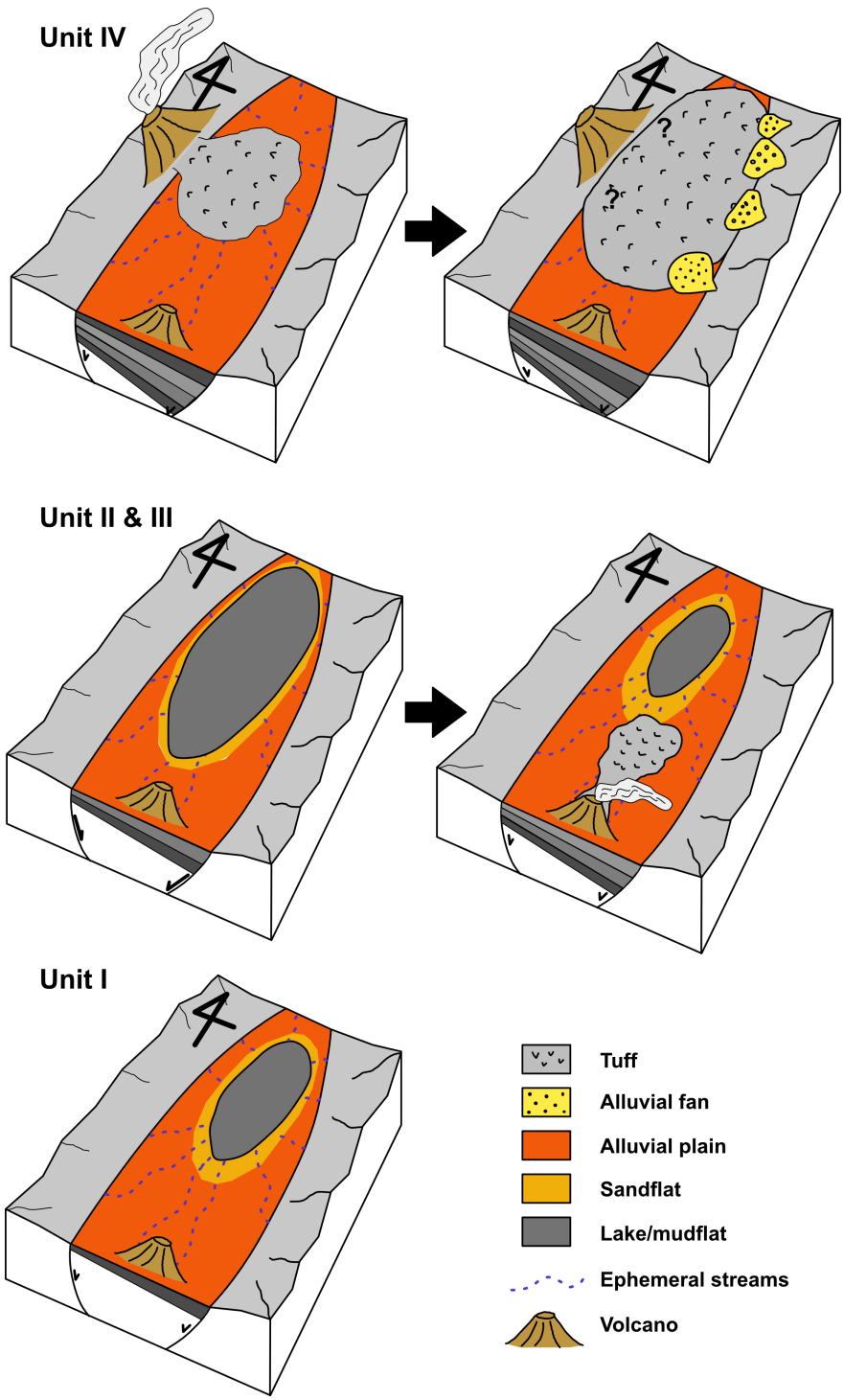

Fig. 1-9. Depositional model illustrating the paleoenvironmental evolution of the Neungju Basin in the study area.

basin (Fig. 1-1). Upsection transition of the facies association in Unit II from FA IV to FA III in the central part of the study area and from FA IV to FA II in the northern part of the study area indicate that the playa lake environment was gradually contracted during the deposition of Unit II, with progradation of proximal facies from nearby source areas.

1.5.4. Stratigraphic Unit III

Stratigraphic Unit III is approximately 200 m thick and shows similar depositional patterns to those of Unit II (Fig. 1-7 and 1-9). In the central part of the study area, this unit initiates with FA II and shows the gradual transition into FA III, indicating another expansion and subsequent contraction of playa lake environments during the deposition. Alluvial fans (FA I) and alluvial plains (FA II) developed in the northern and southern parts of the study area, respectively.

1.5.5. Stratigraphic Unit IV

Stratigraphic Unit IV occurs in an area adjacent to the eastern basin margin, overlying the thick, extensively distributed tuff beds (the Mudeungsan Tuff). Erosional boundaries at the bottom of Unit IV and boulder-size tuff clasts in its conglomerate deposits indicate significant erosion of the underlying amalgamated tuff beds. The upsection transition from alluvial fan (FA I) to sandflat (FA III) environments (Fig. 1-7) indicates retrogradation of proximal facies during the deposition of Unit IV.

1.6. Discussion

1.6.1. Basin Development of the Neungju Basin

According to the stratigraphic changes in unit development of the Neungju Basin, the basin evolution can be subdivided into early (Unit I), middle (Unit II & III), and late (Unit IV) stages. During the early stage of basin evolution (Unit I), alluvial plain (FA II) deposits accumulated with no major transition in depositional environments or sandbody thickness. This unit may have been deposited under consistency of accommodation generation (Paola et al., 1992; Fidolini et al., 2013) after initial basin formation, with no significant changes in extrinsic factors including tectonics and climate.

During the middle stage, two coarsening-upward sequences (Units II & III) were deposited mainly in the central and northern parts of the study area, each representing an early expansion of the playa lake environment and later contraction with progradation of proximal facies from surrounding areas. If the playa lake of the Neungju Basin was under balanced filled or underfilled conditions (*sensu stricto* in Carroll and Bohacs, 1999) due to the prevalence of semi-arid climate conditions in the Korean Peninsula during the Late Cretaceous (Paik et al., 2012), the expansion and contraction of the playa lake could be mainly induced by climatic fluctuations. The abrupt expansion of lacustrine environments at the bases of stratigraphic Units II and III, however, are more likely to be caused by rapid basin subsidence rather than a gradual transition from dry to wet climate conditions. The deposition of fine-grained, distal facies during the early stage and the subsequent, gradual coarsening with progradation of proximal facies are highly similar to tectonically induced

stratigraphic units (or sequences) in extensional basins (Frostick and Steel, 1993; Martins-Neto and Catuneanu, 2010), suggesting that each of these units represents a tectonic pulse comprising an early stage of rapid generation of accommodation space due to basin subsidence and a later stage of gradual filling. Basin subsidence might be focused preferentially on the central and northern parts of the study area, resulting in the limited development of playa lake environments in these regions. Alternatively, reworking of a large volume of tuffaceous materials from the southern volcaniclastic plains might increase the rate of sediment supply in the southern part of the study area, hindering southward expansion of the playa lake environments.

The deposition of thick amalgamated tuff beds before the two lake expansion events suggests that volcanism was closely related to basin subsidence for the development of the Neungju Basin. Volcanic eruptions and following volcano-tectonic subsidence are common characteristics of caldera collapse (e.g., Branney and Kokelaar, 1994; Troll et al., 2000). Caldera structures characterized by ring-like fault systems, however, are not recognized in the study area. Also, deposition of thick volcaniclastic deposits in the southern part of the Neungju Basin and paleocurrent data of the tuff beds suggests that volcanic eruptions occurred outside of the study area. Thus, tectono-volcanic subsidence due to caldera collapse is not a possible explanation for the relation between volcanism and basin subsidence in the study area. Alternatively and more likely, volcanic eruptions near pre-defined fault systems can be a reliable explanation for the development of the middle interval. The Neungju Basin has been bounded by the NE-SW directional fault systems (Fig. 1-1). In areas where fault systems have been already defined, volcanic eruptions may cause caldera-like tectono-volcanic subsidence on the place of volcanic eruption and

nearby areas due to reactivation of the pre-defined fault systems (e.g., Marti, 1991; Holohan et al., 2008), resulting in lake expansion in the basin center soon after deposition of thick pyroclastic flow deposits (e.g., D'Elia and Marti, 2013; D'Elia et al., 2018).

In the later stage (Unit IV), the depositional environments changed from alluvial fan (FA I) to sandflat (FA III) environments, representing retreat of alluvial fan systems. Such a fining-upward, retrograding trend would have been produced in proximal environments by gradual decreases in sediment supply and slope-gradient during tectonic quiescence (Paola et al., 1992; Catuneanu and Elango, 2001). Prior to Unit IV, the Mudeungsan volcanic eruption near the northwestern basin margin resulted in the deposition of the hectometer-thick 3rd amalgamated tuff beds. The occurrence of boulder-size tuff clasts in conglomerates of the lower part of Unit IV (Fig. 1-6f and 1-8c) indicates that the tuff beds were deposited even in the areas close to the eastern basin margins. If accommodation space was fully filled by the significant input of volcaniclastic sediments, sediment bypass of deep channel incision might occur at the top of the 3rd amalgamated tuff beds (e.g., Huerta et al., 2001), instead of deposition of alluvial sediments of Unit IV. Thus, extrusion of a large volume of volcanic materials from the magma chamber and flexural loading might enhance volcano-tectonic subsidence enough to compensate deposition of the hectometer-thick amalgamated tuff beds (Marti, 1991; Smith et al., 2002).

1.6.2. Syn-eruption Versus Inter-eruption Sedimentation

The characteristics of sedimentary environments near active volcanoes were reviewed by Smith (1991). Two different conditions of sedimentation may occur in response to

volcanism. During the syn-eruption period, a large amount of volcaniclastic debris is supplied by floods and debris-flows, resulting in vertical aggradation of laterally extensive sheet-like volcaniclastic deposits. During the inter-eruption period, in contrast, volcaniclastic input is significantly diminished and normal streamflow channels are developed, resulting in incision and deposition of channel conglomerates. Erosional surfaces and paleosols are developed during this period, bounding the top of previous syn-eruption deposits. The facies geometry may also differ in response to basin subsidence (Smith, 1991). If basin subsidence is not sufficient to compensate for the volcaniclastic sediment supply, deeply incised valleys will develop along the erosional surface during the inter-eruption period, with no or minor deposition of inter-eruption deposits (type 1). If basin subsidence matches or exceeds volcaniclastic input, inter-eruption channel conglomerates will be partially preserved within incised channels (types 2a) or extend laterally as sheet-like morphologies (type 2b).

The depositional patterns of the Neungju Basin fill indicate alternation of inter-eruption and syneruption periods. The development of erosive boundary between conglomerate (Gd) of Unit IV and the underlying amalgamated tuff beds (Fig. 1-8a to c) resembles type 2 facies geometry of the depositional model by Smith (1991). In the proximal environments where basin subsidence was less critical than source area rejuvenation (e.g., Hardlari and Rainbird, 2006), tectono-volcanic subsidence might cause minor influence on the depositional pattern. Channels developed in the proximal environments could generate erosional surfaces. In contrast, the lower boundaries of Units II and III with the underlying amalgamated tuff beds differ from the characteristics inferred by the depositional model by Smith (1991), with regional variations. In central and northern parts of the study area, fine-

grained lake sediments (MZd) of Units II and III conformably overlies the amalgamated tuff beds (Fig 1-8e, g, and i). In the southern part of the study area, on the other hand, fine-grained alluvial plain sediments (MZr) overlie the amalgamated tuff beds with minor erosion and paleosol development (Fig. 1-8d, f, and h). In the distal environments, tectono-volcanic subsidence might be the primary control for the development of sedimentary succession. Conformable surface (flooding surface) or minor erosive surface could be formed in the distal environments due to tectono-volcanic subsidence after the volcanic eruption.

1.7. Conclusions

The facies analysis from the northern part of the Neungju Basin reveals that the basin fill is composed of alluvial to lacustrine facies associations. These facies associations represent the deposition of (1) alluvial fan; (2) alluvial plain; (3) sandflat; and (4) playa lake environments. The basin fill can be subdivided into four hectometer-scale stratigraphic units by thickly amalgamated tuff beds. During the early stage (Unit I) of basin development, an alluvial plain developed in the western part of the basin. During the middle stage (Unit II & III), two coarsening-upward sequences were deposited mainly in the central and northern parts of the study area, each representing an earlier expansion of a playa lake environment and later contraction with progradation of proximal facies from surrounding areas. Finally, during the late stage, alluvial fans developed near the eastern basin margin and changed into sandflat environments.

Volcanism and tectonism may have been strongly coupled, controlling the stratigraphic

evolution of the Neungju Basin fill. Two lake expansion events at the lower boundary of Unit II and III were possibly caused by reactivation of pre-defined fault systems due to volcanic eruptions. The coarsening-upward trend in the distal environments (Unit II & III) represents progradation of proximal facies and gradual filling of accommodation space during tectonic quiescence of inter-eruption period, respectively. A significant amount of volcaniclastic sediments were supplied prior to the deposition of Unit IV. Tectono-volcanic subsidence, however, might be enhanced enough to compensate for the increased sediment supply. The fining-upward trend in proximal environments (Unit IV) represent retreat of alluvial fan systems due to decreases in sediment supply and slope-gradient during tectonic quiescence of inter-eruption period.

This study provides insight into a variable relationship between syn-eruptional and inter-eruptional deposits. In proximal environments where basin subsidence is less critical than source area rejuvenation, erosional boundary will be formed at the lower base of inter-eruption deposits, as depicted by the traditional depositional model by Smith (1991). Whereas in distal environments, a conformable boundary will be formed at the base of inter-eruption deposits due to tectono-volcanic subsidence.

2. CONTRASTING GEOCHEMICAL SIGNATURES OF TECTONIC SETTINGS AND WEATHERING INTENSITY BETWEEN PROXIMAL AND DISTAL DEPOSITS: A CASE STUDY FROM THE CRETACEOUS NEUNGJU BASIN, SOUTHWEST KOREA

2.1. Introduction

Provenance study aims to reconstruct the development history of sedimentary basins. Information such as source rocks, tectonic settings, weathering conditions, and sediment transportation and mixing can be delivered from a composition of sedimentary rocks (Nebitt and Young, 1982; Bhatia, 1983; Roser and Korsch, 1988; Ohta, 2008). In nonmarine basins, sediments may preserve the compositional characteristics in the source areas because they are transported in a short distance (Von Eynatten, 2003). However, sediment composition may differ significantly according to relative position and depositional environment due to preferential mixing and separation of sediments derived from different types of source rocks, providing wrong information about a basin (Weltje, 2012). Sediments deposited in a proximal environment (alluvial to fluvial) may reflect the composition of a specific source rock exposed to the nearby areas, whereas sediment deposited in a distal environment (lacustrine) may reflect the mixed composition of the source rocks surrounding a basin (Ingersoll, 1990).

Detrital zircon U-Pb geochronology is a powerful tool to monitor sediment derivation from the source areas and mixing in the depositional areas. In support of paleocurrent data,

detrital zircon U-Pb age data can specify potential source rocks and sediment distribution patterns (e.g., Barth et al., 2004; Dickinson and Gehrels, 2003; Gehrels and Stewart, 1998; Lawton et al., 2009; Rainbird et al., 1997; Raines et al., 2013).

Major element composition of sedimentary rocks can be used to discriminate the tectonic setting of sedimentary basins and weathering conditions in the source areas. Early researchers proposed several tectonic setting discrimination diagrams using the elemental ratios such as SiO_2/Al_2O_3 and K_2O/Na_2O (Bhatia, 1983; Roser and Korsch, 1986, 1988). The diagrams have been widely applied to many provenance studies for over thirty years (e.g., Rahman and Suzuki, 2007; Spalletti et al., 2008; Huntsman-Mapila et al., 2009; Sarki Yandoka, 2015), although their accuracy has been questioned by some researchers because they use only three or four major elements for tectonic setting discrimination, not reflecting the whole compositional characteristics of sedimentary rocks (Armstrong-Altrin and Verma, 2005; Ryan and William, 2007; Pe-Piper et al., 2008; von Eynatten and Dunkl, 2012). Recently, Verma and Armstrong-Altrin (2013) proposed new multi-dimensional diagrams based on a more accurate statistical approach on the extensive compositional database to provide more accurate tectonic setting discrimination than the traditional methods.

Major element composition is also a function of chemical weathering in the source areas. Chemical weathering represents the decomposition of unstable minerals such as feldspars and leaching of mobile elements (e.g., Na_2O, CaO, and K_2O) from the parent rocks. As weathering proceeds, the relative abundance of Al-rich clay minerals increases in the weathering profile. Thus, conventional weathering indices were formulated as a molecular proportion of major elements oxides, measuring leaching of mobile elements against immobile elements such as Al_2O_3 or SiO_2. For example, the Chemical Index of Alteration

(CIA: Nesbitt and Young, 1982) is defined as molecular [$Al_2O_3/(Al_2O_3 + CaO + Na_2O + K_2O)$] x 100. These weathering indices have been used in many studies to assess the climatic condition of sedimentary basins and its temporal changes (e.g., Kotlia and Joshi, 2013; Rashid et al., 2015; Chen et al., 2017).

The Neungju Basin is an extensional nonmarine basin developed in the southwestern Korean Peninsula during Late Cretaceous under arid to semiarid climatic conditions, experiencing intermittent volcanic activities. The basin is surrounded by various types of source rocks including Precambrian granitic gneiss, Mesozoic granites, Paleozoic metasedimentary rocks, and Cretaceous volcaniclastic terrane. Paleocurrent data indicates that sediment detritus originated from these source rocks were transported to the central playa lake through alluvial systems developed near the basin margins (Lee et al., 2019). In this study, mudstones deposited in proximal and distal environments were geochemically analyzed. In support of the detrital zircon U-Pb age data previously reported by Kwon (2018), this study will provide an ideal opportunity to investigate compositional contrast (heterogeneity) in a nonmarine basin and its impact on the tectonic setting and weathering signatures.

2.2. Geological settings

During the Cretaceous, NE-SW-trending sinistral strike-slip fault systems were developed along the East Asian continental margin due to oblique subduction of the Izanagi Plate beneath the East Asian continent (Lee, 1999). Small nonmarine basins were formed under extensional or transtensional tectonic regimes along the NE-SW-trending fault systems in

the southern part of the Korean Peninsula (Ryang, 2013). Subduction-related magmatic activities were initiated in central China and migrated eastward to Korea due to oblique consumption of ridge (Lee, 1999). The Cretaceous nonmarine basins were filled with epiclastic and volcaniclastic deposits, experiencing extensional faulting and acidic to intermediate volcanic activities.

The Neungju Basin is the largest one of the Cretaceous nonmarine basin, located east of the Gwangju City (Fig. 2-1). The eastern and western basin margins are bounded by NNE-SSW-trending fault systems. However, the basin margins are unclear because most part of the margins has been covered by volcaniclastic deposits supplied at the late-stage of basin development (Mudeungsan Tuff). The basin is filled with approximately 2000 m thick succession of epiclastic and volcaniclastic deposits. The basin fill was deposited in alluvial fan, alluvial plain, sandflat, and playa lake environments (You et al., 1998; Huh et al., 2006; Paik et al., 2007; and Lee et al., 2019), and can be subdivided into decameter- to hectometer-thick lithological units: the Oyeri Formation, Manwolsan Tuff, Jangdong Formation (or Jangdong Tuff), Jeokbyeok Formation (or Jeokbyeok Tuff), Mudeungsan Tuff, and Ongam Conglomerate in ascending order (Fig. 2-1; Kim and Park, 1966; Son and Kim, 1966).

The lowermost Oyeri Formation is composed of conglomerates, sandstones, and reddish silty mudstones, representing an alluvial plain environment. The Manwolsan Tuff is gray to greenish lapilli-tuff. The Jangdong and Jeokbyeok formations are mainly composed of dark gray to black silty mudstones and fine sandstones. In some areas of the basin, they also include conglomerates and reddish mudstones. The Jangdong and Jeokbyeok formations mainly represent sandflat to playa lake environment. The Mudeungsan Tuff is

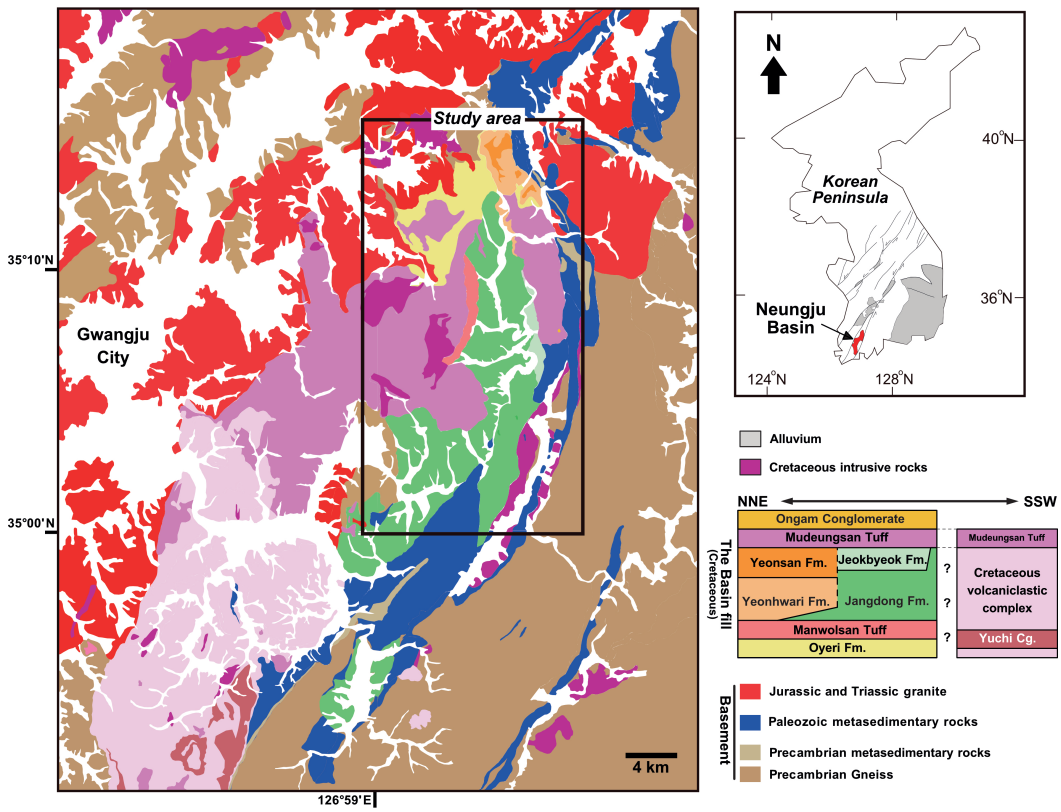

Fig. 2-1. Geological map and stratigraphy of the Neungju Basin (modified after Cheong and Kim, 1966; Kim and Park, 1966; Son and Kim, 1966). Precambrian metamorphic rocks broadly surround the basin. Jurassic granites are mostly distributed near the northern and western basin margins. Paleozoic metasedimentary rocks are narrowly distributed along the eastern margin. The basin fill is dominantly composed of siliciclastic deposits with intercalated volcaniclastic deposits in the northern and central parts of the basin. Whereas, the southern part of the basin is mostly filled with volcaniclastic deposits, indicating the development of volcaniclastic plains.

welded tuffs with a dacitic composition (Jung et al., 2014). The uppermost Ongam Conglomerate is mainly composed of conglomerates, and subordinately sandstones and silty mudstones. Near the northeastern basin margin, the sedimentary succession corresponding to the Jangdong to Jeokbyeok formations is also composed of conglomerates. The conglomerate-dominant succession was defined as the Yeonhwari and Yeonsan formations (Fig. 2-1; Son and Kim, 1966). The Ongam Conglomerate and the Yeonhwari and Yeonsan formations represent an alluvial fan environment. The basin fill mostly is mostly inclined to the southwest to the northeast with an angle of 8–29˚ (Lee et al., 2019).

Previous sedimentological studies show that alluvial fans were developed on the areas close to the basin margins and transited to playa lake toward the central area of the basin (Fig. 2-2; You et al., 1998; Paik et al., 2007; and Lee et al., 2019). Paleocurrent date indicates that sediments originated from the surrounding source areas were transported to the central areas (Lee et al., 2019). Halite and sulfate evaporite traces in the playa lake deposits indicate arid to semiarid climatic conditions during the development of the basin (Paik et al., 2007). Tuff beds interbedded to the lower to upper part of the basin fill provide the youngest zircon age peak of 96 and 87–85 Ma, respectively, indicating deposition of most of the basin fill through Cenomanian to Santonian (Ahn et al., 2014; this study).

The oldest basement rocks are Precambrian granitic gneiss complex (1935 Ma; Turek and Kim, 1995), broadly surrounding The Neungju Basin. Along the eastern to southeastern basin margins, Paleozoic metasedimentary rocks are narrowly distributed as an elongated shape. They are composed of quartzites, carbonates, schists, and coal-bearing shales. Although the depositional ages of the Paleozoic rocks are not well-constrained, they are considered as equivalent to the Upper Paleozoic Pyeongan Supergroup (Seo and Park,

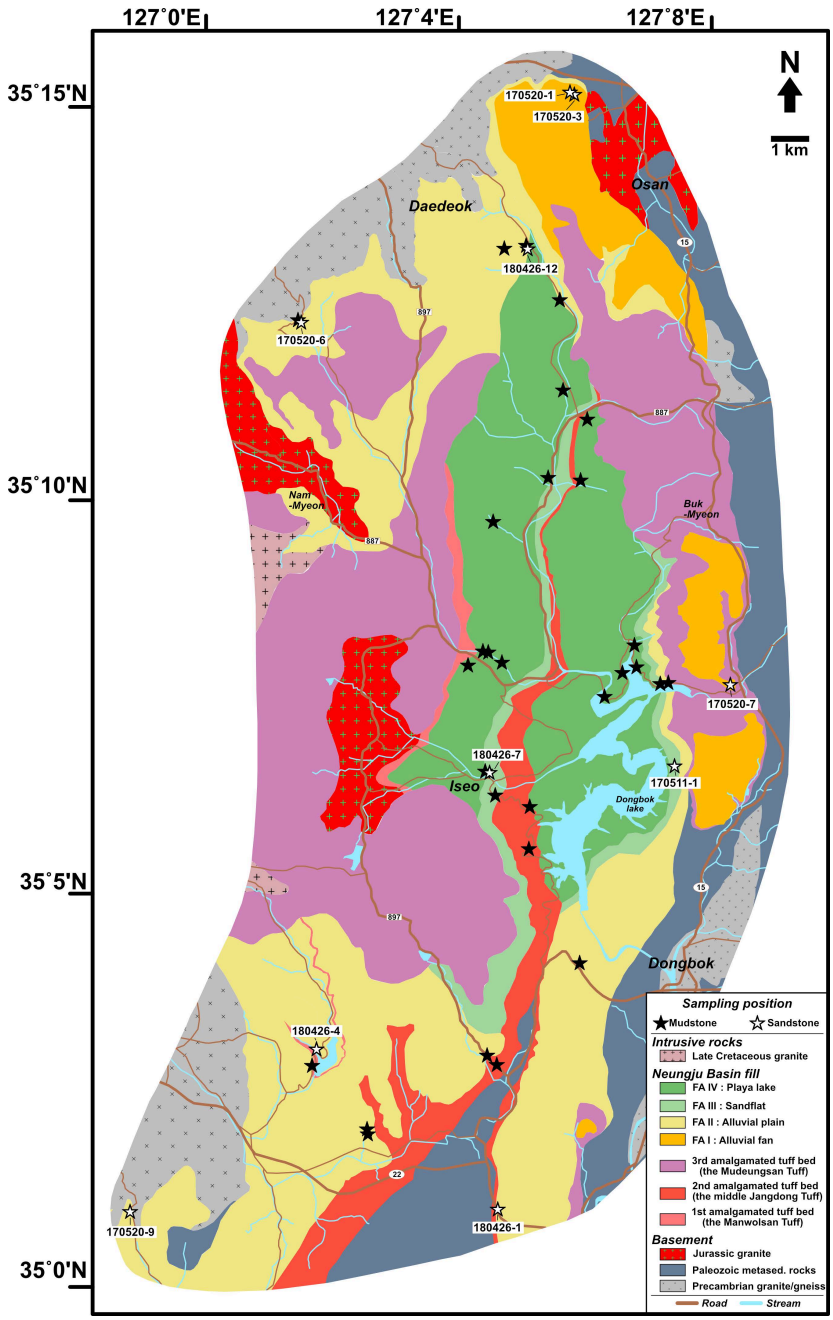

Fig. 2-2. Facies distribution map of the Neungju Basin (modified after Lee et al., 2019). Sample locations for the mudstone samples are indicated by a closed star. Sixteen mudstone samples were collected from the proximal depositional environments (alluvial plain and sandflat), and fourteen mudstone samples from the distal depositional environments (playa lake). To constrain sediment provenance, zircon U-Pb age data of ten sandstone samples from Kwon (2018) was used in this study. The sample locations for zircon age dating analysis is indicated by an open star.

1984). The Precambrian and Paleozoic rocks have been intruded by Triassic and Jurassic granites (219–176 Ma; Turek and Kim, 1995). The Mesozoic granites are widely distributed near the northern and western margins of the Neungju Basin. The southwestern part of the Neungju Basin is filled with rhyolites, dacitic lapilli tuffs, and tuff breccias, with a minor amount of conglomerates, indicating the development of volcaniclastic plains on the areas during basin development (Cheong and Kim, 1966; Kim and Park, 1966; Son and Kim, 1966).

2.3. Analytic methods

To investigate the separation and mixing of sediments in the Neungju Basin, detrital zircon U-Pb age data from ten sandstone samples reported by Kwon (2018) was adopted in this study. The sandstone samples were collected in the northern part of the Neungju Basin (Fig. 2-2). $^{206}Pb/^{238}U$ ages for < 1000 Ma and $^{207}Pb/^{206}Pb$ ages for > 1000 Ma were used for age probability curves, with a discordance of < 15% and a reverse discordance of < 10%.

A total of thirty mudstone samples were also collected from the proximal and distal deposits in the northern part of the Neungju Basin to investigate compositional contrast in tectonic setting and weathering signatures (Fig. 2-2). 16 mudstone samples were collected from the proximal deposits representing alluvial plain (13) and sandflat (3) environments. 14 mudstone samples from the distal deposits representing the playa lake environment. The collected mudstone samples were powdered in agate mortar after they were washed by clean water and dried. The major element composition of the powdered samples was analyzed at Korea Basic Science Institute (KBSI). Phillips PW2404 X-ray fluorescence

spectrometer (XRF) was used to obtain major element contents including SiO_2, Al_2O_3, Fe_2O_3 (total Fe), TiO_2, MnO, MgO, K_2O, Na_2O, and P_2O_4. Loss-on-ignition (LOI) was estimated at 1000˚C for 60 min. The analytic uncertainty is less than 5% for the major element composition.

Sediments deposited during syn-eruption periods may reflect the composition of volcanic and volcaniclastic input only, not presenting the patterns of sediment separation and mixing. Thus, the sandstone and mudstone samples were collected from stratigraphic intervals representing inter-eruption periods (Lee et al., 2019), to avoid direct influence from a volcanic eruption.

2.4. Results and interpretations

2.4.1. Detrital zircon U-Pb ages

Ten sandstone samples provide zircon U-Pb ages (939 grains) ranging from 85.1 ± 1.1 Ma to 3308 ± 3.5 Ma. Most of zircon ages fall into four dominant age groups: Cretaceous (22%; 85.1–100.1 Ma), Jurassic (25%; 161.8–200.1 Ma), Triassic (9%; 201.7–251.0 Ma), and Paleoproterozoic (43%; 1742–2479 Ma). Subordinately, 12 zircons provide Archean ages (1%; 2510–3308 Ma). A single zircon provides Carboniferous age of 309 ± 17 Ma. All zircons of Jurassic to Carboniferous ages have Th/U ratios larger than 0.1, indicating their igneous origin (Vavra et al., 1999). One-third of Paleoproterozoic zircons (152 grains) have Th/U ratios smaller than 0.1, indicating their metamorphic origin. The zircons of Cretaceous to Triassic ages are characterized by euhedral prismatic shapes, whereas Precambrian zircons show rounded shapes (Fig. 2-3).

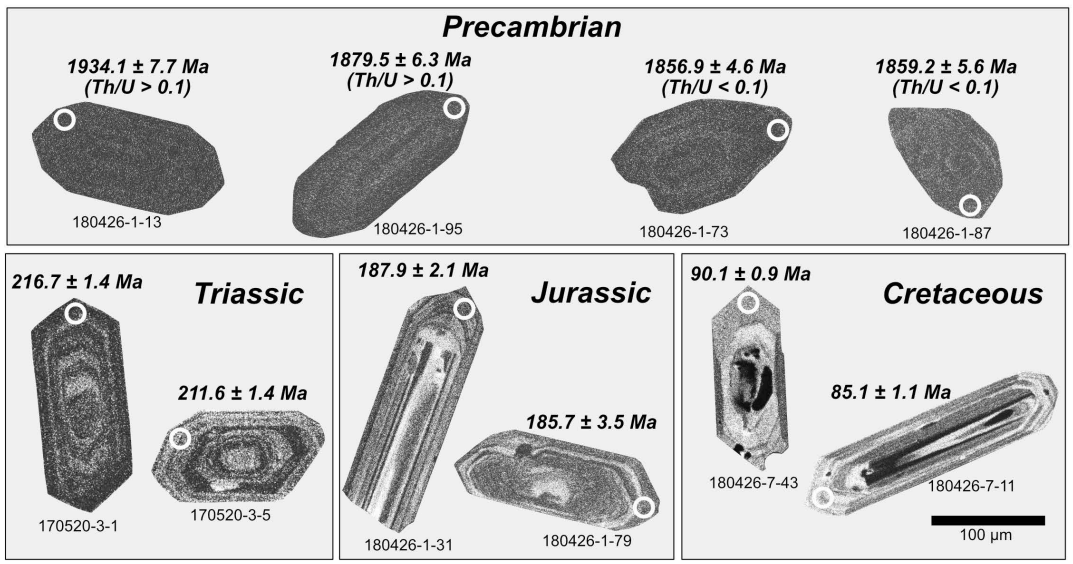

Fig. 2-3. Scanning-electron-microscope (SEM) cathodoluminescence images of selected zircon grains from the sandstone samples in the Neungju Basin. The original SEM images from Kwon (unpublished data). The zircon grains of Cretaceous to Triassic ages show euhedral prismatic shapes, whereas those of Precambrian ages show subrounded shapes.

The distribution of ages for the sandstone samples is presented in the form of a relative age probability curve (Fig. 2-4). Two sandstone samples were collected near the western basin margin (170520-6, 170520-9). 170520-6 shows Jurassic to Triassic ages between 173.0 to 227.6 Ma with an age peak at 187 Ma, and Paleoproterozoic to Archean ages between 1830 to 2596 Ma with age peaks at 1854 and 2440 Ma. 170520-9 has the Carboniferous zircon of 309 Ma. Except for the single Carboniferous zircon, 170520-9 shows Jurassic ages between 178 to 199.7 Ma with a prominent age peak at 186 Ma, and Paleoproterozoic to Archean ages between 1841 to 3308 Ma.

Two sandstone samples were collected near the northeastern basin margin (170520-3, 180220-4). 170520-3 shows Jurassic to Triassic ages between 177.9 to 225.8 Ma with an age peak at 187 Ma, and Paleoproterozoic to Archean ages between 1939 to 2620 Ma with an age peak at 1920 Ma. 180220-4 shows Cretaceous ages between 89.4 to 99.1 Ma (5 grains) and Jurassic to Triassic ages between 171.6 to 251.0 Ma with prominent age peaks at 184 and 220 Ma. Two sandstone samples collected near the eastern basin margin (170520-7, 170511-1) show Paleoproterozoic to Archean ages only. 170520-7 shows ages between 1846 to 3254 Ma with a prominent age peak at 1848 Ma. 170511-1 shows ages between 1905 to 2690 Ma with age peaks at 1853, 2184, and 2467 Ma.

Four sandstone samples collected in the central part of the study area (180426-12, 180426-7, 180426-4, 180426-1) are distinguished by prominent age peaks at Cretaceous with the rest of the samples. 180426-12 shows Cretaceous ages between 88.1 to 94.6 Ma with an age peak at 94 Ma, Jurassic ages between 161.8 to 185.8 Ma with an age peak at 181 Ma, and Paleoproterozoic to Archean ages between 1998 to 2663 Ma with an age peak at 1995 Ma. 180426-7 shows Cretaceous ages between 85.1 to 94.1 Ma with a prominent

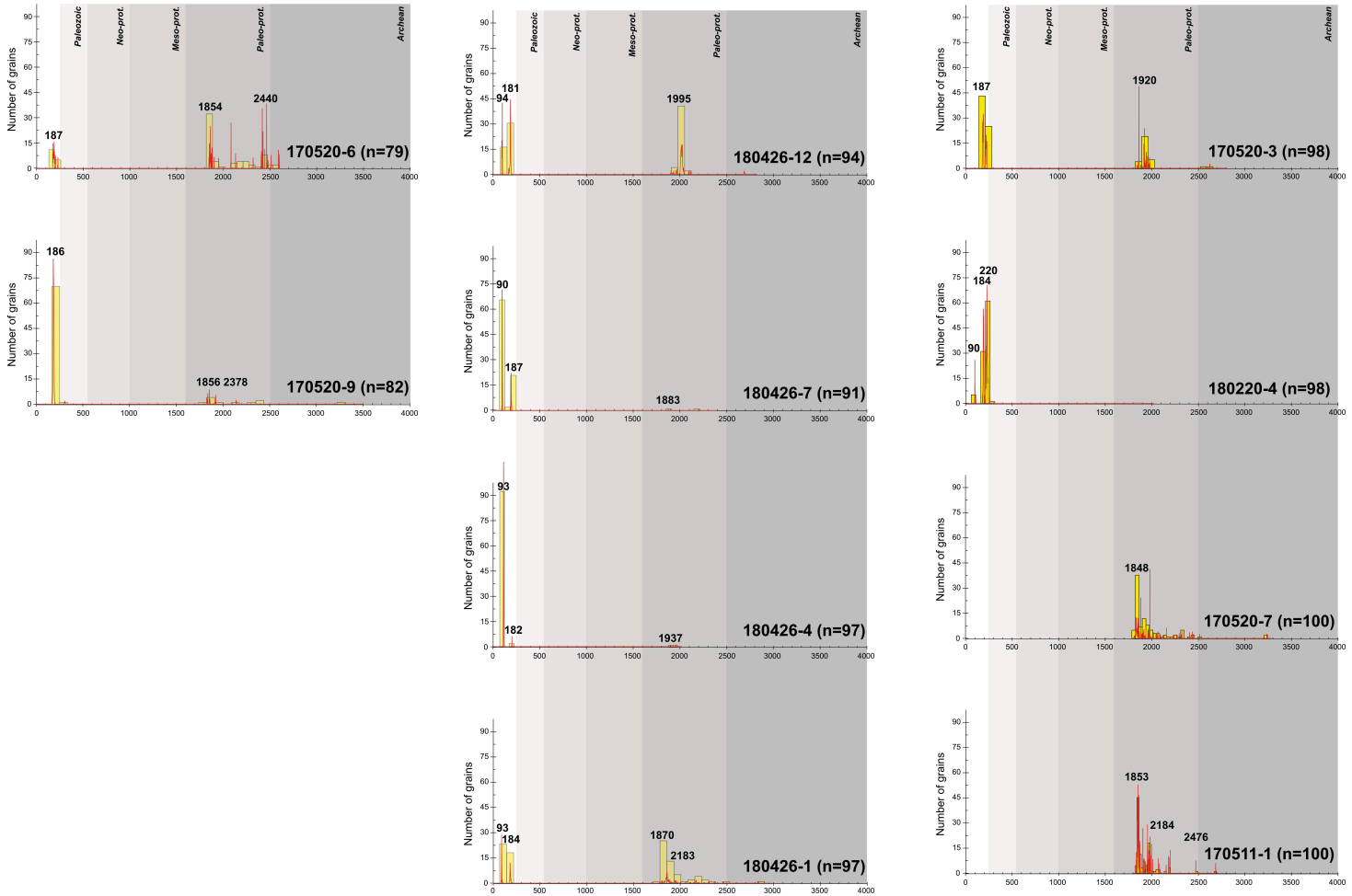

Fig. 2-4. Relative probability plots and histograms of detrital-zircon U-Pb ages from the sandstone samples of the Neungju Basin. The original zircon U-Pb data from Kwon (2018).

age peak at 90 Ma, Jurassic ages between 178.4 to 191.3 Ma with an age peak at 187 Ma, and Paleoproterozoic ages between 1899 to 2215 Ma. 180426-4 shows Cretaceous ages between 89.0 to 97.5 Ma with a prominent age peak at 93 Ma, two Jurassic ages of 181.5 and 182 Ma, and two Paleoproterozoic ages of 1879 and 1937 Ma. 180426-1 shows Cretaceous ages between 88.0 to 100.1 Ma with an age peak at 93 Ma, Jurassic ages between 178.7 to 193.3 Ma with an age peak at 184 Ma, and Paleoproterozoic to Archean ages between 1742 to 2855 Ma with age peaks at 1878 and 2183 Ma.

2.4.2. Major element composition for mudstones

The major element composition of the mudstone samples is presented in Table 2-1. The SiO_2 content ranges from 56.65% to 72.01% with an average of 64.71%, showing similar values with that of Post-Archean Average Shale (PAAS; SiO_2 = 62.8 wt%) (Taylor and Mclennan, 1985). In general, the mudstone samples show higher Na_2O, CaO, and K_2O contents relative to those of PAAS (Na_2O = 1.2 wt%; CaO = 1.3 wt%; K_2O = 3.7 wt%; Fig. 2-5). Although the samples from the proximal and distal environments show no significant differences in many of major element contents, they are clearly distinguished in the Na_2O content (Fig. 2-5). The proximal samples show the Na_2O content ranging from 1.07% to 3.40% with an average of 1.99%, whereas the distal samples show the Na_2O content ranging from 1.35% to 4.95% with an average of 3.50%. Thus, the distal samples are characterized by high Na_2O content. Additionally, the distal samples show slightly lower Al_2O_3 and K_2O contents relative to the proximal samples.

The proximal and distal samples show no spatial contrast in major element composition,

Table 2-1. Major element composition of the mudstone sample from the Neungju Basin (wt %)

Depositional environment	Sample code	SiO_2	Al_2O_3	K_2O	Na_2O	CaO	MgO	Fe_2O_3*	TiO_2	MnO	P_2O_5	L.O.I	Total
Alluvial plain	180220-1	59.34	15.78	4.43	1.27	3.08	2.91	6.27	0.81	0.07	0.18	5.46	99.6
Alluvial plain	180426-4	68.07	14.83	4.10	2.30	1.50	1.39	4.03	0.54	0.09	0.08	3.76	100.7
Alluvial plain	180426-6	65.39	16.57	4.49	2.08	0.89	1.45	5.30	0.64	0.06	0.15	3.35	100.3
Alluvial plain	180426-12	72.01	14.84	4.21	2.50	0.62	1.16	3.15	0.36	0.06	0.04	2.10	101.1
Alluvial plain	180426-13	70.52	13.56	3.10	2.91	2.30	0.87	2.74	0.33	0.05	0.04	2.82	99.2
Alluvial plain	4-26-1050	68.81	15.12	4.38	1.74	0.41	1.27	3.50	0.47	0.05	0.08	3.24	99.1
Alluvial plain	4-26-1104	64.19	15.60	4.22	1.62	1.86	1.67	4.12	0.52	0.10	0.27	4.43	98.6
Alluvial plain	180426-11	59.02	18.07	4.97	2.23	2.07	2.28	7.27	0.98	0.06	0.11	2.74	99.8
Alluvial plain	180427-12-7	64.82	16.34	5.22	1.93	2.10	1.30	4.05	0.48	0.09	0.19	3.07	99.6
Alluvial plain	4-11-425	64.88	15.46	4.54	1.49	2.61	1.54	4.01	0.51	0.07	0.11	4.07	99.3
Alluvial plain	4-17-239-r	64.37	15.25	5.45	1.24	1.41	2.10	5.84	0.68	0.05	0.09	3.18	99.7
Alluvial plain	4-17-239-g	56.65	14.89	4.68	1.07	3.90	4.09	6.87	0.79	0.11	0.16	5.66	98.9
Alluvial plain	4-46-420	64.03	15.35	3.93	3.40	1.33	1.51	5.12	0.71	0.05	0.08	2.76	98.3
Sandflat	180426-7	70.01	15.49	4.49	1.92	0.30	0.84	4.98	0.64	0.01	0.14	2.49	101.3
Sandflat	4-11-1150	69.97	11.41	3.86	2.40	3.53	0.79	2.25	0.40	0.05	0.07	3.47	98.2
Sandflat	4-17-300	63.49	14.97	4.33	1.74	3.28	1.71	4.39	0.56	0.11	0.10	4.53	99.2
Playa lake	180426-8	61.68	15.36	2.67	4.94	3.36	2.02	5.29	0.61	0.10	0.10	4.61	100.7
Playa lake	4-10-239	65.44	12.08	2.99	3.92	3.12	2.03	3.51	0.41	0.06	0.10	4.46	98.1
Playa lake	4-10-445	61.71	11.71	3.58	2.55	4.67	2.50	4.00	0.46	0.06	0.08	6.99	98.3
Playa lake	0307-1-905	63.07	14.57	4.69	3.49	3.27	1.64	4.13	0.53	0.08	0.06	3.34	98.9
Playa lake	1129-1-1	65.22	14.65	3.40	4.27	1.63	1.98	4.51	0.54	0.12	0.08	3.28	99.7
Playa lake	1129-1-2	67.29	13.92	2.64	4.96	1.35	1.33	3.88	0.43	0.20	0.07	2.92	99.0
Playa lake	1129-3-2	59.86	13.93	4.41	3.53	5.01	1.84	4.15	0.52	0.11	0.08	4.85	98.3
Playa lake	180426-9	63.30	13.89	4.37	1.35	3.78	2.22	3.90	0.51	0.17	0.16	6.55	100.2
Playa lake	180427-14-37	63.92	15.55	6.52	2.75	0.63	1.90	4.92	0.61	0.03	0.12	2.91	99.9
Playa lake	180427-15-24	66.76	15.26	5.46	3.74	0.43	1.48	3.76	0.51	0.09	0.08	2.46	100.0
Playa lake	180427-15-39	62.69	15.86	4.60	4.07	0.66	2.63	4.33	0.61	0.03	0.09	3.88	99.5
Playa lake	4-10-408	68.43	13.85	3.17	4.24	0.52	1.73	3.51	0.44	0.05	0.09	3.04	99.1
Playa lake	4-11-110	64.94	16.37	4.13	2.66	0.51	1.69	4.27	0.54	0.04	0.12	2.86	98.1
Playa lake	4-17-340	61.43	12.87	4.43	2.56	5.11	2.31	3.61	0.53	0.09	0.10	6.16	99.2

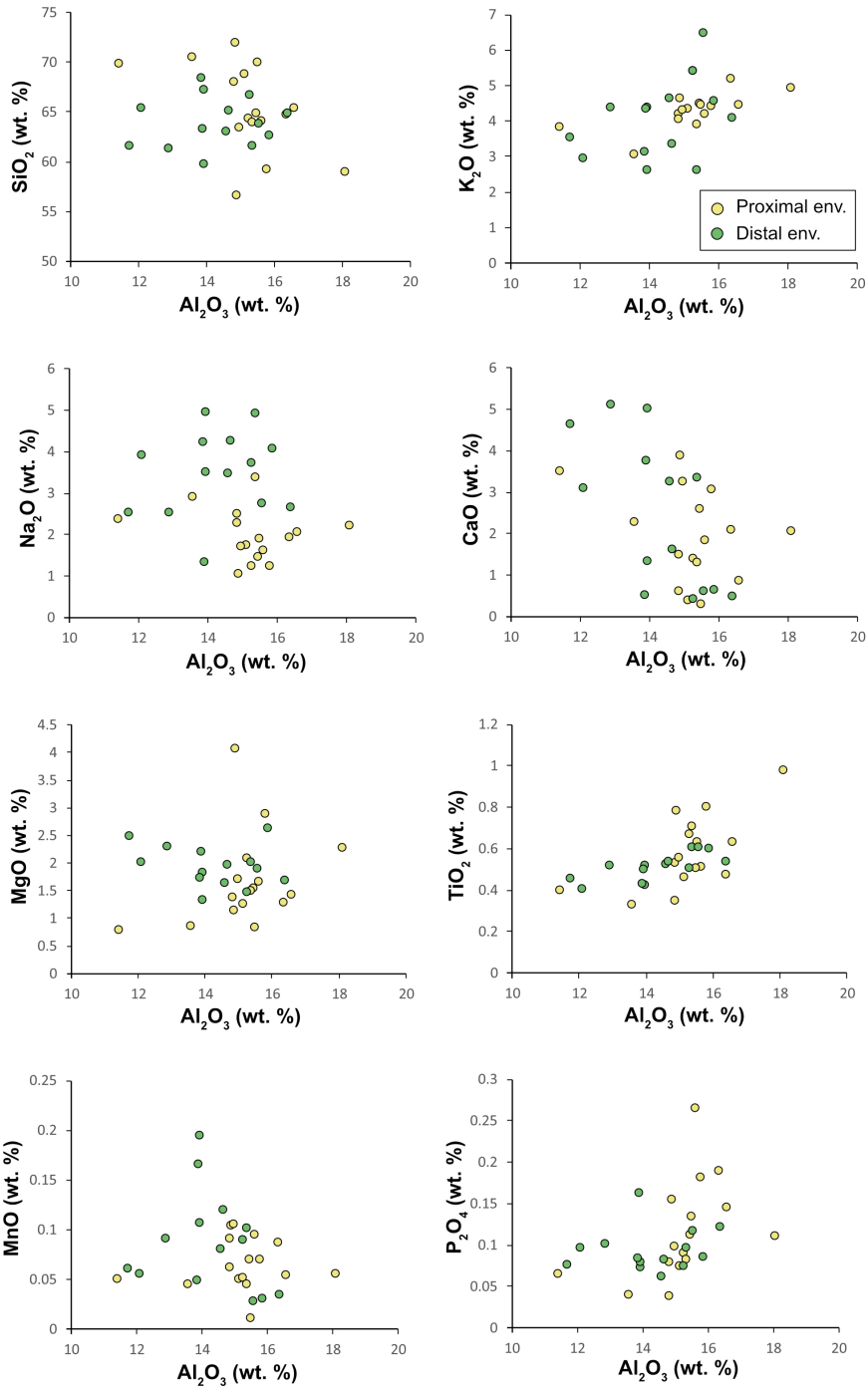

Fig. 2-5. Binary plots of major elements against Al_2O_3 for the mudstone samples. The mudstone samples collected from the proximal and distal depositional environments show a clear distinction in Na_2O content.

respectively. As presented in Fig. 2-6, the proximal samples deposited in the northern, central, and southern parts of the study area are not distinguished from each other. Also, the distal samples deposited in the northern and central parts of the study show similar compositional characteristics.

2.4.3. Tectonic setting signatures for mudstones

In the $K_2O/Na_2O–SiO_2$ diagram by Roser and Korsch (1986), the proximal and distal samples are separately assigned to two different types of tectonic settings (Fig. 2-7a). 81% (13 of 16) of the proximal samples are plotted in the passive margin field and the rest 19% (3 of 16) in the active continental margin field. Whereas 86% (12 of 14) of the distal samples are plotted in an active continental margin, and the remaining two distal samples are plotted in the passive margin and arc fields.

The proximal and distal samples are also assigned to two different types of tectonic settings in $SiO_2/Al_2O_3–K_2O/Na_2O$ diagram (Fig. 2-7b). 75% (12 of 16) of the proximal samples are plotted in the passive margin field. Two of them are plotted at the boundary between the passive margin and active continental margin fields, and the rest two samples are plotted in the active continental margin field. Whereas, 64% (9 of 14) of the distal samples are plotted in the active continental margin field. 29% (4 of 14) of the distal samples are plotted in the passive margin field and the remaining one sample in the evolved arc field.

New discriminant-function-based diagrams by Verma and Armstrong-Altrin (2013) can discriminate tectonic settings of sedimentary rocks to three types: island or continental arc,

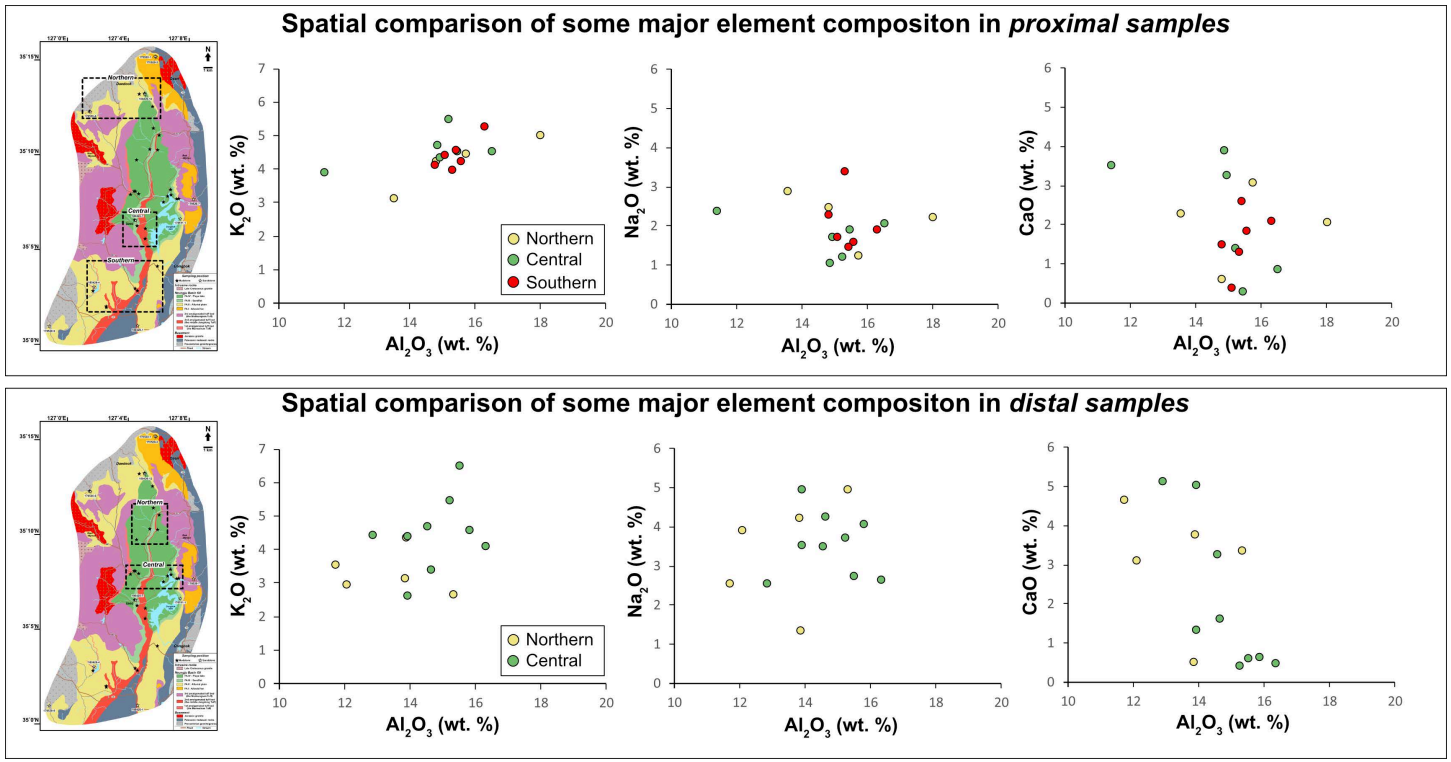

Fig. 2-6. Spatial comparison of some major element composition in *proximal* and *distal* samples. Each sample group shows no distinctive spatial contrast in major element composition.

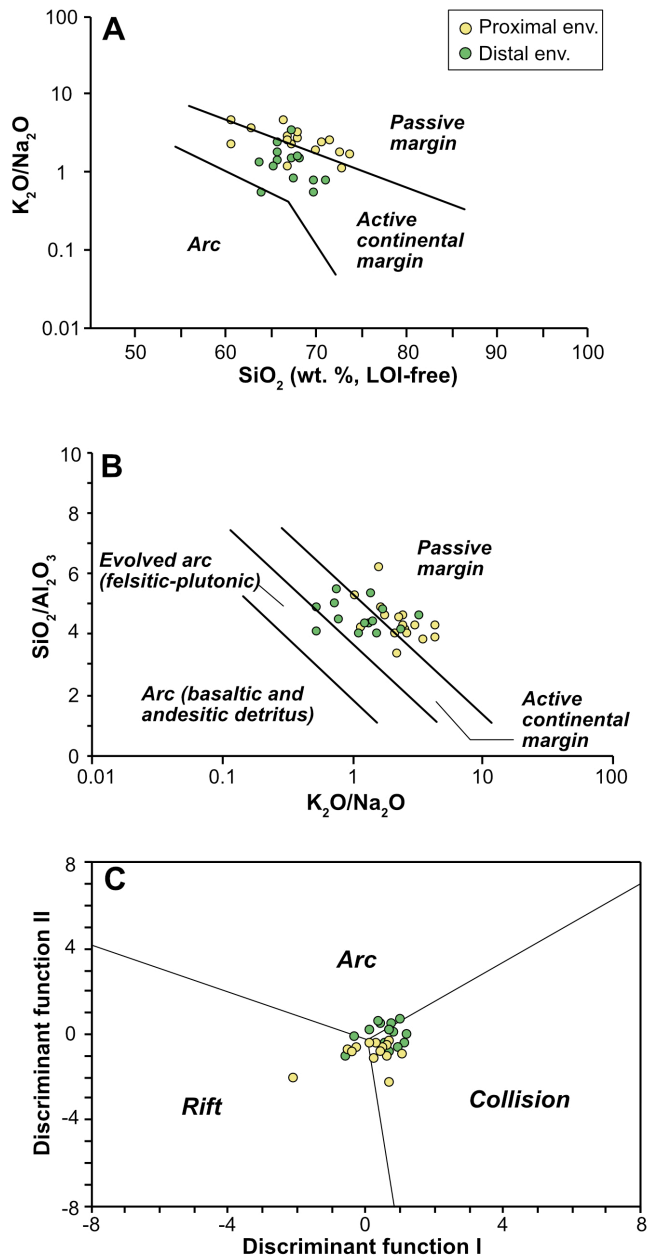

Fig. 2-7. Tectonic setting discrimination diagrams for the mudstone samples. (a) K_2O/Na_2O – SiO_2 diagram (Roser & Korsch, 1986). (b) SiO_2/Al_2O_3 – K_2O/Na_2O diagram (Roser & Korsch, 1986). (c) Discriminant function diagram for high-silica [$(SiO_2)_{adj}$ = 63–95%] samples by Verma & Armstrong-Altrin (2013), where $(SiO_2)adj$ refers to the modified SiO_2 value after volatile-free recalculation of the major elements to 100%. Two mudstone samples classified as low-silica [$(SiO_2)_{adj}$ = 35–63%] are plotted in the rift field. Clear separations in the diagrams are observed for the proximal and distal samples.

continental rift, and collision. Most of the proximal and distal samples are plotted together in the collision field (Fig. 2-7c), indicating sediment derivation dominantly from old metamorphic and metasedimentary rocks. However, two sample groups show no major overlap in the diagram, indicating a clear compositional contrast between two sample groups. The proximal samples are mostly plotted close to the rift and collision fields, whereas the distal samples close to the boundary between arc and collision fields.

2.4.4. Weathering intensities for mudstones

Various weathering indices have been proposed to assess the degree of chemical weathering quantitatively for sediments and sedimentary rocks. The representative indices for the mudstone samples from the Neungju Basin are presented in Table 2-2 and are also visualized in Figure 2-8.

The chemical index of alteration (Nesbitt and Young, 1982) is the most widely used weathering index, monitoring decomposition of feldspar grains and consequent formation of Al-rich clay minerals such as illite and kaolinite. Fresh igneous rocks tend to provide the CIA value of 45 to 55, whereas moderately weathered shales such as PAAS yield the value close to 70 (Nesbitt and Young, 1982). The CIA values of the mudstone samples range from 44 to 64 with an average of 56, indicating a minor degree of chemical weathering. Although the CIA values of the proximal and distal samples are overlapped, they can be separated roughly at the CIA value of 54 (Fig. 2-8). The CIA values of the proximal samples range from 49 to 64 with an average of 59, indicating minor chemical weathering in the source areas. On the other hand, the value of the distal samples ranges from 44 to 63 with an

Table 2-2. Weathering indices for the mudstone samples from the Neungju Basin

Depositional environment	Sample code	CIA	PIA	CPA	WIP	V	STI
Alluvial plain	180220-1	56	59	88	65	1.37	81.8
Alluvial plain	180426-4	57	61	80	64	1.92	85.1
Alluvial plain	180426-6	63	70	83	64	2.46	83.5
Alluvial plain	180426-12	60	66	78	64	2.37	86.8
Alluvial plain	180426-13	52	53	74	61	1.52	87.4
Alluvial plain	4-26-1050	64	74	84	58	2.92	85.5
Alluvial plain	4-26-1104	59	65	85	60	1.96	84.3
Alluvial plain	180426-11	59	63	83	74	1.78	80.0
Alluvial plain	180427-12-7	56	60	84	71	2.14	84.3
Alluvial plain	4-11-425	56	59	86	63	1.84	84.6
Alluvial plain	4-17-239-r	59	67	88	67	2.13	83.6
Alluvial plain	4-17-239-g	52	53	89	71	1.04	81.8
Alluvial plain	4-46-420	56	58	73	72	1.66	83.3
Sandflat	180426-7	64	74	83	59	3.49	84.5
Sandflat	4-11-1150	44	41	74	66	1.26	87.6
Sandflat	4-17-300	53	54	84	66	1.49	84.3
Playa lake	180426-8	47	47	65	82	0.94	83.5
Playa lake	4-10-239	44	42	65	75	0.89	86.8
Playa lake	4-10-445	41	38	74	73	0.82	86.1
Playa lake	0307-1-905	46	45	72	85	1.24	84.5
Playa lake	1129-1-1	52	52	68	78	1.22	84.8
Playa lake	1129-1-2	51	51	63	75	1.20	86.1
Playa lake	1129-3-2	41	38	71	88	0.96	84.4
Playa lake	180426-9	50	50	86	65	1.26	85.0
Playa lake	180427-14-37	55	60	77	88	2.16	83.8
Playa lake	180427-15-24	54	57	71	86	1.98	84.9
Playa lake	180427-15-39	55	58	70	86	1.43	83.5
Playa lake	4-10-408	55	57	67	72	1.40	86.3
Playa lake	4-11-110	63	69	79	66	2.18	84.0
Playa lake	4-17-340	41	37	75	81	0.91	85.1

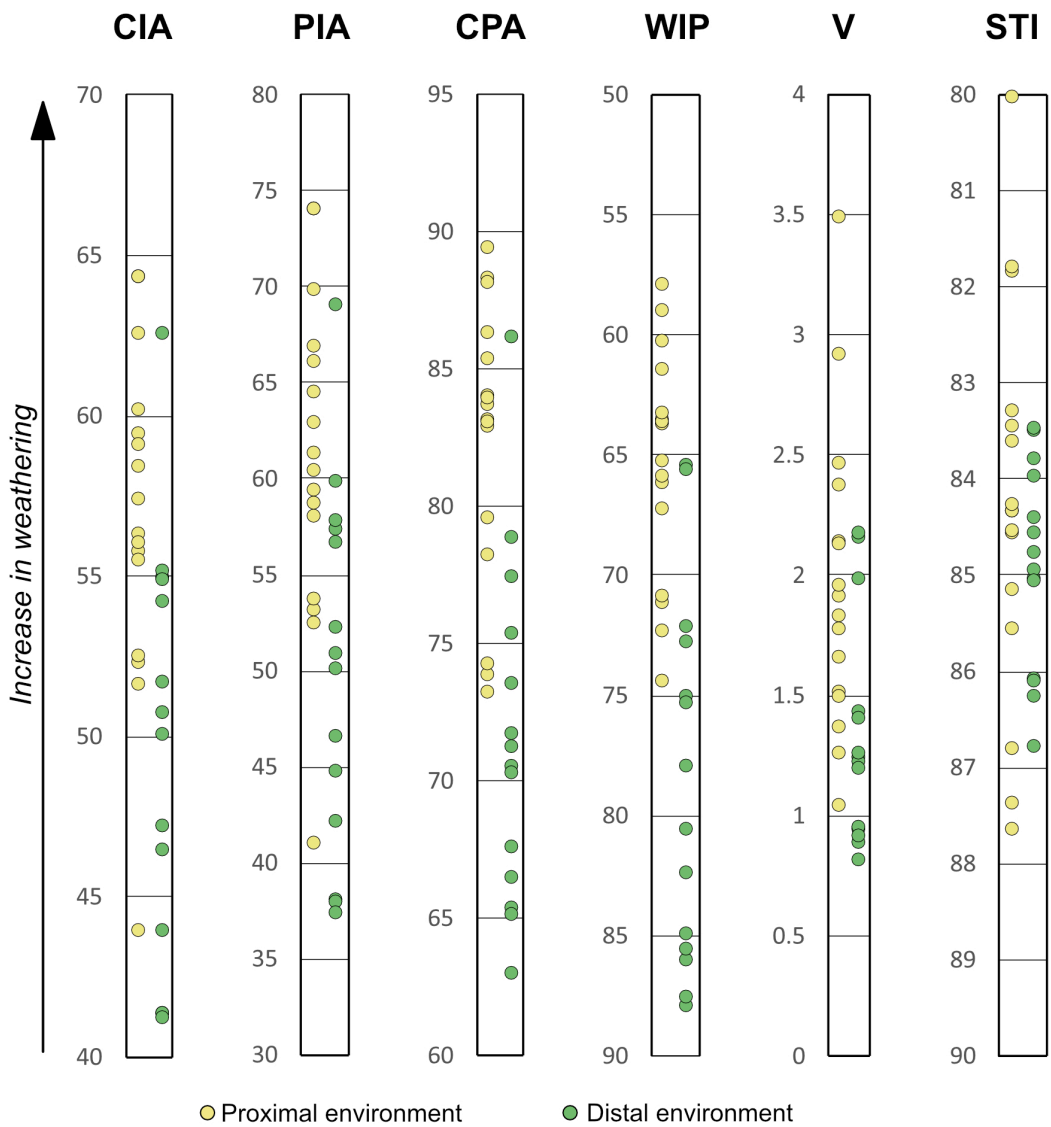

Fig. 2-8. Conventional weathering indices for the mudstone samples. CIA = [Al_2O_3 / (Al_2O_3 + CaO + Na_2O + K_2O)] x 100 (Nesbitt & Young, 1982). PIA = (Al_2O_3 - K_2O) / (Al_2O_3 + CaO + Na_2O - K_2O) x 100 (Fedo et al., 1995). CPA = Al_2O_3 / (Al_2O_3 + Na_2O) x 100 (Buggle et al., 2011). WIP = ($2Na_2O$ / 0.35 + MgO / 0.9 + $2K_2O$ / 0.25 + CaO / 0.7) x 100 (Parker, 1970). V = (Al_2O_3 + K_2O) / (MgO + CaO + Na_2O) (Vogt, 1927). STI = (SiO_2 / TiO_2) / [(SiO_2 / TiO_2) + (SiO_2 / Al_2O_3) + (Al_2O_3 / TiO_2)] x 100 (Jayawardena & Izawa, 1994). The distal samples clearly show a lower degree of chemical weathering intensities relative to the proximal samples in most of the weathering indices, except for the STI index.

average of 52, indicating that they are almost unaltered in the source areas. The weathering indices such as the Plagioclase Index of Alteration (PIA; Fedo et al., 1995), CPA (Buggle et al., 2011), the Vogt's residual index (V; Vogt, 1927), and the weathering Index of Parker (WIP; Parker, 1970) are also formulated to assess the leaching of mobile elements such as Na_2O, CaO, and MgO during the weathering processes. In this study, they provide similar results with those of the CIA value (Fig. 2-8). Very low degree of chemical weathering is inferred for the distal samples, and the distal samples are distinguished with the more weathered proximal samples. The Silica–Titania Index (STI = molar $[(SiO_2/TiO_2)/[(SiO_2/TiO_2) \times (Al_2O_3/TiO_2) \times (SiO_2/Al_2O_3)] \times 100$; Jayawardena and Izawa, 1994) is the only weathering index that showed a similar degree of chemical weathering for the proximal and distal samples. The STI value of the proximal and distal samples range from 80 to 88 (av. = 84) and 83 to 87 (av. = 85), respectively, indicating slightly weathered condition (Jayawardena and Izawa, 1994).

2.5. Discussion

2.5.1. Sediment mixing and separation

The detrital zircon U-Pb age data (Kwon, 2018) shows that sediment detritus derived from nearby source rocks were spatially separated and were not fully mixed especially in the proximal areas close to the basin margins. The sandstone samples (170520-7, 170511-1) from the areas near the eastern margin show zircon age clusters of Paleoproterozoic to Archean ages, suggesting sediment derivation from the Precambrian metamorphic rocks

distributed east of the basin. On the other hand, the samples collected from the areas near the northeastern (170520-3, 180220-4) and western margins (170520-6, 170520-9) show zircon age clusters of Mesozoic ages between Jurassic to Triassic as well as Paleoproterozoic to Archean ages, although 180220-4 have 5 grains of Cretaceous age. Most of the sediment detritus were supplied from the Jurassic and Triassic granites and Precambrian metamorphic rocks broadly distributed on the north and west of the basin. In contrast to the sandstone samples collected from the eastern, northern and western marginal areas, those collected from the southern and central part of the study area (180526-1, 180426-4, 180526-7, 180426-12) show the prominent age peaks at Cretaceous ages, with a relatively minor amount of Jurassic and Paleoproterozoic to Archean zircons. Previous sedimentological study shows a central playa lake had been developed in the central areas of the basin (Lee et al., 2019). Sediment detritus derived from the surrounding source rocks were possibly mixed in the central areas, resulting in a wide range of zircon ages. The Cretaceous zircons were possibly reworked from the southern volcaniclastic plain and transported northward to the central playa lake (e.g., Nakayama and Yoshikawa, 1997; Ashley and Hay, 2002). Paleocurrent data support the derivation of the Cretaceous zircon grains from the south (Lee et al., 2019). Direct derivation of the Cretaceous zircon grains from syndepositional volcanism is a less reliable explanation because tuff beds are not observed in the outcrop sections where the sandstone samples were collected, and their stratigraphic positions correspond to inter-eruption periods (Lee et al., 2019).

2.5.2. Contrasting geochemical signatures of tectonic settings and weathering intensities.

Based on the support of zircon age dating, the compositional contrast between the proximal and distal mudstone samples can be easily explained. The most notable contrast is observed in the Na_2O content. Cretaceous volcanic activities that occurred in the areas near the Neungju Basin were generated from calk-alkaline magma, resulting in deposition of felsic pyroclastic rocks, andesitic and dacitic rocks, and rhyolite (Kim et al., 2008; Koh et al., 2009; Jung et al., 2014). Although the various type of volcanic rocks was formed, they are characterized by abundant plagioclase content. As discussed above, if the reworked sediments from the southern volcaniclastic plains were supplied to the central playa lake, it is natural that the distal samples show higher Na_2O content relative to the proximal samples.

The zircon age data indicate that the relative contribution of Jurassic to Triassic granites and Precambrian metamorphic rocks may differ spatially in the marginal areas (Fig. 2-4). However, the mudstone samples from the proximal environments show no distinctive compositional contrast spatially. Because Jurassic to Triassic granites and Precambrian metamorphic rocks show similar characteristics in major element composition (Lee and Kim, 2012), the spatial difference in the relative contribution of these source rocks might not produce noticeable compositional contrast in the proximal samples. On the other hand, the distal samples collected from the northern and central parts of the study area show similar major element composition, mostly characterized by relatively high Na_2O content. Reworked sediment detritus derived from the southern volcaniclastic plains might be transported throughout the playa lake to the northern part of the study area. The occurrence of Cretaceous zircons in the sandstone sample 180426-12 also supports northward transportation of Cretaceous sediment detritus to the northern part of the study area.

The Neungju Basin was developed in intra-arc to active continental margin settings (Lee, 1999), experiencing episodic faulting and volcanism. However, the preferential mixing and separation of sediment detritus generate significant problems to interpret the tectonic setting of the Neungju Basin using conventional discrimination methods. In the tectonic setting discrimination methods by Roser and Korsch (1986), the mudstone samples deposited in the proximal and distal environments show different tectonic setting signatures. The proximal samples are assigned as passive margin sediments, mainly reflecting the geochemical composition of the Precambrian gneiss and Mesozoic granites. This result, however, is not correct because it does not reflect volcanic activities commonly occurred in the areas adjacent to the Neungju Basin. On the other hand, the distal samples are assigned to active continental margin sediments, reflecting the input of Na_2O-rich sediments originated from volcanic activities. In the southern part of the Korean Peninsula, the Cretaceous Hayang Group was deposited in the Gyeongsang Basin during the depositional period of the Neungju Basin (Paik et al., 2012 and references therein). The mudstone samples collected from the Hayang Group also show active continental margin signatures (Lee and Lee, 2003), supporting the tectonic setting interpretation based on the distal samples of the Neungju Basin. Verma and Armstrong-Altrin (2013) proposed an improved tectonic setting discrimination method using the whole major element composition. However, it also provides inappropriate information about the tectonic setting of the Neungju Basin, assigning most of the mudstone samples as collisional sediments. They collected many of the compositional data from the areas including the Japanese island arc to represent the arc signature (Fig. 1 of Verma and Armstrong-Altrin, 2013). In consequence, their discriminant functions tend to be less

sensitive to felsic magmatism, ignoring the reworking of volcanic detritus in the distal samples.

To assess the weathering conditions properly, chemical loss of the mobile elements and physical erosion of the soil profile should occur at a stable rate in the source areas (Nesbitt et al., 1997). Active tectonism and storms may enhance the physical erosion of fresh bedrocks and less altered lower horizons of the soil profile, resulting in a significant lowering of the estimated weathering intensities (e.g., Lee, 2009; Joo et al., 2018). Most of the weathering indices indicate a minor degree of chemical weathering for the proximal mudstone samples, being consistent with arid to semiarid climate conditions inferred by fossil and sedimentological evidences (Huh et al., 2006; Paik et al., 2007). The Hayang Group mudstones shows the CIA values ranging from 54 to 67 with an average of 61 (Lee and Lee, 2003), suggestive of chemical weathering in similar degree with the proximal mudstone samples from the Neungju Basin. In contrast, the distal samples show the weathering intensities lower than expected. Volcanic activities can generate volcanic terranes with high and unstable topography in a very short period of time (Manville et al., 2009). After the large volume of volcaniclastic sediments is rapidly aggraded in the volcanic terrane during the syn-eruption period, the unconsolidated materials are easily eroded, reworked, and transported as debris-flows to the areas far from the volcanic terrane during the inter-eruption period (Smith, 1988, 1991). Naturally, the well-developed soil profile is difficult to be formed on the surface of volcanic terrane in contrast to non-volcanic depositional systems. The lowering of the weathering intensities in the distal samples, thus, could be induced by additional input of reworked volcaniclastic sediments to the central playa lake. The STI index is less sensitive to the

additional input of Na_2O-rich volcaniclastic sediments, providing similar weathering intensities for the proximal and distal mudstone samples. It is because the index is formulated only using the major elements SiO_2, Al_2O_3, and TiO_2.

2.6. Conclusion

To investigate compositional contrast in a nonmarine basin and its influence on the tectonic setting and weathering signatures, the nonmarine Neungju Basin was studied in terms of mudstone geochemistry in support of the previous zircon U-Pb age dating data. The results show that sediment detritus was supplied from three different types of source rocks: Precambrian metamorphic rocks, Mesozoic granites, and Cretaceous volcanic rocks. Mudstones deposited in the proximal environments (alluvial fan to sandflat) close to the basin margins reflect the composition of nearby source rocks. Whereas, mudstones deposited in the distal environment (the central playa lake) reflect the mixed characteristics of three source rocks. Due to the exclusive input of volcaniclastic sediment in the distal samples, tectonic setting signatures differ significantly between the proximal and distal samples. The proximal samples show passive margin signatures, reflecting their derivation from metamorphic and granitic rocks. Whereas, the distal samples show active continental margin signatures, reflecting the overall source rock signatures. In the case of weathering, the proximal samples indicate slightly higher weathering intensities than the distal samples. The rapid development of the southern volcaniclastic terrane and reworking without experiencing enough time of the soil profile might have lowered the weathering intensities of the distal samples. Overall, this study implies that compositional analysis for

reconstructing tectonic settings and weathering conditions should be carefully performed with supports of detailed provenance and paleoenvironmental analysis. A nonmarine basin may have strong spatial contrast in their sediment composition due to preferential mixing of specific source rocks, and a specific location and depositional environment may not reflect the overall characteristics of the basin.

3. POST-COLLISIONAL DENUDATION OF AN OROGENIC BELT TRACED FROM GEOCHRONOLOGICAL AND BULK-ROCK GEOCHEMICAL RECORDS OF THE WESTERN KOREAN PENINSULA

3.1. Introduction

The evolution of an active continental margin in the framework of a tectonic Wilson cycle is controlled by ocean closure, creating various geological features along plate margins (Wilson, 1966). In particular, the orogenic cycle in an active continental margin consists of a period of subduction or collision (continent-continent or arc-continent), which consumes the oceanic crust and thickens the continental crust (Dewey and Bird, 1970). This over-thickened continental crust is affected by gravity-driven flow and mechanical collapse, which eventually forms extensional basins and exhumes deep orogenic crust (Rey et al., 2001; Teyssier and Whitney, 2002). Late- to post-orogenic processes, coupled with orogenic denudation and erosion, effectively leave a record in the sediments that is derived from a mountain belt (e.g., Séguret et al., 1989; Spencer et al., 2015). Thus, understanding the sedimentary response to the tectonic cycle of an orogenic belt provides an important clue for deciphering the interplay between tectonic plates and related thermo-chemo-mechanical processes.

The western Korean Peninsula was situated along convergent continental margins before the Late Paleozoic to Early Mesozoic continental-collision event, although traces of a collisional suture zone have been disputed (e.g., Oh et al., 2005; Kim et al., 2011, 2014,

2015; Park et al., 2014a, b, 2017a; Kwon et al., 2009; Cho et al., 2017). A large volume of geochronological and petrological evidence indicates that the western Korean Peninsula, including the western Gyeonggi Massif and Imjingang Belt, experienced an Early Mesozoic crustal-thickening event (e.g., Oh et al., 2005; Cho et al., 2007, 2018; Kwon et al., 2009), followed by post-collisional extension and the deposition of Early to Middle Mesozoic sedimentary rocks on top of the collapsed orogenic belt (de Jong et al., 2015; Park et al., 2018, 2019). The sporadically distributed post-collisional basin fills, which are traditionally referred to as the Daedong Supergroup (Lee, 1987), has provided a key to studying the timing and deformational features of two major Mesozoic orogenic events that affected the Korean Peninsula, namely, the Songrim collisional and Daebo subduction-related orogenies (Chough et al., 2000; Jeon et al., 2007; Lim and Cho, 2012; Jang et al., 2015; Cho et al., 2018; Park et al., 2018, 2019). Despite its limited exposure, the Daedong Supergroup has played an important role as a natural laboratory in reconstructing the transition from collisional to subduction tectonics along the western Korean Peninsula in the Mesozoic East Asian continental margin (Park et al., 2018, 2019). The recognized tectonic transition in the western Korean Peninsula reflects the diachronous aspects of the crustal evolutionary history within peripheral regions (Park et al., 2019).

This study reports detrital zircon U-Pb geochronological data and bulk-rock geochemical data of mudstone from Early to Middle Mesozoic post-collisional basin fills and the overlying volcano-sedimentary sequence (the Nampo Group, Oseosan Volcanic Complex, Gimpo Group, and Seokmun Formation) along the western Korean Peninsula. Based on these data, spatial/temporal variation in the provenance of the Daedong Supergroup was investigated in relation to the variation to structural architecture and tectonic evolution of

the collapsed orogenic belt during Late Triassic to Early Jurassic. The results should help us to understand sedimentary records from cyclic mountain-building/destruction processes in relation to the paleotectonic history of Far East Asia.

3.2. Geological setting

3.2.1. Tectonic framework

The Korean Peninsula consists of three Archean to Paleoproterozoic basements (from north to south): the Nangrim, Gyeonggi, and Yeongnam massifs (Fig. 3-1; Lee, 1987). These basements have traditionally been thought to have originated from the North China Craton (Wu et al., 2007; Cho et al., 2017; Kim et al., 2019). They are intervened by two mobile belts: the Paleozoic Imjingang Belt and the Neoproterozoic to Paleozoic Okcheon Belt; here, the basin fills are inferred to have been strongly deformed and metamorphosed during the Late Paleozoic to Early Mesozoic subduction-related and/or collisional orogenic events (e.g., Ree et al., 1996; Cheong et al., 2003, 2018; Cho and Kim, 2005; Cho et al., 2007, 2017, 2018; Jang et al., 2015).

Recent advances in the understanding of the geochronological, geochemical, petrological, and structural features of the Imjingang Belt and the western margin of the Gyeonggi Massif have provided insight into the multiple orogenic processes of the Korean Peninsula from the Proterozoic to the Phanerozoic (Fig. 3-2). This area has recently been referred to as the Hongseong-Imjingang Belt (Kim et al., 2017b, 2019) or the Gyeonggi Marginal Belt (Cho et al., 2017). Although the label of this newly defined orogenic belt

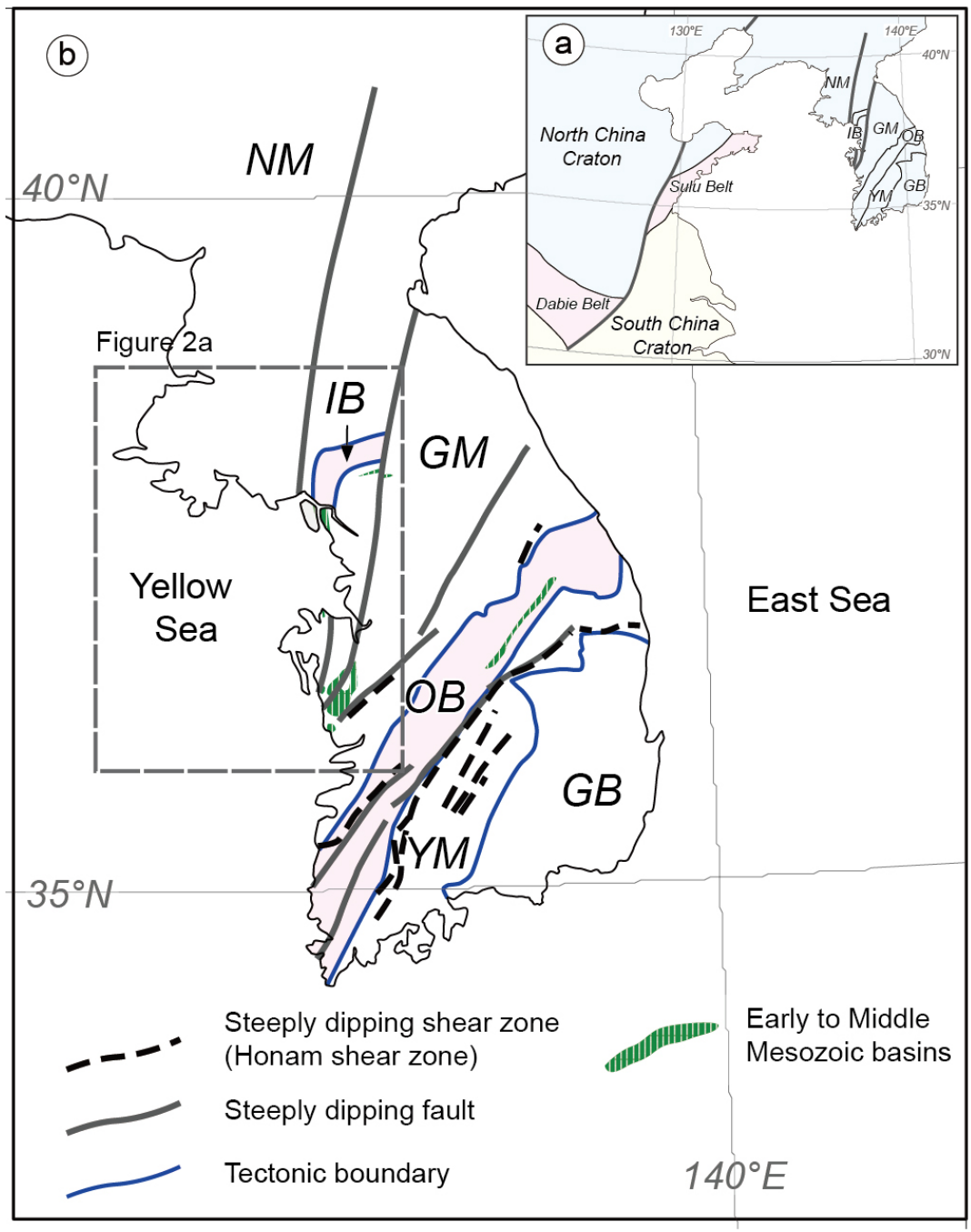

Fig. 3-1. Simplified tectonic map of East Asia (a) and the Korean Peninsula (b), showing the present distribution of the Early-Middle Mesozoic basins in the southern Korean Peninsula (modified from Cluzel, 1992). The gray, rectangular box denotes the area of Figure 2a. NM: Nangrim Massif, IB: Imjingang Belt, GM: Gyeonggi Massif, OB: Okcheon Belt, YM: Yeongnam Massif, GB: Gyeongsang Basin.

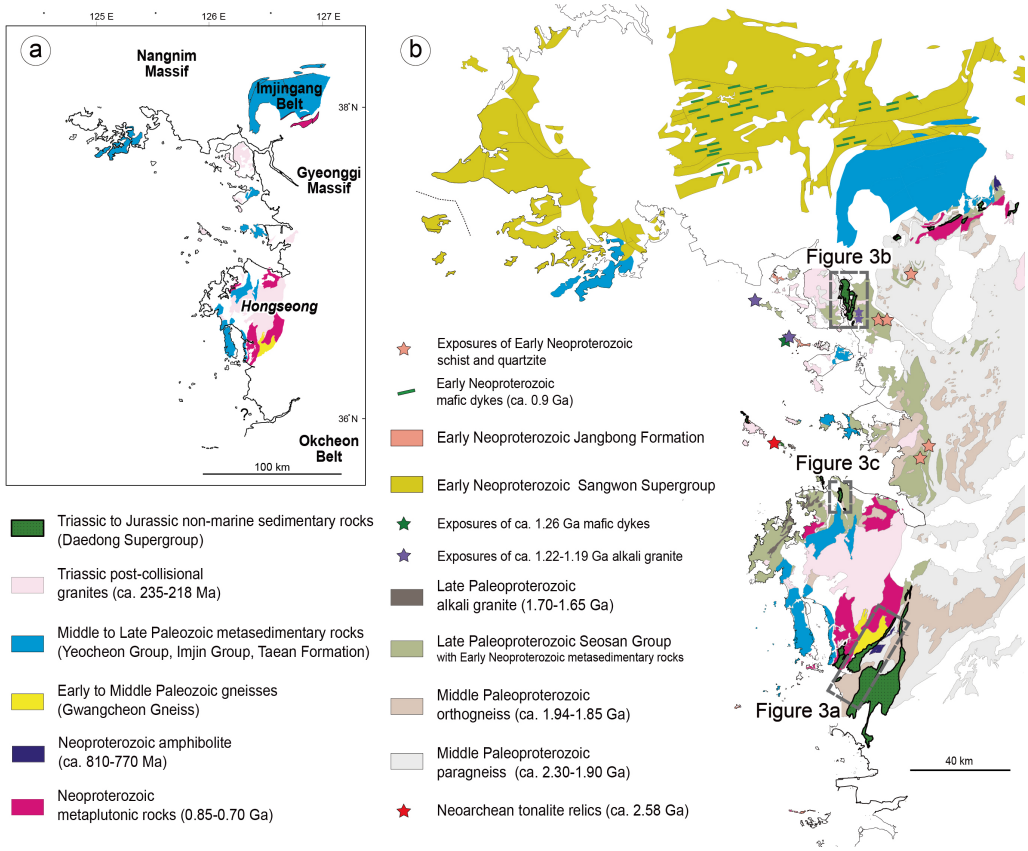

Fig. 3-2. (a) Schematic map of the Late Paleozoic-Early Mesozoic orogenic belt along the western Korean Peninsula as traced by Neoproterozoic granites, Early to Middle Paleozoic gneisses, Middle to Late Paleozoic metasedimentary rocks, and Triassic post-collisional granites. (b) Geologic map of the Late Paleozoic-Early Mesozoic orogenic belt (modified from S.W. Kim et al., 2019). The gray, rectangular boxes denote the areas of Figure 3-3a-c.

along the western Korean Peninsula must be further refined to earn widespread acceptance among geologists, this area provides a unique record of the Early Neoproterozoic arc and post-orogenic magmatism (Park et al., 2017; Kee et al., 2019), following intermittent rifting events from the Late Paleoproterozoic to the Early Neoproterozoic (Cho and Lee, 2017; Kim et al., 2018). Subsequent orogenic cycles were characterized by Early to Middle Paleozoic arc magmatism and metamorphism (Kim et al., 2011, 2015, 2017a; Park et al., 2014a), followed by rift-related magmatism (Kim et al., 2015, 2017b). These Neoproterozoic to Paleozoic continental marginal processes along the western Korean Peninsula were strongly overprinted by a Late Paleozoic to Early Mesozoic crustal-thickening event (Oh et al., 2005; Kim et al., 2006; Cho et al., 2007; Kwon et al., 2009; Sajeev et al., 2010; Park et al., 2014b), which is referred to as the Songrim Collisional Orogeny. The Songrim Orogeny has been correlated with the Central China Orogenic Belt (CCOB), also referred to as Qinling-Dabie-Sulu Belt, between the North and South China blocks in terms of collisional tectonic events (Ree et al., 1996; Chough et al., 2000). However, detailed processes of the Late Paleozoic to Early Mesozoic crustal-thickening event remain controversial (e.g., Cho et al., 2018).

During the Late Triassic collapse of the thickened crust, strong thermal pulses affected the area, causing intrusion of post-collisional granitoids and regional metamorphism along the western Korean Peninsula (Williams et al., 2009; de Jong et al., 2015; Cheong et al., 2015, 2018). These post-collisional processes were accompanied by heterogeneous crustal extension and the rapid exhumation of deeply buried high-grade rocks (de Jong et al., 2015; Park and Kim, 2016), as evidenced by metamorphic paths that are indicative of near-isothermal decompression followed by rapid cooling (Oh et al., 2005; Kim et al., 2006;

Sajeev et al., 2010). This crustal extension finally led to the local deposition of Late Triassic to Early Jurassic non-marine sediments (Kim, 1996; Park et al., 2018), including the Nampo and Gimpo groups and the Seokmun Formation (Figs 3-2 and 3-3).

During the Early to Middle Jurassic, the crustal evolution of the Korean Peninsula was mainly governed by the subduction of the Paleo-Pacific Plate underneath the Eurasian Plate. Continental-arc magmatism and contemporaneous strike-slip shearing (Honam Shear Zone; Fig. 3-1) widely affected the Korean Peninsula (Sagong et al., 2005; Cheong et al., 2006), causing heterogeneous crustal deformation, as identified by local subsidence of the pre-existing post-collisional basins along the western Korean Peninsula (e.g., Oseosan Volcanic Complex: Park et al., 2018, 2019). As the angle of subduction decreased during the Late Jurassic and Early Cretaceous (Sagong et al., 2005), the western Korean Peninsula experienced basement-involved shortening with magmatic quiescence (Park et al., 2018, 2019); this Jurassic to Early Cretaceous subduction-related tectonism in the western Korean Peninsula has been interpreted to be related to the Daebo Orogeny considering spatio-temporal variation in evolutionary style of an orogenic event (Park et al., 2018, 2019).

3.2.2. Stratigraphy and lithology

This study focused on the Late Triassic to Jurassic post-collisional and intra-arc non-marine sedimentary sequences (Daedong Supergroup) along the western Korean Peninsula, including the Nampo Group, the Oseosan Volcanic Complex, the Gimpo Group, and the Seokmun Formation (Fig. 3-3).

The Nampo Group and the Oseosan Volcanic Complex, which are the main

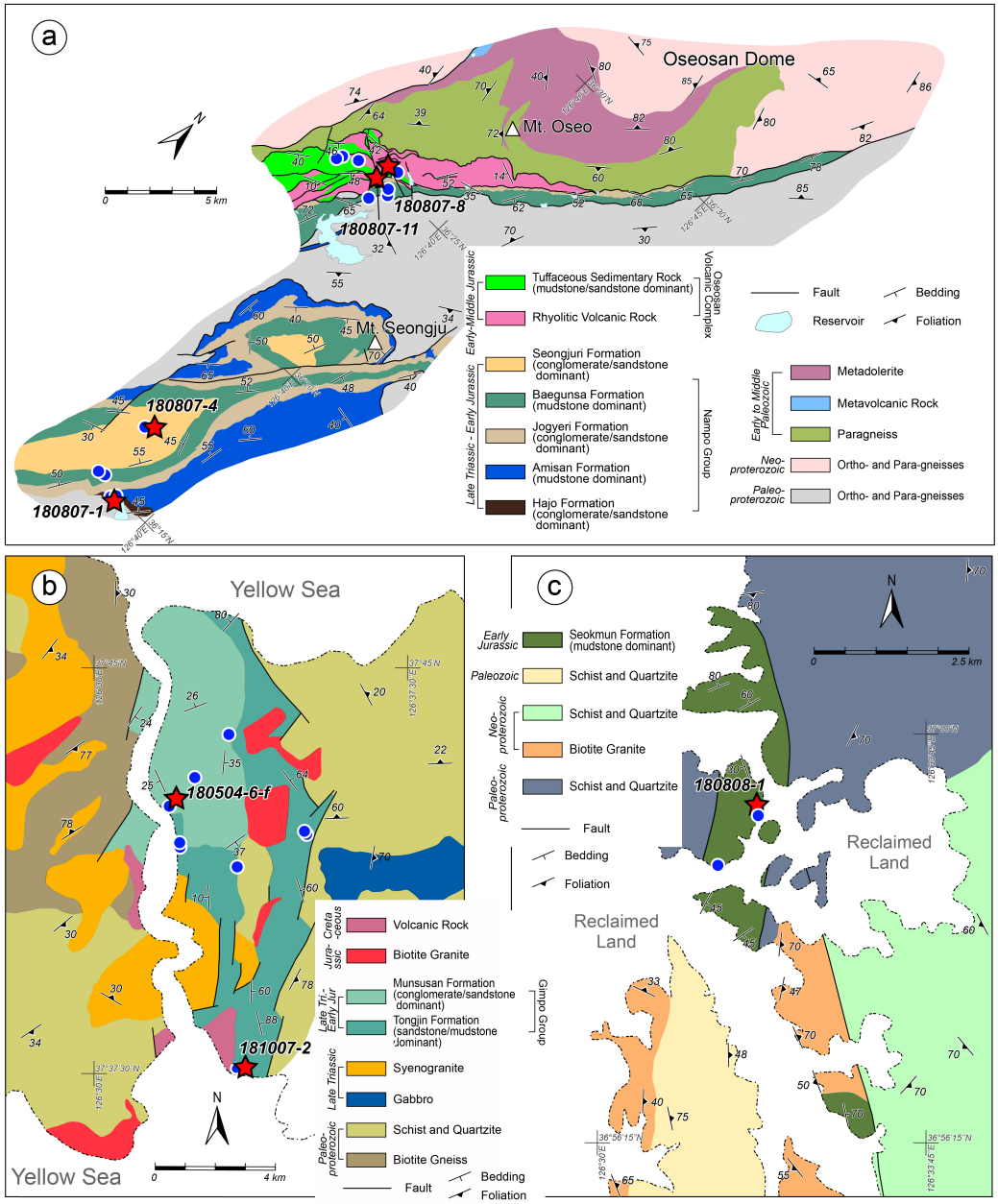

Fig. 3-3. Detailed geological map of the Nampo Group and the Oseosan Volcanic Complex (a), the Gimpo Group (b), and the Seokmun Formation (c), showing the sample locations for detrital-zircon U-Pb age dating (red star) and bulk-rock geochemical analysis (blue circle) (modified from Lee et al., 1989, Cho and Lee, 2017, and Park et al., 2019).

lithostratigraphic units of the Chungnam Basin (Choi et al., 1987, Park et al., 2018, 2019), are situated on top of the basement, which consists of Paleoproterozoic and Neoproterozoic gneisses and Paleozoic gneisses and metavolcanics (Fig. 3-3a). The Nampo Group consists of alluvial fan-fluvial plain-lacustrine sequence, including five lithostratigraphic units, namely, the Hajo, Amisan, Jogyeri, Baegunsan, and Seongjuri formations in ascending order (Choi et al., 1987). The Hajo, Jogyeri, and Seongjuri formations mainly comprise conglomerate and sandstone (Figure 3-4a and b), while the Amisan and Baegunsa formations consist of sandstone, mudstone, and coal. The Nampo Group shows the *Dictyophyllum-Clathropteris* floral province, indicating a Late Triassic to Early Jurassic depositional age (Chun et al., 1987, 1990). The Oseosan Volcanic Complex can be subdivided into a lower rhyolitic-tuff unit and an upper tuffaceous sedimentary unit that includes conglomerate, sandstone, and mudstone deposited in alluvial and lacustrine environments (Figure 3-4c and d; Egawa and Lee, 2009; Park et al., 2018). The rhyolitic-tuff unit yields zircon U-Pb concordia ages between ca. 178 and 172 Ma (Park et al., 2018). These isotopic ages are concordant with paleontological data from the tuffaceous sedimentary unit, which contains *Coniopteris concinna* (Park et al., 2018), suggesting a Middle Jurassic deposition age or younger. The geochemical features of the rhyolitic tuff are represented by a high-K calc-alkaline composition, LREE (Light Rare Earth Element) enrichment, and negative Ba, Ta-Nb, Sr-P, and Eu-Ti anomalies, indicating continental-arc magmatism (Park et al., 2018).

The Gimpo Group covers Paleoproterozoic gneisses and metasedimentary rocks and Triassic granitoids (Cho and Lee, 2017; Fig. 3-3b). This group is made up of fluvial and lacustrine sedimentary rocks (Thomas and Park, 1976; Chun et al., 1990), and can be

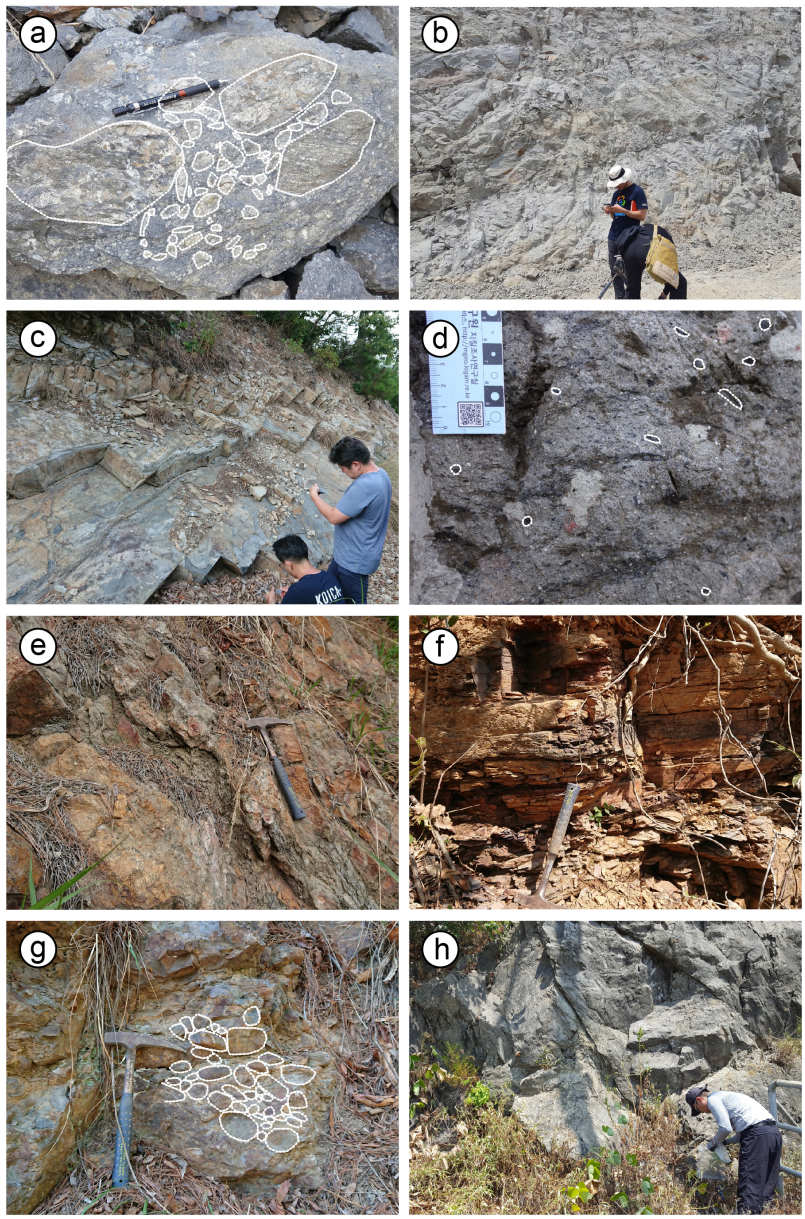

Fig. 3-4. Outcrop photographs of the studied Early-Middle Mesozoic sedimentary units. (a) Conglomerate in the Hajo Formation of the Nampo Group, including pebble- to cobble-size, sub-rounded to sub-angular metamorphic basement clasts. (b) Several meters- to decameter-thick massive sandstone in the Seongjuri Formation of the Nampo Group. (c) Sheet-like tuffaceous sandstones in the Oseosan Volcanic Complex. (d) Rhyolitic tuff from the Oseosan Volcanic Complex, including sub-rounded to sub-angular lithic fragments. (e) Sandstones in the Tongjin Formation of the Gimpo Group. Coarse-grained sandstones are occasionally interbedded with greenish-gray mudstones. (f) Laminated mudstone to siltstone in the Tongjin Formation of the Gimpo Group. (g) Conglomerate in the Munsusan Formation of the Gimpo Group. Sub-rounded to rounded quartzite pebbles are common. (h) Massive sandstones in the Seokmun Formation.

divided into the Tongjin and Munsusan formations. The Tongjin Formation mainly consists of sandstone, mudstone, and coal (Fig. 4e and f), and contains a Late Triassic to Early Jurassic *Dictyophyllum-Clathropteris* floral composition that is identical to that from the Nampo Group (Chun et al., 1990). The Munsusan Formation, which overlies the Tongjin Formation, predominantly consists of conglomerate and sandstone (Fig. 3-4g; Chwae et al., 1995, 1997). Majority of previous studies interpreted the deposition age of the Munsusan Formation to be the Early Jurassic (e.g., Thomas and Park, 1976; Cho and Lee, 2017), although some have argued that this formation represents Cretaceous sedimentation (Chwae et al., 1995, 1997).

The Seokmun Formation is spatially located between the Nampo and Gimpo groups, and sporadically covers Paleoproterozoic and Middle or Late Paleozoic metasedimentary rocks (Fig. 3-3c). This formation comprises mudstone with minor volumes of conglomerate, sandstone, and coal (Fig. 3-4h). The mudstone in the Seokmun Formation has a local calcareous composition (Lee et al., 1989), and its depositional age has been dated to the Jurassic based on lithologic correlations with other post-collisional sedimentary rocks (Lee et al., 1989).

Previous provenance studies based on sandstone petrography (Yu and Lee, 1992; Yu et al., 1992; Egawa and Lee, 2008) showed that the sandstones of the Daedong Supergroup are generally characterized by a low proportion of feldspar grains (Fig. 3-5), suggesting the main supply of detritus to be from mature (meta-)sedimentary rocks. The Oseosan Volcanic Complex's sandstones, meanwhile, include abundant lithic fragments in contrast to the other constituents of the Daedong Supergroup (Fig. 3-5; Egawa and Lee, 2008).

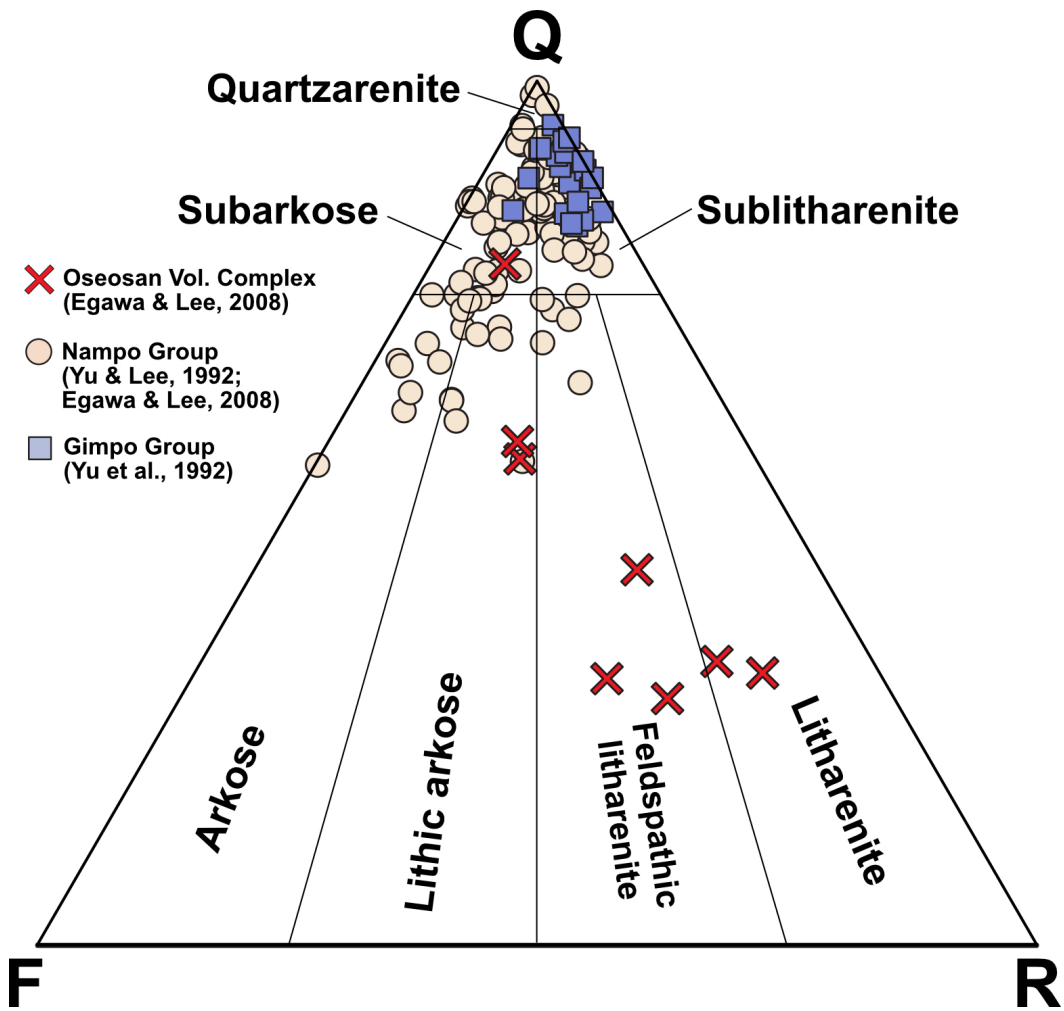

Fig. 3-5. Ternary QFR diagram (Folk et al. 1970) for the classification of the sandstones from the Nampo and Gimpo groups and the Oseosan Volcanic Complex.

3.3. Detrital zircon geochronology

3.3.1. Sample selection and analytical method

A total of seven sandstone samples were collected from the study areas for detrital-zircon U-Pb analysis. Two samples (180807-1 and 180807-4) were taken from the Hajo and Seongjuri formations. These formations are the lowermost and uppermost stratigraphic units in the Nampo Group, respectively. Two other samples (180807-8 and 180807-11) from the tuffaceous sedimentary unit in the Oseosan Volcanic Complex, which stratigraphically overlies the Nampo Group, were also obtained for analysis, alongside three samples (181007-2, 180504-6-f, and 180808-1) from the Tongjin, Munsusan, and Seokmun formations, respectively. Detrital zircons were extracted from the samples by using a conventional heavy-mineral-separation technique and then mounted in epoxy disks with concordant reference zircons 91500 (1065 Ma; Wiedenbeck et al., 1995). Cathodoluminescence (CL) and backscattered electron images (BEIs) were taken by using a scanning electron microscope (JEOL 6610LV) at the Korea Basic Science Institute (KBSI) Ochang Center, South Korea, to examine variation in the internal texture of the zircons before isotopic analysis (Fig. 3-6).

Pb-Th-U isotopic analysis was conducted by using a Nu Plasma II multi-collector inductively coupled plasma mass spectrometer with a 193-nm ArF excimer laser ablation system (LA-MC-ICP-MS) at the KBSI Ochang Center. The following isotopic signals were estimated simultaneously: ^{202}Hg, $^{204}Hg + {}^{204}Pb$, ^{206}Pb, ^{207}Pb, ^{208}Pb, ^{232}Th, and ^{238}U. ^{235}U was calculated from the signal of ^{238}U by a natural ratio of $^{238}U/^{235}U=137.88$. Common ^{204}Pb

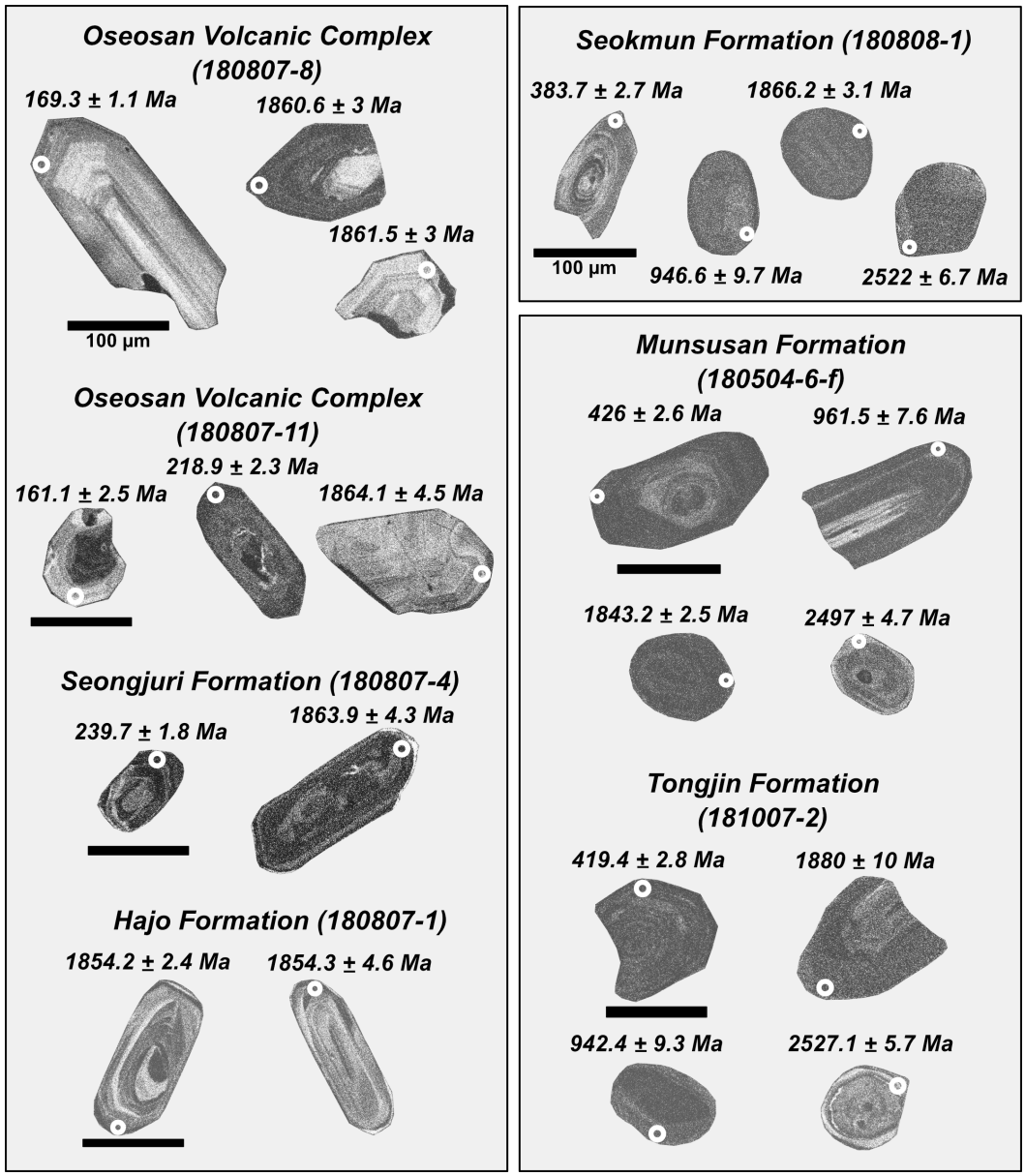

Fig. 3-6. Scanning-electron-microscope (SEM) cathodoluminescence images of selected zircon grains from sandstones in the Late Triassic to Early Jurassic post-collisional basin fills (Nampo and Gimpo groups and Seokmun Formation) and the overlying Middle Jurassic tuffaceous sedimentary rocks (Oseosan Volcanic Complex).

was monitored by mass number 204 after discarding the ^{204}Hg background. The measurement conditions were 15 μm diameter of spot size, 5 Hz repetition rate, and energy density of 3 J/cm^2. Helium was used as carrier gas (650 ml/min). Background signals, dwell time, and wash-out time were 30 s, 30 s, and 20 s, respectively. The measured isotope ratio was examined by a Time-Resolved Analytical (TRA) procedure. Signal intensities for each collector were collected every 0.2 s. Raw data were corrected for background, laser-induced elemental fractionation, mass discrimination, and drift in ion counter grains. For calibration of U-Pb isotope ratios, concordant zircons 91500 were measured at regular intervals during analytical sessions, following protocols by Andersen et al. (2002). Isotopic ages were calculated with 2σ error, and data processing was conducted by using the Iolite 2.5 (Paton et al., 2010, 2011) and Isoplot 3.71 (Ludwig, 2008) software. Age probability curves were plotted by using $^{206}Pb/^{238}U$ ages for < 1000 Ma and $^{207}Pb/^{206}Pb$ ages for > 1000 Ma, with a discordance of < 15% and a reverse discordance of < 10%.

3.3.2. Results

Among the analyzed 700 zircon grains, 592 yielded concordant or slightly discordant Archean to Jurassic U-Pb ages, ranging from 3108 ± 3.9 Ma to 158.0 ± 1.4 Ma (Table 3-1). Except for 91 grains, most of the analyzed zircons had Th/U ratios above 0.1 (Table 3-1), indicating an igneous origin (Hoskin and Black, 2000). Most of the zircons from the Nampo Group and Oseosan Volcanic Complex, which constitute the Chungnam Basin, fell within three major age-peak groups (1864–1854 Ma, 240–218 Ma, and 169–164 Ma), with minor Late Neoproterozoic and Paleozoic peaks (Fig. 3-7; Table 3-1). The grains from the Gimpo Group (Tongjin and Munsusan formations) and Seokmun Formation formed three major

Table 3-1. Detrital-zircon U-Pb isotopic data of sandstones from the Daedong Supergroup along the western Korean Peninsula.

sample name	Th/U	$^{207}Pb/^{235}U$	2σ	$^{206}Pb/^{238}U$	2σ	$^{207}Pb/^{206}Pb$	2σ	^{235}U-^{207}Pb age (Ma)	2σ	^{238}U-^{206}Pb age (Ma)	2σ	$^{207/206}Pb$ age (Ma)	2σ	disc.(%)
Hajo Fm. (n=100)														
180807-1-58	*0.32*	*2.096*	*0.016*	*0.1457*	*0.0009*	*0.1046*	*0.0004*	*1147.5*	*5.2*	*876.5*	*4.9*	*1706.2*	*3.8*	*-29.8*
180807-1-37	*0.33*	*2.962*	*0.017*	*0.1991*	*0.0012*	*0.1079*	*0.0003*	*1397.8*	*4.3*	*1170.3*	*6.3*	*1761.4*	*3.5*	*-49.7*
180807-1-23	*0.21*	*3.927*	*0.038*	*0.2517*	*0.0024*	*0.1122*	*0.0004*	*1618.5*	*7.9*	*1447*	*12*	*1834.4*	*3.6*	*-25.7*
180807-1-81	*0.19*	*4.023*	*0.027*	*0.2619*	*0.0016*	*0.1119*	*0.0003*	*1638.5*	*5.4*	*1499.6*	*7.9*	*1828.3*	*2.7*	*-21.2*
180807-1-34	*0.39*	*4.108*	*0.056*	*0.2643*	*0.0036*	*0.1132*	*0.0004*	*1655*	*11*	*1511*	*19*	*1853.7*	*4.2*	*-21.1*
180807-1-20	*0.24*	*4.100*	*0.029*	*0.2674*	*0.0016*	*0.1112*	*0.0002*	*1653.8*	*5.7*	*1527.3*	*8.4*	*1819.3*	*2.3*	*-18.4*
180807-1-80	*0.26*	*4.134*	*0.042*	*0.2692*	*0.0026*	*0.1113*	*0.0003*	*1661.4*	*8.5*	*1536*	*13*	*1820.8*	*2.5*	*-17.5*
180807-1-62	*0.23*	*4.147*	*0.035*	*0.2695*	*0.0021*	*0.1142*	*0.0002*	*1663*	*6.8*	*1538*	*11*	*1867.2*	*2*	*-20.6*
180807-1-60	*0.16*	*4.191*	*0.043*	*0.2720*	*0.0026*	*0.1138*	*0.0004*	*1671.9*	*8.3*	*1551*	*13*	*1862.9*	*3.6*	*-19.0*
180807-1-94	*0.30*	*4.190*	*0.030*	*0.2723*	*0.0018*	*0.1118*	*0.0003*	*1672.5*	*5.9*	*1552.2*	*8.9*	*1831.8*	*3.1*	*-17.2*
180807-1-32	*0.68*	*4.270*	*0.046*	*0.2731*	*0.0023*	*0.1138*	*0.0005*	*1688.2*	*8.7*	*1558*	*12*	*1859.9*	*6.3*	*-18.2*
180807-1-67	*0.59*	*4.276*	*0.029*	*0.2753*	*0.0019*	*0.1136*	*0.0004*	*1688.4*	*5.5*	*1567.3*	*9.5*	*1858*	*3.7*	*-17.7*
180807-1-28	*0.12*	*4.303*	*0.020*	*0.2761*	*0.0012*	*0.1124*	*0.0003*	*1693.7*	*3.8*	*1571.4*	*6*	*1840*	*2.5*	*-16.6*
180807-1-100	*0.19*	*4.279*	*0.035*	*0.2767*	*0.0023*	*0.1126*	*0.0002*	*1690.9*	*6.7*	*1574*	*11*	*1839.7*	*2.1*	*-16.0*
180807-1-21	*0.38*	*4.431*	*0.053*	*0.2784*	*0.0035*	*0.1138*	*0.0003*	*1717.2*	*9.8*	*1583*	*17*	*1860.9*	*2.7*	*-16.3*
180807-1-6	*0.56*	*4.340*	*0.058*	*0.2793*	*0.0030*	*0.1121*	*0.0011*	*1701*	*11*	*1588*	*15*	*1829*	*12*	*-13.5*
180807-1-46	*0.30*	*4.328*	*0.040*	*0.2798*	*0.0023*	*0.1128*	*0.0003*	*1698.3*	*7.6*	*1590*	*11*	*1844.5*	*3*	*-15.1*
180807-1-86	*0.23*	*4.341*	*0.038*	*0.2810*	*0.0024*	*0.1128*	*0.0002*	*1700.5*	*7.3*	*1596*	*12*	*1843.4*	*2.9*	*-14.6*
180807-1-17	*0.21*	*4.383*	*0.045*	*0.2842*	*0.0027*	*0.1119*	*0.0003*	*1709*	*8.5*	*1612*	*14*	*1830.5*	*4.2*	*-12.4*
180807-1-83	*0.31*	*4.426*	*0.045*	*0.2842*	*0.0026*	*0.1136*	*0.0004*	*1717*	*8.4*	*1612*	*13*	*1857*	*5.2*	*-14.1*
180807-1-52	*0.45*	*4.494*	*0.032*	*0.2855*	*0.0021*	*0.1130*	*0.0002*	*1730.8*	*5.7*	*1619*	*10*	*1848.3*	*2.3*	*-13.4*
180807-1-96	*0.19*	*4.499*	*0.030*	*0.2903*	*0.0018*	*0.1126*	*0.0002*	*1730.5*	*5.5*	*1643.1*	*8.8*	*1843.5*	*2.1*	*-11.5*
180807-1-9	*0.30*	*4.550*	*0.035*	*0.2905*	*0.0021*	*0.1127*	*0.0002*	*1739.5*	*6.5*	*1644*	*11*	*1843.4*	*2.1*	*-11.3*
180807-1-99	*0.65*	*4.574*	*0.032*	*0.2923*	*0.0020*	*0.1137*	*0.0004*	*1745*	*6.1*	*1653*	*9.8*	*1859.6*	*4.5*	*-11.6*
180807-1-8	*0.18*	*4.559*	*0.021*	*0.2924*	*0.0014*	*0.1121*	*0.0002*	*1742.1*	*4*	*1653.5*	*6.9*	*1833.6*	*1.6*	*-10.4*
180807-1-22	0.13	4.566	0.024	0.2932	0.0015	0.1120	0.0003	1742.9	4.4	1657.5	7.7	1831.8	2.3	-9.9
180807-1-40	*0.26*	*4.575*	*0.034*	*0.2934*	*0.0020*	*0.1131*	*0.0003*	*1744.4*	*6.2*	*1658*	*10*	*1847.1*	*3.4*	*-10.6*
180807-1-77	0.32	4.615	0.039	0.2953	0.0023	0.1126	0.0002	1751.5	6.9	1669	12	1840.7	1.7	-9.5
180807-1-19	0.47	4.586	0.034	0.2972	0.0020	0.1128	0.0005	1746.5	6.1	1677	10	1844.8	3.5	-9.2
180807-1-73	0.58	4.714	0.031	0.2974	0.0018	0.1133	0.0004	1769.3	5.5	1678.1	8.8	1851.7	3.6	-9.6
180807-1-18	0.65	4.635	0.028	0.2983	0.0017	0.1134	0.0005	1755.4	5.1	1682.9	8.3	1854.3	4.6	-9.4
180807-1-55	0.52	4.714	0.028	0.2987	0.0017	0.1134	0.0003	1769.3	5	1684.7	8.3	1854.2	2.4	-9.4
180807-1-87	0.59	4.664	0.035	0.2989	0.0020	0.1135	0.0004	1760.4	6.2	1685	10	1855.6	2.9	-9.4
180807-1-53	0.35	4.696	0.037	0.2989	0.0023	0.1131	0.0002	1766.9	6.7	1686	11	1847.4	1.8	-8.8
180807-1-88	0.74	4.685	0.042	0.2993	0.0025	0.1136	0.0003	1764	7.5	1687	13	1860.1	2.7	-9.3
180807-1-39	0.18	4.650	0.078	0.2975	0.0045	0.1133	0.0003	1760	13	1689	24	1854.1	2	-8.2
180807-1-91	0.50	4.698	0.044	0.2998	0.0025	0.1133	0.0004	1766.4	7.9	1690	12	1853.9	3.5	-8.8
180807-1-95	0.59	4.632	0.034	0.2998	0.0021	0.1125	0.0003	1754.6	6	1690	10	1841.4	2.6	-8.2
180807-1-75	0.53	4.762	0.030	0.3004	0.0021	0.1134	0.0004	1777.9	5.4	1693	10	1855.5	4	-8.8
180807-1-97	0.35	4.684	0.033	0.3004	0.0021	0.1132	0.0003	1764.7	5.9	1693	10	1852.7	2.5	-8.7
180807-1-16	0.29	4.653	0.022	0.3004	0.0015	0.1131	0.0002	1758.5	4	1693.3	7.3	1850	2	-8.7
180807-1-65	0.22	4.666	0.047	0.3010	0.0027	0.1143	0.0002	1760.4	8.3	1696	13	1868.5	1.9	-9.3
180807-1-7	0.46	4.752	0.029	0.3011	0.0015	0.1130	0.0003	1776.2	5.1	1696.5	7.6	1850.9	2.4	-8.5
180807-1-35	0.54	4.705	0.049	0.3018	0.0028	0.1140	0.0004	1767.7	8.8	1700	14	1863.8	2.4	-8.7
180807-1-4	0.62	4.752	0.029	0.3019	0.0018	0.1130	0.0003	1776.1	5.2	1700.7	8.9	1848.6	2.1	-8.0
180807-1-25	0.32	4.738	0.032	0.3020	0.0024	0.1131	0.0003	1773.9	5.7	1701	12	1851	2.1	-8.0
180807-1-33	0.63	4.680	0.053	0.3020	0.0035	0.1136	0.0004	1763.2	9.5	1701	17	1859	4.2	-8.0
180807-1-44	0.50	4.771	0.027	0.3030	0.0013	0.1145	0.0004	1779.7	4.7	1706	6.4	1872	4.1	-9.1
180807-1-98	0.37	4.766	0.054	0.3044	0.0032	0.1133	0.0005	1779.7	9.8	1713	16	1852.5	5.3	-6.9
180807-1-72	0.36	4.792	0.033	0.3052	0.0020	0.1131	0.0002	1783.3	5.7	1716.7	9.6	1848.5	1.8	-7.0
180807-1-51	0.49	4.812	0.047	0.3055	0.0024	0.1135	0.0006	1786.7	8.3	1719	12	1853.7	6.8	-6.7
180807-1-36	0.30	4.750	0.058	0.3058	0.0040	0.1139	0.0003	1776	10	1720	20	1861.2	2.4	-6.9
180807-1-93	0.65	4.771	0.032	0.3063	0.0019	0.1132	0.0004	1779.5	5.6	1722.4	9.2	1850.2	3.5	-6.7
180807-1-71	0.67	4.894	0.050	0.3065	0.0028	0.1147	0.0007	1801.1	8.5	1723	14	1872.1	6.4	-7.5
180807-1-47	0.13	4.722	0.061	0.3066	0.0036	0.1118	0.0004	1771	11	1724	18	1827.4	3.4	-4.8
180807-1-76	0.36	4.861	0.040	0.3077	0.0022	0.1142	0.0004	1795.9	7.1	1729	11	1867	3.5	-7.1
180807-1-59	0.70	4.905	0.069	0.3078	0.0042	0.1166	0.0008	1803	12	1730	21	1904.2	8.8	-8.3
180807-1-84	0.53	4.809	0.049	0.3082	0.0026	0.1140	0.0005	1786.1	8.6	1732	13	1864.2	5.2	-6.6
180807-1-90	0.69	4.787	0.040	0.3082	0.0024	0.1131	0.0003	1784	7	1732	12	1848.2	2.9	-5.8
180807-1-92	0.63	4.838	0.028	0.3088	0.0017	0.1135	0.0003	1791.2	5	1734.5	8.6	1857.1	2.7	-6.4
180807-1-61	0.51	4.838	0.048	0.3091	0.0027	0.1164	0.0005	1791.1	8.3	1736	13	1900.7	3.4	-8.5
180807-1-14	0.17	4.740	0.064	0.3094	0.0043	0.1127	0.0004	1774	11	1744	24	1844.3	2	-4.3
180807-1-78	0.33	4.892	0.041	0.3111	0.0025	0.1135	0.0004	1800.6	7.1	1746	12	1854.5	3.1	-5.3
180807-1-49	0.99	4.895	0.026	0.3120	0.0015	0.1141	0.0003	1801.7	4.3	1750.6	7.2	1864.6	2.8	-5.9
180807-1-56	0.61	4.994	0.066	0.3117	0.0037	0.1154	0.0004	1819	11	1751	18	1885.2	3.7	-6.4
180807-1-74	0.62	4.990	0.028	0.3132	0.0015	0.1143	0.0003	1817.4	4.8	1756.1	7.5	1869.9	3	-5.9
180807-1-63	0.78	4.886	0.038	0.3136	0.0022	0.1155	0.0003	1799.4	6.5	1758	11	1886.6	2.2	-6.6
180807-1-89	0.73	4.932	0.048	0.3152	0.0027	0.1139	0.0004	1808.3	8.1	1766	13	1863.2	3.9	-4.5
180807-1-38	0.52	4.891	0.056	0.3157	0.0033	0.1135	0.0005	1800.3	9.8	1768	16	1853.5	4.7	-3.7
180807-1-57	0.75	5.030	0.085	0.3157	0.0051	0.1161	0.0007	1824	14	1768	25	1894.1	6.3	-5.4
180807-1-27	0.12	4.965	0.091	0.3160	0.0058	0.1137	0.0002	1811	15	1769	28	1859	2	-3.4
180807-1-50	0.54	5.024	0.032	0.3160	0.0017	0.1154	0.0004	1823	5.3	1770.2	8.3	1884	4.5	-5.7
180807-1-85	0.74	4.966	0.039	0.3179	0.0022	0.1145	0.0004	1813.9	6.5	1779	11	1867.6	3.1	-4.2
180807-1-2	0.41	5.048	0.027	0.3195	0.0015	0.1135	0.0002	1827.6	4.4	1787	7.3	1855.8	2.4	-3.3
180807-1-5	0.10	4.980	0.150	0.3199	0.0092	0.1134	0.0011	1815	25	1789	45	1855	12	-0.5
180807-1-31	0.40	5.046	0.046	0.3213	0.0025	0.1148	0.0004	1826.7	7.8	1796	12	1876.4	3.2	-3.6
180807-1-24	0.17	4.988	0.042	0.3214	0.0019	0.1128	0.0004	1817.2	7.1	1796.4	9.1	1847.4	2.9	-2.2
180807-1-54	0.77	5.121	0.046	0.3221	0.0028	0.1142	0.0005	1839.3	7.5	1800	13	1864.9	4.5	-2.6
180807-1-64	0.29	5.020	0.140	0.3227	0.0079	0.1146	0.0008	1821	24	1803	39	1881.2	9.1	-1.7
180807-1-79	0.59	5.073	0.078	0.3245	0.0031	0.1131	0.0014	1831	13	1812	15	1856	15	-0.8
180807-1-11	0.22	5.071	0.081	0.3256	0.0053	0.1143	0.0013	1831	14	1817	26	1873	9.1	-1.2
180807-1-68	0.79	5.185	0.065	0.3271	0.0034	0.1155	0.0005	1852	11	1824	17	1885.5	5.6	-2.1
180807-1-69	0.71	5.174	0.085	0.3276	0.0046	0.1147	0.0008	1848	14	1827	22	1874.7	7	-1.0
180807-1-10	0.54	5.132	0.074	0.3280	0.0046	0.1138	0.0016	1841	12	1829	22	1860.4	7.8	-0.1
180807-1-15	0.65	5.094	0.063	0.3280	0.0054	0.1136	0.0008	1835	10	1829	26	1859.5	7.7	0.2
180807-1-12	0.30	5.108	0.058	0.3284	0.0040	0.1137	0.0005	1837	9.6	1831	19	1858.8	4	-0.3
180807-1-26	0.18	5.257	0.055	0.3285	0.0038	0.1169	0.0007	1861.7	8.8	1831	19	1906.9	7.7	-2.7
180807-1-70	1.06	5.212	0.044	0.3294	0.0027	0.1148	0.0006	1854.4	7.1	1836	13	1880.8	4.9	-1.5
180807-1-45	0.17	5.126	0.038	0.3297	0.0026	0.1143	0.0002	1840.2	6.3	1837	13	1869.2	2.3	-0.9
180807-1-66	0.31	5.191	0.035	0.3298	0.0036	0.1160	0.0010	1851.2	5.7	1837	18	1896.8	8	-1.8
180807-1-29	0.25	5.140	0.120	0.3301	0.0075	0.1141	0.0004	1843	20	1839	36	1868.3	9.6	0.9
180807-1-13	0.52	5.163	0.038	0.3313	0.0022	0.1137	0.0004	1846.3	6.2	1845	11	1859.3	3.3	0.0
180807-1-42	0.36	5.171	0.048	0.3315	0.0027	0.1144	0.0007	1847.7	7.8	1846	13	1865.8	7.7	0.0
180807-1-48	0.59	5.174	0.068	0.3316	0.0034	0.1151	0.0013	1848	11	1846	17	1882	12	-0.4
180807-1-30	0.31	5.179	0.046	0.3316	0.0030	0.1140	0.0003	1848.9	7.5	1849	14	1865.9	2.3	0.0
180807-1-43	0.51	5.217	0.054	0.3331	0.0031	0.1151	0.0006	1854.8	8.9	1853	15	1877.4	4.3	-0.3
180807-1-41	0.23	5.260	0.110	0.3352	0.0064	0.1153	0.0009	1863	19	1863	31	1886.8	9.1	0.9
180807-1-1	0.63	5.350	0.220	0.3350	0.0140	0.1146	0.0004	1874	34	1867	65	1876.5	3.5	3.2
180807-1-82	0.41	5.230	0.110	0.3368	0.0074	0.1126	0.0007	1857	18	1871	35	1843.4	5.4	0.7
180807-1-3	0.19	5.410	0.110	0.3405	0.0063	0.1139	0.0007	1886	18	1889	30	1862	4	0.4

Seongjuri Fm. (n=100)

180807-4-61	0.38	0.202	0.010	0.0290	0.0003	0.0496	0.0028	186.8	8.6	184.3	2	277	80	4.4
180807-4-97	0.59	0.206	0.011	0.0291	0.0003	0.0509	0.0027	189.4	9.1	184.9	1.9	410	53	3.5
180807-4-12	0.51	0.209	0.012	0.0298	0.0003	0.0511	0.0030	192	10	189.1	1.8	349	62	4.7
180807-4-36	0.40	0.209	0.004	0.0302	0.0003	0.0505	0.0009	192.6	3.5	191.6	1.7	218	23	2.2
180807-4-44	0.27	0.209	0.003	0.0305	0.0002	0.0496	0.0007	192.7	2.3	193.5	1	181	19	1.3
180807-4-38	0.50	0.212	0.005	0.0306	0.0003	0.0503	0.0012	194.8	4.4	194.4	1.9	225	29	3.0
180807-4-29	0.99	0.215	0.004	0.0310	0.0004	0.0503	0.0008	197.6	3	196.6	2.2	211	18	2.1
180807-4-93	0.42	0.216	0.004	0.0312	0.0004	0.0493	0.0009	198.2	3.3	198	2.2	167	21	2.7
180807-4-51	0.62	0.232	0.020	0.0328	0.0006	0.0505	0.0046	211	17	207.7	3.8	400	110	8.4
180807-4-96	0.70	0.237	0.005	0.0336	0.0003	0.0507	0.0010	216	4.1	213.3	2.1	216	27	1.6
180807-4-17	0.21	0.247	0.003	0.0350	0.0003	0.0508	0.0008	223.7	2.8	221.9	1.7	230	21	1.2
180807-4-19	1.38	0.249	0.004	0.0356	0.0002	0.0502	0.0006	225.8	3.2	225.4	1.5	212	13	1.9
180807-4-78	0.25	0.252	0.004	0.0360	0.0002	0.0505	0.0007	228	3	227.8	1.3	226	18	1.8
180807-4-85	0.31	0.258	0.004	0.0368	0.0003	0.0514	0.0007	233.6	3.6	232.9	2.1	247	18	2.1
180807-4-46	0.72	0.261	0.003	0.0370	0.0002	0.0511	0.0005	235.1	2.6	234	1.4	242	12	1.2
180807-4-74	0.34	0.256	0.006	0.0371	0.0003	0.0500	0.0011	231.3	5	234.9	2.1	191	26	1.5
180807-4-84	0.47	0.263	0.003	0.0376	0.0003	0.0513	0.0005	236.9	2.5	238.1	1.6	254.7	9.5	1.2
180807-4-76	0.60	0.266	0.003	0.0379	0.0002	0.0511	0.0006	239.6	2.6	239.5	1.5	243	15	1.7
180807-4-70	0.63	0.266	0.003	0.0379	0.0003	0.0513	0.0004	239.4	2.1	239.7	1.8	250.1	9.5	1.5
180807-4-32	0.44	0.267	0.003	0.0379	0.0005	0.0514	0.0007	239.8	2.3	239.8	2.9	258	15	2.2
180807-4-7	0.44	0.272	0.003	0.0383	0.0003	0.0514	0.0004	244.6	2.7	242.3	2	250	11	1.0
180807-4-42	0.42	0.268	0.014	0.0386	0.0004	0.0500	0.0026	242	11	243.9	2.4	392	62	4.8
180807-4-47	0.45	0.272	0.004	0.0386	0.0003	0.0508	0.0009	244	3.2	244.1	2	230	24	2.1
180807-4-5	0.27	0.274	0.005	0.0389	0.0003	0.0511	0.0009	245.7	3.6	245.7	2.1	244	22	2.3
180807-4-49	0.45	0.277	0.006	0.0389	0.0003	0.0513	0.0010	248.2	4.7	245.9	2	262	24	1.8
180807-4-28	0.25	0.277	0.004	0.0391	0.0003	0.0515	0.0005	248	2.8	247.2	1.8	259	12	1.5
180807-4-69	0.72	0.279	0.007	0.0393	0.0003	0.0513	0.0013	249	5.7	248.7	2	291	32	3.0
180807-4-39	0.18	0.277	0.008	0.0394	0.0004	0.0506	0.0013	247.8	6.3	249.4	2.4	257	31	2.9
180807-4-40	0.31	0.280	0.010	0.0395	0.0004	0.0519	0.0019	250.6	8.2	249.5	2.6	296	28	3.9
180807-4-65	0.51	0.279	0.014	0.0395	0.0004	0.0507	0.0026	248	12	249.8	2.4	348	49	5.1
180807-4-91	0.37	0.287	0.003	0.0405	0.0002	0.0510	0.0004	256	2.1	255.8	1.4	244	10	1.3
180807-4-64	0.54	0.289	0.004	0.0407	0.0005	0.0519	0.0006	257.4	3.5	257.3	2.9	278	15	2.4
180807-4-6	0.36	0.304	0.006	0.0427	0.0008	0.0518	0.0007	269.3	4.7	269.6	4.9	275	13	3.5
180807-4-100	0.06	0.334	0.008	0.0460	0.0005	0.0523	0.0011	292.4	5.7	289.9	2.8	306	24	2.1
180807-4-75	0.12	0.335	0.007	0.0463	0.0003	0.0525	0.0011	293.7	5.3	291.5	1.9	309	24	1.7
180807-4-81	0.34	0.334	0.006	0.0463	0.0005	0.0520	0.0011	292.1	4.7	291.6	2.9	306	27	2.4
180807-4-9	0.11	0.354	0.007	0.0485	0.0005	0.0525	0.0009	307.2	5.2	305.4	2.7	298	23	2.0
180807-4-80	0.57	0.367	0.006	0.0504	0.0004	0.0523	0.0007	317.4	4.3	316.8	2.4	301	21	1.9
180807-4-60	1.13	0.385	0.008	0.0526	0.0005	0.0521	0.0009	330.3	5.5	330.2	3	291	29	2.5
180807-4-52	0.40	0.407	0.008	0.0552	0.0005	0.0531	0.0010	346.1	5.6	346.2	2.8	335	25	2.4
180807-4-34	0.59	0.577	0.013	0.0741	0.0006	0.0559	0.0012	461.6	8.4	461	3.8	485	32	2.5
180807-4-92	0.23	0.804	0.009	0.0973	0.0006	0.0597	0.0004	598.9	5.2	598.4	3.5	597.7	7.7	1.4
180807-4-4	*0.06*	*1.628*	*0.017*	*0.1168*	*0.0011*	*0.1010*	*0.0004*	*980.8*	*6.6*	*711.9*	*6.1*	*1639.1*	*5.1*	*-36.0*
180807-4-41	*0.15*	*3.219*	*0.034*	*0.2061*	*0.0020*	*0.1129*	*0.0005*	*1463*	*7.6*	*1208*	*11*	*1842.3*	*5.8*	*-51.1*
180807-4-22	*0.12*	*3.481*	*0.030*	*0.2296*	*0.0020*	*0.1102*	*0.0003*	*1522.7*	*6.9*	*1333*	*11*	*1803*	*2.8*	*-34.2*
180807-4-90	*0.02*	*3.896*	*0.047*	*0.2547*	*0.0023*	*0.1120*	*0.0006*	*1612.5*	*9.7*	*1462*	*12*	*1830.8*	*6.8*	*-23.9*
180807-4-79	*0.03*	*4.337*	*0.057*	*0.2779*	*0.0036*	*0.1145*	*0.0006*	*1700*	*11*	*1580*	*18*	*1872.5*	*6.4*	*-17.0*
180807-4-11	0.56	4.628	0.050	0.2957	0.0034	0.1131	0.0005	1754	9	1673	17	1851.3	5.4	-9.3
180807-4-59	-0.01	4.764	0.083	0.2999	0.0050	0.1151	0.0004	1782	16	1691	25	1883.4	4.1	-9.7
180807-4-37	0.68	4.740	0.087	0.3074	0.0040	0.1114	0.0008	1774	15	1728	20	1825.3	8	-4.0
180807-4-53	0.10	4.837	0.098	0.3095	0.0057	0.1138	0.0006	1791	17	1738	28	1863.9	4.3	-5.4
180807-4-58	0.55	4.912	0.076	0.3153	0.0044	0.1132	0.0009	1804	13	1767	22	1852.8	6.4	-3.2
180807-4-3	0.38	4.909	0.075	0.3198	0.0048	0.1107	0.0007	1803	13	1793	22	1810.2	7.4	0.7
180807-4-14	0.38	4.967	0.055	0.3219	0.0034	0.1109	0.0004	1813.5	9.3	1799	16	1815.5	4.6	0.2
180807-4-57	0.34	5.008	0.064	0.3224	0.0042	0.1126	0.0004	1820	11	1801	21	1843	2.7	-1.0
180807-4-24	0.02	5.202	0.060	0.3230	0.0035	0.1168	0.0004	1852.4	9.8	1804	17	1909.2	3.1	-4.7
180807-4-45	0.26	5.151	0.061	0.3244	0.0038	0.1141	0.0003	1844	10	1811	19	1866.9	3.4	-1.8
180807-4-82	0.26	5.000	0.120	0.3260	0.0075	0.1141	0.0009	1819	19	1818	37	1862.9	5	-0.2
180807-4-21	0.07	5.065	0.049	0.3269	0.0029	0.1128	0.0004	1831.1	8.1	1823	14	1847.4	4.3	-0.3
180807-4-15	0.22	5.100	0.053	0.3280	0.0032	0.1128	0.0002	1835.8	8.8	1828	16	1845.1	2.2	0.1
180807-4-73	0.93	5.053	0.066	0.3272	0.0036	0.1127	0.0005	1827	11	1828	18	1845.7	4.4	0.3
180807-4-20	0.39	5.207	0.037	0.3284	0.0021	0.1150	0.0003	1853.4	6.1	1830.2	9.9	1879.4	3.1	-2.0
180807-4-23	0.32	5.165	0.080	0.3286	0.0048	0.1129	0.0008	1846	13	1831	23	1848	6.1	0.7
180807-4-26	0.09	5.165	0.073	0.3288	0.0047	0.1142	0.0006	1847	12	1832	23	1866.2	5.2	-0.3
180807-4-86	0.03	5.100	0.049	0.3293	0.0031	0.1144	0.0002	1835.5	8.1	1834	15	1870.4	2.3	-1.0
180807-4-10	0.33	5.170	0.120	0.3296	0.0063	0.1139	0.0010	1852	17	1836	30	1866.2	6.6	0.3
180807-4-13	0.44	5.170	0.110	0.3298	0.0041	0.1130	0.0014	1847	18	1837	20	1848	15	1.3
180807-4-89	0.68	5.126	0.047	0.3301	0.0028	0.1134	0.0006	1839.6	7.9	1838	14	1853.3	5.5	0.2
180807-4-71	0.12	5.129	0.040	0.3301	0.0026	0.1134	0.0004	1841.1	6.7	1840	13	1854.2	3.4	0.1
180807-4-63	0.38	5.128	0.034	0.3305	0.0022	0.1128	0.0003	1840.5	5.6	1841	11	1842.3	3.3	0.7
180807-4-25	0.24	5.183	0.044	0.3309	0.0023	0.1136	0.0005	1849.3	7.2	1843	11	1857.4	4.2	0.0
180807-4-33	0.50	5.206	0.087	0.3316	0.0058	0.1147	0.0004	1853	14	1846	28	1876.2	3.4	0.1
180807-4-8	0.64	5.238	0.063	0.3325	0.0031	0.1136	0.0008	1860	10	1850	15	1856.7	6.9	0.8
180807-4-27	0.05	5.260	0.036	0.3333	0.0023	0.1147	0.0003	1862.1	5.8	1854	11	1875.6	2.7	-0.4
180807-4-68	0.13	5.215	0.035	0.3334	0.0024	0.1144	0.0003	1854.9	5.8	1855	12	1869.8	2.7	0.0
180807-4-99	0.02	5.220	0.039	0.3334	0.0023	0.1132	0.0003	1856.4	6.4	1855	11	1850.9	2.6	0.5
180807-4-66	0.12	5.207	0.063	0.3339	0.0041	0.1138	0.0003	1853	10	1857	20	1863.3	3.5	0.9
180807-4-87	0.12	5.232	0.037	0.3339	0.0019	0.1142	0.0004	1857.6	6	1857.1	9	1864.3	3.5	0.3
180807-4-67	0.27	5.243	0.051	0.3341	0.0029	0.1146	0.0005	1859.1	8.2	1858	14	1871.3	6.1	0.4
180807-4-72	0.96	5.216	0.042	0.3339	0.0027	0.1149	0.0004	1855	6.9	1859	13	1876.5	3.6	0.0
180807-4-62	0.02	5.257	0.059	0.3341	0.0031	0.1141	0.0004	1861.4	9.6	1861	16	1863.7	4.5	1.0
180807-4-77	0.15	5.264	0.044	0.3348	0.0027	0.1148	0.0003	1863.7	6.8	1861	13	1877.1	2.6	0.0
180807-4-35	0.02	5.300	0.043	0.3359	0.0026	0.1147	0.0003	1868.7	6.9	1867	12	1874.5	2	0.3
180807-4-2	0.13	5.332	0.042	0.3362	0.0024	0.1144	0.0004	1873.8	6.7	1868	11	1869.2	3.5	0.7
180807-4-56	0.09	5.331	0.097	0.3366	0.0052	0.1149	0.0006	1873	16	1870	25	1875.7	5	1.3
180807-4-43	0.79	5.332	0.077	0.3369	0.0041	0.1149	0.0005	1876	13	1872	20	1877.1	3.9	1.0
180807-4-50	0.43	5.314	0.072	0.3370	0.0036	0.1144	0.0006	1871	12	1872	17	1870.9	7.4	1.2
180807-4-95	0.59	5.365	0.061	0.3384	0.0038	0.1138	0.0006	1879.7	9.6	1878	18	1858.6	4.1	0.1
180807-4-18	0.68	5.428	0.036	0.3389	0.0021	0.1160	0.0004	1889	5.8	1881	10	1894.7	3	0.0
180807-4-48	*0.25*	*7.172*	*0.059*	*0.3396*	*0.0025*	*0.1529*	*0.0006*	*2133.6*	*7.6*	*1884*	*12*	*2379.4*	*4.7*	*-25.4*
180807-4-98	0.12	5.400	0.051	0.3399	0.0031	0.1151	0.0004	1884.3	8.1	1886	15	1883.9	3.8	0.9
180807-4-1	*0.04*	*7.504*	*0.074*	*0.3570*	*0.0032*	*0.1516*	*0.0003*	*2172.9*	*8.9*	*1968*	*15*	*2365.7*	*1.9*	*-19.3*
180807-4-31	0.08	6.158	0.043	0.3631	0.0023	0.1233	0.0007	1999	5.9	1997	11	2003.4	8.9	0.7
180807-4-94	0.21	6.820	0.078	0.3823	0.0031	0.1282	0.0007	2088	10	2087	15	2073	6.4	0.4
180807-4-30	0.57	7.530	0.110	0.4006	0.0054	0.1357	0.0010	2176	14	2171	25	2172.4	9	1.5
180807-4-83	*0.50*	*8.970*	*0.072*	*0.4006*	*0.0031*	*0.1653*	*0.0005*	*2334.7*	*7.4*	*2172*	*14*	*2510.3*	*2.6*	*-14.8*
180807-4-16	*0.08*	*9.082*	*0.091*	*0.4086*	*0.0027*	*0.1609*	*0.0008*	*2345.7*	*9.1*	*2208*	*12*	*2465*	*6.2*	*-10.8*
180807-4-55	0.21	8.490	0.230	0.4251	0.0080	0.1433	0.0012	2282	25	2283	36	2268	11	1.4
180807-4-88	0.17	8.870	0.110	0.4341	0.0050	0.1500	0.0003	2324	12	2326	23	2347.1	2.5	0.2
180807-4-54	0.46	10.710	0.130	0.4714	0.0054	0.1650	0.0009	2498	11	2489	24	2508.4	6	0.4

Oseosan volcanic complex (180807-11; n=100)

180807-11-99	0.66	0.170	0.006	0.0248	0.0002	0.0500	0.0016	159.6	5	158	1.4	181	41	3.0
180807-11-66	0.48	0.171	0.008	0.0250	0.0002	0.0499	0.0024	159.8	7.2	159.1	1.5	264	48	5.0
180807-11-46	0.55	0.175	0.007	0.0251	0.0002	0.0506	0.0022	163.2	6.4	160	1.4	236	50	2.9
180807-11-90	0.51	0.172	0.005	0.0253	0.0002	0.0496	0.0016	161	4.4	161	1.3	184	41	3.5
180807-11-87	0.50	0.172	0.005	0.0254	0.0002	0.0491	0.0013	161.2	4.2	161.4	1.2	180	27	3.2
180807-11-3	0.48	0.172	0.005	0.0255	0.0002	0.0486	0.0012	160.7	4.1	162.1	1.3	126	23	2.5
180807-11-77	0.29	0.175	0.002	0.0255	0.0002	0.0498	0.0006	163.7	1.9	162.4	1.4	184	18	1.2
180807-11-100	*0.98*	*0.213*	*0.004*	*0.0256*	*0.0002*	*0.0593*	*0.0012*	*195.8*	*3.4*	*162.9*	*1.4*	*581*	*31*	*-17.2*
180807-11-63	0.75	0.175	0.008	0.0256	0.0004	0.0493	0.0026	163.3	7.2	163.1	2.5	207	50	5.8
180807-11-68	0.79	0.177	0.005	0.0257	0.0002	0.0503	0.0014	165.4	4.3	163.8	1.3	270	41	2.4
180807-11-28	1.28	0.180	0.008	0.0258	0.0002	0.0506	0.0023	167.4	7.2	164	1.5	243	52	3.2
180807-11-79	0.64	0.176	0.002	0.0258	0.0002	0.0493	0.0003	164.9	1.8	164.4	1.1	169	12	1.5
180807-11-38	0.44	0.176	0.007	0.0259	0.0003	0.0492	0.0021	165.3	6.2	164.7	1.6	322	42	4.4
180807-11-45	0.72	0.177	0.005	0.0259	0.0002	0.0501	0.0013	165.3	4.4	164.8	1.2	195	37	3.1
180807-11-33	0.58	0.176	0.003	0.0261	0.0002	0.0487	0.0010	164.3	2.9	166.1	1.2	133	22	1.4
180807-11-75	0.50	0.178	0.010	0.0263	0.0005	0.0492	0.0029	168.2	9.4	167.4	2.8	293	73	6.8
180807-11-18	0.43	0.179	0.003	0.0265	0.0002	0.0488	0.0007	167.4	2.9	168.9	1.1	145	15	1.5
180807-11-1	0.77	0.192	0.002	0.0267	0.0002	0.0517	0.0004	178	1.7	169.6	1.1	268	11	-3.3
180807-11-34	0.35	0.183	0.002	0.0267	0.0002	0.0498	0.0006	170.5	2.1	169.8	1.2	194	16	1.5
180807-11-23	0.75	0.183	0.002	0.0269	0.0002	0.0493	0.0003	170.8	1.5	171.1	1.4	162.3	9.6	1.5
180807-11-96	0.29	0.189	0.002	0.0271	0.0002	0.0502	0.0003	175.7	1.7	172.4	1.4	200.1	4.5	-0.1
180807-11-43	0.24	0.187	0.005	0.0272	0.0002	0.0497	0.0014	173.5	4.1	173	1.1	195	24	2.7
180807-11-80	0.41	0.188	0.007	0.0274	0.0004	0.0498	0.0014	174.9	5.6	174	2.8	194	32	4.3
180807-11-25	*0.41*	*0.255*	*0.006*	*0.0287*	*0.0003*	*0.0642*	*0.0015*	*230.5*	*4.9*	*182.3*	*2.1*	*743*	*41*	*-22.6*
180807-11-71	0.27	0.236	0.005	0.0337	0.0002	0.0509	0.0009	214.8	4	213.4	1.3	228	22	1.8
180807-11-29	0.65	0.239	0.016	0.0341	0.0004	0.0506	0.0030	217	13	216.1	2.6	268	62	6.8
180807-11-56	0.06	0.241	0.008	0.0341	0.0004	0.0520	0.0016	220.2	6.6	216.3	2.2	267	34	2.3
180807-11-39	0.31	0.241	0.002	0.0344	0.0002	0.0511	0.0005	219.2	1.8	218.3	1.3	246	13	1.0
180807-11-8	0.81	0.239	0.007	0.0345	0.0004	0.0508	0.0015	219	5.6	218.5	2.4	243	35	3.4
180807-11-44	0.01	0.241	0.004	0.0346	0.0004	0.0512	0.0006	219.5	3.1	218.9	2.3	245	16	2.2
180807-11-12	0.64	0.248	0.009	0.0348	0.0003	0.0516	0.0018	224.1	6.9	220.7	1.9	303	32	2.4
180807-11-50	0.66	0.242	0.009	0.0352	0.0003	0.0501	0.0017	219.8	7.1	222.8	1.9	282	33	2.7
180807-11-55	0.04	0.253	0.005	0.0359	0.0005	0.0516	0.0009	228.5	4	227.3	3.1	259	21	2.6
180807-11-9	0.04	0.255	0.008	0.0363	0.0003	0.0507	0.0015	230.6	6.3	229.6	2	261	30	3.2
180807-11-97	0.03	0.257	0.008	0.0367	0.0003	0.0508	0.0014	232.8	6.1	232.1	1.9	266	34	3.1
180807-11-4	-0.24	0.274	0.013	0.0381	0.0004	0.0524	0.0025	247	11	241.1	2.2	427	51	3.0
180807-11-83	*0.00*	*0.455*	*0.005*	*0.0475*	*0.0004*	*0.0695*	*0.0006*	*380.7*	*3.4*	*298.9*	*2.1*	*916*	*14*	*-25.5*
180807-11-42	0.37	0.572	0.005	0.0705	0.0004	0.0591	0.0003	459.4	3.2	438.9	2.5	569.8	8.4	-3.4
180807-11-91	*0.05*	*0.933*	*0.017*	*0.0779*	*0.0009*	*0.0871*	*0.0011*	*669*	*8.9*	*483.4*	*5.6*	*1357*	*13*	*-35.4*
180807-11-85	*0.02*	*1.260*	*0.022*	*0.0962*	*0.0011*	*0.0940*	*0.0011*	*827*	*10*	*592.2*	*6.4*	*1515*	*12*	*-36.9*
180807-11-98	0.87	1.062	0.023	0.1201	0.0013	0.0641	0.0011	734	11	731	7.7	759	19	2.1
180807-11-88	1.02	1.069	0.068	0.1214	0.0023	0.0635	0.0034	736	33	739	13	767	57	5.8
180807-11-37	0.67	1.149	0.026	0.1269	0.0016	0.0668	0.0017	777	12	770	9	835	26	1.8
180807-11-52	0.37	1.282	0.023	0.1382	0.0025	0.0681	0.0003	837	10	835	14	870.5	3.3	2.6
180807-11-13	*0.63*	*3.023*	*0.051*	*0.2020*	*0.0028*	*0.1078*	*0.0006*	*1413*	*13*	*1186*	*15*	*1767.2*	*4.2*	*-47.4*
180807-11-82	*0.10*	*3.266*	*0.034*	*0.2144*	*0.0018*	*0.1105*	*0.0004*	*1472.7*	*8.1*	*1252*	*9.4*	*1806.9*	*4.2*	*-43.2*
180807-11-31	*0.08*	*3.431*	*0.047*	*0.2234*	*0.0026*	*0.1126*	*0.0006*	*1511*	*11*	*1300*	*14*	*1837.1*	*5.7*	*-39.8*
180807-11-73	*0.70*	*3.545*	*0.040*	*0.2246*	*0.0023*	*0.1148*	*0.0005*	*1536.6*	*8.9*	*1308*	*12*	*1874.8*	*3.9*	*-42.1*
180807-11-54	*0.27*	*3.599*	*0.027*	*0.2303*	*0.0015*	*0.1139*	*0.0003*	*1548.9*	*5.9*	*1336*	*7.9*	*1863.7*	*3*	*-38.7*
180807-11-27	*0.21*	*3.596*	*0.045*	*0.2365*	*0.0024*	*0.1111*	*0.0007*	*1548*	*10*	*1368*	*12*	*1818.9*	*6.2*	*-31.6*
180807-11-84	*0.13*	*3.768*	*0.027*	*0.2470*	*0.0018*	*0.1107*	*0.0003*	*1586.4*	*5.6*	*1423*	*9.1*	*1811.1*	*3*	*-26.4*
180807-11-58	*0.38*	*3.777*	*0.032*	*0.2482*	*0.0019*	*0.1111*	*0.0004*	*1587.4*	*6.8*	*1429.2*	*9.7*	*1815.5*	*3.9*	*-26.1*
180807-11-69	*0.12*	*3.810*	*0.024*	*0.2486*	*0.0014*	*0.1116*	*0.0003*	*1595.1*	*5.2*	*1431.1*	*7.1*	*1827.4*	*2.7*	*-27.0*
180807-11-89	*0.01*	*4.025*	*0.045*	*0.2541*	*0.0027*	*0.1158*	*0.0005*	*1640.3*	*9.5*	*1459*	*14*	*1891.6*	*4.8*	*-28.4*
180807-11-41	*0.07*	*4.081*	*0.036*	*0.2637*	*0.0019*	*0.1129*	*0.0004*	*1650.2*	*7.2*	*1508.4*	*9.5*	*1848*	*2.5*	*-21.7*
180807-11-59	*0.15*	*4.292*	*0.057*	*0.2714*	*0.0032*	*0.1151*	*0.0007*	*1693*	*10*	*1548*	*16*	*1882.7*	*7.1*	*-20.1*
180807-11-61	*0.02*	*4.272*	*0.071*	*0.2743*	*0.0038*	*0.1139*	*0.0005*	*1687*	*14*	*1563*	*19*	*1861.4*	*4.3*	*-17.6*
180807-11-16	*0.29*	*4.295*	*0.052*	*0.2796*	*0.0028*	*0.1119*	*0.0005*	*1691.9*	*9.9*	*1589*	*14*	*1833.9*	*4.8*	*-14.2*
180807-11-2	*0.56*	*4.390*	*0.059*	*0.2826*	*0.0033*	*0.1125*	*0.0007*	*1712*	*12*	*1604*	*17*	*1838.1*	*6.7*	*-13.1*
180807-11-35	*0.07*	*4.418*	*0.027*	*0.2837*	*0.0017*	*0.1134*	*0.0002*	*1715.9*	*5.1*	*1610*	*8.6*	*1854.4*	*2.3*	*-14.5*
180807-11-94	*0.31*	*4.507*	*0.079*	*0.2900*	*0.0042*	*0.1126*	*0.0008*	*1732*	*15*	*1642*	*21*	*1840.3*	*7*	*-10.4*
180807-11-74	*0.42*	*4.601*	*0.037*	*0.2950*	*0.0019*	*0.1131*	*0.0004*	*1749.4*	*6.6*	*1666.1*	*9.7*	*1849.9*	*4.3*	*-10.2*
180807-11-60	*0.16*	*4.628*	*0.054*	*0.2967*	*0.0029*	*0.1141*	*0.0007*	*1754*	*9.7*	*1675*	*15*	*1865.5*	*6.4*	*-10.1*
180807-11-64	0.41	4.633	0.046	0.3014	0.0030	0.1130	0.0006	1756.7	8.6	1698	15	1846.1	6.4	-7.5
180807-11-78	0.01	4.764	0.046	0.3041	0.0031	0.1139	0.0004	1778.2	8.1	1711	15	1862	4.6	-7.7
180807-11-93	0.61	4.774	0.062	0.3040	0.0032	0.1130	0.0007	1782	10	1711	16	1841.8	8.2	-6.2
180807-11-49	0.02	4.724	0.038	0.3042	0.0024	0.1129	0.0002	1771.3	6.7	1712	12	1846.7	2.3	-7.0
180807-11-22	0.01	4.761	0.076	0.3067	0.0045	0.1127	0.0004	1778	13	1724	22	1842.8	2.8	-5.5
180807-11-20	0.01	4.973	0.057	0.3077	0.0033	0.1167	0.0005	1814.5	9.6	1729	16	1904.1	4.4	-8.9
180807-11-72	0.22	4.820	0.054	0.3087	0.0026	0.1132	0.0007	1788	9.4	1734	13	1855.9	5.6	-6.0
180807-11-21	0.13	4.837	0.080	0.3091	0.0054	0.1137	0.0008	1791	14	1736	27	1859.1	3.8	-5.3
180807-11-57	0.36	4.858	0.045	0.3093	0.0027	0.1144	0.0004	1794.7	7.8	1737	13	1873.1	3.2	-6.9
180807-11-95	0.18	4.940	0.048	0.3137	0.0030	0.1138	0.0005	1808.9	8.1	1759	15	1864.1	4.5	-4.9
180807-11-47	0.02	4.850	0.100	0.3153	0.0061	0.1127	0.0005	1792	18	1766	30	1846.4	4.3	-2.6
180807-11-76	0.53	5.031	0.064	0.3166	0.0031	0.1155	0.0008	1826	11	1773	15	1885.6	6.6	-5.1
180807-11-70	0.19	4.918	0.069	0.3187	0.0046	0.1142	0.0007	1805	12	1783	23	1865.2	4.2	-3.1
180807-11-19	0.76	4.970	0.160	0.3237	0.0085	0.1119	0.0012	1812	27	1807	41	1837	11	1.2
180807-11-5	0.17	5.010	0.071	0.3238	0.0036	0.1128	0.0006	1821	12	1808	18	1847.2	3.2	-1.0
180807-11-51	0.22	5.076	0.072	0.3243	0.0061	0.1133	0.0011	1832	12	1811	30	1865	14	-0.6
180807-11-86	1.27	5.119	0.073	0.3276	0.0043	0.1136	0.0008	1839	12	1826	21	1861.1	8.3	-0.3
180807-11-7	0.38	5.072	0.074	0.3283	0.0043	0.1130	0.0007	1831	12	1830	21	1850.5	7.9	0.5
180807-11-62	0.36	5.103	0.077	0.3284	0.0050	0.1143	0.0009	1836	13	1831	24	1870.3	7.5	-0.4
180807-11-32	0.24	5.136	0.095	0.3289	0.0053	0.1141	0.0006	1845	15	1833	26	1867.6	5.2	-0.2
180807-11-67	0.53	5.122	0.080	0.3290	0.0045	0.1146	0.0009	1839	13	1833	22	1867.2	8.1	-0.2
180807-11-53	0.17	5.144	0.073	0.3295	0.0046	0.1137	0.0003	1842	12	1836	22	1860.2	3.9	0.1
180807-11-81	0.27	5.227	0.077	0.3312	0.0032	0.1154	0.0010	1857	13	1844	15	1880	10	-0.6
180807-11-26	0.29	5.171	0.074	0.3314	0.0044	0.1136	0.0010	1848	12	1845	21	1855.4	9.3	1.1
180807-11-65	0.25	5.260	0.110	0.3320	0.0061	0.1150	0.0010	1862	18	1848	29	1878.7	9.5	0.4
180807-11-40	0.17	5.226	0.056	0.3327	0.0030	0.1148	0.0004	1856.5	9.1	1851	14	1873.9	3.5	-0.3
180807-11-92	0.12	5.287	0.084	0.3336	0.0054	0.1157	0.0007	1867	14	1856	26	1887	7.8	0.2
180807-11-17	0.24	5.499	0.072	0.3429	0.0043	0.1167	0.0007	1901	11	1900	21	1906.1	5.7	1.1
180807-11-6	0.23	5.585	0.091	0.3436	0.0049	0.1173	0.0015	1913	14	1904	24	1914	14	1.5
180807-11-15	*0.19*	*7.292*	*0.088*	*0.3645*	*0.0036*	*0.1462*	*0.0006*	*2149*	*11*	*2003*	*17*	*2302.7*	*5.1*	*-13.9*
180807-11-48	0.11	7.360	0.150	0.3866	0.0057	0.1404	0.0006	2155	18	2107	27	2234.7	2.7	-4.7
180807-11-10	*0.31*	*8.360*	*0.110*	*0.3928*	*0.0047*	*0.1551*	*0.0008*	*2271*	*11*	*2136*	*22*	*2406.7*	*5.6*	*-11.4*
180807-11-11	0.09	8.483	0.061	0.3997	0.0027	0.1540	0.0003	2284.3	6.6	2168	13	2390.8	1.9	-9.6
180807-11-24	0.26	8.720	0.120	0.4105	0.0053	0.1551	0.0005	2309	12	2217	24	2404.7	3.6	-7.2
180807-11-36	0.75	8.760	0.190	0.4301	0.0071	0.1494	0.0016	2319	20	2308	32	2346	12	0.3
180807-11-30	0.55	9.650	0.130	0.4514	0.0052	0.1557	0.0010	2402	12	2401	23	2411.9	8	0.8
180807-11-14	1.11	10.060	0.260	0.4597	0.0093	0.1587	0.0012	2439	24	2438	41	2442.6	9.9	1.9

Oseosan volcanic complex (180807-8; n=100)

180807-8-32	0.29	0.178	0.003	0.0261	0.0002	0.0497	0.0008	166.3	2.4	166.2	1.2	179	25	2.1
180807-8-82	0.29	0.178	0.003	0.0261	0.0002	0.0496	0.0011	166.7	2.7	166.3	1	180	36	2.0
180807-8-15	0.43	0.179	0.003	0.0262	0.0002	0.0493	0.0009	167.1	2.7	166.9	1.1	158	25	2.2
180807-8-65	0.43	0.179	0.003	0.0262	0.0002	0.0493	0.0009	167.1	2.7	167	1.1	158	25	2.2
180807-8-87	0.52	0.179	0.002	0.0263	0.0001	0.0496	0.0006	167.4	1.6	167.23	0.77	168	17	1.3
180807-8-37	0.52	0.180	0.002	0.0263	0.0001	0.0495	0.0005	168.4	1.7	167.53	0.79	170	17	1.0
180807-8-38	0.53	0.185	0.009	0.0263	0.0002	0.0502	0.0024	171.5	7.5	167.6	1.5	336	49	3.0
180807-8-88	0.54	0.185	0.008	0.0264	0.0002	0.0505	0.0022	171.6	6.8	167.6	1.3	374	46	2.4
180807-8-97	0.75	0.178	0.005	0.0264	0.0002	0.0493	0.0012	166.3	4.1	167.7	1.3	173	26	2.4
180807-8-93	0.56	0.179	0.002	0.0264	0.0002	0.0495	0.0004	167.4	1.7	168.19	0.98	171.4	7.2	1.1
180807-8-12	0.65	0.183	0.009	0.0265	0.0002	0.0498	0.0024	170.4	7.3	168.5	1.1	234	86	3.9
180807-8-43	0.55	0.180	0.002	0.0265	0.0002	0.0496	0.0003	168.2	1.4	168.69	0.95	174.6	7.8	1.1
180807-8-23	0.62	0.183	0.004	0.0265	0.0002	0.0501	0.0008	170.6	3.2	168.8	1.2	211	25	1.5
180807-8-50	1.05	0.182	0.008	0.0265	0.0003	0.0501	0.0023	170.7	7.4	168.8	1.6	330	42	4.2
180807-8-100	1.05	0.183	0.008	0.0265	0.0002	0.0501	0.0021	170.5	6.7	168.8	1.5	326	39	3.9
180807-8-62	0.65	0.178	0.009	0.0265	0.0003	0.0484	0.0023	165.8	7.4	168.9	1.6	205	70	3.6
180807-8-47	0.69	0.181	0.002	0.0266	0.0002	0.0492	0.0005	168.5	1.7	169.3	1.1	162	11	1.2
180807-8-73	0.62	0.183	0.003	0.0266	0.0002	0.0498	0.0007	170.5	2.7	169.3	1.1	204	19	1.5
180807-8-51	0.65	0.185	0.003	0.0267	0.0002	0.0499	0.0010	172	2.7	169.7	1.4	184	21	1.1
180807-8-36	0.39	0.182	0.002	0.0267	0.0002	0.0497	0.0004	170.1	1.8	169.74	0.97	177	11	1.4
180807-8-86	0.40	0.182	0.002	0.0267	0.0001	0.0497	0.0004	169.6	1.5	169.74	0.79	175	11	1.3
180807-8-1	0.65	0.184	0.003	0.0267	0.0002	0.0495	0.0009	171.7	2.6	169.9	1.3	184	21	1.2
180807-8-14	0.48	0.183	0.006	0.0267	0.0003	0.0492	0.0015	170.2	4.9	169.9	2	152	30	3.9
180807-8-53	0.33	0.187	0.004	0.0268	0.0002	0.0502	0.0009	174.1	3.2	170.6	1.1	195	29	0.5
180807-8-96	0.35	0.183	0.003	0.0268	0.0001	0.0495	0.0007	170.2	2.6	170.64	0.88	175	23	1.8
180807-8-42	0.43	0.183	0.002	0.0268	0.0002	0.0496	0.0006	170.8	1.3	170.68	0.95	184	15	1.2
180807-8-46	0.38	0.184	0.003	0.0269	0.0001	0.0495	0.0008	171.1	2.3	171.1	0.77	175	13	1.8
180807-8-3	0.33	0.187	0.004	0.0269	0.0002	0.0502	0.0009	173.8	3.5	171.3	1.3	195	28	1.3
180807-8-92	0.43	0.186	0.002	0.0270	0.0001	0.0499	0.0005	173.2	1.4	171.52	0.82	192	12	0.3
180807-8-19	0.33	0.184	0.002	0.0270	0.0002	0.0491	0.0005	171.2	1.5	171.6	1	155.6	6.4	1.2
180807-8-69	0.34	0.184	0.002	0.0270	0.0002	0.0492	0.0004	171.4	1.4	171.6	1	156	6.3	1.3
180807-8-27	0.29	0.188	0.005	0.0272	0.0002	0.0498	0.0011	174.7	4.2	172.9	1.5	200	21	2.3
180807-8-35	0.29	0.187	0.002	0.0273	0.0002	0.0500	0.0002	174.2	1.8	173.4	1.2	186.9	7	1.3
180807-8-64	0.48	0.187	0.004	0.0273	0.0002	0.0493	0.0009	174.1	3	173.6	1.2	176	21	2.1
180807-8-41	0.62	0.185	0.009	0.0274	0.0003	0.0488	0.0023	171.9	7.4	174.5	1.8	181	44	3.8
180807-8-91	0.64	0.189	0.008	0.0276	0.0003	0.0496	0.0023	175.3	6.8	175.2	1.8	179	42	4.9
180807-8-31	0.39	0.189	0.005	0.0276	0.0003	0.0491	0.0013	176.1	4.4	175.5	1.9	155	41	3.2
180807-8-77	0.39	0.192	0.004	0.0279	0.0002	0.0502	0.0010	178.2	3.2	177.3	1.2	198	20	2.0
180807-8-81	0.39	0.192	0.004	0.0279	0.0002	0.0494	0.0010	177.8	3.6	177.4	1.5	163	30	2.6
180807-8-85	0.31	0.195	0.001	0.0285	0.0002	0.0497	0.0002	181.01	0.99	181.34	0.93	182.4	5.4	0.9
180807-8-25	*0.37*	*0.331*	*0.005*	*0.0329*	*0.0003*	*0.0730*	*0.0010*	*290.2*	*4.1*	*208.7*	*1.8*	*1016*	*25*	*-36.2*
180807-8-75	*0.37*	*0.329*	*0.005*	*0.0329*	*0.0003*	*0.0727*	*0.0011*	*288.7*	*3.9*	*208.7*	*1.9*	*1003*	*25*	*-35.6*
180807-8-34	-0.33	0.254	0.023	0.0356	0.0006	0.0515	0.0050	229	18	225.7	3.8	300	130	8.2
180807-8-8	0.00	0.254	0.004	0.0363	0.0003	0.0505	0.0009	229.4	3.6	229.6	1.8	224	23	2.3
180807-8-58	0.00	0.253	0.004	0.0363	0.0003	0.0505	0.0008	229.3	3.1	229.8	1.8	221	21	1.9
180807-8-84	0.08	0.254	0.025	0.0364	0.0005	0.0498	0.0044	228	20	230.5	2.9	380	93	8.9
180807-8-22	1.77	0.638	0.013	0.0807	0.0006	0.0571	0.0012	501.1	8.2	500.3	3.5	503	30	2.2
180807-8-72	1.77	0.638	0.013	0.0807	0.0006	0.0571	0.0012	500.8	8.2	500.3	3.5	501	30	2.2
180807-8-16	*0.03*	*1.257*	*0.032*	*0.0955*	*0.0021*	*0.0949*	*0.0009*	*826*	*14*	*588*	*12*	*1522*	*15*	*-36.1*
180807-8-66	*0.05*	*1.306*	*0.032*	*0.1014*	*0.0022*	*0.0944*	*0.0015*	*848*	*14*	*622*	*13*	*1508*	*21*	*-32.0*
180807-8-17	*0.01*	*3.379*	*0.029*	*0.2247*	*0.0017*	*0.1098*	*0.0004*	*1500.4*	*7*	*1306.4*	*8.8*	*1795.5*	*3.3*	*-36.5*
180807-8-67	*0.01*	*3.379*	*0.028*	*0.2247*	*0.0016*	*0.1098*	*0.0004*	*1499.3*	*6.5*	*1306.7*	*8.5*	*1795.7*	*3.2*	*-36.5*
180807-8-98	*0.10*	*3.580*	*0.027*	*0.2364*	*0.0018*	*0.1101*	*0.0004*	*1545*	*5.9*	*1368*	*9.2*	*1801.6*	*3.6*	*-30.8*
180807-8-48	*0.11*	*3.676*	*0.032*	*0.2425*	*0.0023*	*0.1105*	*0.0004*	*1565.9*	*6.9*	*1399*	*12*	*1805.5*	*4.5*	*-27.9*
180807-8-83	*0.08*	*3.794*	*0.026*	*0.2460*	*0.0014*	*0.1122*	*0.0003*	*1591*	*5.5*	*1417.7*	*7.3*	*1834.5*	*2.3*	*-28.7*
180807-8-78	*0.34*	*3.836*	*0.030*	*0.2483*	*0.0017*	*0.1123*	*0.0004*	*1601.3*	*6.5*	*1429.6*	*8.7*	*1838.8*	*4.1*	*-27.7*
180807-8-28	*0.34*	*3.832*	*0.027*	*0.2485*	*0.0016*	*0.1121*	*0.0003*	*1599.3*	*5.6*	*1430.7*	*8.3*	*1836.3*	*3.6*	*-27.5*
180807-8-33	*0.08*	*3.861*	*0.030*	*0.2487*	*0.0017*	*0.1126*	*0.0003*	*1606.2*	*6*	*1431.8*	*8.8*	*1839.2*	*2.6*	*-27.7*
180807-8-71	*0.06*	*3.898*	*0.027*	*0.2540*	*0.0016*	*0.1112*	*0.0002*	*1613*	*5.6*	*1458.9*	*8.3*	*1819.7*	*2.1*	*-24.0*
180807-8-21	*0.06*	*3.896*	*0.027*	*0.2540*	*0.0016*	*0.1112*	*0.0002*	*1612.7*	*5.5*	*1459*	*8.2*	*1819.9*	*2.1*	*-24.0*
180807-8-44	*0.17*	*4.090*	*0.030*	*0.2660*	*0.0015*	*0.1122*	*0.0004*	*1652.1*	*5.9*	*1520.3*	*7.5*	*1839.4*	*3.7*	*-20.3*
180807-8-94	*0.17*	*4.095*	*0.030*	*0.2661*	*0.0015*	*0.1123*	*0.0004*	*1653*	*5.9*	*1520.7*	*7.5*	*1839.9*	*3.7*	*-20.3*
180807-8-6	*0.04*	*4.335*	*0.037*	*0.2823*	*0.0022*	*0.1114*	*0.0002*	*1701*	*7.2*	*1602*	*11*	*1823.3*	*2.3*	*-13.0*
180807-8-56	*0.04*	*4.333*	*0.037*	*0.2824*	*0.0022*	*0.1114*	*0.0002*	*1701.2*	*7.2*	*1603*	*11*	*1822.9*	*2.3*	*-12.9*
180807-8-79	0.26	4.657	0.031	0.3008	0.0019	0.1127	0.0002	1759	5.6	1694.9	9.5	1842.6	1.9	-8.0
180807-8-39	0.06	4.705	0.073	0.3041	0.0045	0.1130	0.0005	1768	13	1712	22	1846.4	4.4	-6.3
180807-8-40	0.06	4.880	0.033	0.3063	0.0020	0.1153	0.0004	1798.7	5.7	1723	10	1886	3.7	-8.7
180807-8-89	0.06	4.799	0.085	0.3068	0.0058	0.1138	0.0004	1784	15	1725	29	1860.2	4.3	-5.9
180807-8-4	*0.07*	*5.847*	*0.054*	*0.3075*	*0.0028*	*0.1383*	*0.0006*	*1953.1*	*8.1*	*1728*	*14*	*2207.7*	*6.2*	*-26.6*
180807-8-54	*0.07*	*5.913*	*0.083*	*0.3095*	*0.0035*	*0.1380*	*0.0007*	*1963*	*12*	*1738*	*17*	*2203.2*	*6.7*	*-25.4*
180807-8-29	0.28	4.867	0.085	0.3121	0.0048	0.1129	0.0005	1796	15	1751	23	1850.8	3.2	-4.2
180807-8-90	0.06	5.056	0.068	0.3165	0.0039	0.1159	0.0005	1829	11	1773	19	1894.7	2.7	-5.6
180807-8-10	0.38	4.957	0.069	0.3222	0.0051	0.1120	0.0007	1812	12	1800	25	1831.8	6.3	0.0
180807-8-60	0.38	4.979	0.065	0.3233	0.0047	0.1121	0.0007	1816	11	1806	23	1833.3	6.5	0.1
180807-8-99	0.31	5.024	0.085	0.3242	0.0054	0.1133	0.0008	1823	14	1810	26	1852.5	5.5	-0.6
180807-8-49	0.31	5.017	0.091	0.3252	0.0049	0.1136	0.0010	1822	15	1815	24	1857.1	8.6	-0.5
180807-8-13	0.20	5.034	0.066	0.3254	0.0040	0.1126	0.0005	1825	11	1816	19	1841.7	3.9	-0.2
180807-8-76	0.42	5.040	0.033	0.3264	0.0038	0.1130	0.0009	1826.1	5.5	1821	18	1850.2	6.8	-0.2
180807-8-26	0.42	5.044	0.036	0.3270	0.0040	0.1129	0.0010	1826.8	6	1824	19	1846.1	8.8	0.3
180807-8-63	0.20	5.071	0.062	0.3273	0.0039	0.1126	0.0005	1831	10	1825	19	1843.3	3.3	0.2
180807-8-95	0.73	5.052	0.063	0.3277	0.0040	0.1130	0.0003	1828	11	1827	19	1846.1	4.1	0.2
180807-8-45	0.72	5.068	0.065	0.3283	0.0041	0.1130	0.0003	1830	11	1830	20	1847.7	3.6	0.3
180807-8-57	0.35	5.088	0.044	0.3282	0.0030	0.1131	0.0004	1833.9	7.4	1830	14	1851.7	3.8	-0.2
180807-8-2	0.14	5.154	0.043	0.3294	0.0028	0.1140	0.0003	1844.8	7.1	1835	13	1861.1	3	-0.6
180807-8-52	0.14	5.151	0.045	0.3294	0.0028	0.1139	0.0003	1844.3	7.5	1836	14	1860.6	3	-0.4
180807-8-7	0.36	5.138	0.055	0.3297	0.0038	0.1135	0.0004	1842.1	9.1	1837	18	1856.3	3.3	0.1
180807-8-70	0.51	5.098	0.067	0.3297	0.0053	0.1135	0.0008	1835	11	1837	25	1858.6	8.8	0.7
180807-8-24	0.22	5.166	0.051	0.3321	0.0033	0.1139	0.0007	1846.7	8.3	1848	16	1863.8	5.8	0.3
180807-8-5	0.62	5.227	0.041	0.3324	0.0025	0.1139	0.0004	1856.4	6.6	1850	12	1861.9	3.2	0.2
180807-8-55	0.62	5.224	0.039	0.3324	0.0025	0.1139	0.0003	1856	6.4	1850	12	1861.5	3	0.2
180807-8-20	0.51	5.155	0.099	0.3330	0.0067	0.1135	0.0009	1850	18	1852	32	1862.3	9.7	1.7
180807-8-74	0.21	5.207	0.045	0.3341	0.0030	0.1143	0.0006	1853.5	7.3	1858	15	1870	5	0.4
180807-8-59	0.01	5.316	0.051	0.3354	0.0034	0.1153	0.0003	1871.3	8.1	1864	16	1885.8	2.4	-0.2
180807-8-9	0.01	5.317	0.052	0.3356	0.0035	0.1153	0.0003	1871.5	8.4	1865	17	1885.6	2.3	-0.1
180807-8-18	0.58	6.770	0.120	0.3796	0.0066	0.1287	0.0008	2081	16	2074	31	2079.3	9.4	1.7
180807-8-68	0.58	6.780	0.130	0.3807	0.0067	0.1286	0.0008	2082	17	2079	31	2081.6	7.8	1.7
180807-8-61	0.55	9.390	0.110	0.4286	0.0036	0.1598	0.0009	2376	11	2299	16	2455.6	8.3	-5.8
180807-8-11	0.55	9.430	0.110	0.4292	0.0036	0.1598	0.0009	2380	11	2302	16	2457.7	7.2	-5.8
180807-8-80	*0.08*	*14.790*	*0.120*	*0.5009*	*0.0034*	*0.2137*	*0.0006*	*2801.2*	*7.6*	*2618*	*15*	*2934.3*	*4*	*-11.4*
180807-8-30	*0.09*	*15.170*	*0.150*	*0.5050*	*0.0044*	*0.2161*	*0.0008*	*2828*	*10*	*2635*	*19*	*2952*	*3.8*	*-11.2*

Tongjin Fm. (n=100)

181007-2-68	*1.37*	*0.441*	*0.011*	*0.0502*	*0.0008*	*0.0639*	*0.0018*	*371.9*	*7.7*	*315.9*	*4.7*	*734*	*47*	*-13.8*
181007-2-42	0.50	0.420	0.017	0.0552	0.0007	0.0540	0.0023	355	12	346.5	4.5	361	44	2.3
181007-2-94	0.62	0.405	0.011	0.0556	0.0007	0.0532	0.0014	345.1	8	349	4.2	352	34	2.4
181007-2-15	0.37	0.410	0.014	0.0563	0.0015	0.0539	0.0015	349	10	353	9	397	34	4.3
181007-2-54	0.55	0.418	0.010	0.0568	0.0009	0.0536	0.0009	354.3	6.8	355.9	5.6	360	27	3.0
181007-2-73	0.47	0.433	0.011	0.0570	0.0008	0.0548	0.0015	365.2	7.8	357	4.6	393	33	1.2
181007-2-100	0.38	0.421	0.007	0.0571	0.0005	0.0540	0.0009	357.2	5.2	357.9	2.7	376	20	2.0
181007-2-88	0.50	0.439	0.026	0.0575	0.0010	0.0560	0.0035	367	19	360.2	6.1	533	77	5.1
181007-2-50	0.31	0.434	0.008	0.0576	0.0007	0.0548	0.0007	365.9	6	361	4.1	400	18	1.4
181007-2-70	0.40	0.439	0.008	0.0581	0.0005	0.0542	0.0008	369.7	5.4	364	3.2	398	24	0.8
181007-2-82	0.68	0.452	0.006	0.0603	0.0006	0.0545	0.0007	378.6	4.2	377.6	3.4	393	11	1.7
181007-2-26	0.65	0.459	0.007	0.0614	0.0004	0.0541	0.0008	382.9	5.2	384	2.4	380	18	1.7
181007-2-55	0.45	0.459	0.020	0.0617	0.0006	0.0545	0.0022	383	14	386.2	3.9	428	42	3.8
181007-2-40	0.46	0.477	0.011	0.0618	0.0007	0.0556	0.0011	397.1	7.9	386.7	4.5	442	21	0.5
181007-2-74	1.38	0.476	0.011	0.0627	0.0009	0.0537	0.0010	395	7.9	391.7	5.5	368	20	2.6
181007-2-59	0.72	0.490	0.012	0.0649	0.0010	0.0566	0.0016	406.3	9.1	405.5	6.1	480	32	3.6
181007-2-5	0.35	0.501	0.004	0.0655	0.0005	0.0555	0.0004	412.5	2.8	408.8	2.9	423	11	0.5
181007-2-25	0.62	0.507	0.007	0.0666	0.0008	0.0555	0.0006	417.6	4.3	415.8	4.7	429	16	1.7
181007-2-1	0.52	0.512	0.005	0.0669	0.0005	0.0557	0.0004	419.4	3.6	417.4	3.1	436.6	9.3	1.1
181007-2-9	0.92	0.509	0.009	0.0669	0.0008	0.0555	0.0006	417.4	5.7	417.4	4.8	436	13	2.5
181007-2-69	0.74	0.515	0.005	0.0672	0.0005	0.0551	0.0004	422.1	3.4	419.4	2.8	415.2	8.6	0.8
181007-2-2	0.70	0.518	0.007	0.0677	0.0005	0.0551	0.0008	423.6	5	422.3	2.9	421	18	1.6
181007-2-52	0.31	0.522	0.009	0.0679	0.0006	0.0559	0.0008	426.3	6	423.4	3.8	439	19	1.6
181007-2-35	0.53	0.526	0.008	0.0684	0.0007	0.0550	0.0007	428.7	5.4	426.2	3.9	420	18	1.6
181007-2-57	0.12	0.525	0.006	0.0687	0.0006	0.0559	0.0005	428.6	4.2	428.4	3.6	449.2	9.7	1.8
181007-2-22	0.33	0.529	0.005	0.0689	0.0005	0.0557	0.0003	431.3	3.1	429.8	3.3	435.1	8.4	1.1
181007-2-17	0.48	0.538	0.008	0.0701	0.0005	0.0557	0.0008	437	5.1	436.8	3.2	440	16	1.9
181007-2-23	0.03	0.539	0.011	0.0702	0.0007	0.0560	0.0010	437.2	7.4	437.4	4.3	445	27	2.6
181007-2-37	0.98	0.574	0.016	0.0726	0.0006	0.0566	0.0015	460	10	451.5	3.6	500	34	1.1
181007-2-28	0.49	0.580	0.009	0.0742	0.0011	0.0561	0.0008	463.9	6	461.4	6.4	460	23	2.1
181007-2-58	0.41	0.588	0.019	0.0754	0.0021	0.0579	0.0007	469	12	468	12	525.4	6.4	4.9
181007-2-20	0.04	0.867	0.043	0.1042	0.0023	0.0609	0.0025	634	24	639	13	655	51	5.0
181007-2-38	0.62	1.095	0.027	0.1206	0.0014	0.0659	0.0017	750	13	733.8	8.3	808	27	0.7
181007-2-16	0.55	1.113	0.020	0.1255	0.0019	0.0651	0.0007	759.1	9.5	762	11	782	15	2.3
181007-2-46	0.74	1.141	0.023	0.1259	0.0014	0.0651	0.0013	772	11	764.6	*7.9*	789	23	1.5
181007-2-60	0.84	1.193	0.015	0.1313	0.0012	0.0662	0.0006	796.9	7.2	795	7	812.3	9.1	1.5
181007-2-14	0.15	1.371	0.035	0.1353	0.0028	0.0745	0.0006	875	14	820	15	1060	13	-3.2
181007-2-33	*0.04*	*1.832*	*0.014*	*0.1439*	*0.0011*	*0.0915*	*0.0003*	*1056.9*	*5*	*866.4*	*6.2*	*1454.5*	*3.7*	*-20.7*
181007-2-79	0.73	1.408	0.024	0.1478	0.0015	0.0689	0.0011	891	10	888.5	8.1	891	20	1.8
181007-2-45	0.78	1.514	0.015	0.1556	0.0013	0.0698	0.0004	935.8	6.1	932.5	7.2	930.8	8.1	1.1
181007-2-75	0.53	1.541	0.018	0.1566	0.0015	0.0711	0.0005	946	7.4	937.8	8.6	963.1	7.7	0.8
181007-2-6	0.20	1.530	0.018	0.1568	0.0018	0.0705	0.0004	941.9	7.3	939	10	942.4	7.1	1.5
181007-2-77	0.49	1.538	0.013	0.1574	0.0010	0.0708	0.0004	946	5.2	942.2	5.6	953	5.8	0.7
181007-2-71	0.52	1.547	0.028	0.1574	0.0017	0.0702	0.0011	949	11	942.4	9.3	934	19	1.5
181007-2-89	0.52	1.552	0.019	0.1580	0.0014	0.0712	0.0005	951	7.4	945.7	8	962.1	7.9	1.1
181007-2-48	0.11	1.569	0.020	0.1594	0.0017	0.0709	0.0006	957.5	7.7	953.5	9.6	948	12	1.4
181007-2-62	0.65	1.572	0.018	0.1595	0.0016	0.0717	0.0004	960.5	6.9	954.1	9.2	980	5.8	1.0
181007-2-81	0.17	1.593	0.018	0.1612	0.0012	0.0715	0.0006	967	7.1	963.2	6.6	974	10	1.0
181007-2-10	0.14	1.934	0.043	0.1859	0.0035	0.0761	0.0012	1094	14	1099	19	1103	18	3.0
181007-2-11	0.21	1.985	0.024	0.1888	0.0030	0.0775	0.0008	1110.2	8.3	1115	16	1141	13	0.3
181007-2-78	0.09	2.032	0.025	0.1910	0.0019	0.0776	0.0004	1125.6	8.5	1127	10	1133.5	7	0.9
181007-2-92	0.64	2.106	0.036	0.1934	0.0024	0.0795	0.0013	1150	12	1139	13	1175	19	-0.4
181007-2-90	0.88	2.123	0.088	0.1956	0.0054	0.0837	0.0017	1164	27	1150	30	1274	28	-5.7
181007-2-83	0.25	2.235	0.029	0.1953	0.0016	0.0829	0.0006	1191.7	9	1150.1	8.6	1270.2	7.8	-9.0
181007-2-84	0.68	2.491	0.043	0.2173	0.0022	0.0832	0.0011	1269	12	1268	12	1266	17	2.1
181007-2-63	*0.02*	*4.006*	*0.047*	*0.2312*	*0.0029*	*0.1254*	*0.0006*	*1635.2*	*9.6*	*1341*	*15*	*2034*	*5.9*	*-50.1*
181007-2-39	*1.06*	*3.437*	*0.046*	*0.2387*	*0.0025*	*0.1030*	*0.0007*	*1512*	*10*	*1380*	*13*	*1675.4*	*8.2*	*-19.9*
181007-2-36	*0.47*	*4.360*	*0.110*	*0.2465*	*0.0050*	*0.1263*	*0.0009*	*1703*	*21*	*1420*	*26*	*2043.8*	*8.4*	*-41.5*
181007-2-47	0.67	3.205	0.025	0.2523	0.0017	0.0917	0.0002	1459.1	5.9	1450.2	8.9	1461.8	2.7	0.0
181007-2-95	1.15	3.630	0.024	0.2692	0.0016	0.0982	0.0004	1555.8	5.3	1536.6	8.1	1589.9	4.1	-2.7
181007-2-56	0.71	3.777	0.094	0.2788	0.0048	0.0986	0.0014	1588	20	1585	24	1600	12	1.3
181007-2-12	*1.02*	*4.300*	*0.110*	*0.2821*	*0.0074*	*0.1125*	*0.0017*	*1691*	*21*	*1601*	*37*	*1842*	*15*	*-11.8*
181007-2-98	*0.14*	*4.350*	*0.030*	*0.2825*	*0.0016*	*0.1123*	*0.0004*	*1702.4*	*5.8*	*1604.6*	*8.3*	*1838.1*	*3.1*	*-13.8*
181007-2-96	*0.74*	*4.473*	*0.031*	*0.2903*	*0.0016*	*0.1122*	*0.0003*	*1725.5*	*5.7*	*1643*	*8*	*1835.3*	*3.2*	*-11.0*
181007-2-80	0.64	4.630	0.055	0.2986	0.0031	0.1121	0.0005	1753.2	9.8	1684	15	1836.7	4.9	-7.9
181007-2-24	0.78	4.293	0.078	0.2991	0.0040	0.1033	0.0010	1692	15	1687	20	1686	11	1.8
181007-2-72	1.08	4.711	0.056	0.3123	0.0031	0.1085	0.0006	1769	10	1752	15	1773.8	5.5	-0.1
181007-2-41	0.30	4.952	0.038	0.3137	0.0022	0.1128	0.0005	1810.9	6.5	1759	11	1846.3	4.5	-4.1
181007-2-43	-0.25	4.944	0.084	0.3138	0.0049	0.1132	0.0011	1809	14	1759	24	1849.7	9.1	-3.3
181007-2-13	*0.62*	*5.957*	*0.088*	*0.3145*	*0.0046*	*0.1387*	*0.0006*	*1971*	*12*	*1765*	*22*	*2208.8*	*5*	*-23.6*
181007-2-99	1.00	4.670	0.120	0.3179	0.0060	0.1083	0.0025	1762	21	1779	29	1768	22	2.3
181007-2-53	0.10	5.172	0.040	0.3233	0.0022	0.1162	0.0002	1847.5	6.6	1806	11	1899.9	1.8	-4.5
181007-2-4	0.73	5.104	0.053	0.3277	0.0030	0.1120	0.0007	1836.1	8.7	1827	14	1834.9	7.8	0.8
181007-2-64	0.22	5.183	0.070	0.3295	0.0043	0.1137	0.0004	1849	12	1836	21	1858.4	3.6	0.1
181007-2-49	0.07	5.173	0.043	0.3299	0.0027	0.1134	0.0003	1847.4	7.2	1837	13	1854.1	2.2	-0.1
181007-2-7	0.41	5.180	0.038	0.3313	0.0021	0.1136	0.0003	1849.7	6.3	1844	10	1859.6	3.2	-0.1
181007-2-18	0.27	5.301	0.059	0.3351	0.0031	0.1154	0.0010	1868.2	9.6	1863	15	1880.7	7.4	0.3
181007-2-91	0.23	5.343	0.077	0.3367	0.0031	0.1152	0.0011	1875	12	1870	15	1880	10	0.8
181007-2-30	0.54	5.351	0.089	0.3371	0.0036	0.1149	0.0014	1876	14	1873	17	1879	10	1.1
181007-2-65	0.11	5.510	0.100	0.3417	0.0063	0.1164	0.0003	1900	16	1894	30	1900.8	2.3	1.3
181007-2-8	0.21	5.935	0.080	0.3498	0.0042	0.1230	0.0006	1966	12	1933	20	1998.9	6.4	-2.0
181007-2-34	0.62	5.998	0.085	0.3588	0.0048	0.1196	0.0006	1975	12	1976	23	1952.9	5.1	0.3
181007-2-31	0.98	6.510	0.130	0.3724	0.0080	0.1258	0.0009	2049	19	2040	38	2039.9	9.5	2.3
181007-2-93	0.58	8.692	0.077	0.4218	0.0029	0.1497	0.0007	2305.6	8	2270	13	2341.4	4.5	-2.4
181007-2-67	0.22	8.590	0.300	0.4260	0.0130	0.1467	0.0020	2291	32	2284	60	2311	12	2.0
181007-2-44	0.63	9.600	0.200	0.4325	0.0092	0.1599	0.0011	2396	19	2316	41	2450.2	7.8	-3.7
181007-2-87	1.32	9.717	0.063	0.4423	0.0025	0.1589	0.0004	2408	6	2361	11	2442	2.8	-2.8
181007-2-29	0.20	9.718	0.099	0.4517	0.0042	0.1557	0.0004	2409.5	9.1	2402	19	2409.4	2.6	0.6
181007-2-85	0.64	10.098	0.079	0.4530	0.0032	0.1620	0.0005	2443.8	7.1	2408	14	2476.5	3.3	-2.1
181007-2-66	0.61	10.142	0.098	0.4600	0.0034	0.1586	0.0008	2447.5	9	2440	15	2443	4.8	0.7
181007-2-86	0.14	10.970	0.130	0.4606	0.0051	0.1717	0.0007	2520	11	2442	23	2573.8	5.5	-4.2
181007-2-51	0.68	10.347	0.078	0.4658	0.0032	0.1614	0.0003	2466.6	6.9	2465	14	2469.4	2	0.5
181007-2-3	0.14	10.600	0.260	0.4710	0.0100	0.1626	0.0005	2490	22	2487	46	2484.5	4.2	1.9
181007-2-61	0.60	10.830	0.110	0.4724	0.0047	0.1665	0.0008	2508	9.8	2496	20	2523.6	3.7	-0.2
181007-2-76	0.40	10.914	0.094	0.4737	0.0041	0.1661	0.0006	2515.6	8	2500	18	2520.2	3.4	0.0
181007-2-97	0.80	10.920	0.130	0.4746	0.0056	0.1678	0.0010	2516	11	2503	25	2537.8	5.9	-0.2
181007-2-27	0.41	11.020	0.210	0.4747	0.0094	0.1669	0.0013	2525	18	2519	48	2527.1	5.7	1.8
181007-2-32	0.97	11.585	0.099	0.4924	0.0039	0.1693	0.0003	2570.9	8.1	2580	17	2551.3	2.1	-0.4
181007-2-21	0.82	13.560	0.360	0.5178	0.0094	0.1893	0.0040	2732	33	2690	40	2733	21	0.7
181007-2-19	0.54	15.180	0.110	0.5468	0.0041	0.2013	0.0008	2826.4	7.1	2811	17	2834.4	3.5	-0.1

Munsusan Fm. (n=100)

180504-6-f-5	0.84	0.241	0.008	0.0346	0.0002	0.0502	0.0015	218.5	6.5	219.4	1.4	242	43	3.2
180504-6-f-35	0.97	0.254	0.006	0.0362	0.0002	0.0509	0.0011	229.7	4.6	229.4	1.4	237	24	2.5
180504-6-f-39	1.02	0.443	0.005	0.0594	0.0003	0.0540	0.0006	371.9	3.5	371.8	1.7	365	16	1.4
180504-6-f-30	0.21	0.474	0.005	0.0629	0.0009	0.0545	0.0012	393.8	3.5	393.1	5.5	410	42	2.1
180504-6-f-86	1.09	0.489	0.009	0.0648	0.0004	0.0553	0.0010	403.8	5.9	404.6	2.7	430	21	1.9
180504-6-f-25	0.78	0.509	0.005	0.0670	0.0003	0.0549	0.0005	417.8	3.4	417.9	1.9	417	11	1.2
180504-6-f-47	0.52	0.515	0.009	0.0674	0.0005	0.0556	0.0009	421.8	6.2	420.6	2.7	444	21	1.8
180504-6-f-71	0.46	0.524	0.007	0.0683	0.0006	0.0559	0.0005	427.5	4.5	425.7	3.8	433	12	1.5
180504-6-f-97	0.45	0.520	0.017	0.0683	0.0014	0.0548	0.0015	428	12	425.5	8.3	421	33	4.2
180504-6-f-58	0.56	0.522	0.006	0.0683	0.0004	0.0558	0.0006	426.7	3.7	426	2.6	450.7	9.4	1.3
180504-6-f-40	0.17	0.525	0.009	0.0684	0.0005	0.0551	0.0008	428	6	426.3	2.7	422	16	1.6
180504-6-f-33	0.85	0.522	0.006	0.0684	0.0004	0.0552	0.0006	426.9	3.9	426.4	2.3	422	14	1.3
180504-6-f-24	0.27	0.525	0.007	0.0687	0.0004	0.0555	0.0007	429.3	4.7	428.5	2.2	429	21	1.4
180504-6-f-44	0.82	0.526	0.008	0.0687	0.0005	0.0555	0.0007	429	5.6	428.6	3.1	431	14	1.9
180504-6-f-42	0.44	0.529	0.008	0.0689	0.0008	0.0559	0.0006	431	5.1	429.8	4.9	440	13	2.0
180504-6-f-65	0.11	0.527	0.008	0.0689	0.0005	0.0554	0.0008	429.4	5.5	429.7	3.2	437	19	2.0
180504-6-f-46	0.40	0.538	0.006	0.0699	0.0005	0.0560	0.0005	437.2	3.9	435.6	2.7	437	13	1.1
180504-6-f-63	0.15	0.546	0.005	0.0711	0.0004	0.0558	0.0005	442.2	3.4	442.7	2.6	448	11	1.2
180504-6-f-21	0.74	0.552	0.011	0.0719	0.0005	0.0555	0.0012	446.2	7.4	447.4	2.7	438	35	2.0
180504-6-f-20	0.09	0.691	0.014	0.0825	0.0012	0.0612	0.0007	533.2	8.3	511.1	7.4	631	18	-1.3
180504-6-f-59	0.22	0.671	0.007	0.0842	0.0007	0.0584	0.0005	522.2	4	521	4.1	542	13	1.3
180504-6-f-34	0.85	0.676	0.007	0.0847	0.0005	0.0575	0.0005	524.7	4.2	524.2	3.2	520	9.6	1.3
180504-6-f-76	0.41	0.694	0.013	0.0856	0.0006	0.0582	0.0009	535.1	7.6	529.5	3.3	537	18	1.0
180504-6-f-74	0.01	0.723	0.010	0.0891	0.0008	0.0591	0.0008	552	6.2	550	4.7	577	16	1.6
180504-6-f-38	0.23	0.864	0.011	0.1031	0.0011	0.0607	0.0004	632.3	6.2	632.3	6.6	632	6.3	2.0
180504-6-f-56	*0.08*	*1.455*	*0.023*	*0.1150*	*0.0011*	*0.0924*	*0.0011*	*911.5*	*9.3*	*701.9*	*6.6*	*1475*	*18*	*-27.6*
180504-6-f-53	*0.18*	*1.744*	*0.045*	*0.1234*	*0.0035*	*0.1020*	*0.0006*	*1024*	*17*	*750*	*20*	*1657.1*	*4.5*	*-31.6*
180504-6-f-27	1.32	1.153	0.023	0.1280	0.0012	0.0654	0.0013	778	11	776.6	7.1	782	25	2.2
180504-6-f-64	0.63	1.168	0.011	0.1296	0.0009	0.0657	0.0004	785.3	5.3	785.6	5.1	802.7	8	1.3
180504-6-f-50	0.32	1.440	0.036	0.1496	0.0018	0.0699	0.0016	905	15	899	10	927	23	2.1
180504-6-f-57	0.46	1.438	0.020	0.1505	0.0017	0.0702	0.0005	904.7	8.2	903.8	9.3	935.6	6.6	1.8
180504-6-f-13	0.15	1.487	0.012	0.1542	0.0009	0.0701	0.0004	924.9	5.1	924.1	5.2	926.8	6.6	1.0
180504-6-f-7	1.87	1.540	0.011	0.1583	0.0008	0.0712	0.0004	946.8	4.3	947.1	4.3	959	6.6	0.9
180504-6-f-90	0.59	1.548	0.045	0.1584	0.0022	0.0714	0.0019	952	18	948	12	968	28	2.7
180504-6-f-17	0.29	1.552	0.015	0.1590	0.0013	0.0704	0.0002	950.9	5.9	951.4	7.4	940.1	3.2	1.3
180504-6-f-52	0.55	1.555	0.027	0.1593	0.0012	0.0703	0.0012	952	11	952.6	6.9	946	24	1.8
180504-6-f-60	0.04	1.554	0.013	0.1593	0.0010	0.0715	0.0004	952	5.1	952.8	5.8	970.5	5.5	1.1
180504-6-f-83	0.74	1.565	0.011	0.1598	0.0008	0.0710	0.0004	956.2	4.3	955.6	4.4	955.6	6.5	0.8
180504-6-f-41	0.48	1.579	0.022	0.1609	0.0014	0.0711	0.0010	961.6	8.6	961.5	7.6	968	11	1.7
180504-6-f-22	0.13	1.587	0.017	0.1615	0.0013	0.0709	0.0005	965.1	6.6	965.3	7.2	954	6	1.4
180504-6-f-85	0.15	1.665	0.030	0.1661	0.0016	0.0725	0.0010	995	11	990.7	8.6	1005	16	1.5
180504-6-f-69	0.18	1.674	0.017	0.1674	0.0015	0.0722	0.0006	998.5	6.5	997.7	8.2	996	11	1.4
180504-6-f-23	0.25	1.747	0.038	0.1725	0.0034	0.0737	0.0005	1026	14	1025	19	1035.6	7.5	1.6
180504-6-f-70	0.57	1.907	0.025	0.1825	0.0015	0.0751	0.0009	1083.4	8.7	1080.8	8.1	1081	11	1.7
180504-6-f-15	*0.23*	*2.303*	*0.041*	*0.1845*	*0.0029*	*0.0908*	*0.0006*	*1213*	*13*	*1092*	*16*	*1439.2*	*9.2*	*-29.5*
180504-6-f-81	0.25	1.980	0.020	0.1876	0.0018	0.0766	0.0004	1108.9	6.7	1108.3	9.7	1107.3	6.2	1.3
180504-6-f-18	0.35	1.983	0.040	0.1880	0.0018	0.0766	0.0010	1109	14	1110.5	9.5	1110	11	1.8
180504-6-f-98	0.30	2.023	0.044	0.1907	0.0031	0.0777	0.0010	1126	14	1125	17	1145	18	1.3
180504-6-f-26	0.54	2.135	0.043	0.1939	0.0040	0.0798	0.0005	1160	14	1142	22	1193.2	6.8	-2.0
180504-6-f-54	1.18	2.193	0.021	0.2003	0.0012	0.0802	0.0006	1178.2	6.8	1176.8	6.5	1201.3	8.4	-0.8
180504-6-f-37	0.25	2.206	0.035	0.2017	0.0022	0.0794	0.0009	1183	11	1184	12	1180.6	8.8	1.5
180504-6-f-32	0.57	2.231	0.020	0.2031	0.0013	0.0796	0.0006	1190.6	6.2	1192.1	7.2	1180.8	9.5	0.5
180504-6-f-31	0.52	2.257	0.017	0.2045	0.0012	0.0799	0.0003	1198.7	5.2	1199.1	6.5	1193.8	5.3	0.5
180504-6-f-77	0.37	2.315	0.022	0.2077	0.0017	0.0809	0.0005	1217.8	6.7	1216.6	9	1226.3	6	0.4
180504-6-f-91	0.05	2.491	0.047	0.2167	0.0024	0.0832	0.0010	1269	14	1264	13	1275.5	6.6	0.6
180504-6-f-66	1.05	2.510	0.031	0.2186	0.0023	0.0835	0.0006	1274	8.8	1274	12	1282.4	7.7	0.9
180504-6-f-14	*0.67*	*3.980*	*0.041*	*0.2226*	*0.0020*	*0.1300*	*0.0005*	*1631.2*	*8.6*	*1296*	*11*	*2094.6*	*4.2*	*-60.4*
180504-6-f-79	0.87	2.585	0.023	0.2227	0.0017	0.0837	0.0004	1295.8	6.5	1295.9	9.2	1287.4	5.3	0.5
180504-6-f-36	0.47	2.600	0.046	0.2237	0.0041	0.0845	0.0005	1300	13	1301	22	1305.4	5.1	1.7
180504-6-f-82	1.53	3.198	0.037	0.2422	0.0023	0.0947	0.0003	1457.3	9	1400	11	1523.9	4.8	-7.7
180504-6-f-4	0.23	3.410	0.050	0.2564	0.0056	0.0963	0.0017	1507	12	1471	29	1546.1	8.8	-2.5
180504-6-f-55	*0.04*	*4.001*	*0.065*	*0.2706*	*0.0034*	*0.1075*	*0.0008*	*1634*	*13*	*1544*	*17*	*1756.3*	*9*	*-12.1*
180504-6-f-96	0.82	3.874	0.067	0.2821	0.0023	0.0992	0.0015	1608	14	1602	11	1614	20	1.2
180504-6-f-8	*0.87*	*5.239*	*0.071*	*0.2878*	*0.0026*	*0.1331*	*0.0011*	*1861*	*12*	*1630*	*13*	*2139*	*10*	*-29.8*
180504-6-f-51	*0.07*	*4.607*	*0.043*	*0.2916*	*0.0025*	*0.1148*	*0.0004*	*1750.2*	*7.7*	*1649*	*12*	*1874.9*	*4.4*	*-12.7*
180504-6-f-84	0.29	4.298	0.043	0.3001	0.0028	0.1037	0.0005	1693.1	8.4	1692	14	1690.5	5	1.0
180504-6-f-6	0.56	4.762	0.042	0.3073	0.0024	0.1128	0.0004	1779.1	7.2	1727	12	1845.2	3.5	-5.9
180504-6-f-43	0.12	4.811	0.034	0.3074	0.0020	0.1133	0.0005	1786.4	6	1727.7	9.7	1853.3	4.6	-6.4
180504-6-f-29	0.05	4.550	0.100	0.3087	0.0041	0.1075	0.0004	1739	19	1734	20	1758.6	5.4	0.0
180504-6-f-2	0.47	4.800	0.170	0.3096	0.0080	0.1124	0.0021	1784	29	1738	39	1837	11	-2.8
180504-6-f-68	*0.65*	*6.722*	*0.094*	*0.3102*	*0.0032*	*0.1571*	*0.0010*	*2077*	*12*	*1742*	*16*	*2429.4*	*6.5*	*-38.2*
180504-6-f-28	0.07	5.020	0.045	0.3267	0.0024	0.1113	0.0003	1823.7	7.8	1822	12	1823.3	2.7	0.7
180504-6-f-100	0.23	5.040	0.027	0.3271	0.0019	0.1120	0.0003	1826.2	4.6	1824.2	9.2	1833.5	3.1	0.2
180504-6-f-62	0.22	5.033	0.035	0.3273	0.0020	0.1119	0.0003	1824.4	5.8	1825.3	9.9	1831.3	2.6	0.4
180504-6-f-94	0.40	5.053	0.043	0.3276	0.0023	0.1121	0.0005	1828.2	7.1	1827	11	1830.2	4.1	0.7
180504-6-f-16	*0.34*	*6.115*	*0.076*	*0.3281*	*0.0032*	*0.1356*	*0.0008*	*1992*	*11*	*1829*	*16*	*2173.9*	*8.1*	*-17.5*
180504-6-f-19	0.49	5.138	0.054	0.3308	0.0036	0.1122	0.0009	1842.1	9	1842	18	1837.2	7.5	1.1
180504-6-f-72	0.07	5.193	0.056	0.3318	0.0038	0.1128	0.0003	1850.7	9.2	1847	18	1843.2	2.5	0.9
180504-6-f-73	0.36	5.173	0.050	0.3319	0.0026	0.1123	0.0007	1847.9	8.2	1848	13	1835.5	7.1	0.4
180504-6-f-92	0.29	5.170	0.050	0.3319	0.0027	0.1130	0.0005	1848.4	8	1850	13	1847.4	5.3	0.8
180504-6-f-87	0.22	5.226	0.056	0.3326	0.0025	0.1135	0.0008	1856.7	9	1851	12	1852.4	6.8	0.9
180504-6-f-78	0.46	5.234	0.059	0.3340	0.0029	0.1131	0.0009	1857.8	9.5	1858	14	1843.4	8.2	0.4
180504-6-f-88	0.14	5.291	0.046	0.3354	0.0028	0.1146	0.0004	1867	7.5	1866	14	1873.1	3.3	0.5
180504-6-f-12	0.15	5.286	0.088	0.3372	0.0052	0.1142	0.0007	1866	14	1873	25	1864.6	8	1.3
180504-6-f-9	0.37	5.317	0.066	0.3386	0.0042	0.1139	0.0006	1871	10	1880	20	1860.3	6.9	0.4
180504-6-f-95	0.21	5.794	0.095	0.3521	0.0055	0.1193	0.0003	1943	14	1943	26	1946.6	3	1.3
180504-6-f-1	*0.41*	*7.625*	*0.072*	*0.3577*	*0.0046*	*0.1543*	*0.0015*	*2187.8*	*8.5*	*1971*	*22*	*2395*	*12*	*-19.8*
180504-6-f-48	0.22	8.339	0.070	0.4005	0.0028	0.1507	0.0006	2267.9	7.6	2171	13	2354	4.3	-7.6
180504-6-f-67	0.81	9.050	0.150	0.4364	0.0063	0.1510	0.0016	2342	15	2334	28	2346	15	1.3
180504-6-f-3	0.63	9.938	0.076	0.4397	0.0027	0.1633	0.0005	2428.6	7	2349	12	2491.9	2.9	-5.4
180504-6-f-10	0.22	9.991	0.068	0.4587	0.0026	0.1590	0.0004	2434.5	6.1	2434	12	2443.9	2.4	0.2
180504-6-f-49	0.88	10.579	0.088	0.4697	0.0030	0.1639	0.0007	2486.2	7.7	2484	14	2497	4.7	0.2
180504-6-f-80	0.22	10.660	0.180	0.4713	0.0062	0.1651	0.0016	2494	16	2489	27	2509.3	9.2	0.6
180504-6-f-89	0.35	10.710	0.110	0.4722	0.0044	0.1642	0.0005	2498.2	9.2	2493	19	2498.3	2.9	0.7
180504-6-f-61	0.47	10.722	0.094	0.4737	0.0037	0.1641	0.0006	2498.9	8.1	2500	16	2499.6	2.3	0.7
180504-6-f-75	0.43	10.980	0.140	0.4777	0.0053	0.1659	0.0009	2523	11	2517	23	2519.2	5.6	1.0
180504-6-f-11	0.78	10.957	0.089	0.4778	0.0038	0.1666	0.0005	2519.1	7.5	2520	16	2526.2	2.7	0.5
180504-6-f-99	0.75	11.100	0.110	0.4800	0.0037	0.1672	0.0010	2531.1	9.5	2527	16	2531.3	4.7	0.6
180504-6-f-93	0.35	11.350	0.520	0.4870	0.0220	0.1686	0.0009	2543	49	2578	86	2542.5	5.8	2.2
180504-6-f-45	0.49	12.750	0.170	0.5119	0.0059	0.1810	0.0010	2660	13	2664	25	2663	5.2	1.1

Seokmun Fm. (n=100)

180808-1-73	0.33	0.423	0.023	0.0561	0.0007	0.0549	0.0032	357	17	351.7	4.4	538	63	4.6
180808-1-70	0.41	0.417	0.006	0.0562	0.0003	0.0543	0.0008	353.8	4	352.3	1.8	378	19	1.2
180808-1-67	0.33	0.419	0.009	0.0562	0.0004	0.0546	0.0012	356.6	6.8	352.7	2.5	400	22	1.5
180808-1-80	0.61	0.420	0.006	0.0566	0.0006	0.0538	0.0005	357.3	4.2	355.1	3.8	359	11	1.6
180808-1-97	0.39	0.425	0.006	0.0568	0.0004	0.0536	0.0008	359.3	4.2	356.1	2.4	358	20	1.0
180808-1-86	0.61	0.422	0.006	0.0568	0.0005	0.0535	0.0006	357.3	4.2	356.3	3	350	19	1.7
180808-1-1	0.45	0.428	0.006	0.0574	0.0004	0.0541	0.0008	361.3	4.3	359.9	2.5	369	22	1.5
180808-1-84	1.04	0.449	0.009	0.0596	0.0004	0.0541	0.0011	375.7	6.6	373.2	2.6	361	22	1.8
180808-1-93	1.23	0.455	0.016	0.0596	0.0004	0.0552	0.0020	380	11	373.4	2.6	457	45	1.9
180808-1-51	0.77	0.454	0.009	0.0605	0.0004	0.0545	0.0009	379.4	5.9	378.4	2.4	395	24	1.9
180808-1-30	0.82	0.461	0.020	0.0610	0.0006	0.0550	0.0026	384	14	381.4	3.9	403	80	4.0
180808-1-3	1.23	0.459	0.005	0.0611	0.0004	0.0544	0.0005	383.4	3.7	382.4	2.4	386	14	1.3
180808-1-49	0.60	0.462	0.008	0.0613	0.0004	0.0549	0.0008	386.2	5.7	383.7	2.7	407	23	1.5
180808-1-52	0.97	0.473	0.014	0.0614	0.0007	0.0563	0.0014	392.6	9.8	384.3	4	466	33	1.4
180808-1-59	0.45	0.463	0.010	0.0617	0.0005	0.0545	0.0010	385.7	6.8	386	3.1	382	21	2.5
180808-1-29	0.90	0.468	0.014	0.0620	0.0008	0.0546	0.0015	389.6	9.5	387.8	5	408	37	3.3
180808-1-91	0.54	0.483	0.020	0.0620	0.0006	0.0567	0.0022	401	13	387.8	3.5	490	52	0.9
180808-1-98	0.26	0.486	0.015	0.0626	0.0006	0.0564	0.0018	404	11	391.2	3.5	488	36	0.4
180808-1-55	0.62	0.476	0.011	0.0628	0.0006	0.0550	0.0012	395.9	8	392.8	3.3	427	24	2.1
180808-1-78	0.08	0.502	0.005	0.0656	0.0004	0.0558	0.0004	413	3.3	409.3	2.3	435.7	8.8	0.5
180808-1-72	0.34	0.522	0.008	0.0679	0.0004	0.0559	0.0008	426.7	5.2	423.5	2.1	438	17	1.0
180808-1-44	0.33	0.522	0.005	0.0682	0.0005	0.0557	0.0005	426.8	3.4	425.5	2.8	441	11	1.2
180808-1-68	0.05	0.729	0.005	0.0894	0.0004	0.0597	0.0003	556	2.6	551.9	2.5	591.3	5.3	0.2
180808-1-42	0.22	0.810	0.009	0.0973	0.0007	0.0607	0.0006	602.4	4.8	598.8	4	621	12	0.9
180808-1-8	0.45	0.851	0.029	0.1006	0.0012	0.0614	0.0019	623	16	618.1	6.9	639	39	2.9
180808-1-54	*0.33*	*1.294*	*0.015*	*0.1226*	*0.0011*	*0.0764*	*0.0004*	*842.6*	*6.7*	*745.3*	*6.1*	*1106.6*	*7.8*	*-11.3*
180808-1-90	0.71	1.142	0.011	0.1262	0.0007	0.0654	0.0005	773.3	5.1	766.3	3.9	784.3	8.3	0.3
180808-1-7	*0.73*	*1.666*	*0.038*	*0.1273*	*0.0027*	*0.0953*	*0.0007*	*998*	*14*	*776*	*16*	*1534.6*	*7.1*	*-24.7*
180808-1-74	1.01	1.418	0.027	0.1470	0.0017	0.0711	0.0012	896	11	884.3	9.3	964	19	1.0
180808-1-33	0.78	1.402	0.015	0.1471	0.0012	0.0698	0.0005	890.7	6.4	884.5	6.6	915.9	9.7	0.8
180808-1-87	0.44	1.434	0.016	0.1485	0.0010	0.0700	0.0007	902.5	6.7	892.7	5.5	939	12	0.3
180808-1-31	0.40	1.450	0.016	0.1507	0.0010	0.0703	0.0007	909.4	6.7	904.8	5.7	930	13	0.9
180808-1-83	0.23	1.525	0.018	0.1559	0.0012	0.0714	0.0006	940.3	7.4	933.6	6.9	964.2	8.2	0.8
180808-1-6	0.36	1.550	0.020	0.1582	0.0017	0.0715	0.0006	950.9	8.1	946.6	9.7	964.5	9.8	1.4
180808-1-69	0.18	1.555	0.015	0.1584	0.0010	0.0714	0.0005	952.6	6	947.9	5.8	974.3	7.8	0.7
180808-1-76	0.32	1.578	0.041	0.1603	0.0020	0.0714	0.0018	961	16	958	11	955	22	2.5
180808-1-22	0.33	1.652	0.036	0.1649	0.0029	0.0738	0.0009	990	14	984	16	1032	10	2.4
180808-1-99	0.05	1.654	0.023	0.1657	0.0017	0.0719	0.0003	992.1	8.7	988.5	9.5	983.5	4.7	1.5
180808-1-17	0.35	1.908	0.022	0.1820	0.0019	0.0765	0.0008	1083.4	7.6	1078	11	1103	14	0.0
180808-1-23	0.40	1.885	0.021	0.1881	0.0015	0.0737	0.0005	1076.2	7.2	1110.9	7.9	1033.2	7.8	-6.0
180808-1-43	1.62	2.142	0.015	0.1969	0.0010	0.0789	0.0003	1163.1	5	1159	5.5	1167.5	4.1	0.1
180808-1-53	0.19	2.229	0.022	0.2009	0.0017	0.0814	0.0004	1189.8	7	1179.8	9.2	1230.9	5.6	-3.1
180808-1-88	0.45	2.276	0.022	0.2033	0.0013	0.0811	0.0007	1204.2	6.7	1193.9	6.8	1224.7	9	-1.3
180808-1-79	*0.13*	*3.129*	*0.056*	*0.2144*	*0.0035*	*0.1077*	*0.0004*	*1439*	*14*	*1252*	*19*	*1760.2*	*3.2*	*-38.8*
180808-1-38	*0.11*	*3.387*	*0.030*	*0.2205*	*0.0016*	*0.1111*	*0.0005*	*1501.3*	*6.9*	*1284.5*	*8.7*	*1816.7*	*3.2*	*-40.5*
180808-1-19	0.13	2.786	0.026	0.2318	0.0021	0.0882	0.0003	1351.5	6.8	1344	11	1389.4	4.6	-2.2
180808-1-25	0.65	3.180	0.050	0.2507	0.0031	0.0929	0.0008	1453	12	1442	16	1486	10	-1.2
180808-1-26	0.94	3.212	0.040	0.2535	0.0022	0.0922	0.0008	1460.9	9.5	1456	11	1474.3	8.5	0.1
180808-1-50	0.71	3.650	0.160	0.2707	0.0092	0.0968	0.0032	1553	35	1542	46	1562	35	4.0
180808-1-15	0.90	3.697	0.040	0.2756	0.0023	0.0978	0.0007	1571.4	8.6	1570	11	1585	7.8	0.2
180808-1-12	*0.48*	*4.616*	*0.052*	*0.2961*	*0.0035*	*0.1142*	*0.0004*	*1752.8*	*9.3*	*1672*	*17*	*1867*	*3.9*	*-10.4*
180808-1-39	0.42	4.664	0.069	0.2987	0.0040	0.1131	0.0008	1760	12	1685	20	1850.3	7.3	-8.2
180808-1-64	0.43	4.377	0.034	0.3011	0.0021	0.1071	0.0005	1707.6	6.3	1698	11	1749.6	4.1	-2.1
180808-1-21	0.26	4.802	0.061	0.3041	0.0036	0.1142	0.0007	1784	11	1711	18	1862.4	6.3	-7.4
180808-1-37	0.18	4.759	0.060	0.3041	0.0028	0.1123	0.0008	1777	11	1711	14	1838.3	7	-6.2
180808-1-9	0.74	4.803	0.063	0.3173	0.0032	0.1106	0.0009	1785	11	1779	15	1813.8	6.7	-0.7
180808-1-16	0.53	4.924	0.037	0.3220	0.0022	0.1116	0.0005	1806	6.4	1799	11	1827.4	4.9	-0.7
180808-1-89	0.62	4.963	0.040	0.3219	0.0023	0.1119	0.0007	1812.6	6.8	1799	11	1828.8	4.9	-0.8
180808-1-95	0.39	5.090	0.200	0.3240	0.0110	0.1137	0.0016	1843	37	1808	55	1859	18	1.2
180808-1-34	0.04	5.030	0.043	0.3251	0.0027	0.1135	0.0003	1824	7.2	1814	13	1855.3	3.2	-1.4
180808-1-57	0.45	5.015	0.037	0.3251	0.0020	0.1130	0.0006	1821.8	6.2	1814.5	9.8	1848.5	5	-1.1
180808-1-24	0.42	5.034	0.032	0.3265	0.0019	0.1124	0.0003	1824.7	5.4	1821	9.4	1837.7	2.7	-0.3
180808-1-71	0.08	5.043	0.042	0.3264	0.0026	0.1135	0.0003	1826	7.1	1821	13	1854.4	2.2	-1.0
180808-1-13	0.16	5.075	0.044	0.3273	0.0026	0.1129	0.0004	1831.6	7.3	1825	13	1845.1	2.8	-0.2
180808-1-62	0.28	5.126	0.044	0.3272	0.0021	0.1146	0.0006	1839.7	7.3	1825	10	1871.2	5.5	-1.7
180808-1-18	0.44	5.119	0.067	0.3275	0.0036	0.1149	0.0006	1839	11	1826	18	1874.5	8.9	-1.2
180808-1-60	0.07	5.061	0.055	0.3279	0.0034	0.1128	0.0004	1829.2	9.2	1828	17	1843.5	5.4	0.4
180808-1-61	0.44	5.137	0.039	0.3278	0.0024	0.1153	0.0005	1841.9	6.5	1828	12	1882.4	3.4	-2.1
180808-1-11	0.52	5.052	0.057	0.3282	0.0039	0.1110	0.0006	1827.7	9.6	1829	19	1816.6	5.3	0.7
180808-1-77	0.17	5.131	0.030	0.3287	0.0019	0.1134	0.0004	1841.1	5	1833.2	9	1854.9	3.6	-0.5
180808-1-82	0.35	5.158	0.043	0.3294	0.0022	0.1133	0.0006	1846	7	1835	10	1855.6	5.1	-0.3
180808-1-4	0.09	5.140	0.055	0.3299	0.0032	0.1131	0.0002	1841.8	9	1838	16	1850.9	1.9	0.3
180808-1-27	0.06	5.252	0.058	0.3325	0.0034	0.1157	0.0003	1860.5	9.4	1850	16	1892.1	2.2	-1.3
180808-1-14	0.27	5.211	0.051	0.3326	0.0025	0.1140	0.0007	1853.4	8.4	1851	12	1864	8	0.4
180808-1-36	0.37	5.300	0.120	0.3335	0.0073	0.1173	0.0011	1868	19	1855	35	1917	10	-0.9
180808-1-10	0.38	5.246	0.031	0.3335	0.0019	0.1144	0.0003	1860.5	5.2	1856.4	9.2	1869.7	2.8	-0.1
180808-1-28	0.14	5.278	0.088	0.3352	0.0048	0.1139	0.0005	1865	14	1863	23	1862.5	5.5	1.5
180808-1-35	0.10	5.128	0.033	0.3357	0.0020	0.1111	0.0003	1841.1	5.3	1867.1	9.3	1817	2.6	-2.1
180808-1-66	0.16	5.155	0.038	0.3361	0.0028	0.1114	0.0003	1844.9	6.4	1868	13	1822.3	2.5	-1.7
180808-1-2	0.13	5.328	0.036	0.3369	0.0019	0.1142	0.0003	1872.9	5.8	1872.7	9.2	1866.2	3.1	0.3
180808-1-75	0.03	5.221	0.031	0.3374	0.0018	0.1143	0.0002	1855.9	5	1874.1	8.8	1868.2	2.8	0.3
180808-1-81	0.45	5.364	0.079	0.3379	0.0037	0.1148	0.0009	1879	12	1876	18	1878	7.8	1.3
180808-1-85	0.41	5.423	0.037	0.3374	0.0019	0.1169	0.0005	1888.8	6	1876.3	9.3	1911	5	-1.1
180808-1-100	0.16	5.269	0.054	0.3415	0.0032	0.1113	0.0003	1863	8.7	1894	15	1819.9	2.3	-3.1
180808-1-63	0.07	5.594	0.044	0.3440	0.0023	0.1190	0.0006	1916	6.9	1907	11	1938.3	5.4	-0.8
180808-1-96	0.52	6.250	0.110	0.3470	0.0051	0.1303	0.0010	2009	16	1919	25	2110	10	-8.1
180808-1-65	0.23	5.737	0.056	0.3491	0.0031	0.1218	0.0006	1938.3	8.8	1930	15	1981.7	5.6	-1.6
180808-1-94	0.10	5.447	0.032	0.3529	0.0015	0.1132	0.0005	1892.2	5	1948.5	6.9	1849.9	4.3	-4.7
180808-1-20	*0.83*	*8.235*	*0.085*	*0.3791*	*0.0037*	*0.1569*	*0.0004*	*2256.6*	*9.4*	*2072*	*17*	*2423.5*	*2.3*	*-16.0*
180808-1-47	0.51	7.615	0.066	0.3803	0.0028	0.1452	0.0007	2185.8	7.8	2077	13	2290.9	4.7	-9.4
180808-1-58	0.58	8.813	0.070	0.4138	0.0027	0.1568	0.0005	2318.4	7.3	2232	13	2419.7	4.5	-7.6
180808-1-48	0.48	7.870	0.083	0.4220	0.0036	0.1350	0.0006	2216.5	9.3	2269	16	2161.4	5.1	-4.0
180808-1-40	1.56	10.140	0.240	0.4586	0.0087	0.1655	0.0021	2446	22	2433	38	2504	14	-0.8
180808-1-32	0.60	10.325	0.076	0.4628	0.0034	0.1629	0.0007	2465	6.6	2451	15	2485.8	6.2	-0.6
180808-1-46	0.67	10.600	0.150	0.4671	0.0049	0.1663	0.0012	2488	13	2470	22	2522	6.7	-0.9
180808-1-45	0.84	10.865	0.082	0.4740	0.0036	0.1666	0.0005	2511.7	6.9	2502	16	2526.3	3	-0.2
180808-1-92	0.05	11.040	0.170	0.4770	0.0060	0.1669	0.0009	2524	14	2513	26	2532.1	8.5	0.6
180808-1-41	0.44	12.190	0.120	0.4980	0.0046	0.1797	0.0006	2618.3	9.5	2605	20	2649.4	2.7	-0.8
180808-1-5	0.21	12.010	0.180	0.4982	0.0064	0.1765	0.0010	2605	14	2606	27	2619.8	6.3	0.7
180808-1-56	0.50	19.560	0.140	0.6057	0.0035	0.2383	0.0013	3071.8	7.9	3053	14	3108.3	3.9	-1.2

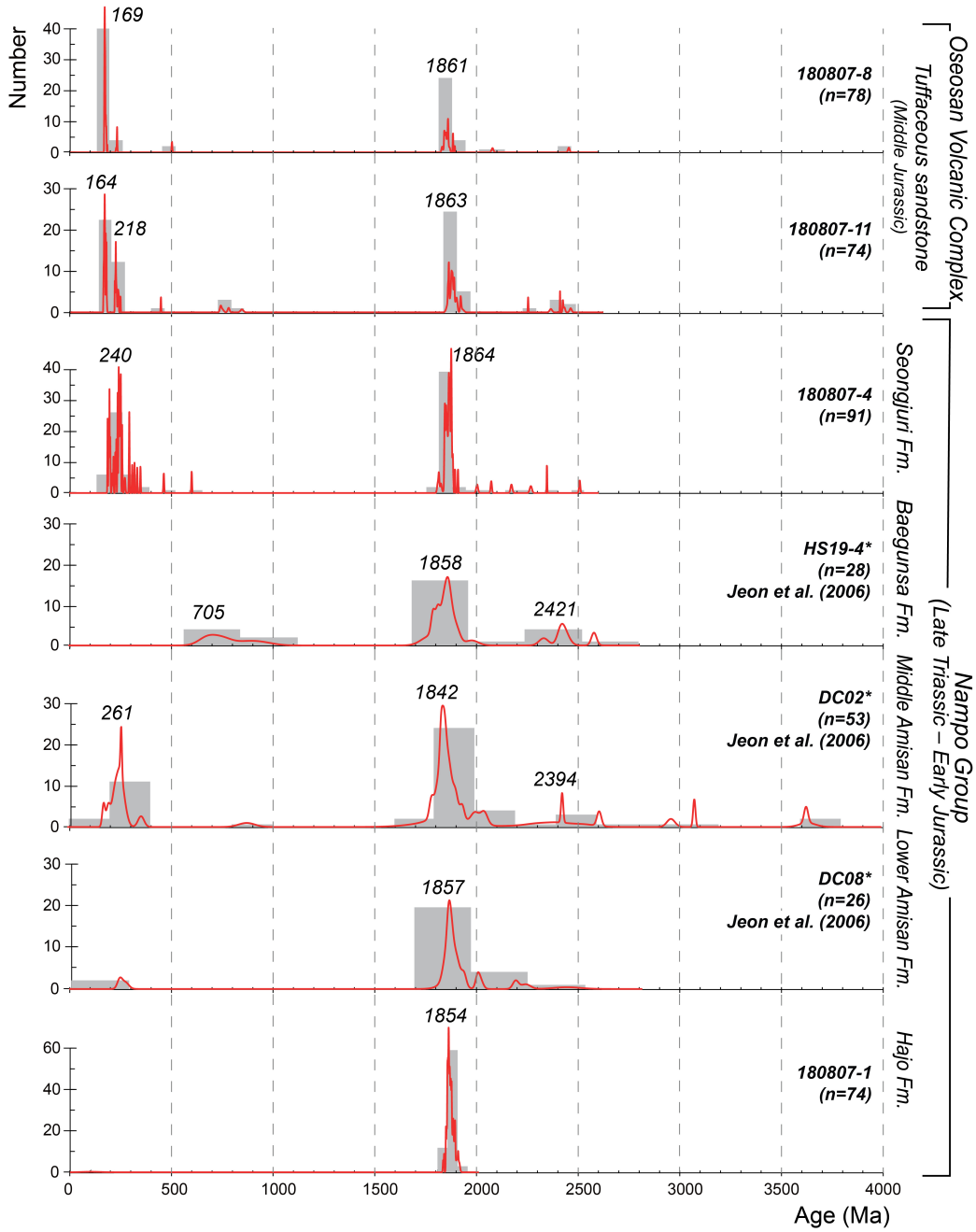

Fig. 3-7. Probability-density plots and histograms of detrital-zircon U-Pb ages from sandstones of the Nampo Group and the Oseosan Volcanic Complex. For comparison, detrital-zircon-age patterns were also constructed by using concordant or slightly discordant (discordance < 15%) isotopic data from Jeon et al. (2007).

age groups (1880–1843 Ma, 955–942 Ma, and 426–384 Ma), with a few exhibiting Late Archean, Meso-Neoproterozoic, Paleozoic, and Triassic ages (Fig. 3-8; Table 3-1).

3.3.2.1. Nampo Group and Oseosan Volcanic Complex

The Nampo Group exhibited obvious variation in detrital-zircon age distribution among the formations (Fig. 3-7; Tables 3-1 and 3-2). The Hajo Formation, which is the lowermost unit of the Nampo Group, characteristically contained only Paleoproterozoic zircons (1906–1827 Ma). The Seongjuri Formation, which is the uppermost unit of the Nampo Group, had Paleoproterozoic to Late Archean zircons (2508–1810 Ma; 54%) alongside Triassic (250–208; 24%), Paleozoic (461–256; 12%), Early Jurassic (198–184; 9%), and Neoproterozoic (598 Ma; 1%) zircons (Table 3-2).

For comparison, detrital-zircon age patterns from the middle portion of the Nampo Group (i.e., the Amisan and Baegunsa formations) are presented in Table 3-2 and are illustrated in Figure 3-7 by using concordant or slightly discordant (discordance < 15%) isotopic data from Jeon et al. (2007). The lower Amisan Formation mainly included Paleoproterozoic (2434–1832 Ma; 92%) zircons with some Permian (271 Ma; 4%) and Triassic (244 Ma; 4%) zircons. The middle Amisan Formation was dominated by Archean to Paleoproterozoic (3638–1755 Ma; 74%) zircons, with others from the Permian (273–257 Ma; 11%), Late Triassic (238–224 Ma; 8%), Early Jurassic (197–175 Ma; 4%), Neoproterozoic (879 Ma; 2%), and Devonian (359 Ma; 2%). The detrital zircons from the Baegunsa Formation were primarily Archean to Paleoproterozoic (2577–1765 Ma; 79%) and Neoproterozoic (947–671 Ma; 21%).

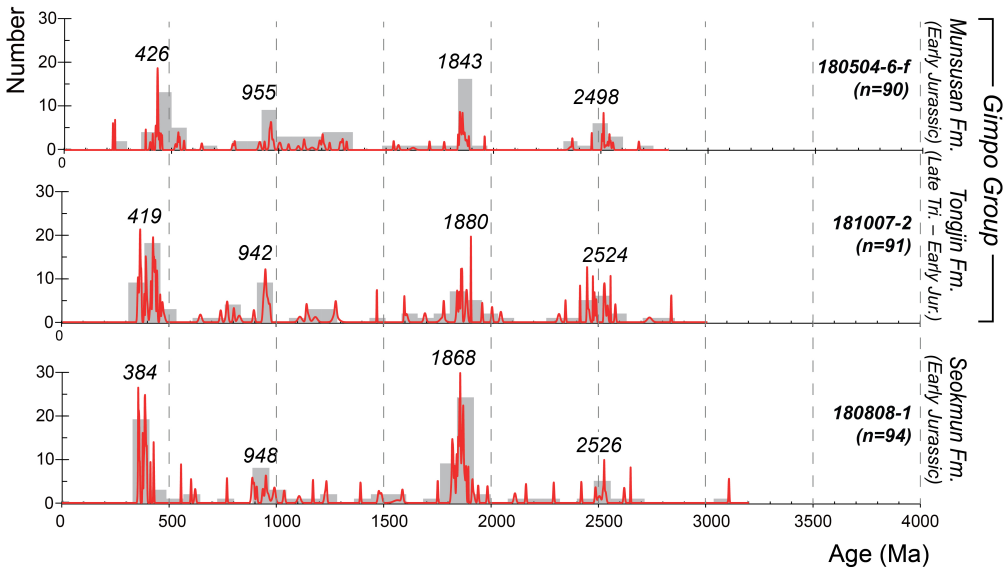

Fig. 3-8. Probability-density plots and histograms of detrital-zircon U-Pb ages from sandstones of the Gimpo Group and the Seokmun Formation.

Table 3-2. Summary of the detrital-zircon-age distribution in the Daedong Supergroup along the western Korean Peninsula. The age distributions in the Amisan and Baegunsa formations are presented by using the concordant or slightly discordant (discordance < 15%) data from Jeon et al. (2007).

	Hajo Fm. (180807-1)			Lower Amisan Fm. (DC08)			Middle Amisan Fm. (DC02)			Baegunsa Fm. (HS19-4)			Seongjuri Fm. (180807-4)			Oseosan volcanic complex (180807-8)			Oseosan volcanic complex (180807-11)			Tongjin Fm. (181007-2)			Munsusan Fm. (180504-6-f)			Seokmun Fm. (180808-1)		
	grain number	range (Ma)	(%)	grain number	range (Ma)	(%)	grain number	range (Ma)	(%)	grain number	range (Ma)	(%)	grain number	range (Ma)	(%)	grain number	range (Ma)	(%)	grain number	range (Ma)	(%)	grain number	range (Ma)	(%)	grain number	range (Ma)	(%)	grain number	range (Ma)	(%)
Jurassic							2	197-175	3.77				8	198-184	9	40	181-166	54	22	174-158	28									
Triassic				1	244	3.85	4	238-224	7.55				22	250-208	24	4	231-226	5	12	241-213	15				2	229-219	2			
Permian				1	271	3.85	6	273-257	11.3				6	292-256	7															
Carboniferous													4	346-305	4							6	358-347	7				6	356-352	6
Devonian							1	359	1.89													13	417-360	14	4	418-372	4	14	409-360	15
Silurian																			1	439	1	8	437-419	9	12	443-421	13	2	426-424	2
Ordovician													1	461	1							3	468-451	3	1	447	1			
Cambrian																2	500	3							4	530-511	4			
Paleozoic (total)				1	271	3.85	7	359-257	13.2				11	461-256	12	2	500	3	1	439	1	30	468-347	33	21	530-372	23	22	426-352	23
Neoproterozoic							1	879	1.89	6	947-671	21.4	1	598	1				4	835-731	5	16	963-639	18	17	998-550	19	14	989-552	15
Mesoproterozoic																						10	1600-1103	11	17	1546-1036	19	10	1585-1033	11
Paleoproterozoic & Archearn	74	1906-1827	100	24	2434-1832	92.3	39	3638-1755	73.6	22	2577-1765	78.6	49	2508-1810	54	32	2458-1832	43	35	2443-1837	45	35	2834-1686	38	33	2663-1614	37	48	3108-1750	51

The Oseosan Volcanic Complex, which stratigraphically overlies the Nampo Group, included Paleoproterozoic (2458–1832 Ma; 44%), Early to Late Jurassic (181–158 Ma; 41%), Triassic (241–213 Ma; 11%), Neoproterozoic (835–731 Ma; 3%), and Paleozoic zircons (500–439 Ma; 2%) (Fig. 3-7; Tables 3-1 and 3-2). Two samples (180807-8 and 180807-11) from the Oseosan Volcanic Complex showed a variation in the relative abundance of the Jurassic and Triassic zircons.

3.3.2.2. Gimpo Group

A total of 181 zircon grains yielded concordant or slightly discordant Late Archean to Triassic U-Pb ages (Fig. 3-8; Tables 3-1 and 3-2). The detrital-zircon age distributions of the Tongjin and Munsusan formations differed considerably from those of the Nampo Group and the Oseosan Volcanic Complex in the Chungnam Basin. In particular, the zircon ages were widely spread between the Paleoproterozoic and Triassic. The Tongjin Formation had Late Archean and Paleoproterozoic (2834–1686 Ma; 38%), Ordovician-Carboniferous (468–347 Ma; 33%), Neoproterozoic (963–639 Ma; 18%), and Mesoproterozoic (1600–1103 Ma; 11%) zircon grains, with no Mesozoic record (Table 3-2). The zircon-age spectrum of the Munsusan Formation, which overlies the Tongjin Formation, consisted of Archean and Paleoproterozoic (2663–1614 Ma; 37%), Mesoproterozoic (1546–1036 Ma; 19%), Neoproterozoic (998–550 Ma; 19%), Silurian (443–421 Ma; 13%), Cambrian (530–511 Ma; 4%), Devonian (418–372 Ma; 4%), Triassic (229–219 Ma; 2%), and Ordovician (447 Ma; 1%) records (Table 3-2). Carboniferous zircons were found only in the Tongjin Formation, while Cambrian and Triassic zircons were present only in the Munsusan Formation.

3.3.2.3. Seokmun Formation

A total of 94 concordant or slightly discordant detrital-zircon ages were found in the Seokmun Formation. The zircon ages were also widely spread, ranging from 3108 Ma to 352 Ma (Fig. 3-8; Tables 3-1 and 3-2). The zircon ages fell within four groups: Archean and Paleoproterozoic (3108–1750 Ma; 51%), Silurian-Carboniferous (426–352 Ma; 23%), Mesoproterozoic (1585–1033 Ma; 11%), and Neoproterozoic (989–552 Ma; 15%).

3.4. Geochemistry

3.4.1. Sample preparation and analytical method

Twenty-four mudstone samples were collected from the study areas to analyze their major, trace, and rare earth elements (REEs). In the Chungnam Basin, eight samples were taken from the Nampo Group (the Amisan, Baegunsa, and Seongjuri formations), and five samples were taken from the Oseosan Volcanic Complex. Nine samples were collected from the Gimpo Group (the Tongjin and Munsusan formations) and two from the Seokmun Formation (Fig. 3-3). Most of the analyzed samples were taken from dark gray to black, horizontally or ripple-cross laminated lacustrine mudstones. Only three samples from the Munsusan Formation were obtained from reddish mudstones alternated with conglomerates, likely indicating flood plain sedimentary environment.

After powdering the collected samples with an agate mortar, the bulk-rock geochemistry

of the powdered samples was analyzed at the Korea Basic Science Institute (KBSI), Seoul Center, South Korea. Major-element oxides, including SiO_2, Al_2O_3, Fe_2O_3 (total), TiO_2, MnO, MgO, K_2O, Na_2O, and P_2O_4, were analyzed by using a Phillips PW2404 X-ray fluorescence spectrometer (XRF). The loss-on-ignition (LOI) was estimated by weighing the samples before and after 60 min of heating at 1000°C. Trace elements, including REEs, were analyzed by using an Optima 4300DV inductively coupled plasma-atomic emission spectrometer (ICP-AES) and a PQ II Plus inductively coupled plasma mass spectrometer (ICP-MS). The analytical accuracy and precision were checked by using the USGS standard materials STM-2, QLO-1, and W-2 for major elements and BCR-2 for trace and rare earth elements (Tables 3-3 and 3-4). The analytical precision was generally within 5–10 %. The measured values for the standards mostly differed by less than 5% of the certified values. All the measured concentrations of major, trace, and rare earth elements were above the detection limits for the analytic instruments at KBSI.

3.4.2. Results and interpretation

3.4.2.1. Major elements

The major elements that were found in the analyzed mudstone samples are presented in Table 3-3. Compared to post-Archean average shale (PAAS; Taylor and McLennan, 1985), most of the samples were enriched with SiO_2 and K_2O. The samples from the Oseosan Volcanic Complex were characterized by high SiO_2 and low Al_2O_3, Fe_2O_3, and TiO_2, and could be clearly distinguished from the other samples in the binary plots of major elements

Table 3-3. Major-element contents of mudstones from the Daedong Supergroup along the western Korean Peninsula (wt. %).

Group	Nampo Group								-					-		Gimpo Group								
Formation	Hajo		Baegunsa					Seongjuri	Oseosan Volcanic Complex					Seokmun		Tongjin						Munsusan		
Sample ID	0807-1-C	0807-1-D	0807-2	0807-3	0807-10	0807-12	0807-13	0807-4-D	0807-5	0807-6-A	0807-7	0807-9-D	0807-11-C	0808-1-C	0808-2	0504-1-A	0504-3-A	0504-5-C	0504-5-D	0508-4-A	0508-4-D	0504-6-A	0504-7-B	0508-3
SiO_2	63.56	61.67	58.73	64.60	65.64	66.88	62.89	52.02	77.69	72.38	71.67	74.98	71.63	64.47	58.77	66.74	70.85	53.94	67.84	64.79	65.60	74.90	63.87	68.84
TiO_2	1.28	0.90	0.90	0.81	0.87	0.78	0.78	1.10	0.16	0.17	0.19	0.14	0.34	0.85	0.75	0.91	0.76	0.84	0.85	0.73	0.93	0.94	0.85	1.29
Al_2O_3	17.15	21.18	20.10	19.61	18.53	18.94	18.40	20.69	13.01	13.79	13.42	13.07	16.09	18.98	16.86	16.02	15.63	24.91	19.38	15.02	18.97	13.10	18.34	15.18
Fe_2O_3	5.38	2.19	7.15	2.72	5.11	4.64	5.75	9.38	1.47	3.24	2.42	1.62	2.50	5.80	7.52	7.01	6.14	6.81	2.02	8.75	4.57	4.42	7.51	6.51
MnO	0.03	0.02	0.06	0.01	0.03	0.02	0.01	0.17	0.01	0.04	0.07	0.04	0.00	0.01	0.15	0.07	0.00	0.01	0.19	0.04	0.00	0.00	0.02	0.01
MgO	0.89	0.77	0.50	0.35	0.61	0.73	0.94	0.95	0.64	1.17	0.47	0.26	0.77	0.91	2.99	0.77	0.45	0.89	0.50	2.47	0.81	0.67	0.41	0.55
CaO	0.47	0.06	0.03	0.02	0.07	0.04	0.27	0.18	0.02	0.28	0.05	0.68	0.05	0.01	1.94	0.02	0.03	0.08	0.03	0.19	0.06	0.01	0.04	0.03
Na_2O	0.10	0.32	0.21	0.20	0.40	1.63	0.85	0.31	0.08	0.26	0.49	3.05	0.70	0.27	0.55	0.32	0.14	0.22	0.19	0.06	0.11	0.13	0.15	0.12
K_2O	5.87	6.61	4.68	5.16	4.45	3.30	3.87	6.36	4.16	4.13	9.20	4.65	5.75	5.16	3.38	4.42	2.80	6.04	4.95	3.39	2.14	3.03	4.14	4.31
P_2O_5	0.33	0.09	0.13	0.02	0.11	0.03	0.18	0.09	0.02	0.03	0.03	0.03	0.05	0.07	0.15	0.11	0.04	0.12	0.05	0.09	0.03	0.07	0.09	0.03
L.O.I	3.59	4.67	5.92	4.93	4.42	3.25	5.67	6.81	2.39	2.70	1.17	1.29	2.64	3.43	5.24	4.10	3.81	5.68	3.95	4.45	5.94	3.21	4.45	3.13
Total	98.65	98.48	98.41	98.43	100.26	100.24	99.59	98.06	99.65	98.18	99.17	99.80	100.52	99.95	98.29	100.50	100.65	99.54	99.95	99.99	99.17	100.48	99.86	99.99

Table 3-4. Trace- and rare earth-element contents of mudstones from the Daedong Supergroup along the western Korean Peninsula (ppm).

Group	Nampo Group								Gimpo Group													
Formation	Hajo		Baegunsa					Seongjuri	Oseosan Vol. complex					Seokmun		Tongjin					Munsusan		
Sample ID	0807-1-C	0807-1-D	0807-2	0807-3	0807-10	0807-12	0807-13	0807-4-D	0807-5	0807-6-A	0807-7	0807-9-D	0807-11-C	0808-1-C	0808-2	0504-1-A	0504-3-A	0504-5-C	0504-5-D	0508-4-A	0508-4-D	0504-6-A	0504-7-B	0508-3
Trace elements																								
Ba	1440.0	1377.0	1032.0	775.6	785.8	667.3	679.8	1562.0	1249.0	975.1	346.5	825.2	501.1	794.1	362.4	607.6	371.9	704.9	668.8	350.0	398.9	435.2	543.8	287.3
Rb	496.69	507.32	390.41	380.18	273.49	273.37	247.08	561.94	377.49	312.88	676.15	314.11	519.28	388.61	328.31	211.53	189.65	396.25	332.13	192.39	149.94	178.12	212.70	226.93
Sr	56.70	101.30	91.81	78.46	60.15	190.20	81.12	57.22	13.38	40.79	25.02	94.67	25.58	77.44	73.26	53.43	43.25	135.30	77.98	< 1.00	18.93	38.10	44.37	22.24
Cs	6.20	9.33	5.84	5.94	10.29	8.43	7.19	11.90	10.05	9.00	9.53	4.53	15.45	13.51	13.00	10.04	11.28	57.64	29.61	20.44	10.67	16.00	8.78	16.83
Sc	13.53	16.00	16.80	11.48	12.99	12.31	12.25	18.01	3.25	3.58	4.33	3.53	7.34	15.90	15.82	7.52	5.51	14.09	8.36	5.87	7.36	3.30	10.32	6.41
V	49.94	97.97	103.30	66.02	81.93	76.43	88.14	100.60	6.12	10.15	14.58	6.47	30.66	98.07	99.24	83.32	75.69	143.50	110.40	86.34	83.94	74.44	92.66	96.17
Co	23.69	13.92	22.68	16.13	24.52	19.88	16.92	37.99	22.88	18.20	21.57	26.40	19.92	21.98	34.52	72.08	34.19	9.05	53.92	33.82	34.19	60.51	5.84	36.53
Ni	9.50	4.10	55.80	34.92	40.78	24.40	36.39	30.98	3.43	3.96	7.61	3.52	10.24	52.83	38.69	36.37	34.94	51.59	29.63	37.03	46.48	39.68	29.75	20.11
Cr	36.21	101.10	97.48	91.29	81.53	63.72	67.06	149.70	13.76	8.56	18.12	12.54	27.84	72.70	72.28	59.41	85.32	114.50	136.10	62.06	79.31	59.91	96.99	75.53
Zr	66.65	155.80	186.40	219.90	221.40	184.90	208.80	187.50	143.60	151.20	108.50	102.90	136.40	175.30	140.90	140.40	92.99	130.40	129.00	56.77	90.04	108.80	68.51	56.50
Nb	57.56	12.58	23.70	14.95	18.01	14.10	18.82	30.39	3.41	13.39	16.33	10.44	10.99	10.95	25.81	15.09	12.55	26.25	27.40	8.60	18.99	6.33	19.49	25.05
Hf	2.82	5.46	6.61	8.24	7.43	6.32	6.84	6.71	5.94	5.60	4.75	4.58	5.56	5.76	4.96	4.90	3.29	3.68	4.87	2.12	3.32	3.99	1.93	3.60
Pb	27.23	20.16	32.01	33.08	20.28	21.71	18.33	31.95	24.56	26.76	30.39	31.53	7.63	18.42	20.29	20.01	50.00	45.47	39.87	19.37	26.62	33.94	43.32	25.23
Th	40.95	64.12	56.61	49.61	14.03	18.77	17.59	54.51	57.70	52.65	43.85	43.05	59.14	15.11	18.41	18.18	17.82	33.95	21.59	14.46	18.70	16.53	19.08	20.57
U	3.52	6.55	4.93	6.16	3.59	4.24	3.89	8.67	7.68	7.01	5.23	5.13	7.15	2.11	2.46	3.07	1.93	3.71	2.92	1.67	4.42	2.93	2.31	2.64
Y	103.28	31.07	88.75	21.26	22.80	18.55	22.07	89.58	17.34	15.90	21.53	16.60	21.69	30.12	27.10	11.50	11.00	35.76	17.48	22.95	11.14	13.92	8.67	10.47
Rare earth elements																								
La	143.17	131.47	165.19	76.41	77.27	92.93	92.45	72.80	94.79	99.85	52.05	93.07	87.85	82.06	87.84	48.98	46.74	94.45	56.22	42.20	51.15	58.31	31.23	59.65
Ce	336.51	273.64	240.16	125.05	158.16	203.95	196.25	116.46	215.54	175.37	102.36	179.82	177.09	162.34	173.37	100.65	113.09	182.87	106.09	79.61	98.68	102.91	42.32	116.21
Pr	22.66	17.75	22.01	7.97	10.76	12.06	12.38	10.26	10.67	11.11	7.78	10.61	10.88	11.06	11.04	10.95	10.55	21.41	11.48	9.91	11.17	11.66	5.93	12.72
Nd	211.23	161.11	174.58	39.44	53.78	64.45	63.79	46.88	59.59	54.26	36.11	54.51	55.59	55.04	56.44	63.91	66.91	115.17	65.63	54.65	63.53	65.05	28.02	72.40
Sm	19.54	12.29	15.91	5.63	7.94	8.72	9.04	8.64	6.77	6.69	5.71	6.75	7.71	8.27	7.95	8.77	8.21	14.64	7.25	8.16	8.10	7.98	4.32	8.51
Eu	2.34	2.46	3.30	1.08	1.66	1.83	1.65	2.32	1.28	1.07	0.54	1.10	0.97	1.86	1.71	1.76	1.55	2.54	1.36	1.52	1.32	1.59	1.07	1.43
Gd	19.77	11.53	15.66	5.45	7.39	8.25	8.17	9.08	6.36	6.24	5.92	6.33	7.58	8.53	8.37	7.74	6.92	13.98	6.21	7.84	6.72	6.95	3.96	7.34
Tb	2.62	1.50	2.11	0.85	0.94	0.97	0.97	1.46	0.80	0.78	0.85	0.78	0.95	1.18	1.10	0.82	0.67	1.62	0.71	0.99	0.66	0.74	0.51	0.74
Dy	13.32	7.53	10.81	4.76	4.87	4.47	4.78	9.09	4.01	3.73	4.50	3.72	4.73	6.57	5.77	3.49	2.86	8.03	3.65	5.11	2.97	3.46	2.58	3.13
Ho	2.55	1.46	2.11	0.95	0.99	0.85	0.93	2.04	0.76	0.69	0.87	0.68	0.89	1.35	1.15	0.60	0.52	1.51	0.72	1.00	0.56	0.63	0.49	0.54
Er	7.16	4.34	6.19	2.85	3.17	2.69	3.01	6.72	2.29	1.95	2.52	2.02	2.62	4.10	3.43	1.86	1.68	4.59	2.44	2.92	1.76	1.95	1.49	1.68
Tm	0.91	0.60	0.83	0.42	0.47	0.41	0.45	1.02	0.32	0.25	0.35	0.27	0.36	0.59	0.48	0.27	0.24	0.62	0.36	0.40	0.25	0.27	0.23	0.22
Yb	5.52	3.99	5.32	2.92	3.36	3.01	3.21	7.10	2.15	1.67	2.27	1.76	2.41	3.97	3.25	2.13	1.76	4.19	2.68	2.59	1.79	2.03	1.71	1.51
Lu	0.82	0.63	0.78	0.46	0.54	0.49	0.52	1.12	0.36	0.24	0.34	0.27	0.36	0.62	0.49	0.35	0.28	0.64	0.44	0.37	0.28	0.32	0.28	0.24
total REE	788	630	665	274	331	405	398	295	406	364	222	362	360	348	362	252	262	466	265	217	249	264	124	286
Elemental ratios																								
Th/Sc	3.03	4.01	3.37	4.32	1.08	1.52	1.44	3.03	17.75	14.70	10.12	12.20	8.06	0.95	1.16	2.42	3.24	2.41	2.58	2.46	2.54	5.00	1.85	3.21
Cr/Th	0.88	1.58	1.72	1.84	5.81	3.40	3.81	2.75	0.24	0.16	0.41	0.29	0.47	4.81	3.93	3.27	4.79	3.37	6.30	4.29	4.24	3.62	5.08	3.67
Co/Th	0.58	0.22	0.40	0.33	1.75	1.06	0.96	0.70	0.40	0.35	0.49	0.61	0.34	1.45	1.88	3.96	1.92	0.27	2.50	2.34	1.83	3.66	0.31	1.78
La_N/Yb_N	17.53	22.29	20.96	17.68	15.54	20.89	19.47	6.93	29.82	40.29	15.48	35.82	24.66	13.98	18.26	15.56	17.99	15.23	14.16	10.99	19.30	19.38	12.36	26.65
Eu/Eu*	0.36	0.63	0.64	0.59	0.66	0.66	0.59	0.80	0.60	0.51	0.29	0.51	0.39	0.68	0.64	0.65	0.63	0.54	0.62	0.58	0.55	0.65	0.79	0.55

against Al_2O_3 (Fig. 3-9). Although the samples from the Nampo and Gimpo groups could not be clearly distinguished from each other in the binary plots, those from the Nampo Group tended to be more enriched in Al_2O_3 and K_2O, while the Gimpo Group contained more SiO_2 and Fe_2O_3. The samples from the Seokmum Formation tended to fall between those from the Nampo and Gimpo groups in the plot.

3.4.2.2. Trace elements

The results of the trace-element analysis are presented in Table 3-4. The analyzed samples were generally enriched in Rb and depleted in Sr relative to PAAS (Fig. 3-10). Rb showed a strong positive correlation with K_2O ($r = 0.91$), indicating a K-rich clay-mineral (e.g., illite) origin. Sr showed no correlation with CaO ($r = 0.08$), precluding an association with carbonate minerals. Instead, this element exhibited a strong positive correlation with Al_2O_3 ($r = 0.81$) if two outliers were excluded, indicating an association with clay minerals. Given the negative correlation with SiO_2 ($r = -0.72$), the overall Sr depletion in the analyzed samples is considered to have been caused by quartz dilution.

The samples from the Oseosan Volcanic Complex were enriched in Rb, Th, and U and strongly depleted in Sr, Sc, and transition metals such as Cr, Ni, and V. The samples from the Nampo Group were enriched in Rb and Th and slightly depleted in Sr, Sc, and transition metals. The samples from the Gimpo Group also showed Rb and Th enrichment relative to PAAS and could be distinguished from the other samples by their high levels of Cs and transition metals. The samples from the Seokmun Formation exhibited transitional characteristics between those of the Nampo and Gimpo groups.

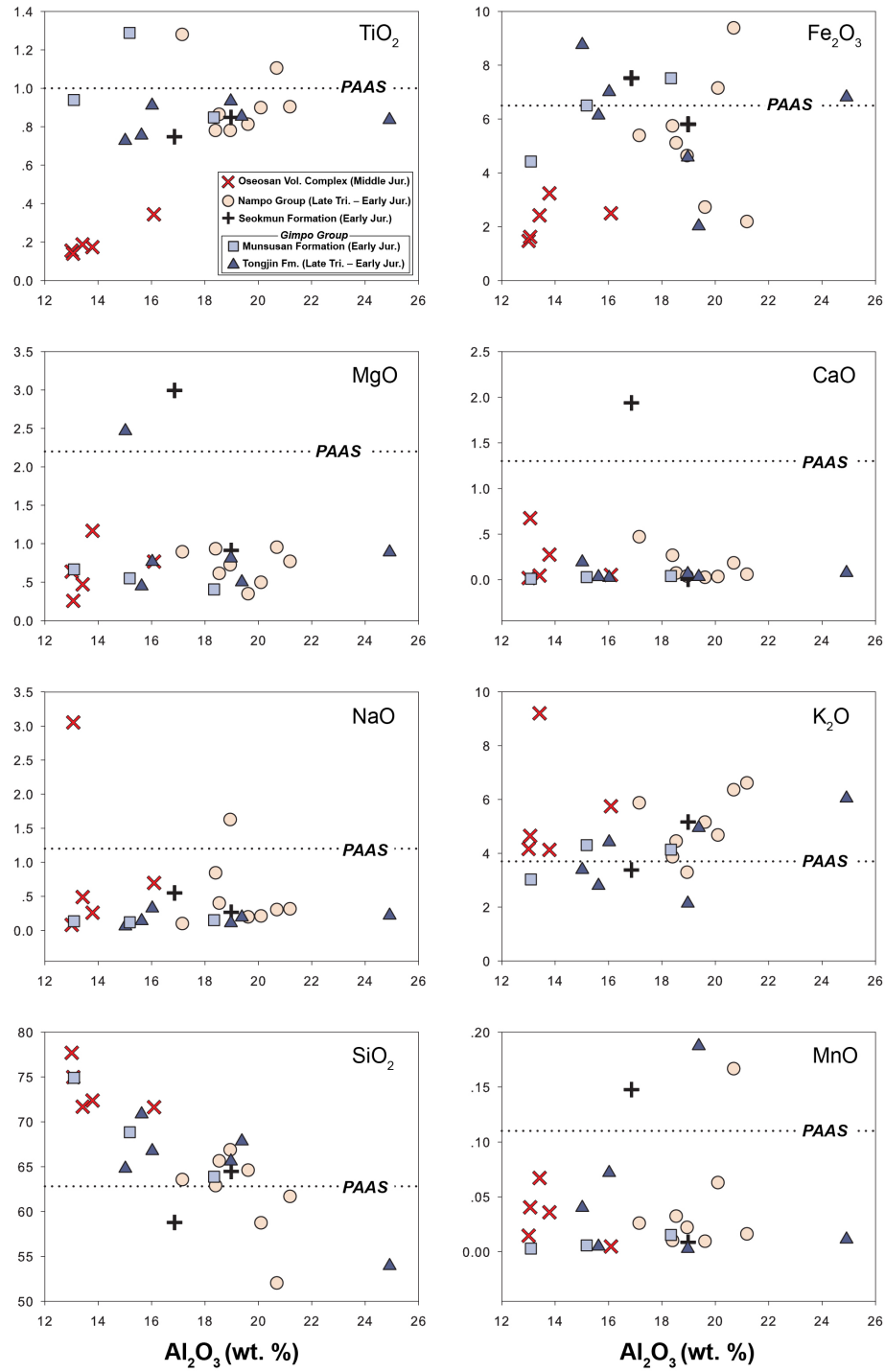

Fig. 3-9. Major element–Al_2O_3 binary plots of the mudstone samples. The dotted line indicates the major-element content of PAAS (Taylor and McLennan, 1985).

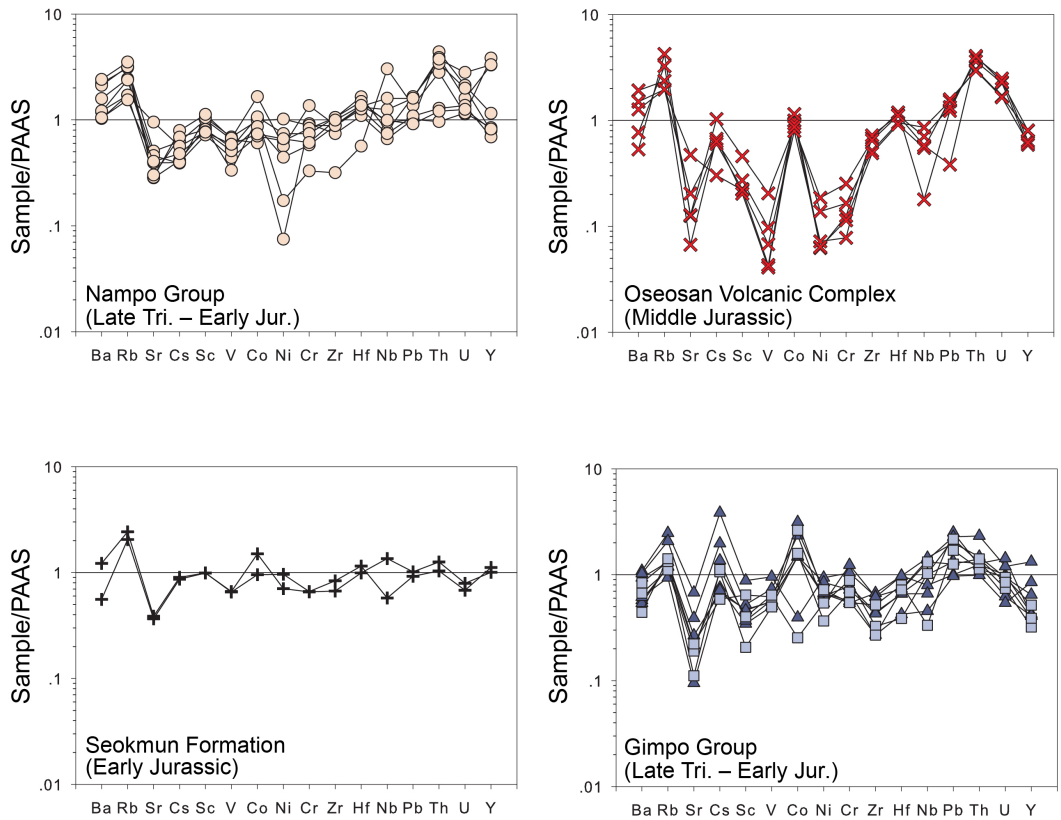

Fig. 3-10. Trace-element composition of the mudstone samples normalized against PAAS (Taylor and McLennan, 1985).

3.4.2.3. Rare earth elements (REEs)

The REE levels and chondrite-normalized REE patterns are presented in Figure 3-11. The total REE abundance (ΣREE) was generally higher than that in PAAS (183 ppm), ranging from 124 to 788 ppm, with an average of 358 ppm. The samples from the Nampo Group showed the highest ΣREE (av. 473 ppm), while the samples from the Gimpo Group exhibited a lower ΣREE (av. 265 ppm) than those from the Seokmun Formation (av. 355 ppm) and Oseosan Volcanic Complex (av. 343 ppm). The REE patterns were all characterized by strong LREE enrichment compared to HREEs.

Most of the analyzed samples showed higher La_N/Yb_N ratios than PAAS (9.20), ranging from 6.93 to 40.29, with an average of 19.64. The samples from the Oseosan Volcanic Complex exhibited the highest La_N/Yb_N ratios (av. 29.21), while the samples from the Nampo Group had slightly higher La_N/Yb_N ratios (av. 17.66) than those from the Gimpo Group (av. 16.80) and Seokmun Formation (av. 16.10).

The REE patterns were also characterized by strong negative Eu anomalies. The Eu/Eu* values ranged from 0.29 to 0.80, with an average of 0.59. The samples from the Oseosan Volcanic Complex showed the lowest Eu/Eu* values (av. 0.46). Although the samples from the Seokmun Formation tended to have slightly higher Eu/Eu* values (av. 0.66) than those from the Nampo and Gimpo groups (the average of both = 0.62), these samples could not be clearly distinguished from each other.

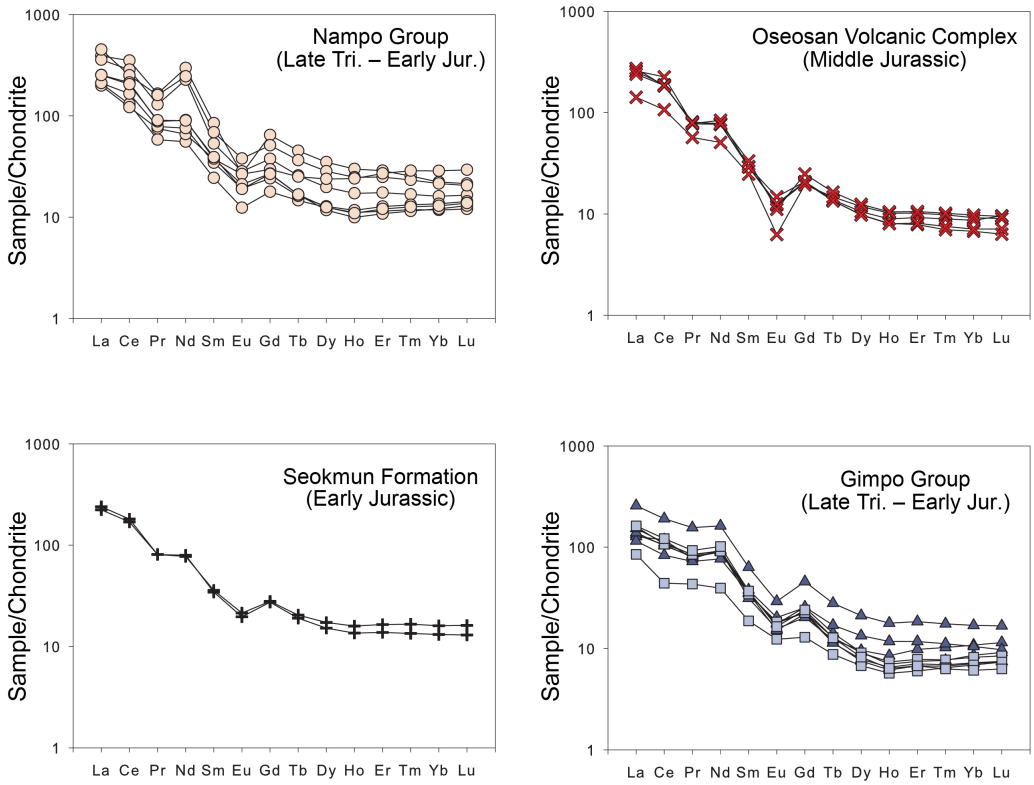

Fig. 3-11. Chondrite-normalized REE plots of the mudstone samples. The chondrite normalizing factors are from Taylor and McLennan (1985).

3.5. Discussion

3.5.1. Geochemical information on the sedimentary provenance

The major-element geochemistry is a useful indicator for deciphering the provenance of sedimentary rocks. Figure 3-12 presents a provenance-discrimination diagram for two functions that use the unstandardized abundance of seven major elements (TiO_2, Al_2O_3, Fe_2O_3, MgO, CaO, Na_2O, and K_2O; Roser and Korsch, 1988). Most of the analyzed samples fell close to the boundary between the P3 and P4 fields, representing a mixed provenance signature of felsic igneous and quartzose (meta-)sedimentary rocks. In detail, however, some variations existed in the provenance signatures of the analyzed sample groups. The samples from the Gimpo Group occurred mostly in or near the P4 field, indicating a high proportion of mature detritus from (meta-)sedimentary rocks. On the other hand, the Nampo Group's samples plotted in the P3 field, most likely indicating a relatively higher ratio of detritus that was derived from felsic igneous rocks. The samples from the Seokmun Formation fell between those from the Gimpo and Nampo groups, but the small number of samples makes drawing conclusions regarding their provenance pattern difficult. The samples from the Oseosan Volcanic Complex were distributed broadly across the P3 and P4 fields. Because the tuffaceous sedimentary rocks of the Oseosan Volcanic Complex overlie thick rhyolitic tuff (highly enriched in SiO_2; Park et al., 2018), this scattering of data points might be interpreted as the result of the significant input of felsic volcanic detritus with the recycling of (meta-)sedimentary rocks.

Trace- and rare earth-element ratios such as Th/Sc, Cr/Th, Co/Th, La_N/Yb_N, and Eu/Eu* can also be used as provenance indicators (e.g., Cullers, 1994; Cullers and Podkovyrov, 2000; Roy and Roser, 2013). These ratios record source-rock signatures during depositional

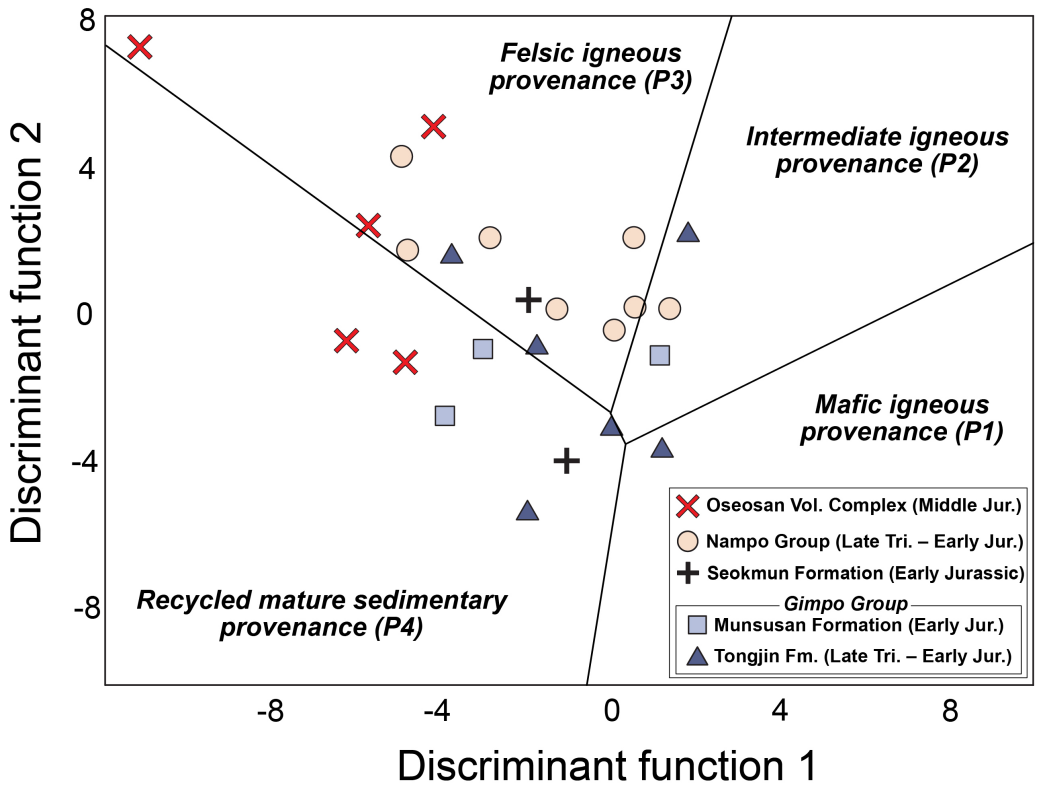

Fig. 3-12. Provenance-discrimination diagram for the major elements of mudstone (Roser and Korsch, 1988). The discriminant functions are calculated as follows: discriminant function 1 = $-1.773TiO_2 + 0.607Al_2O_3 + 0.76Fe_2O_3 - 1.5MgO + 0.616CaO + 0.509Na_2O - 1.224K_2O - 9.09$; discriminant function 2 = $0.445TiO_2 + 0.07Al_2O_3 - 0.25Fe_2O_3 - 1.142MgO + 0.438CaO + 1.475Na_2O + 1.426K_2O - 6.861$ (Roser and Korsch, 1988).

and post-depositional processes (Taylor and McLennan, 1985; McLennan et al., 1993). All the analyzed mudstone samples showed higher Th/Sc ratios than that of PAAS (0.91), ranging from 0.95 to 17.75 with an average of 4.49 (Table 3-4). This result suggests that the sediment was predominantly derived from felsic igneous rocks and/or mature sedimentary rocks (McLennan et al., 1993). The relatively high La_N/Yb_N ratios and strong negative Eu anomalies in the REE patterns (Table 3-4 and Figure 3-11) also support an overall felsic nature for the source rocks.

The spatial variation in the provenance of the Early to Middle Mesozoic sedimentary units along the western Korean Peninsula was also illustrated by their trace- and rare earth-element patterns. On the binary plot of Cs/Th against Co/Th (Fig. 3-13a), the Gimpo Group and Seokmun Formation, which had relatively high Cs/Th and Co/Th ratios, were clearly distinguishable from the Nampo Group and Oseosan Volcanic Complex. Cs is strongly enriched in fine-grained sedimentary rocks or their metamorphic products rather than igneous rocks (Parker, 1967; Tanaka and Watanabe, 2015; Zaunbrecher et al., 2015), so (meta-)sedimentary rocks such as shale and schist may have been broadly distributed in the source areas of the Gimpo Group and Seokmun Formation. On the binary plot of Th/Sc against Cr/Th (Fig. 3-13b), the samples from the Oseosan Volcanic Complex, which had relatively high Th/Sc and low Cr/Th ratios, were distinguishable from the other analyzed samples, which suggests considerable detritus input from extremely felsic volcanic rocks, as outlined above.

Previous provenance studies (e.g., Yu and Lee, 1992; Yu et al., 1992) proposed that the Nampo and Gimpo groups were mainly derived from quartzose sedimentary rocks based on petrographic observation that was characterized by a high proportion of quartzite clasts

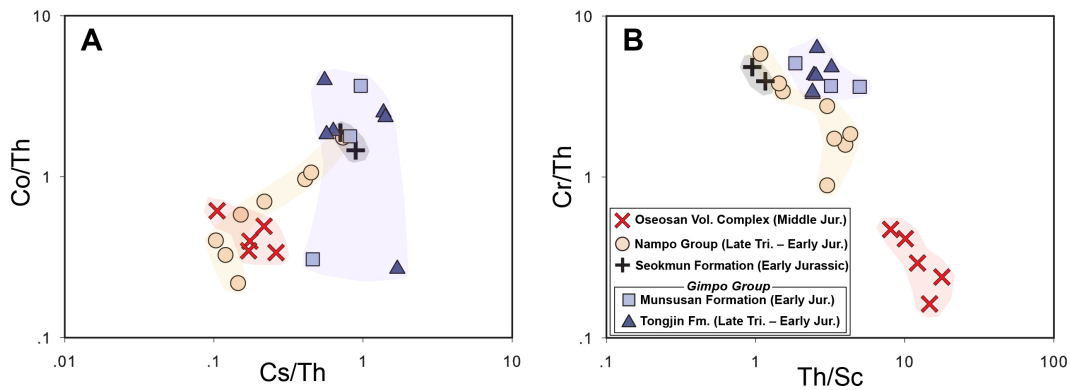

Fig. 3-13. Binary plots for the trace-element ratios of the mudstone samples. (a) Cs/Th vs. Co/Th. (b) Th/Sc vs. Cr/Th.

in conglomerates and a low proportion of feldspar grains in sandstones (Fig. 3-5). The previous interpretation differs from that based on the mudstone geochemistry of the Nampo Group, which reflects a felsic igneous provenance (Fig. 3-12). Recent provenance studies have emphasized that geochemical data of fine-grained rocks may provide more accurate information about the source rocks than traditional petrological and petrographic analyses for conglomerate and sandstones (von Eynatten et al., 2003; Weltje and von Eynatten, 2003; Hessler and Lowe, 2006; Kutterolf et al., 2008). It is because that labile minerals such as feldspars are transformed into clay minerals during weathering processes and durable quartz-dominant detritus are accumulated in conglomerates and sandstones (e.g., Hessler and Lowe, 2006), making the provenance signature of conglomerate and sandstone more mature than those of the source rocks. The Nampo Group was deposited under tropical to subtropical climate conditions (Chun et al., 1988), and thus, the sediment contribution from felsic igneous rocks to the Nampo Group might be difficult to be recognized from the previous petrographic observation about coarse-grained sedimentary rocks. Additionally, diagenetic replacement of feldspars and rock fragments by mica in the sandstones of the Nampo Group (Egawa and Lee, 2008) might contribute to underestimation of felsic igneous provenance signature for the Nampo Group.

3.5.2. Orogenic denudation and post-collisional basin filling

Expansion and/or relocation of catchment areas may induce changes in type and ages of the dominant source rocks, consequently resulting in upsection changes in zircon age distribution and composition of sedimentary successions (e.g., Shao et al., 2015; Yang et al., in press). In fault-bounded basins, however, catchment areas are difficult to expanded

far from the bounding faults due to their episodic reactivations (e.g., Leeder et al., 1991; Cecil et al., 2010; Fosdick and Blisniuk, 2018). Considering that the Daedong Supergroup consists of repeated alluvial-lacustrine sequences deposited under tropical or subtropical climate (Chun et al., 1987, 1990), the cyclic changes in depositional environments were likely caused by repeated events of basin subsidence and uplift of the source areas, and the detritus was mainly derived from nearby source rocks without significant widening of drainage area (Blair and Bilodeau, 1988). It means that detrital-zircon U-Pb geochronological data of this study, coupled with geochemical data, can increase understanding of the relationship between orogenic denudation and post-collisional basin filling within the western Korean Peninsula. However, it should be noted that some spot analyses, dated at a few isolate ages, might result from radiogenic Pb loss. Early Jurassic zircon ages, dated at ca. 197 Ma and 175 Ma, from the Amisan Formation (DC02: Table 3-2) have been interpreted to be ascribed to Pb loss (Jeon et al., 2007). Thus, these ages, likely resulting from radiogenic Pb loss, were excluded from further discussion.

The Gimpo Group and Seokmun Formation exhibited a variety of zircon-age clusters, including the Archean, Paleoproterozoic, Mesoproterozoic, Neoproterozoic, Cambrian–Carboniferous, and Triassic, although these formations exhibited different peak intensities (Table 3-2 and Fig. 3-8). Most of these age groups were identified in nearby metasedimentary units (Fig. 3-14), including the Middle or Late Paleozoic Taean Formation (e.g., Cho et al., 2010; Kim et al., 2014, 2017b; Han et al., 2017), the Middle Paleozoic Yeoncheon and Imjin groups (e.g., Kim et al., 2014, 2017b; Han et al., 2017; Zhang et al., 2018), the Early Neoproterozoic Sangwon Supergroup (e.g., Kim et al., 2016), and Late Paleoproterozoic Seosan Group (Cho et al., 2006). These detrital-zircon records

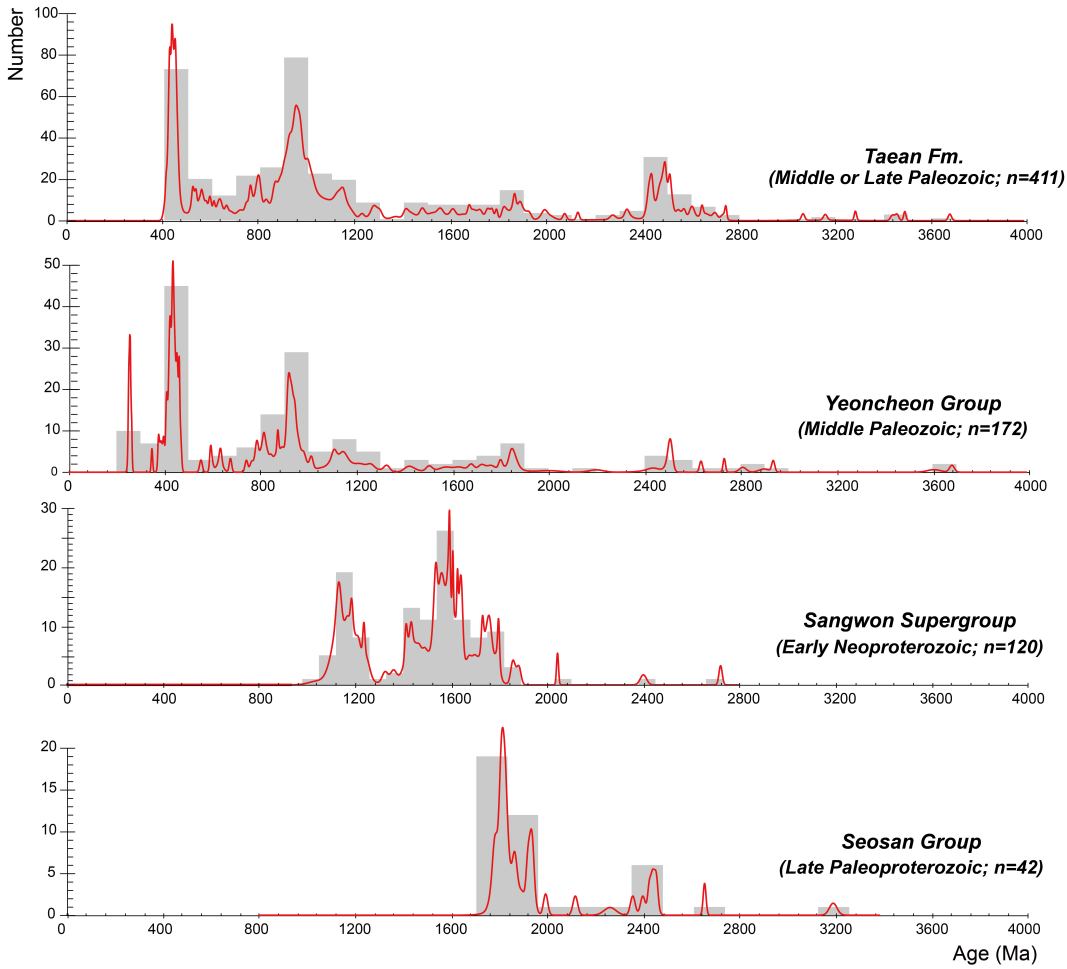

Fig. 3-14. Probability-density plots and histograms of detrital-zircon U-Pb ages that were previously reported from the Middle or Late Paleozoic Taean Formation (Cho, 2007; Cho et al., 2010; So et al., 2013; Kim et al., 2014), the Middle Paleozoic Yeoncheon Group (Kim et al., 2017b), the Early Neoproterozoic Sangwon Supergroup (Kim et al., 2016), and the Late Paleoproterozoic Seosan Group (Cho et al., 2006) as the possible source rocks of the Daedong Supergroup's sandstones.

support geochemical signatures indicative of major role of sediment recycling in the detritus supply (Figs. 3-12 and 3-13). Small groups of Late Devonian, Late Triassic, and Early Carboniferous zircons (Table 3-2 and Fig. 3-8) were likely derived from nearby igneous bodies or metasedimentary rocks. Late Triassic granitoids (ca. 235 to 218 Ma; Williams et al., 2009; Cheong et al., 2015; Cho and Lee, 2017) are common in the western Korean Peninsula (Fig. 3-2). Late Devonian felsic and mafic igneous rocks (ca. 370 Ma; Kim et al., 2011, 2015, 2017b) or Late Paleozoic metasedimentary rocks with Late Devonian (ca. 370 to ca. 360 Ma; Kim et al., 2011) detrital zircons are sporadically distributed in this area. The Late Devonian and the Late Triassic igneous rocks preserve evidence of post-collisional or post-orogenic extensions that were associated with plate convergence along the western Korean Peninsula (Kim et al., 2015). However, an Early Carboniferous igneous body is seldom recognized in and around the western Korean Peninsula. Early Carboniferous detrital zircons (ca. 360 to 331 Ma: Kim et al., 2011) have been reported in Late Paleozoic metasedimentary rocks locally distributed in the western Korean Peninsula. The Early Carboniferous zircons in the Gimpo Group and Seokmun Formation (ca. 358 to 347 Ma; Table 3-2) are possibly a window to the Late Paleozoic subduction-related magmatism in the orogenic belt along the western Korean Peninsula before final continental amalgamation, although its product is now undetectable because of complete denudation. However, further work is required to precisely track ultimate source rocks of the Early Carboniferous detrital zircons.

The detrital-zircon age patterns from the Nampo Group are more monotonous than those from the Gimpo Group and Seokmun Formation, but those of the stratigraphic formations exhibited conspicuous variations that are indicative of temporal and/or spatial changes in

sediment provenance (Fig. 3-7). Given the geochemical signatures (Figs. 3-12 and 3-13), the main age peaks from the Nampo Group suggest sediment input from nearby Paleoproterozoic, Neoproterozoic, and Late Paleozoic to Middle Mesozoic felsic igneous rocks or geochemically equivalent migmatitic basement gneisses. This interpretation was confirmed by the reported ages of the Paleoproterozoic, Neoproterozoic, and Mesozoic crystallization and metamorphism in the felsic ortho- and paragneisses and granites around the Nampo Group (e.g., Park et al., 2009, 2014b). However, Late Paleozoic to Early Mesozoic zircons with ages ranging from ca. 359 to ca. 240 Ma (Table 3-2 and Fig. 3-7) in the Nampo Group have seldom been reported from igneous rocks in and around the western Korean Peninsula. Carboniferous detrital zircons might be supplied from nearly Late Paleozoic metasedimentary rocks (Kim et al., 2011), as discussed above. However, sources rocks of the Permian to Middle Triassic detrital zircons are enigmatic at this moment. Various hypotheses including 1) Permian to Middle Triassic subduction and/or collision-related magmatism along the western Korean Peninsula, and 2) local zircon supply from other orogenic belts, such as the northern margin of the North China Craton (Zhang et al., 2016; Cao et al., 2013) and the Okcheon Belt of the Korean Peninsula (Kim and Lee, 2018; references therein), are required to be tested through further work.

In summary, the sediments in the sporadic post-collisional basins along the western Korean Peninsula might have been derived from the denudation of nearby collapsed mountainous regions that consisted of metasedimentary cover rocks and basements. Variations in geochemical and detrital-zircon geochronological data between the basins depended on their structural position in the orogenic belt. In other words, the spatial variations in the sources of the basin fills indicated that the Nampo Group was located on

the hinterland side of the mountain belt, mainly exposing crystalline basements (migmatitic gneisses and granites), whereas the Gimpo Group and Seokmun Formation on the foreland side mainly consisted of metasedimentary rocks (Figure 3-2).

3.5.3. Tectonic transition during basin evolution: insights from the Chungnam Basin

Recent research found that the Chungnam Basin evolved as a two-phase extensional basin system in relation to an orogenic cycle from the closure of the Paleo-Tethys Ocean to the subduction of the Paleo-Pacific Plate (Park et al., 2018, 2019). This observation implies that the transition between the orogenic processes in the continental margin can be tracked based on temporal variations in the sedimentary responses.

The detrital-zircon ages from the Hajo Formation, the lowermost strata of the Nampo Group, were monotonous only for the Paleoproterozoic signature (Table 3-2 and Fig. 3-7), which is much older than the depositional age. The considerable difference between the detrital-zircon and depositional ages has been interpreted as a diagnostic feature of rift or passive-margin basins, which generally lack syn-depositional igneous activity and are mainly filled with detritus from old cratons (Hawkesworth et al., 2009; Cawood et al., 2012). However, the Late Triassic post-collisional tectonic framework in the southwestern Gyeonggi massif (Williams et al., 2009; de Jong et al., 2015) suggests a plausible alternative interpretation, where igneous intrusions that were related to the closure of the Paleo-Tethys Ocean were not exposed in the drainage basin during the initial stages of basin formation. Only nearby Paleoproterozoic crystalline basements, probably in the hinterland highlands, were sources of detritus to the basin. In contrast, the middle to upper Nampo

Group (the Amisan to Seongjuri formations) were characterized by younger detrital-zircon spectra (Permian to Early Jurassic) that were closer to the sedimentation age (Table 3-2 and Fig. 3-7), except for the sample from the Baegunsa Formation, which was probably affected by local variations in sources. The Chungnam Basin experienced the increased input of younger detritus likely from nearby exhumed Permo–Triassic igneous rocks during the sedimentation of the middle to upper Nampo Group. The minor presence of Early Jurassic zircons suggests an incipient stage of Jurassic subduction-related magmatism in the western Korean Peninsula because of the interplay between the Paleo-Pacific and Eurasian plates (Sagong et al., 2005; Cheong et al., 2018). The emergence of the Archean to Paleoproterozoic episodic age peaks in the middle to upper Nampo Group strongly indicates the exhumation of migmatized felsic paragneisses with Paleoproterozoic and older detrital zircons in the source area, as reported by Park et al. (2014b). The exhumation of the migmatite might have been caused, at least partially, by the crustal extension and/or diapiric upwelling of low-density, partially molten rocks, which are ubiquitous thermo-mechanical phenomena in relation to late- or post-orogenic processes in various mountain belts (e.g., Coney, 1980; Axen et al., 1995). Late Triassic near-isothermal decompression and subsequent rapid cooling, which were recorded in metabasite bodies that were embedded in migmatite (Oh et al., 2005; Kim et al., 2006), can be considered a diagnostic feature of diapiric upwelling (Vanderhaeghe and Teyssier 2001; Teyssier and Whitney, 2002).

Once the sedimentation of the Nampo Group ended in the Early Jurassic, the Chungnam Basin was further expanded in an intra-arc environment associated with the subduction of the Paleo-Pacific Plate underneath the Eurasian Plate (Park et al., 2018, 2019). Volcanic

materials with geochemical features of the continental arc filled the basin from 178 to 172 Ma, producing the lower rhyolitic-tuff unit of the Oseosan Volcanic Complex (Park et al., 2018). The analyzed samples from the upper tuffaceous sedimentary unit (180807-8 and 180807-11) overlying the lower tuff unit had a high proportion of Early to Middle Jurassic detrital zircons (ca. 181 to 158 Ma), although differences between their age ranges and abundances existed (Table 3-2 and Fig. 3-7). Notably, the proportion of young detrital zircons with ages close to the sedimentation age of the strata in sample 180807-8 was over 50%. This pattern is typical of basins along convergent plate margins, where magmatism actively generates zircons (Hawkesworth et al., 2009; Cawood et al., 2012).

In summary, the Nampo Group and Oseosan Volcanic Complex in the Chungnam Basin exhibited temporal variations in their zircon age-spectra patterns. Archean to Paleoproterozoic zircons tended to decrease with ascending stratigraphic order in the Nampo Group, while Phanerozoic zircons increased in number and diversity. On the other hand, the Oseosan Volcanic Complex included a high proportion of zircons with ages close to the deposition age. The detrital-zircon record was most likely controlled by orogenic exhumation and sediment input from the adjoining volcanic arc, reflecting the transition from collisional to convergent tectonic settings (Figs. 3-15 and 3-16).

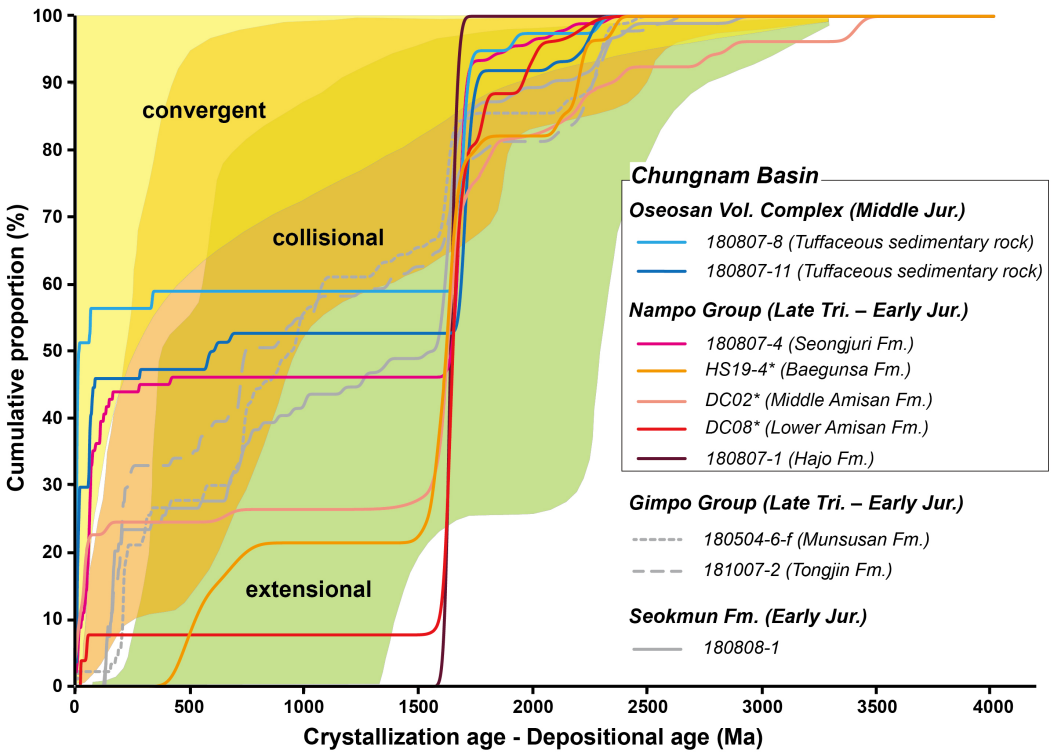

Fig. 3-15. Cumulative-age probability curves of detrital zircons from the Nampo Group and the Oseosan Volcanic Complex in the Chungnam Basin, along with the Gimpo Group (the Tongjin and Munsusan formations) and the Seokmun Formation for comparison. The proposed tectonic settings for sedimentary rocks are based on differences between the zircon-crystallization and -depositional ages (Cawood et al., 2012). The depositional age was assumed 1) as 223 Ma (the youngest age of post-collisional granite as a basement in the western Gyeonggi Massif: Cho and Lee, 2017) for the lower to middle Nampo Group (Hajo, Amisan, and Baegunsa formations), the Tongjin and Seokmun formations, and 2) as the youngest zircon age for the Upper Nampo Group (Seongjuri Formation), Oseosan Volcanic Complex, the Munsusan Formation, which contain zircon grains younger than 223 Ma. The detrital zircon data for the Amisan and Baekunsa formations were abapted from Jeon et al. (2007) and are marked with *.

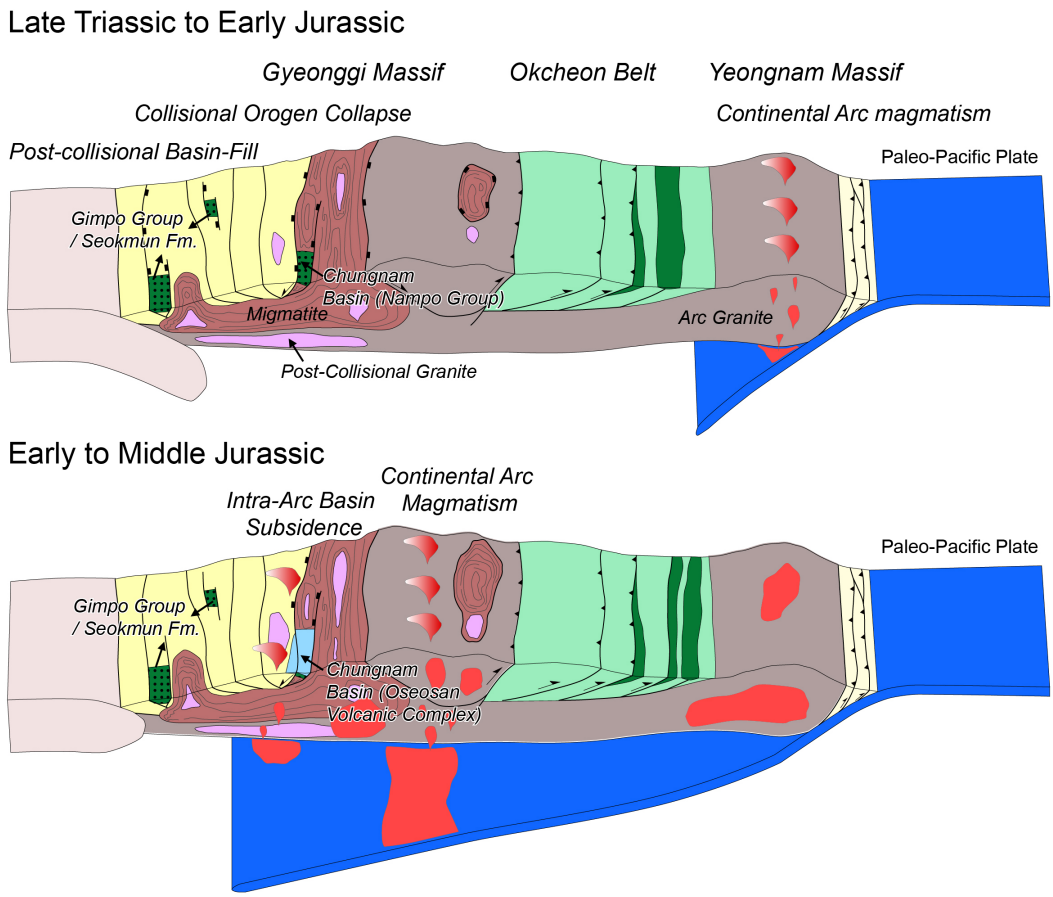

Fig. 3-16. Schematic diagrams that show a tectonic transition from post-collision (Late Triassic to Early Jurassic) to subduction (Early to Middle Jurassic) in the western Korean Peninsula (modified from Park et al., 2018, 2019).

SUMMARY AND CONCLUSION

Facies analysis, geochemical analysis for mudstones and zircon U-Pb analysis were carried out on the Mesozoic nonmarine basins located on the western Korean Peninsula to investigate evolution history of the basins.

The Cretaceous Nenungju Basin was filled during Late Cretaceous (ca. Cenomanian to Santonian) in nonmarine environments, experiencing intermittent volcanic activities and resultant input of volcaniclastic sediments. Based on facies analysis in the northern part of the Neungju Basin, four facies associations are recognized, representing (1) alluvial fan, (2) alluvial plain, (3) sandflat, and (4) playa lake environments. The basin fill can be subdivided into four stratigraphic units by thick amalgamated tuff beds. The lowermost unit (Unit I) is composed of alluvial plain deposits. The lack of any vertical depositional trend indicates a balance between basin subsidence and sediment supply. The middle units (Units II and III) show spatial differences in depositional environments. Playa lake was extensively distributed in the central to northern parts of the study area, which was later gradually filled by prograding proximal depositional systems. Playa lake was not expanded to the southern part of the study area during the deposition of the middle units. Instead, alluvial plains were prevailed in the areas. The uppermost unit (Unit IV) shows a vertical transition from alluvial fan to sandflat, comprising a fining-upward trend that reflects a gradual decrease of sediment supply. Vertical and spatial changes in depositional environments were strongly controlled by tectono-volcanic subsidence and source area rejuvenation after volcanism. Tectono-volcanic subsidence followed by volcanism increased accommodation generation, resulting in two events of lake expansion in the distal environments (Units II and III). Influence of tectono-volcanic subsidence might be minor

in the proximal environments, resulting in the conglomerate deposition (Unit IV). Due to coupling of volcanism and tectono-volcanic subsidence, various type of boundary (conformable to unconformable) can be formed according to the relative position of a basin between syneruption and inter-eruption deposits. The traditional depositional model composed of syneruption aggradation and inter-eruption degradation may not be sufficient to explain the development of sedimentary succession.

Provenance interpretation for the Neungju Basin based on previous zircon U-Pb data and paleocurrent data shows that sediment detritus was derived from three types of different source rocks: (1) Precambrian metamorphic rocks, (2) Jurassic to Triassic granites, and (3) Cretaceous volcaniclastic plains developed on the southern part of the basin. Precambrian and Jurassic (to Triassic) age peaks are identified from the sandstone samples collected in the marginal areas close to the western, northern and eastern basin margins. Prominent Cretaceous age peaks are identified in the sandstone samples collected in the southern and central parts of the study area, indicating exclusive input of Cretaceous volcanic zircons from the southern volcaniclastic plains to the areas. Due to the additional input of plagioclase-rich materials from the volcaniclastic plains to the central area, the mudstone samples deposited in distal environment (playa lake) are distinguished by those deposited in proximal environment (alluvial fan to sandflat) by their higher Na_2O content. The compositional contrast induces differences in tectonic setting signatures for the proximal and distal mudstone samples: passive margin signature for the proximal samples, whereas active continental margin signatures for the distal samples. Because mixing of sediment detritus from different source rocks occurred in the central areas of the basin, the mudstone samples collected from the distal environments can be considered as a proper representative

of tectonic setting signatures. On the other hand, the distal mudstone samples provide the weathering indices lower than expected by sedimentological and paleontological evidences. Derivation of less- or un-altered materials from the southern volcaniclastic plains might result in the lowering of weathering signatures for the distal mudstones. Overall, the results imply that geochemical data obtained from a specific position (or specific depositional environment) of a nonmarine basin may deliver inappropriate information about tectonic setting and weathering conditions. Geochemical analysis should be applied in support of various analytic methods and background information for proper interpretation of a basin.

Early Mesozoic (Triassic to Jurassic) nonmarine basins scattered on the western Korean Peninsula are an ideal target to investigate Mesozoic tectonic evolution of the Korean Peninsula. Provenance analysis using detrital zircon U-Pb age dating and mudstone geochemistry was performed on the Chungnam and Gimpo basin fills with the Seokmun Formation. The results show that the lower Chungnam Basin fills (the Nampo Group) was mainly derived from nearby felsic igneous rocks or geochemically equivalent migmatitic gneisses, whereas the Gimpo Basin fills (Tongjin and Munsusan formations) and the Seokmun Formation contemporary with the Nampo Group were mainly derived from metasedimentary rocks. This difference in provenance signature may reflect their structural positions in the Early Mesozoic orogeny belt: the exhumed basement-dominant hinterland side for the Chungnam Basin (south), and the cover rock-dominant foreland side for the Gimpo Basin (north). Additionally, the change of the youngest zircon age peaks in the Chungnam Basin fills from 1854 Ma in the lowermost unit to 164 Ma in the uppermost unit indicates a transition of tectonic settings from a post-collision to a convergent margin setting with intensified magmatic activities.

This study implies that application of single provenance analysis technique may deliver wrong information about a sedimentary basin. Sandstone petrography and bulk rock geochemistry are useful to discriminate tectonic setting of sedimentary basin and weathering conditions in the source areas. These methods, however, are vulnerable to preferential mixing and separation of sediment. If sediments were not well-mixed, petrographic and geochemical composition of sedimentary rocks may not reflect the overall compositional characteristics of a basin. Information such as depositional environments and sediment dispersal patterns should be considered together to validate the results obtained from petrographic and geochemical analysis. Also, sediment composition, especially petrographic composition of sandstones, can be easily homogenized by combination of intense chemical weathering and post-depositional alterations. Ancient sedimentary rocks deposited under warm and humid climatic conditions and modified after through diagenesis may provide similar compositional characteristics regardless of differences in their original source rock signatures. To reconstruct paleogeographic and paleoclimatic history properly, multi-disciplinary approach for provenance study is required.

REFERENCES

Acocella, V., 2010, Coupling volcanism and tectonics along divergent plate boundaries: collapsed rifts from central Afar, Ethiopia. Geological Society of America Bulletin, 122, 1717–1728.

Ainsworth, R.B., Hasiotis, S.T., Amos, K.J., Krapf, C.B.E., Payenberg, T.H.D., Sandstrom, M.L., Vakarelov, B.K., and Lang, S.C., 2012, Tidal signatures in an intracratonic playa lake. Geology, 40, 607–610.

Ahn, K.S., Huh, M., and Son, J.M., 2014, Geological history and landscape of Mudeungsan National Park. Journal of the Geological Society of Korea, 50, 91–105. (in Korean with English abstract)

Allen, J.P., Fielding, C.R., Rygel, M.C., and Gibling, M.R., 2013, Deconvolving signals of tectonic and climatic controls from continental basins: an example from the Late Paleozoic Cumberland Basin, Atlantic Canada. Journal of Sedimentary Research, 83, 847–872.

Allen, J.R.L., 1983, Studies in fluviatile sedimentation: bars, bar-complexes and sandstone sheets (low-sinuosity braided streams) in the Brownstones (L. Devonian), Welsh Border. Sedimentary Geology, 33, 237–293.

Andersen, T., 2002, Correction of common lead in U-Pb analyses that do not report ^{204}Pb. Chemical Geology, 192, 59–79.

Armstrong-Altrin, J.S. and Verma, S.P., 2005. Critical evaluation of six tectonic setting discrimination diagrams using geochemical data of Neogene sediments from known tectonic settings. Sedimentary Geology, 177, 115–129.

Ashley, G.M. and Hay, R.L., 2002, Sedimentation patterns in a Plio-Pleistocene volcaniclastic rift-platform Basin, Olduvai Gorge, Tanzania. In: Renaut, R.W. and Ashley, G.M. (eds.), Sedimentation in Continental Rifts. Society for Sedimentary Geology (SEPM), Special Publication 73, p. 107–122.

Axen, G.J., Bartley, J.M. and Selverstone, J., 1995, Structural expression of a rolling hinge in the footwall of the Brenner Line normal fault, eastern Alps. Tectonics, 14, 1380–1392.

Barth, A.P., Wooden, J.L., Jacobson, C.E., and Probst, K., 2004, U-Pb geochronology and geochemistry of the McCoy Mountains, southeastern California: a Cretaceous retroarc foreland basin. Geological Society of America Bulletin, 116, 142–153.

Best, J.I.M. and Bridge, J., 1992, The morphology and dynamics of low amplitude bedwaves upon upper stage plane beds and the preservation of planar laminae. Sedimentology, 39, 737–752.

Bhatia, 1983, Plate tectonics and geochemical composition of sandstones. Journal of Geology, 91, 611–627.

Blair, T.C., 1987, Sedimentary processes, vertical stratification sequences, and geomorphology of

the Roaring River alluvial fan, Rocky Mountain National Park, Colorado. Journal of Sedimentary Petrology, 57, 1–18.

Branney, M.J. and Kokelaar, P., 1994, Volcanotectonic faulting, soft-state deformation, and rheomorphism of tuffs during development of a piecemeal caldera, English Lake District. Geological Society of America Bulletin, 106, 507–530.

Branney, M.J. and Kokelaar, P., 1997, Giant bed from a sustained catastrophic density current flowing over topography: Acatlan ignimbrite, Mexico. Geology, 25, 115–118.

Branney, M.J. and Kokelaar, P. (eds.), 2002, Pyroclastic Density Currents and the Sedimentation of Ignimbrites. Geological Society of London, Memoir, 27, 143 p.

Bridge, J.S. and Best, J.L., 1988, Flow, sediment transport and bedform dynamics over the transition from dunes to upper-stage plane beds: implications for the formation of planar laminae. Sedimentology, 35, 753–763.

Buggle, B., Glaser, B., Hambach, U., Gerasimenko, N., and Markovic, S., 2011, An evaluation of geochemical weathering indices in loess-paleosol studies. Quaternary International, 240, 12–21.

Cao, H.-H., Xu, W.-L., Pei, F.-P., Wang, Z.-W., Wang, F., and Wang, Z.-J., 2013, Zircon U–Pb geochronology and petrogenesis of the Late Paleozoic–Early Mesozoic intrusive rocks in the eastern segment of the northern margin of the North China Block. Lithos, 170–171, 191–207.

Caracciolo, L., von Eynatten, H., Tolosana-Delgado, R., Critelli, S., Manetti, P., and Marchev, P., 2012, Petrological, geochemical, and statistical analysis of Eocene-Oligocene sandstones of the western Thrace Basin, Greece and Bulgaria. Journal of Sedimentary Research, 82, 482–498.

Carroll, A.R., and Bohacs, K.M., 1999, Stratigraphic classification of ancient lakes: Balancing tectonic and climatic controls. Geology, 27, 99–102.

Cas, R.A.F., and Wright, J.V., 1987. Volcanic Successions. Modern and Ancient. Chapman & Hall, London, 528 p.

Catuneanu, O. and Elango, H.N., 2001, Tectonic control on fluvial styles: the Balfour Formation of the Karoo Basin, South Africa. Sedimentary Geology, 140, 291–313.

Cawood, P.A., Hawkesworth, C.J., and Dhuime, B., 2012, Detrital zircon record and tectonic setting. Geology, 40, 875–878.

Cecil, M.R., Ducea, M.N., Reiners, P., Gehrels, G., Mulch, A., Allen, C., and Campbell, I., 2010, Provenance of Eocene river sediments from the central northern Sierra Nevada and implications for paleotopography. Tectonics, 29, TC6010.

Cheong, C.H. and Kim, G.S., 1966, Explanatory text of the geological map of Neungju Sheet (1:50,000). Geological Survey of Korea, 42 p. (in Korean and Engish)

Cheong, C.-S., Jeong, G.Y., Kim, H., Choi, M.-S., Lee, S.-H., and Cho, M., 2003, Early Permian peak metamorphism recorded in U–Pb system of black slates from the Ogcheon metamorphic belt, South Korea, and its tectonic implication. Chemical Geology, 193, 81–92.

Cheong, C.-S., Kee, W.-S., Jeong, Y.-J., and Jeong, G.Y., 2006, Multiple deformations along the Honam shear zone in southwestern Korea constrained by Rb–Sr dating of synkinematic fabrics: implications for the Mesozoic tectonic evolution of northeastern Asia. Lithos, 87, 289–299.

Cheong, C.-S., Kim, N., Jo, H.J., Cho, M., Choi, S.H., Zhou, H., and Geng, J.-Z., 2015, Lithospheric mantle signatures as revealed by zircon Hf isotopes of Late Triassic post-collisional plutons from the central Korean peninsula, and their tectonic implications. Terra Nova, 27, 97–105.

Cheong, A.C.-S., Jo, H.J., Jeong, Y.-J., and Li, X.-H., 2018, Magmatic response to the interplay of collisional and accretionary orogenies in the Korean Peninsula: Geochronological, geochemical, and O-Hf isotopic perspectives from Triassic plutons. Geological Society of America Bulletin, 131, 609–634.

Cho, D.-L., 2007, SHRIMP zircon dating of a low-grade meta-sandstone from the Taean Formation: Provenance and its tectonic implications. KIGAM Bulletin, 11, 3–14.

Cho, D.-L. and Lee, S.-B., 2017, 1:100,000 Tectonostratigraphic map of the Gimpo-Incheon area: Korea Institute of Geoscience and Mineral Resources.

Cho, D.-L., Kim, Y.-J., and Armstrong, R., 2006, SHRIMP U-Pb geochronology of detrital zircons from iron-bearing quartzite of the Seosan Group: constraints on age and stratigraphy. Journal of the Petrological Society of Korea, 15, 119–127 (in Korean with English abstract).

Cho, M., and Kim, H., 2005, Metamorphic evolution of the Ogcheon Belt, Korea: a review and new age constraints. International Geology Review, 47, 41–57.

Cho, M., Kim, Y., and Ahn, J., 2007, Metamorphic evolution of the Imjingang belt, Korea: Implications for Permo-Triassic collisional orogeny. International Geology Review, 49, 30–51.

Cho, M., Na, J., and Yi, K., 2010, SHRIMP U-Pb ages of detrital zircons in metasandstones of the Taean Formation, western Gyeonggi massif, Korea: tectonic implications. Geosciences Journal, 14, 99–109.

Cho, M., Lee, Y., Kim, T., Cheong, W., Kim, Y., and Lee, S.R., 2017, Tectonic evolution of Precambrian basement massifs and an adjoining fold-and-thrust belt (Gyeonggi Marginal Belt), Korea: An overview. Geosciences Journal, 21, 845–865.

Cho, M., Min, K., and Kim, H., 2018, Geology of the 2018 Winter Olympic site, Pyeongchang, Korea. International Geology Review, 60, 267–287.

Choi, H.-I., Kim, D.S., and Seo, H.G., 1987, Stratigraphy, Depositional Environment and Basin Evolution of the Daedong Strata in the Chungnam Coalfield. KIER Research Report (KR-

87-(B)-3), Daejeon, 97 p. (in Korean with English abstract)

Chough, S.K., Kwon, S.-T., Ree, J.-H., and Choi, D.K., 2000, Tectonic and sedimentary evolution of the Korean Peninsula: a review and new view. Earth-Science Reviews, 52, 175–235.

Chun, H.Y., Bong, P.Y., Lee, H.Y., and Choi, S.J., 1987, Paleontology and Stratigraphy of the Chungnam Coalfield. KIER Research Report (KR-87-28), Daejeon, 52 p. (in Korean with English abstract)

Chun, H.Y., Kim, D.H., Um, S.H., Bong, P.Y., Lee, H.Y., Choi, S.J., Kim, B.C., and et al., 1990, The Study on the Organic Remains of the Separated Sedimentary Basin in Korea. Korea Institute of Energy and Resources, 288 p (in Korean).

Chwae, U., Kim, G.B., Choi, S.J., Yun, U., and Jin, M.S., 1995, Geological report of the Kimpo-Incheon sheets (1:50,000). Korea Institute of Geology, Mining and Materials, 34 p. (in Korean with English abstract)

Chwae, U., Choi, S.-J., and Kim, K.B., 1997, Explanatory text of the geological map of Tongjin sheet (1:50,000). Korea Institute of Geology, Mining, and Materials, 63 p. (in Korean with English abstract)

Cluzel, D., 1992, Formation and tectonic evolution of early Mesozoic intramontane basin in the Ogcheon belt (South Korea): a reappraisal of the Jurassic “Daebo orogeny”. Journal of Southeast Asian Earth Sciences, 7, 223–235.

Coney, P.J., 1980, Cordilleran metamorphic core complexes: An overview. Geological Society of America, special publication, 153, 7–31.

Cullers, R.L., 1994, The controls on the major and trace element variation of shales, siltstones, and sandstones of Pennsylvanian–Permian age from uplifted continental blocks in Colorado to platform sediment in Kansas, USA. Geochimica et Cosmochimica Acta, 58, 4955–4972.

Cullers, R.L. and Podkovyrov, V.N., 2000, Geochemistry of the Mesoproterozoic Lakhanda shales in southeastern Yakutia, Russia: implications for mineralogical and provenance control, and recycling. Precambrian Research, 104, 77–93.

de Jong, K., Han, S., and Ruffet, G., 2015, Fast cooling following a Late Triassic metamorphic and magmatic pulse and their bearing on the tectonic evolution of the Korean Collision Belt. Tectonophysics, 662, 271–290.

D’Elia, L. and Marti, J., 2013, Caldera events in a rift depocentre: an example from the Jurassic Neuguen basin, Argentina. Journal of the Geological Society, London, 170, 571–584.

D'Elia, L., Martí, J., Muravchik, M., Bilmes, A., and Franzese, J.R., 2018, Impact of volcanism on the sedimentary record of the Neuquén rift basin, Argentina: towards a cause and effect model. Basin Research, 30, 311–335.

Dewey, J.F. and Bird, J.M., 1970, Mountain belts and the new global tectonics. Journal of Geophysical Research, 75, 2625–2647.

Dickinson, W.R., 1970, Interpreting detrital modes of graywacke and arkose. Journal of sedimentary Petrology, 40, 695–707.

Dickinson, W.R. and Suczek, C., 1979, Plate tectonics and sandstone composition. AAPG Bulletin, 63, 2164–2182.

Dickinson, W.R. and Gehrels, G.E., 2003, U-Pb ages of detrital zircons from Permian and Jurassic eolian sandstones of the Colorado Plateau, USA: paleogeographic implications. Sedimentary Geology, 163, 29–66.

Egawa, K. and Lee, Y.I., 2008, Thermal maturity assessment of the Upper Triassic to Lower Jurassic Nampo Group, mid-west Korea: Reconstruction of thermal history. Island Arc 17, 109–128.

Egawa, K. and Lee, Y.I., 2009, Jurassic synorogenic basin filling in western Korea: sedimentary response to inception of the western Circum-Pacific orogeny Basin Research, 21, 407–431.

Fedo, C.M., Nesbitt, H.W., and Young, G.M., 1995, Unraveling the effects of potassium metasomatism in sedimentary rocks and paleosols, with implications for paleoweathering conditions and provenance. Geology, 23, 921–924.

Fidolini, F., Ghinassi, M., Aldinucci, M., Billi, P., Boaga, J., Deiana, R., and Brivio, L., 2013, Fault-sourced alluvial fans and their interaction with axial fluvial drainage: An example from the Plio-Pleistocene Upper Valdarno Basin (Tuscany, Italy). Sedimentary Geology, 289, 19–39.

Fielding, C.R., 1984, A coal depositional model for the Durham Coal Measures of NE England. Journal of the Geological Society, 141, 919–931.

Fielding, C.R., 1986, Fluvial channel and overbank deposits from the Westphalian of the Durham coalfield, NE England. Sedimentology, 33, 119–140.

Floyd, P.A. and Leveridge, B.E., 1987, Tectonic environment of the Devonian Gramscatho basin, south Cornwall: framework mode and geochemical evidence from turbiditic sandstones. Journal of the Geological Society, London, 144, 531–542.

Folk, R.L., Andrews, P.B., and Lewis, D.W., 1970, Detrital sedimentary rock classification and nomenclature for use in New Zealand. New Zealand Journal of Geology and Geophysics, 13, 937–968.

Fosdick, J.C. and Blisniuk, K., 2018, Sedimentary signals of recent faulting along an old strand of the San Andreas Fault, USA. Scientific Report, 8, 12132.

Friend, P.F., 1966, Clay fractions and colours of some Devonian red beds in the Catskill Mountains, U.S.A. Quarterly Journal of the Geological Society, 122, 273–288.

Frostick, L.E. and Steel, R.J., 1993, Sedimentation in divergent plate-margin basins. In: Frostick, L.E. and Steel, R.J. (eds.), Tectonic Controls and Signatures in Sedimentary Successions. International Association of Sedimentologists, Special Publication, 20, p. 111–128.

Gawthorpe, R.L. and Leeder, M.R., 2000, Tectono-sedimentary evolution of active extensional basins. Basin Research, 12, 195–218.

Gawthorpe, R.L., Fraser, A.J., and Collier, R.E.L., 1994, Sequence stratigraphy in active extensional basins: implications for the interpretation of ancient basin-fills. Marine and Petroleum Geology, 11, 642–658.

Gehrels, G.E. and Stewart, J.H., 1998, Detrital zircon U-Pb geochronology of Cambrian to Triassic miogeoclinal and eugeoclinal strata of Sonora, Mexico. Journal of Geophysical Research, 103, 2471–2487.

Hadlari, T. and Rainbird, R.H., 2006, Tectonic accommodation and alluvial sequence stratigraphy of a Paleoproterozoic continental rift, Baker Lake Basin, Canada. Stratigraphy, 3, 263–283.

Han, S., de Jong, K., and Yi, K., 2017, Detrital zircon ages in Korean mid-Paleozoic meta-sandstones (Imjingang Belt and Taean Formation): Constraints on tectonic and depositional setting, source regions and possible affinity with Chinese terranes. Journal of Asian Earth Sciences, 143, 191–217.

Hawkesworth, C., Cawood, P., Kemp, T., Storey, C., and Dhuime, B., 2009, A Matter of Preservation. Science, 323, 49–50.

Hessler, A.M. and Lowe, D.R., 2006, Weathering and sediment generation in the Archean: an integrated study of the evolution of siliciclastic sedimentary rocks of the 3.2 Ga Moodies Group, Barberton Greenstone Belt, South Africa. Precambrian Research, 151, 185–210.

Holohan, E.P., Van Wyk de Vries, B., and Troll, V.R., 2008, Analogue models of caldera collapse in strike-slip tectonic regimes. Bulletin of Volcanology, 79, 773–796.

Huerta, P., Armenteros, I., and Silva, P.G., 2011, Large-scale architecture in non-marine basins: the response to the interplay between accommodation space and sediment supply. Sedimentology, 58, 1716–1736.

Huh, M., Paik, I.S., Chung, C.H., Hwang, K.G., and Kim, B.S., 2003, Theropod tracks from Seoyuri in Hwasung, Jeollanamdo, Korea: occurrence and paleontological significance. Journal of the Geological Society of Korea, 39, 461–478. (in Korean with English abstract)

Huh, M., Paik, I.S., Lockley, M.G., Hwang, K.G., Kim, B.S., and Kwak, S.K., 2006, Well-preserved theropod tracks from the Upper Cretaceous of Hwasun County, southwestern South Korea, and their paleobiological implications. Cretaceous Research, 27, 123–138.

Huntsman-Mapila, P., Tiercelin, J.-J., Benoit, M., Ringrose, S., Diskin, S., Cotton, J., and Hemond, C., 2009, Sediment geochemistry and tectonic setting: Application of discrimination diagrams to early stages of intracontinental rift evolution, with examples from the Okavango and Southern Tanganyika rift basins. Journal of African Earth Sciences, 53, 33–44.

Ingersoll, R.V., 1990, Actualistic sandstone petrofacies: discriminating modern and ancient source rocks. Geology, 18, 733–736.

Jang, Y., Kwon, S., and Yi, K., 2015, Structural style of the Okcheon fold-thrust belt in the Taebaeksan zone, Korea. Journal of Asian Earth Sciences, 105, 140–154.

Jayawardena, U.de S. and Izawa, E., 1994, A new chemical index of weathering for metamorphic silicate rocks in tropical regions: a study from Sri Lanka. Engineering Geology, 36, 303–310.

Jeon, H., Cho, M., Kim, H., Horie, K., and Hidaka, H., 2007, Early Archean to Middle Jurassic evolution of the Korean Peninsula and its correlation with Chinese cratons: SHRIMP U-Pb zircon age constraints. The Journal of Geology, 115, 525–539.

Jo, H.R., 2003, Non-marine successions in the northwestern part of Kyongsang Basin (Early Cretaceous): fluvial styles and stratigraphic architecture. Geosciences Journal, 7, 89–106.

Joo, Y.J., Lee, Y.I., and Hisada, K., 2007, Provenance of Jurassic accretionary complex: Mino terrane, inner zone of south-west Japan – implications for paleogeography of eastern Asia. Sedimentology, 54, 515–543.

Joo, Y.J., Elwood Madden, M.E., and Soreghan, G.S., 2018, Anomalously low chemical weathering in fluvial sediment of a tropical watershed (Puerto Rico). Geology, 46, 691–694.

Jung, W., Ki, Y. and Huh, M., 2014, A petrological study of the Mudeungsan Tuff focused on Cheonwangbong and Anyangsan. The Journal of the Petrological Society of Korea, 23, 325–336. (in Korean with English abstract)

Kim, C.B. and Kang, S.S., 2012, K-Ar ages of Cretaceous fossil sites, Seoyuri, Hwasun, Southern Korea. Journal of the Korean Earth Science Society, 33, 618–626. (in Korean with English abstract)

Kee, W.-S., Kim, S. W., Kwon, S., Santosh, M., Ko, K., and Jeong, Y.-J., 2019, Early Neoproterozoic (ca. 913 – 895 Ma) arc magmatism along the central-western Korean Peninsula: Implications for the amalgamation of Rodinia supercontinent. Precambrian Research, 105498.

Kelly, S.B. and Olsen, H., 1993, Terminal fans - a review with reference to Devonian examples. Sedimentary Geology, 85, 339–374.

Kim, B.G. and Park, B.G., 1966, Geological report of the Dongbok sheet (1:50,000). Geological Survey of Korea, 33 p. (in Korean)

Kim, J.H., 1996, Mesozoic tectonics in Korea. Journal of Southeast Asian Earth Sciences, 13, 251–265.

Kim, M.G., and Lee, Y.I., 2018, The Pyeongan Supergroup (upper Paleozoic–Lower Triassic) in the Okcheon Belt, Korea: A review of stratigraphy and detrital zircon provenance, and its implications for the tectonic setting of the eastern Sino-Korean Block. Earth-Science Reviews, 185, 1170–1186.

Kim, M.J., Park, J.-W., Lee, T.-H., Song, Y.-S., and Park, K.-H., 2016, LA-MC-ICPMS U-Pb ages of the detrital zircons from the Baengnyeong Group: Implications of the dominance of the Mesoproterozoic zircons. Economic and Environmental Geology, 49, 433–444. (in Korean with English abstract)

Kim, S.W., Oh, C.W., Williams, I.S., Rubatto, D., Ryu, I.C., 2006. Phanerozoic high-pressure eclogite and intermediate-pressure granulite facies metamorphism in the Gyeonggi Massif, south Korea: implications for the eastward extension of the Dabie–Sulu continental collision zone. Lithos 92, 357–377.

Kim, S.W., Kwon, S., Santosh, M., Williams, I.S., and Yi, K., 2011, A Paleozoic subduction complex in Korea: SHRIMP zircon U–Pb ages and tectonic implications. Gondwana Research, 20, 890–903.

Kim, S.W., Kwon, S., Santosh, M., Cho, D.-L., and Ryu, I,-C., 2014, Detrital zircon U–Pb geochronology and tectonic implications of the Paleozoic sequences in western South Korea. Journal of Asian Earth Sciences, 95, 217–227.

Kim, S.W., Kwon, S., Park, S.-I., Yi, K., Santosh, M., and Ryu, I.-C., 2015, Early to Middle Paleozoic arc magmatism in the Korean Peninsula: constraints from zircon geochronology and geochemistry. Journal of Asian Earth Sciences, 113, 866–882.

Kim, S.W., Kwon, S., Park, S.-I., Yi, K., Santosh, M., and Kim, H.S., 2017a, Early to Middle Paleozoic tectonometamorphic evolution of the Hongseong area, central western Korean Peninsula: tectonic implications. Gondwana Research, 47, 308–322.

Kim, S.W., Park, S.-I., Jang, Y., Kwon, S, Kim, S.J., and Santosh, M., 2017b, Tracking Paleozoic evolution of the South Korean Peninsula from detrital zircon records: Implications for the tectonic history of East Asia. Gondwana Research, 50, 95–215.

Kim, S.W., Cho, D.-L., Lee, S.-B., Kwon, S., Park, S.-I., Santosh, M., and Kee, W.-S., 2018, Mesoproterozoic magmatic suites from the central-western Korean Peninsula: imprints of Columbia disruption in East Asia. Precambrian Research, 306, 155–173.

Kim, S.W., Kwon, S., Santosh, M., Cho, D.-L., Kee, W.-S., Lee, S.-B., and Jeong, Y.-J., 2019, Detrital zircon U-Pb and Hf isotope characteristics of the Early Neoproterozoic successions in the central-western Korean Peninsula: Implication for the Precambrian tectonic history of East Asia. Precambrian Research, 322, 24–41.

Kim, Y.-L., Koh, J.-S., Lee, J.-H., and Yun, S.-H., 2008, Petrological study on the Cretaceous volcanic rocks in the southwest Ryeongnam Massif: (1) the Mt. Moonyu volcanic mass, Seungju-gun. Journal of the Petrological Society of Korea, 17, 57–82. (in Korean with English abstract)

Koh, J.-S., Yun, S.-H., and Kim, Y.-L., 2009, Petrology of the Mt. Dungjuribong Volcanic Complex, Gurye-gun, Southwest of Ryeongnam Massif. Journal of the Petrological Society of Korea, 18, 349–370. (in Korean with English abstract)

Kotlia, B.S. and Joshi, L.M., 2013, Late Holocene climatic changes in Garhwal Himalaya. Current Sciences, 104, 911–919.

Kumon, F. and Kiminami, K., 1994, Modal and chemical compositoins of the representative sandstones from the Japanese Islands and their tectonic implications. Proceedings of the 29th International Geological Congress, Part A., 135–151.

Kutterolf, S., Diener, R., Schacht, U., and Krawinkel, H., 2008, Provenance of the Carboniferous Hochwipfel Formation (Karawanken Mountains, Austria/Slovenia) – Geochemistry versus petrography. Sedimentary Geology, 203, 246–266.

Kwon, M.G., 2018, Provenance of the Cretaceous Neungju Basin, southwestern Korea. MS Thesis, Chosun University, 118 p. (in Korean with English abstract)

Kwon, S., Sajeev, K., Mitra, G., Park, Y., Kim, S.W., and Ryu, I.-C., 2009, Evidence for Permo-Triassic collision in Far East Asia: the Korean collisional orogen. Earth and Planetary Science Letters, 279, 340–349.

Lawton, T.F., Bradford, I.A., Vega, F.G., Gehrels, G.E., and Amato, J.M., 2009, Provenance of Upper Cretaceous−Paleogene sandstones in the foreland basin system of the Sierra Madre Oriental, northeastern Mexico, and its bearing on fluvial systems of the Mexican Laramide Province. Geological Society of America Bulletin, 121, 820–836.

Lee, D.S., 1987, Geology of Korea. Geological Society of Korea, Kyohaksa, Seoul, 514 p.

Lee, D.W., 1999, Strike–slip fault tectonics and basin formation during the Cretaceous in the Korean Peninsula. Island Arc, 8, 218–231.

Lee, Y.I., 2009, Geochemistry of shales of the Upper Cretaceous Hayang Group, SE Korea: implications for provenance and source weathering at an active continental margin. Sedimentary Geology, 215, 1–12.

Lee, J.I. and Lee, Y.I., 2003, Geochemistry and provenance of Lower Cretacceous Sindong and Hayang mudrocks, Gyeongsang Basin, Southeastern Korea. Geosciences Journal, 7, 107–122.

Lee, S.-G. and Kim, D.Y., 2012, Geochemical composition of the continental crust in Korean Peninsula. Journal of Petrological Society of Korea, 21, 113–128.

Lee, H., Sim, M.S., and Choi, T., 2019, Stratigraphic evolution of the northern part of the Cretaceous Neungju Basin, South Korea. Geosciences Journal, 23, 849–865.

Lee, S.M., Kim, H.S., Na, K.C., and Park, B.Y., 1989, Geological report of the Tangjin-Changgohang sheet: Korea Institute of Energy and Resources, 15 p. (in Korean with English abstract)

Leeder, M.R., Seger, M.J., and Stark, C.P., 1991, Sedimentation and tectonic geomorphology adjacent to major active and inactive normal faults, southern Greece. Journal of the Geological Society, London, 148, 331–343.

Lim, C., and Cho, M., 2012. Two-phase contractional deformation of the Jurassic Daebo Orogeny, Chungnam Basin, Korea, and its correlation with the early Yanshanian movement of China. Tectonics, 31, TC1004.

Ludwig, K.R., 2008, User's Manual for Isoplot 3.6: A Geochronological Toolkit for Microsoft Excel. Berkeley Geochronology Center Special Publication, Berkeley.

McLennan, S.M., Hemming, S., McDaniel, D.K., and Hanson, G.N., 1993, Geochemical approaches to sedimentation, provenance, and tectonics. Geological Society of America Special Papers, 284, 21–40.

Manville, V., Nemeth, K., and Kano, K., 2009, Source to sink: a review of three decades of progress in the understanding of volcaniclastic processes, deposits, and hazards. Sedimentary Geology, 220, 136–161.

Marti, J., 1991, Caldera-like structures related to Permo-Carboniferous volcanism of the Catalan Pyrenees (NE Spain). Journal of Volcanology and Geothermal Research, 45, 173–186.

Martin, A.J., 2000, Flaser and wavy bedding in ephemeral streams: a modern and an ancient example. Sedimentary Geology, 136, 1–5.

Martins-Neto, M.A. and Catuneanu, O., 2010, Rift sequence stratigraphy. Marine and Petroleum Geology, 27, 247–253.

Miall, A.D., 1977, A review of the braided-river depositional environment. Earth-Science Reviews, 13, 1–62.

Miall, A.D., 1985, Architectural-element analysis: A new method of facies analysis applied to fluvial deposits. Earth-Science Reviews, 22, 261–308.

Miall, A.D., 1996, The Geology of Fluvial Deposits: Sedimentary Facies, Basin Analysis, and Petroleum Geology. Springer-Verlag, Berlin, 582 p.

Milliken, K.L., 1988, Loss of provenance information through subsurface diagenesis in Plio-Pleistocene sandstones, northern gulf of Mexico. Journal of Sedimentary Petrology, 58, 992–1002.

Mtelela, C., Roberts, E.M., Downie, R., and Hendrix, M.S., 2016, Interplay of structural, climatic, and volcanic controls on late Quaternary lacustrine-deltaic sedimentation patterns in the western branch of the East African Rift system, Rukwa Rift Basin, Tanzania. Journal of Sedimentary Research, 86, 1179–1207.

Nakayama, K. and Yoshikawa, S., 1997, Depositional processes of primary to reworked volcaniclastics on an alluvial plain: an example from the Lower Pliocene Ohta tephra bed of the Tokai Group, central Japan. Sedimentary Geology, 107, 211–229.

Nemec, W. and Steel, R.J., 1984, Alluvial and coastal conglomerates: their significant features and some comments on gravelly mass-flow deposits. In: Koster, E.H. and Steel, R.J. (eds.), Sedimentology of Gravel and Conglomerates. Canadian Society of Petroleum Geologists, Memoir, 10, p. 1–31.

Nemec, W. and Postma, G., 1993, Quaternary Alluvial Fans in Southwestern Crete: Sedimentation Processes and Geomorphic Evolution. In: Marzo, M. and Puigdefabregas, C. (eds.), Alluvial Sedimentation. International Association of Sedimentologists, Special Publication, 17, p. 235–276.

Nesbitt, H.W. and Young, G.M., 1982, Early Proterozoic climates and plate motions inferred from

major element chemistry of lutites. Nature, 299, 715–717.

Nilsen, T.H., 1982, Alluvial Fan Deposits. In: Scholle, P.A. and Spearing, D. (eds.), Sandstone Depositional Environments. American Association of Petroleum Geologists, Memoir, 31, p. 49-86.

Oh, C.W., Kim, S.W., Choi, S.G., Zhai, M., Guo, J., and Sajeev, K., 2005, First finding of eclogite facies metamorphic event in South Korea and its correlation with the Dabie-Sulu collision belt in China. The Journal of Geology, 113, 226–232.

Ohta, T., 2008, Measuring and adjusting the weatheirng and hydraulic sorting effects for rigorous provenance analysis of sedimentary rocks: a case study from the Jurassic Ashikita Group, south-west Japan. Sedimentology, 55, 1687–1701.

Olsen, H., 1987, Ancient ephemeral stream deposits: a local terminal fan model from the Bunter Sandstone Formation (L. Triassic) in the Tonder-3, -4 and -5 wells, Denmark. In: Frostick, L.E. and Reid, I. (eds.), Desert Sediments: Ancient and Modern. Geological Society, Special Publication, 35, p. 69–86.

Olsen, H., 1989, Sandstone-body structures and ephemeral stream processes in the Dinosaur Canyon Member, Moenave Formation (Lower Jurassic), Utah, U.S.A. Sedimentary Geology, 61, 207–221.

Paik, I.S. and Kim, H.J., 2006, Playa lake and sheetflood deposits of the Upper Cretaceous Jindong Formation, Korea: Occurrences and palaeoenvironments. Sedimentary Geology, 187, 83–103.

Paik, I.S., Huh, M., So, Y.H., Lee, J.E., and Kim, H.J., 2007, Traces of evaporites in Upper Cretaceous lacustrine deposits of Korea: Origin and paleoenvironmental implications. Journal of Asian Earth Sciences, 30, 93–107.

Paik, I.S., Lee, Y.I., Kim, H.J., and Huh, M., 2012, Time, space and structure on the Korea Cretaceous dinosaur coast: Cretaceous stratigraphy, geochronology, and paleoenvironments. Ichnos, 19, 6–16.

Paola, C., Heller, P.L., and Angevine, C.L., 1992, The large-scale dynamics of grain-size variation in alluvial basins, 1: Theory. Basin Research, 4, 73–90.

Park, S.-I. and Kim, S.W., 2016, A report on gneiss dome in the Hongseong area, southwestern margin of the Gyeonggi massif. Economic and Environmental Geology, 49, 315–323. (in Korean with English abstract)

Park, S.-I., Kim, S.W., Kwon, S., Thanh, N.X., Yi, K., and Santosh, M., 2014a, Paleozoic tectonics of the southwestern Gyeonggi massif, South Korea: insight from geochemistry, chromian-spinel chemistry and SHRIMP U–Pb geochronology. Gondwana Research, 26, 684–698.

Park, S.-I., Kwon, S., Kim, S.W., Yi, K., and Santosh, M., 2014b, Continental origin of the Bibong eclogite, southwestern Gyeonggi massif, South Korea. Journal of Asian Earth Science, 95, 192–202.

Park, S.-I., Kim, S.W., Kwon, S., Santosh, M., Ko, K., and Kee, W.-S., 2017, Nature of Late Mesoproterozoic to Early Neoproterozoic magmatism in the western Gyeonggi massif, Korean Peninsula and its tectonic significance. Gondwana Research, 47, 291–307.

Park, S.-I., Kwon, S., Kim, S.W., Hong, P.S., and Santosh, M., 2018, A Mesozoic orogenic cycle from post-collision to subduction in the southwestern Korean Peninsula: new structural, geochemical, and chronological evidence. Journal of Asian Earth Sciences, 157, 166–186.

Park, S.-I., Noh, J., Cheong, H.J., Kwon, S., Song, Y., Kim, S.W., and Santosh, M., 2019, Inversion of two-phase extensional basin systems during subduction of the Paleo-Pacific Plate in the SW Korean Peninsula: Implication for the Mesozoic "Laramide-style" orogeny along East Asian continental margin. Geoscience Frontiers, 10, 909–925.

Park, Y.S., Kim, S.W., Kee, W.-S., Jeong, Y.-J., Yi, K. and Kim, J., 2009, Middle Jurassic tectono-magmatic evolution in the southwestern margin of the Gyeonggi Massif, South Korea. Geosciences Journal, 13, 217–231.

Parker, A., 1970, An index of weathering for silicate rocks. Geological Magazine, 107, 501–504.

Parker, R.L., 1967, Composition of the Earth's Crust. Professional Paper 440-D, U.S. Geological Survey, 19 p.

Paton, C., Woodhead, J.D., Hellstrom, J.C., Hergt, J.M., Greig, A., and Maas, R., 2010, Improved laser ablation U-Pb zircon geochronology through robust downhole fractionation correction. Geochemistry, Geophysics, Geosystems, 11, Q0AA06.

Paton, C., Hellstrom, J., Paul, B., Woodhead, J., and Hergt, J., 2011, Iolite: freeware for the visualization and processing of mass spectrometric data. Journal of Analytical Atomic Spectrometry, 26, 2508–2518.

Pierson, T.C. and Scott, K.M., 1985, Downstream dilution of a lahar: transition from debris flow to hyperconcentrated streamflow. Water Resources Research, 21, 1511–1524.

Rainbird, R.H., Mcnicoll, V.J., Theriault, R.J., Heaman, L.M., Abbott, J.G., Long, D.G.F., and Thorkelson, D.J., 1997, Pan-continental river system draining Grenville orogeny recorded by U-Pb and Sm-Nd geochronology of Neoproterozoic quartzarenites and mudrocks, northwestern Canada. The Journal of Geology, 105, 1–17.

Raines, M.K., Hubbard, S.M., Kukulski, R.B., Leier, A.L., and Gehrels, G.E., 2013, Sedimentary dispersal in an evolving foreland: Detrital zircon geochronology from Upper Jurassic to lowermost Cretaceous strata, Alberta Basin, Canada. Geological Society of America Bulletin, 125, 741–755.

Rashid, S.A., Ganai, J.A., Masoodi, A., and Khan, F.A., 2015, Major and trace element geochemistry of lake sediments, India: implications for weathering and climate control. Arabian Journal of Geosciences, 8, 5677–5684.

Ree, J.-H, Cho, M., Kwon, S.-T., and Nakamura, E., 1996, Possible eastward extension of Chinese collision belt in South Korea: the Imjingang belt. Geology, 24, 1071–1074.

Reid, I. and Frostick, L.E., 1984, Particle interaction and its effect on the thresholds of initial and final bedload motion in coarse alluvial channels. In: Koster, E.H. and Steel, R.J. (eds.), Sedimentology of Gravels and Conglomerates. Canadian Society of Petroleum Geologists, Memoir, 10, p. 61–68.

Reineck, H.E., 1967, Layered sediments of tidal flats, beaches, and shelf bottoms of the North Sea. In: Lauff, G.H. (ed.), Estuaries: Sediments and Sedimentation. American Association for the Advancement, Science Publication, 83, p. 191–206.

Reineck, H.E. and Wunderlich, F., 1968, Classification and origin of flaser and lenticular bedding. Sedimentology, 11, 99–104.

Rey, P., Vanderhaeghe, O., and Teyssier, C., 2001, Gravitational collapse of the continental crust: definitions, regimes, mechanisms, and modes. Tectonophysics, 342, 435–449.

Rhee, C.W. and Chough, S.K., 1993, The Cretaceous Pyonghae sequence, southeast Korea: terminal fan facies. Palaeogeography, Palaeoclimatology, Palaeoecology, 105, 139–156.

Roh, Y., Park, C.W., Kim, H.J., Lee, S.K., Seo, H., Choi, B.D., and Jung, J.Y., 2017, Geoheritage monitoring and geosite academic supplement for Mudeungsan geopark - final report. GPRN 55-6290000-000458-01, Gwangju ciy, 144 p. (in Korean)

Roser, B.P. and Korsch, R.J., 1986, Determination of tectonic setting of sandstone-mudstone suites using SiO_2 content and K_2O/Na_2O ratio. Journal of Geology, 94, 635–650.

Roser, B.P. and Korsch, R.J., 1988, Provenance signatures of sandstone-mudstone suites determined using discriminant function analysis of major-element data. Chemical Geology, 67, 119–138.

Roy, D.K., and Roser, B.P., 2013, Geochemical evolution of the Tertiary succession of the NW self, Bengal basin, Bangladesh: Implications for provenance, paleoweathering, and Himalayan erosion. Journal of Asian Earth Sciences, 78, 248–262.

Ryan, K.M. and Williams, D.M., 2007, Testing the reliability of discrimination diagrams for determining the tectonic depositional environment of ancient sedimentary basins. Chemical Geology, 242, 103–125.

Ryang, W.-H., 2013, Characteristics of strike-slip basin formation and sedimentary fills and the Cretaceous small basins of the Korean Peninsula. Journal of the Geological Society of Korea, 49, 31–45.

Ryang, W.H. and Chough, S.K., 1997, Sequential development of alluvial/lacustrine system: southeastern Eumsung Basin (Cretaceous), Korea. Journal of Sedimentary Research, 67, 274–285.

Sajeev, K., Jeong, J., Kwon, S., Kee,W.-S., Kim, S.W., Komiya, T., Itaya, T., Jung, H.-S., and Park, Y., 2010, High P–T granulite relicts from the Imjingang belt, South Korea: tectonic significance. Gondwana Research, 17, 75–86.

Sagong, H., Kwon, S.-T., and Ree, J.-H., 2005, Mesozoic episodic magmatism in South Korea and

its tectonic implication. Tectonics, 24, TC5002.

Séguret, M., Séranne, M., Chauvet, A., and Brunel, A., 1989, Collapse basin: A new type of extensional sedimentary basin from the Devonian of Norway. Geology, 17, 127–130.

Seo, H.G. and Paik, S.H., 1984, Researches on coal resources (II), north part of the Iyang area, Honam coal field, 83-coal resources-3-16. Geological Survey of Korea, 205 p. (in Korean).

Shao, L., Yuan, S., Li, C., Kang, C., Zhu, W., Liu, Y., and Wang, J., 2015, Changing provenance of late Cenozoic sediments in the Jianghan Basin. Geoscience Frontiers, 6, 605–615.

Shultz, A.W., 1984, Subaqueous debris-flow deposits in the Upper Paleozoic Culter Formation, western Colorado. Journal of Sedimentary Petrology, 54, 759–772.

Smith, G.A., 1986, Coarse-grained nonmarine volcaniclastic sediment: terminology and depositional process. Geological Society of America Bulletin, 97, 1–10.

Smith, G.A., 1987, The influence of explosive volcanism on fluvial sedimentation; the Deschutes Formation (Neogene) in central Oregon. Journal of Sedimentary Research, 57, 613–629.

Smith, G.A., 1988, Sedimentology of proximal to distal volcaniclastics dispersed across an active foldbelt: Ellensburg Formation (late Miocene), central Washington. Sedimentology, 35, 953–977.

Smith, G.A., 1991, Facies sequences and geometries in continental volcaniclastic sediments. In: Fisher, R.V. and Smith, G.A. (eds.), Sedimentation in Volcanic Settings. Society for Sedimentary Geology (SEPM), Special Publication, 45, p. 109–122.

Smith, G.A., Moore, J.D., and McIntosh, W.C., 2002, Assessing roles of volcanism and basin subsidence in causing Oligocene-lower Miocene sedimentation in the northern Rio Grande Rift, New Maxico, U.S.A. Journal of Sedimentary Research, 72, 836–848.

Smoot, J.P., 1983, Depositional subenvironmnets in an arid closed basin; the Wilins Peak Member of the Green River Formation (Eocene), Wyoming, U.S.A. Sedimentology, 30, 801–827.

So, Y.S., Rhee, C.W., Choi, P.-Y., Kee, W.-S., Seo, J.Y., and Lee, E.-J., 2013, Distal turbidite fan/lobe succession of the Late Paleozoic Taean Formation, western Korea. Geosciences journal, 17, 9–25.

Sohn, Y.K., Ki, J.S., Jung, S., Kim, M.-C., Cho, H. and Son, M., 2013, Synvolcanic and syntectonic sedimentation of the mixed volcaniclastic–epiclastic succession in the Miocene Janggi Basin, SE Korea. Sedimentary Geology, 288, 40–59.

Son, C.M. and Kim, S.J., 1966, Geological report of the Changpyeong sheet (1:50,000). Geological Survey of Korea, 205 p. (in Korean)

Spearing, D.R., 1974, Summary sheets of sedimentary deposits, Mc-8, Sheet 1. Geological Society of America.

Spencer, C.J., Cawood, P.A., Hawkesworth, C.J., Prave, A.R., Roberts, N.M.W., Horstwood, M.S.A., Whitehouse, M.J., and EIMF, 2015, Generation and preservation of continental crust in the

Grenville Orogeny. Geoscience Frontiers, 6, 357–372.

Steel, R.J. and Thompson, D.B., 1983, Structures and textures in Triassic braided stream conglomerates ('Bunter' Pebble Beds) in the Sherwood Sandstone Group, North Staffordshire, England. Sedimentology, 30, 341–367.

Taylor, S.R. and McLennan, S.M., 1985, The Continental Crust: Its Composition and Evolution. Blackwell Scientific Publications, Oxford, 315 p.

Teyssier, C., and Whitney, D.L., 2002, Gneiss domes and orogeny. Geology, 30, 1139–1142.

Thomas, L.P., and Park, S.H., 1976, Geology of the Kimpo and Yeoncheon coalfields, Gyeonggi Province, Republic of Korea. Korea Research Institute of Geoscience and Mineral Resources, 80 p.

Troll, V.R., Walter, T.R., and Schmincke, H.-U., 2002, Cyclic caldera collapse: piston or piecemeal subsidence? Field and experimental evidence. Geology, 30, 135–138.

Tunbridge, I.P., 1984, Facies model for a sandy ephemeral strea and clay playa complex; the Middle Devonian Trentishoe Formation of North Devon, U.K. Sedimentology, 31, 697–715.

Turek, A. and Kim, C.-B., 1995, U-Pb zircon ages of Mesozoic plutons in the Damyang-Geochang area, Ryongnam massif, Korea. Geochemical Journal, 29, 243–258.

Vavra, G., Schmid, R., and Gebauer, D., 1999. Internal morphology, habit and U–Th–Pb microanalysis of amphibolite-to-granulite facies zircons: geochronology of the Ivrea Zone (Southern Alps). Contributions to Mineralogy and Petrology, 134, 380–404.

Vanderhaeghe, O., and Teyssier, C., 2001, Partial melting and flow of orogens. Tectonophysics, 342, 451–472.

Vernam S.P. and Armstrong-Altrin, J.S., 2013, New multi-dimentional diagrams for tectonic discrimination of siliciclastic sediments and their application to Precambrian basins. Chemical Geology, 355, 117–133.

Vogt, T., 1927, Sulitjelmafeltets geologi og petrografi. Norges Geologiske Undersokelse, 121, 1–560 (in Norwegian with English abstract).

von Eynatten, H., Barcelo-Videl, C., and Pawlowsky-Glahn, V., 2003, Composition and discrimination of sandstones: a statistical evaluation of different analytical methods. Journal of Sedimentary Research, 73, 47–57.

Wasson, R.J., 1977, Last-glacial alluvial fan sedimentation in the Lower Derwent Valley, Tasmania. Sedimentology, 24, 781–799.

Weltje, G.J., 2012, Quantitative models of sediment generation and provenance: state of the art and future developments. Sedimentary Geology, 280, 4–20.

Weltje, G.J. and von Eynatten, H., 2004, Quantitative provenance analysis of sediments: review and outlook. Sedimentary Geology, 171, 1–11.

Wiedenbeck, M., Alle, P., Corfu, F., Griffin, W.L., Meier, M., Oberli, F., von Quadt, A., Roddick, J.C., and Spiegel, W., 1995, Three natural zircon standards for U–Th–Pb, Lu–Hf, trace element and REE analyses. Geostandards and Geoanalytical Research, 19, 1–23.

Wilson, J.T., 1966, Did the Atlantic close and then re-open?. Nature, 211, 676–681.

Williams, I.S., Cho, D.L., and Kim, S.W., 2009, Geochronology, and geochemical and Nd–Sr isotopic characteristics, of Triassic plutonic rocks in the Gyeonggi Massif, South Korea: constraints on Triassic post-collisional magmatism. Lithos, 107, 239–256.

Wu, F.-Y., Yang, J.-H., Wilde, S.A., Liu, X.-M., Guo, J.-H., and Zhai, M.-G., 2007, Detrital zircon U-Pb and Hf isotopic constraints on the crustal evolution of North Korea. Precambrian Research, 159, 155–177.

Yandoka, B.M.S., Abullah, W.H., Abubakar, M.B., Hakimi, M.H., and Adegoke, A.K., 2015, Geochemical characterization of Early Cretaceous lacustrine sediments of Bima Formation, Yola Sub-basin, Northern Benue Trough, NE Nigeria: organic matter input, preservation, paleoenvironment and palaeoclimatic conditions. Marine and Petroleum Geology, 61, 82–94.

Yang, R., Suhail, H.A., Gourbet, L., Willett, S.D., Fellin, M.G., Lin, X., Gong, J., Wei, X., Maden, C., Jiao, R., and Chen, H., in press, Early Pleistocene drainage pattern changes in Eastern Tibet: constraints from provenance analysis, thermochronometry, and numerical modeling. Earth and Planetary Science Letters.

You, H.S., Moon, B.C., Koh, Y.K., Kim, H.G. and Lyu, S.O., 1998, A study on the paleodepositional environment of Cretaceous sedimentary rocks - northeastern area of Chonnam. Journal of the Korean Earth Science Society, 19, 318–328. (in Korean with English abstract)

Yu, K.M. and Lee, Y., 1992, Sedimentary petrology of the sandstones of the Daedong Group in western part of the Chungnam Coalfield. Journal of the Geological Society of Korea, 28, 284–297. (in Korean with English abstract)

Yu, K.M., Kwon, Y.I., and Chun, H.Y., 1992, Stratigraphy and mineral composition of sandstones from the Daedong Group in Yeoncheon Area. Journal of the Geological Society of Korea, 28, 152–166. (in Korean with English abstract)

Zaunbrecher, L.K., Elliott, W.C., Wampler, J.M., Perdrial, N., and Kaplan, D.I., 2015, Enrichment of cesium and rubidium in weathered micaceous materials at the Savannah River site, South Carolina. Environmental Science and Technology, 49, 4226–4234.

Zhang, Y., Hu, B., Zhai, M., Wu, F., Hou, Q., Peng, P., Zhang, X., and Li, Q., 2018, In situ U-Pb zircon dating of Devonian sandstones and Paleoproterozoic gneissic granites in the Imjingang Belt: Tectonic implications for the Korean Peninsula and North China. Lithos, 316–317, 232–242.

Zhang, S.-H., Zhao, Y., Liu, J.-M., and Hu, Z.-C., 2016, Different sources involved in generation of continental arc volcanism: The Carboniferous–Permian volcanic rocks in the northern margin of the North China block. Lithos, 240–243, 382–401.

국문 초록

한반도 남부의 중생대 퇴적분지들의 발달에 대한 지화학적, 퇴적학적 및 쇄설성 저어콘 연대측정 연구

한반도 중생대 지질사를 복원하기 위해서는 중생대 퇴적분지들의 발달에 해한 이해가 요구된다. 본 연구는 한반도 서부에 분포하고 있는 두 시기의 중생대 퇴적분지에 대한 세 가지 주제를 다루고 있다. 연구 대상은 백악기의 능주분지와 삼첩기-쥬라기의 충남분지, 김포층군, 그리고 석문층이다. 제1장에서는 능주분지의 발달사를 조사하기 위해 퇴적상분석 통한 연구를 수행하였다. 능주분지에서는 선상지, 선상지평원, 사질평원 및 플라야호수 환경을 지시하는 네 종의 퇴적상조합이 확인되었다. 퇴적환경의 시공간적 분포는 화산활동 이후 수발된 분지침강과 기원지의 융기에 의해 결정되었다. 화산활동기와 비활동기 퇴적물 사이의 경계면은 분지 내에서의 상대적 위치에 따라 다양하다. 근부환경에서는 화산활동과 관계된 침강의 영향이 적어 화산활동기 퇴적물 위에 침식면이 발달할 수 있으나, 원부환경에서는 침강의 영향이 지배적이기 때문에 화산활동기 퇴적물 위에 정합적으로 호수퇴적이 쌓이게 된다. 제2장에서는 서로 다른 기원지로부터 공급된 퇴적물이 분리/혼합되는 양상을 연구하기 위해 기존 연구들에서 제시된 능주분지 사암의 저어콘 U-Pb 연대자료와 함께 능주분지 이암의 지화학적 조성을 조사하였다. 연구지역 능주분지의 분지충진물은 선캄브리아기 변성암, 삼첩기-쥬라기 화강암 및 분지남부지역 내에

발달한 화산쇄설물평원에서 기원하였다. 서로 다른 기원지로부터 공급된 퇴적물질은 근부환경(선상지에서 사질평원)에서는 완전한 혼합을 이루지 않았으며, 따라서 근부환경 퇴적물은 분지를 둘러쌓은 기원암 전반의 조성적 특징을 반영하지 않아 분지의 지구조환경에 대한 부적절한 정보를 제공한다. 한편 원부환경(플라야호수)의 퇴적물은 화산쇄설물평원으로부터 충분히 풍화받지 않은 퇴적물질을 공급받았기 때문에 다른 퇴적학적, 고생물학적 증거들로부터 제시되는 풍화강도에 비해 낮은 풍화강도를 산출한다. 제3장에서는 이암의 지화학 분석과 사암의 저어콘 연대 분석을 통하여 전기 중생대 동안 한반도 서부에서 발생한 지구조적 진화를 조사하였다. 그 결과 전기중생대 동안 한반도 서부에 발달한 조산대는 기반암이 노출된 북쪽의 후방지(hinterland side)와 변성퇴적암류가 노출된 남부의 전방지(foreland side)로 구성되어 있었으며, 전기중생대의 퇴적분지들이 발달하는 동안 한반도 서부는 충돌성(collision) 지구조환경에서 수렴성(convergent) 지구조 환경으로 전이했다는 것을 확인할 수 있었다.

주요어: 지화학, 퇴적상분석, 저어콘 U-Pb 연대측정, 중생대, 육성환경
학 번: 2010-30111